

# **Geological Storage of CO<sub>2</sub>: Sensitivity and Risk Analysis**

**Meisam Ashraf**



Dissertation for the degree of Philosophiae Doctor (PhD)

Department of Mathematics  
University of Bergen

November 2013



# **Scientific environment**

This dissertation is submitted as a partial fulfillment of the requirements for the degree Doctor of Philosophy (PhD) at the University of Bergen. It is part of the project Mathematical Modeling and Risk Assessment of CO<sub>2</sub> storage, MatMoRA, which was funded by the Norwegian Research Council of Norway, Statoil and Norske Shell under grant no. 178013/I30 and lead by Professor Helge Dahle at the Department of Mathematics, University of Bergen (UiB).

The working environment have been SINTEF-ICT in Oslo, CIPR in Bergen, and SIMTECH in Stuttgart. Professor Knut-Andreas Lie, chief scientist at SINTEF-ICT, has been the main adviser and Professor Jan M. Nordbotten at the Department of Mathematics, UiB, along with Halvor M. Nilsen, research scientist at SINTEF, have been co-advisers. With warm supports from Professor Rainer Helmig, head of Department of Hydromechanics and Modelling of Hydrosystems at Stuttgart University, last parts of the work is benefited from advices of professor Wolfgang Nowak, head of Stochastic Modelling of Hydrosystems, Dr. Sergey Oladyshkin, postdoctoral fellow at SIMTECH, and Professor Holger Class at Stuttgart University.



# Acknowledgements

*I dedicate this to my father.*

With them the seed of Wisdom did I sow,  
And with mine own hand wrought to make it grow;  
And this was all the Harvest that I reap'd-  
"I came like Water, and like Wind I go."

*Omar Khayyam, 1048 – 1131.*

*Translated by Edward FitzGerald, 1809-1883.*

My great thanks go to Knut-Andreas Lie who supported me throughout my study. I always enjoyed discussions with Halvor M. Nilsen, who initially was my only friend in Norway. Jan M. Nordbotten always inspired me in my works. Many thanks to Helge Dahle, who supported me during my stay in Bergen. I have enjoyed working with Segrey Oladyshkin, Wolfgang Nowak, and Holger Class while spending a semester in Stuttgart University. Special thanks go to friends and family that made my life more beautiful.

I would like also to acknowledge the sponsors of the MatMora project defined in the University of Bergen in partnership with SINTEF-ICT and the University of Stuttgart, and the German Research Foundation (DFG) for financial support of the project within the Cluster of Excellence in Simulation Technology (EXC310/1) at the University of Stuttgart.

Meisam Ashraf  
Trondheim, November 2013



# Abstract

Geological CO<sub>2</sub> storage is a key technology utilized in the prevention of industrial CO<sub>2</sub> emission into the atmosphere. A successful storage operation requires safe geological structures with large storage capacity. The practicality of the technology is challenged by various operational concerns, ranging from site selection to long-term monitoring of the injected CO<sub>2</sub>. The research in this report addresses the value of using sophisticated geological modeling to help in predicting storage performance.

In the first part, we investigate the significance of assessing the geological uncertainty and its consequences in site selection and the early stages of storage operations. This includes the injection period and the early migration time of the injected CO<sub>2</sub> plume. The extensive set of realistic geological realizations used in the analysis makes the key part of this research. Heterogeneity is modelled using the most influential geological parameters in a shallow-marine system, including aggradation angle, levels of barriers in the system, faults, lobosity, and progradation direction.

A typical injection scenario is simulated over 160 realizations and major flow responses are defined to measure the success of the early stages of CO<sub>2</sub> storage operations. These responses include the volume of trapped CO<sub>2</sub> by capillarity, dynamics of the plume in the medium, pressure responses, and the risk of leakage through a failure in the sealing cap-rock. The impact of geological uncertainty on these responses is investigated by comparing all cases for their performance. The results show large variations in the responses due to changing geological parameters. Among the main influential parameters are aggradation angle, progradation direction, and faults in the medium.

A sophisticated geological uncertainty study requires a large number of detailed simulations that are time-consuming and computationally costly. The second part of the research introduces a workflow that employs an approximating response surface method called arbitrary polynomial chaos (aPC). The aPC is fast and sophisticated enough to be used practically in the process of sensitivity analysis and uncertainty and risk assessment. We demonstrate the workflow by combining the aPC with a global sensitivity analysis technique, the Sobol indices, which is a variance-based method proven to be practical for complicated physical problems. Probabilistic uncertainty analysis is performed by applying the Monte Carlo process using the aPC. The results show that the aPC can be used successfully in an extensive geological uncertainty study.



# List of papers

1. M. Ashraf, K.A. Lie, H.M. Nilsen and A. Skorstad, "*Impact of geological heterogeneity on early-stage CO<sub>2</sub> plume migration: CO<sub>2</sub> spatial distribution sensitivity study*", Submitted to the Groundwater.
2. M. Ashraf, "*Impact of geological heterogeneity on early-stage CO<sub>2</sub> plume migration: pressure sensitivity study*", Submitted to the International Journal of Greenhouse Gas Control(IJGGC).
3. M. Ashraf, S. Oladyshkin, W. Nowak, "*Geological storage of CO<sub>2</sub>: Application, feasibility and efficiency of global sensitivity analysis and risk assessment using the arbitrary polynomial chaos.*" , Published in the International Journal of Greenhouse Gas Control (2013).



# Contents

<b>Scientific environment</b>	<b>i</b>
<b>Acknowledgements</b>	<b>iii</b>
<b>Abstract</b>	<b>v</b>
<b>List of papers</b>	<b>vii</b>
<b>1 Introduction</b>	<b>1</b>
1.1 Introduction . . . . .	2
1.2 Carbon storage . . . . .	3
1.3 Modeling procedure . . . . .	4
1.4 Uncertainty Sources . . . . .	6
1.5 Geological modeling . . . . .	7
1.5.1 Geological description . . . . .	7
1.5.2 Geological parameters . . . . .	10
1.6 Flow equations . . . . .	17
1.6.1 Single phase flow . . . . .	17
1.6.2 Two-phase flow . . . . .	19
1.7 Flow regimes . . . . .	24
1.7.1 Injection and early migration . . . . .	25
1.7.2 Long term migration . . . . .	27
1.8 Flow modeling . . . . .	28
1.8.1 Numerical scheme . . . . .	28
1.8.2 Flow scenarios . . . . .	31
1.8.3 Flow responses . . . . .	33
1.8.4 ECLIPSE input file . . . . .	35
1.9 Sensitivity and risk analysis . . . . .	46
1.9.1 Stochastic analysis . . . . .	46
1.9.2 Arbitrary polynomial chaos expansion . . . . .	46
1.9.3 Sensitivity analysis . . . . .	49
1.9.4 Risk analysis . . . . .	51
1.10 General summary . . . . .	51
1.10.1 Implementation of the work-flow . . . . .	52
1.10.2 Generic application of results . . . . .	52
<b>2 Introduction to the papers</b>	<b>55</b>
2.1 Introduction . . . . .	56
2.2 Summary of papers . . . . .	56

<b>3 Scientific results</b>	<b>61</b>
3.1 Impact of geological heterogeneity on early-stage CO <sub>2</sub> plume migration: Sensitivity study	63
3.2 Geological storage of CO <sub>2</sub> : Heterogeneity impact on pressure behavior . . . . .	89
3.3 Geological storage of CO <sub>2</sub> : Application, feasibility and efficiency of global sensitivity analysis and risk assessment using the arbitrary polynomial chaos. . . . .	115
<b>A Additional supporting material</b>	<b>133</b>
A.1 Impact of geological heterogeneity on early-stage CO <sub>2</sub> plume migration . . . . .	135
A.2 Impact of geological heterogeneity on early-stage CO <sub>2</sub> plume migration: sensitivity study	145
A.3 Field-case simulation of CO <sub>2</sub> plume migration using vertical-equilibrium models. . . . .	161

# List of Figures

1.1	Green-house gases act like a blanket trapping part of the heat received from the sun. The low frequency radiations from the earth surface can not pass through the layer of green-house gas on the upper part of the atmosphere (shown by a red line in the figure).	3
1.2	The injected CO <sub>2</sub> (the yellow part) in the aquifer (the dark blue part) can be stored under the sealing geological structures (the brown part). . . . .	4
1.3	Modeling procedure diagram. The tasks are shown in yellow boxes and they fall in three main categories that are indicated by big cyan boxes. Arrows depict the flow of the procedure based on the sequence order of the tasks. . . . .	5
1.4	Schematic plots of heterogeneities in fluvial and beach depositions. The top view is illustrated in Figure (a) and Figure (b) shows the side view. The arrow in Figure (b) shows that the deposition mass is less heterogeneous than the fluvial systems. . . . .	8
1.5	Stratigraphic heterogeneity levels in lateral and vertical directions. Arrows direction indicates the increase in the heterogeneity level. Modified from [47]. . . . .	12
1.6	Fine grid perspective view. Colors depict rock types; see Figures 1.7 and 1.8. The geological structure is divided in two parts due to a faulting process. The eleveated part is considered in the study. . . . .	12
1.7	Perspective view of the rock type variations for a selected case mapped on a uniform grid.	13
1.8	Six different rock types used in modeling the stratigraphic heterogeneities. Compare with Figure 1.7 . . . . .	13
1.9	Histogram of lateral transmissibility for different facies in a selected case. Scales are logarithmic in units cP.m <sup>3</sup> /day/bar. Only the x-axis is logarithmic. . . . .	14
1.10	Logarithmic of lateral transmissibility plotted for four layers in fine grid versus their representative layer in the coarse grid. The top view is plotted in all figures and units are cP.m <sup>3</sup> /day/bar. . . . .	15
1.11	Top view illustration of faults used in the faulted grids. The fault plotted in red divides the medium in two parts (compare with Figure 1.6) and only the part below the red line in the top view is considered in the study. . . . .	15
1.12	Lobosity levels are defined based on the shoreline shape, which is caused by the interplay between fluvial and wave forces. From Figure (a) to (c) the system changes from wave to fluvial dominated. . . . .	16
1.13	Periodic floods and fluctuactions in fluvial system can result in shale draped surfaces. These surfaces act as barriers to flow in both vertical and horizontal directions. The barries are modeled in the SAIGUP study by modifying the transmissibility of cells across the barrier (red surface in the plot). Barrier level variations are specified by areal coverage of zero transmissibility multipliers (indicated by blue color). . . . .	16
1.14	The change in the fluvial flux results in a shift in the depositional rock types from the river to the sea. The shift varies from very extensive in amount resulting in near horizontal layers of facies stocked on top of each other (low aggradation angles) to slight shifts resulting in near vertical rock type patterns (high aggradation angles). . . . .	17
1.15	Techtonic activies in shallow marine systems can result in various orientations of river to sea depositions that is considered as progradation direction in the SAIGUP study. . . . .	17

1.16 The flow problem is solved over domain $\Omega$ that is bounded by $\Gamma_i$ . The injection well is modeled as source point $q$ . Geological heterogeneities can be in the form of discontinuity $\gamma_i$ .	18
1.17 Permeability is an indication of how easy it is for the fluids to flow through the medium.	18
1.18 In a multiphase system, phases wet the medium with different degrees of preference. Wettability is defined by the angle between two phases' interface and the solid surface ( $\Theta$ ). The wetting phase makes an acute angle with the solid phase. Water is the wetting phase in this example.	20
1.19 The $\text{CO}_2$ (yellow parts) is the non-wetting phase and it flows through the water (blue parts) that wets the rock grains (brown parts) easier than $\text{CO}_2$ . The cross section of the medium is illustrated here.	20
1.20 Relative permeability is an indication of how easy it is for the two phases to flow together through the medium. Relative permeability depends on the wettability of phases and the relative volumes occupied by each phase (phase saturation).	21
1.21 Capillary pressure can be expressed as a function of wetting saturation. The plot shows a typical Van Genuchten curve for capillary pressure. The scale in the vertical axis is only for demonstration. For application, see for example [46] and [40].	22
1.22 Capillary force is caused by the interaction of fluid phases with the pore walls. Capillary pressure is calculated from the force balance at the interface and depends on the curvature of the interface and the pore radius.	22
1.23 Water saturation ( $S_w$ ) distribution in the capillary transition zone. In the hydrostatic equilibrium condition, phases exist at different depths with saturations that depend on the balance between capillary and gravity forces.	23
1.24 Flow regimes in geological $\text{CO}_2$ storage; (a) During injection, the main physical processes are the flow advection due to the imposed pressure by the injection, the gravity segregation due to the phase density differences, and the dissolution of $\text{CO}_2$ into water. (b) During the long-term $\text{CO}_2$ migration, the main physical processes in the medium are the gravity segregation, the molecular diffusion, the $\text{CO}_2$ dissolution in water, the water capillary imbibition, and the convection mixing due to gravity instabilities.	29
1.25 Transmissibility between two cells $a$ and $b$ depends on the interface area perpendicular to the flow ( $A_{ab}$ ) and transmissibilities between the center and the cell side within each cell ( $T_a$ and $T_b$ ).	30
1.26 Injection operation causes pressure increase near the well-bore. The red color in the figure demonstrates the regions with pressure build-up. The well-bore pressure is calculated by a relation that models the pressure distribution around the well. The black curve in the figure shows a schematic incline of the pressure near the injector.	30
1.27 In the models used for flow simulation, the top, bottom, and upper side boundaries are closed and the rest are open to the flow. Arrows point to the boundaries and their color indicates if the boundary is open (green) or closed (red). Colors on the grid show the depth of different locations.	32
1.28 The aquifer can be connected to neighboring aquifer systems and the flow from those aquifers (red arrows in the plot) is modeled by imposing external pressure on the open sides of the model. The dotted box in the figure schematically indicates a domain considered for study. Aquifer layers outside the frame are considered external. The yellow color demonstrates the injected $\text{CO}_2$ in the aquifer.	33
1.29 Mobile and residual $\text{CO}_2$ volumes; the injected $\text{CO}_2$ plume travels upward within the geological formation and leaves behind a volume of residual $\text{CO}_2$ that is trapped due to capillarity.	33
1.30 We use a 2D Gaussian distribution for leakage probability on the cap-rock.	34

1.31 Transmissibility in the vertical direction for two selected cases. The left plots correspond to case A in Table 1.4, and the right plots belong to case B. Colors are in log scale and the scale in Figures (a) and (b) are powers of ten in cP.m <sup>3</sup> /day/bar units. . . . .	36
1.32 Transmissibility in the lateral direction for two selected cases. The left plots correspond to case A in Table 1.4, and the right plots belong to case B. Colors are in log scale and the scale in Figures (a) and (b) are powers of ten in cP.m <sup>3</sup> /day/bar units. . . . .	37
1.33 CO <sub>2</sub> distribution at the end of injection for two selected cases. The left plots correspond to case A in Table 1.4, and the right plots belong to case B. . . . .	38
1.34 CO <sub>2</sub> distribution at the end of simulation for two selected cases. The left plots correspond to case A in Table 1.4, and the right plots belong to case B. . . . .	39
1.35 Flow sign in the Y direction at the end of injection for two selected cases. The left plots correspond to case A in Table 1.4, and the right plots belong to case B. Blue color corresponds to down-dip direction, red to up-dip direction, and green represents the stagnant fluid. . . . .	40
1.36 Mobile CO <sub>2</sub> distribution at different times for two selected cases. Cases A and B are described in Table 1.4. Compare with Figures 1.31 and 1.32 for transmissibility values in different directions. Colors represent the same ranges shown in Figure 1.34. . . . .	41
1.37 Pressure development during injection and early migration. Pressure differences from hydrostatic pressure are shown for two selected cases. Values are in bar. Cases A and B are described in Table 1.4. Compare with Figures 1.31 and 1.32 for transmissibility values in different directions. . . . .	42
1.38 Marker codes used to plot the simulation results of all cases together. Aggradation is shown by different colors. Faults are shown by marker thickness; the thickest marker shows a case with close fault, medium thickness represents a case with open faults, and the thin markers indicate a case with no faults. All cases plotted in triples for the three degrees of faults. Therefor, plots contain 54 number of cases in the x-axis. The first 27 case numbers represent the up-dip progradation, and case numbers 28 to 54 have down-dip progradation. . . . .	43
1.39 Flowchart of workflow implemented in an automated procedure. . . . .	52



# **Chapter 1**

## **Introduction**

## 1.1 Introduction

“We won’t have a society if we destroy the environment”

– Margaret Mead, American cultural anthropologist, 1901-1978

Climate changes resulting from CO<sub>2</sub> emissions caused by human have been shown in studies such as [36]. The underground sequestration of CO<sub>2</sub> produced from localized sources such as power-plants and oil and gas recovery sites is proposed as a possible solution to reduce the rate of CO<sub>2</sub> emission into the atmosphere [11, 35]. The technology required to inject CO<sub>2</sub> is similar to what is in use in the oil and gas and mining industry. However, there are two main challenges that are specific to carbon storage operations. First, the temporal and spatial scales in these problems are larger. Second, the risk of leakage of stored CO<sub>2</sub> up to the surface. The leakage can happen via natural features like fractures and faults or via man-made features such as leakage through ill-plugged wells and broken cap-rock due to high pressure imposed to the system during the injection operations is a major concern.

The main objectives of carbon storage operations are to maximize the storage volume and the volumetric injection rate, and to minimize the risk of leakage of the stored CO<sub>2</sub>. The CO<sub>2</sub> storage operations require multidisciplinary collaborations. The work-flow from initial phases of a project until end of storage operations is divided between government and private sectors, research organizations and industry. In particular, it is the task of research community to investigate the safety of CO<sub>2</sub> sequestration and provide the methodology for CO<sub>2</sub> fate prediction [5].

Bachu [5] discusses a road-map of site selection for geological CO<sub>2</sub> sequestration. He defines the process in three steps: to assess the general suitability of the site, to perform an inventory study on source point, storage location, and operational transport issues, and finally to investigate the safety and assess the capacity of the storage. Safety and storage capacity issues are investigated from different perspectives such as immediate and ultimate results. As an example, the leakage through ill-plugged wells or fractures during the injection time is considered the immediate risk. However, leakage caused by plume migration long time after the injection and contamination to other aquifer systems are considered as ultimated risks.

To predict the fate of the injected CO<sub>2</sub>, it is important to study the dynamics of flow in the storage medium. Study of flow dynamics includes quantification of acting forces in a geological heterogeneous medium as well as solving a complicated system of mathematical equations. It is convenient to replace the geological heterogeneous medium with an equivalent homogeneous medium to simplify the solution of the flow equations. However, proper modeling of geological heterogeneity is important in reservoir assessment and carbon storage studies [6, 19, 50, 51].

In this thesis, we report a series of studies performed within a PhD program. The work in this thesis is focusing on the fundamental uncertainty in geological description. The objective is to perform a sensitivity analysis on a set of geological parameters used to describe the geology of shallow-marine depositional systems. Although the focus is on a particular depositional system, the procedure can be implemented for other systems of interest. The work is reported in a series of papers.

The thesis is structured in three chapters. In the first chapter, we start by discussing the global warming and its causes, and the carbon storage as an interim proposed solution to mitigate the increasing level of industrial CO<sub>2</sub> emission to the atmosphere. Section 1.3 provides the work-flow of the works reported in the thesis. A literature overview is given in that section. A short discussion on different types of uncertainties in CO<sub>2</sub> storage operations is given in Section 1.4.

In Section 1.5, a detailed report on geological description is given, which includes information about the geological upscaling process. Flow equations for single-phase and two-phase flow problems are discussed in Section 1.6. In Section 1.7, various flow regimes occurring during geological storage

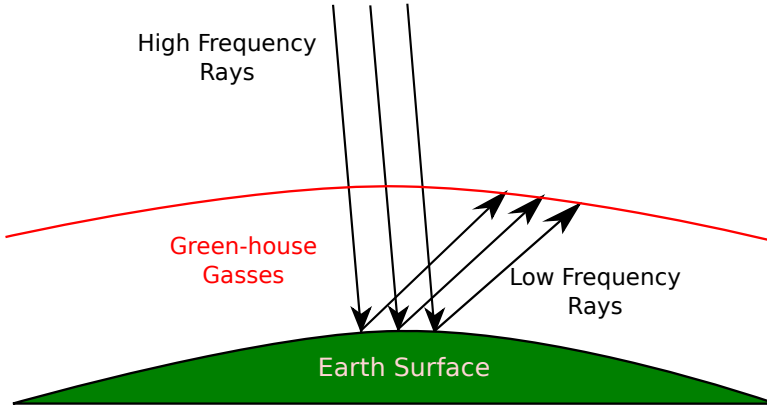


Figure 1.1: Green-house gases act like a blanket trapping part of the heat received from the sun. The low frequency radiations from the earth surface can not pass through the layer of green-house gas on the upper part of the atmosphere (shown by a red line in the figure).

of CO<sub>2</sub> are briefly described by discussing the force balance within the medium at different times. This section helps in evaluation of the simplifying physical assumptions taken in the study. For example, we discuss the circumstances under which the capillary pressure can be ignored in the study.

The introduction chapter continues in Section 1.8 by a discussion of flow simulation scenario and assumptions taken in the work. We use a set of flow responses to monitor the performance of the operation in a typical carbon storage process, with a special emphasis on the injection and early migration of CO<sub>2</sub> in the medium. Flow dynamics and a linear sensitivity analysis on the simulation results are discussed in this section.

Section 1.9 provides an overview of the techniques that can be used for fast flow simulations. We use a response surface method to evaluate the flow responses. This proxy model is then used in a global sensitivity analysis and Monte Carlo risk assessment process. At the end of this chapter, an overview of the work-flow and the limiting assumptions made in the study are discussed.

The second chapter consists of a summary of the included papers. A report on the comments and issues regarding each part of the research is given. In the last chapter, we present the scientific results of our studies.

## 1.2 Carbon storage

Causes of climate change are explained in numerous theories. Milankovich theory [29] relates the energy received from the sun to the cyclical variation of earth orbit around the sun, and earth rotation around its axis. The earth orbit changes eccentricity between circular and elliptical; This influences the distance between earth and sun, and in its peak it can reach to about 20% difference in the energy received from the sun. The second variation occurs in the rotation of earth around its plane axis. This rotation wobbles approximately every 13600 years and the summer solstice switches from June to January. Furthermore, a tilt variation of earth rotational axis happens approximately after every 41000 years. This can cause warmer winters and colder summers in high latitudes [29]. The solar radiation changes by a small amount of 0.1% over a 11 year cycle. On the scale of tens to thousands of years, variations in the earth orbit result in seasonal changes, which in the past caused glacial and inter-glacial cycles.

The theory of green house effect relates the earth climatic change to the fact that the long wave radiation from earth back to atmosphere is absorbed by the green-house gases, mainly carbon dioxide, water vapor, and methane existing in the atmosphere. This results in trapping of heat energy and an increase in atmosphere temperature level (Figure 1.1) [29].

Human manipulations in the nature has led to approximately 100 ppm increase in carbon dioxide

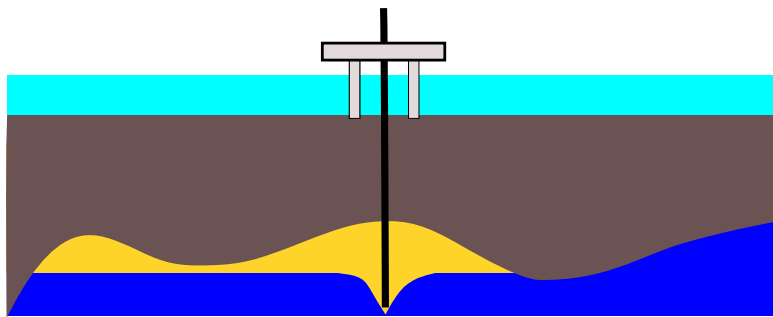


Figure 1.2: The injected CO<sub>2</sub> (the yellow part) in the aquifer (the dark blue part) can be stored under the sealing geological structures (the brown part).

level in the atmosphere. Most scientists believe that we are already experiencing the global warming due to green house effects. The IPCC Second Assessment report states that the observed warming trend since the late 19<sup>th</sup> century is unlikely to be entirely natural in origin and is partly due to anthropogenic causes [14].

Carbon capture and storage (CCS) has received major attention in the industry and the scientific communities. According to the International Energy Agency (IEA), the cost of mitigating climate change by 2050 is estimated to be 70% higher without implementing CCS [39].

The CCS is considered as an interim solution, because it is valid due to fossil fuel consumption, and the long term strategy of replacing fossil fuel with renewable energy will terminate the validity of the CCS. Therefore, initiating CCS has to be conducted in a reasonable fashion such that it does not slow down the research for renewable energy. Another concern regarding CCS is the acceleration of coal and fossil fuel consumption with the excuse of availability of CCS technology.

Sequestration of CO<sub>2</sub> at the ocean floor and also in deep underground aquifers (Figure 1.2) are some of the available options for permanent storage of CO<sub>2</sub>. The geological sequestration is considered an attractive solution because of availability of large storage capacity in the aquifers. Nevertheless, this alternative is not free from economical, social and industrial concerns.

In the last decades, the scientific community has been putting efforts into convincing the public regarding the feasibility of CO<sub>2</sub> storage operations. Social awareness is the first step in public agreement regarding the geological CO<sub>2</sub> storage. The EU has conducted a survey to assess the public awareness in 12 European states, which is published in the Eurobarometer report in May 2011. People's awareness of climate change and its causes, and their acceptance of the methods to avoid or mitigate the problems, in particular the CCS technology, was examined in the survey. The majority of European participants are either fairly or very well informed about causes and consequences of climate change. However, the awareness of the CCS among the European respondents was low. Two third of the participants in the survey have had not heard about the CCS.

The same survey suggests that the overall trust in Europe in the sources of information regarding the CCS is best in universities and other scientific institutions. Governments are investing in research, not only to move toward industrialization of the CCS, but also to make it well received by public. This highlights the importance of researching the storage of CO<sub>2</sub> and the way it is needed both for industrial and social concerns.

### 1.3 Modeling procedure

Predicting the fate of CO<sub>2</sub> storage involves identification and quantification of the relevant uncertainties and risk assessment process. The procedure starts with a geological description and continues with modeling of flow in geological formations. After constructing a deterministic flow model, the stochastic nature of the problem is analyzed by studying the variation in the model outcome due to uncertainties in the system.

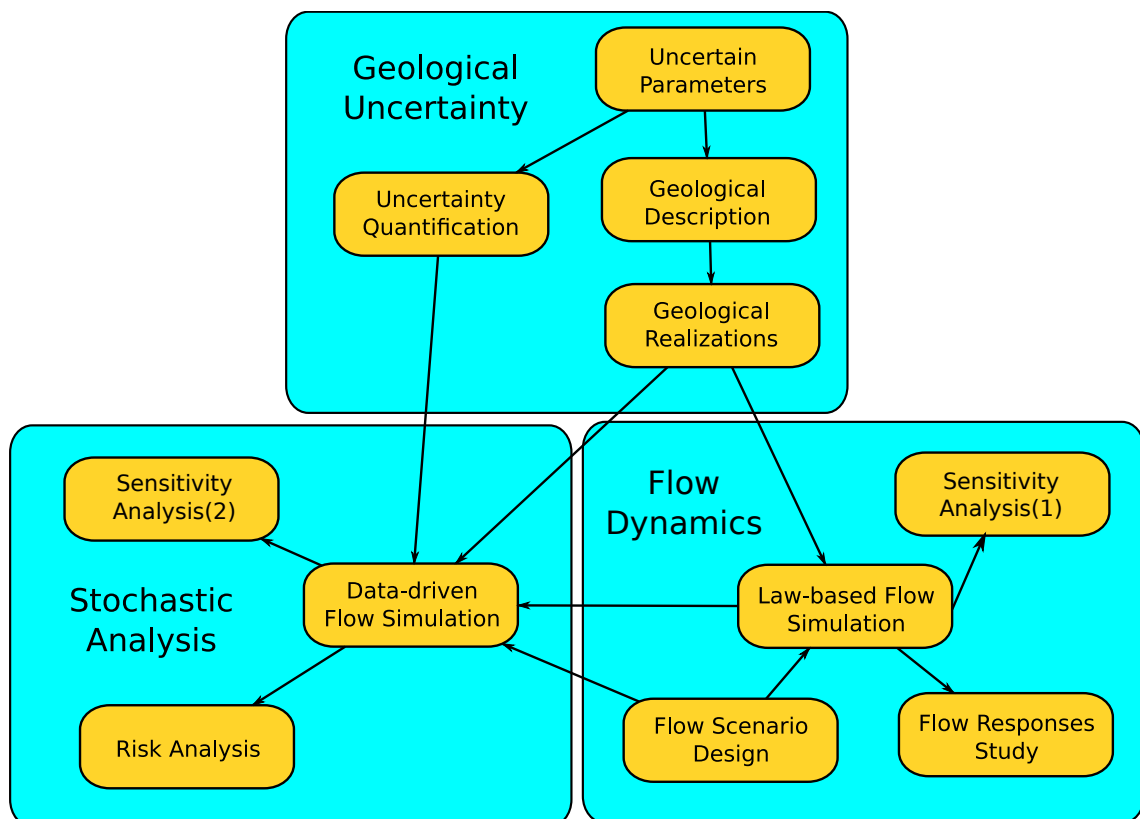


Figure 1.3: Modeling procedure diagram. The tasks are shown in yellow boxes and they fall in three main categories that are indicated by big cyan boxes. Arrows depict the flow of the procedure based on the sequence order of the tasks.

Figure 1.3 shows the modeling work-flow implemented in this thesis. The steps are categorized in three parts: geological uncertainty, flow dynamics, and stochastic analysis. The relations between the steps are plotted by arrows in the flow-chart. In this section, we briefly describe each step. More details will follow in the next sections.

**Uncertain parameters:** In the first step, we identify the uncertain parameters of the model to study their influence on the modeling outcome. It is possible that our knowledge of model sensitivity to the parameters is limited. In a conservative approach we choose a larger number of parameters and by doing a primary sensitivity analysis with a fast technique, we filter out the important parameters. Herein, the focus is on geological parameters that are determined to be the most influential source of geological uncertainty for shallow-marine environments [38].

**Uncertainty quantification:** After identification of the uncertain geological parameters, we assign a likelihood value to each of the parameters. It is hardly possible to have a unique likelihood profile that applies to every geological location. Thus, we note that probabilities of existence for an uncertain geological feature can change from place to place. The uncertainty enters the modeling in the form of parameter frequency histograms. The conventional practice is to consider an analytical distribution function to be assigned to the parameters. However, the sampling procedure normally ends in scarce frequency histograms that are difficult to fit into a unique analytical distribution function.

**Geological description:** Geological uncertainty study is normally done by series of runs to measure the sensitivity of the model to the parameter variations. Results are valid, only if the geology used in the work-flow is representative of reality. The process of geological description results in a large number of realizations to be used in the next steps of the study. Herein, we will use a set of equiprobable geological realizations of a shallow-marine reservoir.

**Flow scenario design:** Herein we define the initial and boundary conditions of the CO<sub>2</sub> injection problem. Also, we specify the injection scenarios. Simplifying physical assumptions will be taken here. Each scenario is implemented for all geological realizations.

**Law-based flow modeling:** After defining the injection problem, we simulate the flow dynamics in the available realizations. We use a two-phase flow model and a standard commercial simulator.

**Data-driven flow modeling:** Modeling the flow dynamics via formulation of physical laws normally results in complicated equations with many degrees of freedom. The computational cost of solving these equations is high, in particular for uncertainty related studies that require a large number of simulations to cover the variation in the uncertain parameters. So called data-driven methods, are mathematical functions that are specified by correlating a set of unknown flow attributes to their corresponding uncertain parameter values. These methods need to be tuned by a law-based method before employment. Because these methods are designed to be only dependent on the uncertain parameters, they are normally low in computational costs. However, they may exhibit the pitfall of not following the physical rules and in some cases produce unrealistic results.

**Flow responses study:** Once the simulation results are obtained from the flow modeling procedure, it is possible to calculate the important flow responses from simulation results. The fate of carbon storage and assessment of the operations can be inferred from these responses. Storage capacity, injection rate, and leakage risk are evaluated from flow responses. Responses include pressure distribution over time, CO<sub>2</sub> plume development, and other quantities describing the dynamics of flow.

**Sensitivity and risk analysis:** The sensitivity analysis is performed in two ways: In the first method, we use three-dimensional, two-phase flow simulations on all realizations available for demonstrating the geological variability. In the second method, we employ an approximating polynomial to perform global sensitivity analysis and stochastic uncertainty studies. Using a relatively fast data-driven method, we perform a Monte Carlo process on 10000 simulation cases.

## 1.4 Uncertainty Sources

Sources of uncertainty can exist in every part of the CO<sub>2</sub> storage modeling process. Herein, we describe each of the possible contributions to the uncertainty in the modeling within various parts.

**Uncertainty in physical modeling:** We may ignore some phenomena during the physical modeling of CO<sub>2</sub> storage that can be influential in the flow behavior. This can happen due to lack of awareness of the phenomena or by underestimating the significance of it. For example, we may ignore the heat exchange within the system, assuming that heat transfer does not play an important role in the flow performance. If some parameters in the modeling are sensitive to the heat and change by temperature variations, then the assumption to ignore heat transfer effect can introduce considerable bias in the outcome of the modeling.

**Mathematical formulation and numerical approximation:** Modeling CO<sub>2</sub> injection and migration in a realistic geological formation results in a complicated mathematical system that in most of the cases can not be solved analytically. The numerical approach to approximate the original mathematical system, normally introduces errors in the results. Mathematical analysis can help in estimating the error or its order, but it might not be doable for complicated models.

A specified physical problem can be formulated mathematically in more than one way. The choice of primary unknowns to be found can change the mathematical form and nature of the equations. Degrees of non-linearity and coupling between unknowns in the equations can vary in different formulations.

**Geological uncertainty:** The high costs of data acquisition and technical limitations introduce a huge amount of geological uncertainties in CO<sub>2</sub> storage modeling. The injected CO<sub>2</sub> may travel in a large spatial scale. Geological characterization of such a large medium is a big challenge.

**User introduced uncertainty:** These type of uncertainties are caused by the errors introduced by the user for his/her biased choice of modeling tools and interpretation of modeling results.

## 1.5 Geological modeling

The central part of a successful CO<sub>2</sub> storage modeling is to provide aquifer models that depict the geological heterogeneity in a realistic manner. This requires having an inclusive understanding about model sensitivity with respect to different geological parameters and quantifications of geological uncertainty and its impact on the process.

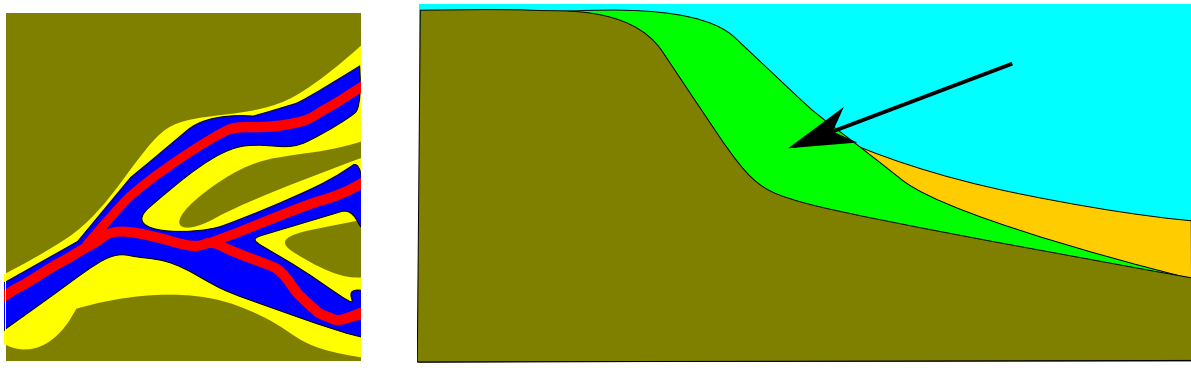
The conventional practice of geological modeling includes using geostatistical models. It is possible that two different heterogeneity patterns produce the same geostatistical model, as discussed by Caers [12]. Therefore, a geostatistical model does not represent a unique reservoir image and if we do not include additive information in the process, we may end-up with an unrealistic heterogeneity texture[12, 19]. The primary attention in our work has been on this issue and to provide a more realistic way of geological uncertainty analysis for CO<sub>2</sub> sequestration by including information of geological features and textures in the process.

### 1.5.1 Geological description

Geological storage of CO<sub>2</sub> requires large accommodation of subsurface volumes. Only sedimentary basins, which hold relative large pore volumes, are generally suitable for this mean. However, not all sedimentary basins are similarly appropriate for CO<sub>2</sub> sequestration.

Convergent basins along active tectonic areas pose a higher risk of CO<sub>2</sub> leakage due to volcanism, earthquakes, and active faults. Divergent basins located on the stable lithosphere are much less prone to earthquakes or other catastrophic event that can lead to accidental release of large CO<sub>2</sub> quantities. Therefore, specific considerations must be done in selecting site locations with respect to security of subsurface storage.

Sedimentary basins are composed of various lithological facies. Stratigraphic architecture and sand-body geometry control the capacity and effectiveness of CO<sub>2</sub> sequestration. As a result of various tectonic depositional and erosional process, low and high permeability rocks are accumulated on top of each other and can form stratigraphic flow-path leading to various directions and speed of subsurface flow. Three types of formations can be characterized as aquifers, aquitards, and aquiclude.



(a) Fluvial depositional system.

(b) Beach depositional system.

Figure 1.4: Schematic plots of heterogeneities in fluvial and beach depositions. The top view is illustrated in Figure (a) and Figure (b) shows the side view. The arrow in Figure (b) shows that the deposition mass is less heterogeneous than the fluvial systems.

Aquifers are high permeability strata that provide major beddings for flow transport. Good rock quality in continuous sandbodies allow for efficient CO<sub>2</sub> storage in an acceptable capacity volumes. Aquitards are made of low permeability strata that provide beddings with orders of magnitude slower flow than aquifers. Layers of aquifers and aquitards are formed by thick accumulation of sediments that undergo burial, compaction, lithification, and uplift over millions of years. They can be covered by aquiclude, which are evaporative beds that are impervious to fluid flow. Typical seal rocks include, from most ductile to most brittle: salt, anhydrite, krogen-rich shales, dense mudstone, tightly cemented sandstones, anhydrite-filled dolomite, carbonate, or silica-cemented sandstones, and cherts.

Aquifer pressure is normally close to hydrostatic, because the conductivity within the medium allows for pressure equilibrium over long time. High pressurized compartments can exist in highly sealed structures. The pressure of the sedimentary basin has a significant impact on its suitability for CO<sub>2</sub> storage [5]. Trapping mechanism for CO<sub>2</sub> can happen due to stratigraphic or structural traps. Stratigraphic trapping is primarily controlled by the geometry of depositional facies and sand body continuity. These factors control the permeability distribution within the medium that controls the efficiency of injection and storage of CO<sub>2</sub>. Structural heterogeneity factors include faults, folds, and fracture intensity. The dip angle of formation layers control the buoyancy forces that govern CO<sub>2</sub> plume migration along the conductive layers. Fractures can enhance the mobility of the plume and sealing faults can provide structural traps for long-term CO<sub>2</sub> storage. Anticline structures can also be permanent traps for stored CO<sub>2</sub>.

Depositional environment varies from fluvial to marine systems. The texture and degree of sandiness of beach deposits are functions of the shore profile, typically consisting of a gently sloping formation layering in a transition from near shore to deep offshore. Deposits range from sandy, coarse grain structure near the shore, to muddy, burrowed, fine grained sand in the lower offshore. High energy near the shore that is a result of interplay between wave, fluvial, and tidal forces, filters out the larger grains in the deposition.

Therefore, formations closer to the shore contain large continuous sand bodies that have good quality rock. This is the reason for shallow-marine systems to be appropriate traps for hydrocarbons and analogously, good candidates for CO<sub>2</sub> storage.

The beach facies normally are homogeneous rocks with internal heterogeneity due to tidal systems. In contrast, mixed-load fluvial deposits that contain both mud and sand are more heterogeneous than beach systems. The presence of numerous mud drapes as a result of periodic floods, serves as barriers to fluid flow. Heterogeneity in the fluvial systems exist on multiple scales, from small-scale variations of rock type near the river bed, to the large-scale heterogeneity in fluvial channel-fill sandstones and over-bank deposits. Heterogeneity also occurs within these systems in the form of muddy abandoned channel-fill deposits.

In theory, we prefer a medium that allows for more lateral movement to overcome the buoyancy bypassing of the flow. Heterogeneity in the vertical direction, such as shale inter-bed barriers can serve for enhancing the lateral flow and disperse the flow in the lateral direction. Structural heterogeneities can have a similar impact. In addition, splitting a large plume into smaller plumes lowers the risk of leakage of huge CO<sub>2</sub> amounts via potential breakings in the integrity of the sealing barriers or abandoned wells.

CO<sub>2</sub> injectivity is related to sequestration capacity and effectiveness, and can be defined by the conductive cross-sectional area. Stratigraphic factors that enhance injectivity are high permeability and injection interval thickness. In addition, the lateral permeability architecture can influence the injectivity quality. The lower the injectivity is, the higher will be the pressure buildup in the medium due to injection.

Over the last two decades, there have been a large number of studies concerning the subsurface storage of CO<sub>2</sub>. Several authors investigate the efficiency of geological CO<sub>2</sub> storage based on regional data in a specific site location. A case study from the Texas Gulf Coast [37] investigates the sequestration capacity and efficiency in accordance to the geological heterogeneity. The study performs a site-scale assessment of brine aquifers for geological CO<sub>2</sub> sequestration. Injection is considered in the Frio formation which is a sandstone-rich, high quality rock, overlain by thick, regionally extensive shale in the upper Texas Gulf Coast. Migration of CO<sub>2</sub> during injection (20 years), and post-injection (40 years) is studied in different geological realizations. The heterogeneity represented by stochastic modeling of geological sediments. Structural heterogeneity is modeled by layers dip angle and faults at different locations. Six models are made based on regional available geological information. The study shows that in a homogeneous rock volume, CO<sub>2</sub> flow paths are dominated by buoyancy, bypassing much of the lateral rock volume. If the permeable rock is inter-bedded with multiple low permeability layers, the flow paths are dispersed, enhancing the lateral movements of CO<sub>2</sub> and allowing for larger percentage of contact with rock volume. The study suggests that dip angle enhances buoyancy forces and decreases storage capacity, while compartmentalization by faulting appears to increase sequestration capacity at the cost of increased pressure, and consequently, increased risk of CO<sub>2</sub> leakage.

A number of pilot sites are established worldwide to test the large-scale injection of CO<sub>2</sub> in the subsurface formation. The In Salah project [60] in Algeria is an industrial-scale injection project into a fracture-influenced, matrix-dominated sandstone formation. The reservoir matrix comprises tidal deltaic sandstone. The project benefits from relatively high level of data acquisition: wireline and LWD well logs, image logs and production and geophysical monitoring [60]. In addition, the most valuable monitoring method has been the use of satellite airborne radar above the injection well. Also, chemical tracers are used in the injected CO<sub>2</sub> to differentiate the natural CO<sub>2</sub> in place from the injected volumes, when the CO<sub>2</sub> breaks through other wells. The detailed analysis highlights the geological controls on the movement and dispersion of CO<sub>2</sub> plumes. The injection is performed via a horizontal well perpendicular to the geomechanical stress field and the faults present in the domain. This, along with the fracture network, enhance the plume migration, which is about three times faster than the flow in a homogeneous domain. Results from In Salah illustrate the value of reducing geological uncertainty by employing sufficient logging tools and monitoring techniques.

The CO<sub>2</sub>-SINK project at Ketzin Germany [28] is another pilot site for practicing subsurface CO<sub>2</sub> injection. The injection is performed in the Stuttgart formation that is geologically heterogeneous within an anticline structure. The Stuttgart formation is made of sandy channel facies of good rock quality alternate with muddy flood-plain-facies. A thick cap-rock section covers the Stuttgart formation.

Practically, including all details of every scale into a flow simulation model is impossible. Various simplifications have been made to account for heterogeneities in modeling. Some earlier studies consider two dimensional modeling, with homogeneous or geostatistically populated permeabilities. The study in [45] simulates an escape rate of CO<sub>2</sub> in a homogeneous medium similar to Utsira formation in Norway. By changing the horizontal permeability, they demonstrate that most of the injected CO<sub>2</sub> volume accumulates in a fine layer beneath the cap-rock due to buoyancy forces in the long-term CO<sub>2</sub> migration process. However, this study assumes no vertical heterogeneities. A layered heterogeneity

is examined in [68]. They used a log normal distribution of permeability in a simplified two dimensional grid to account for viscous and gravity forces. Results suggest that the sweep efficiency of CO<sub>2</sub> in the porous medium is low, and heterogeneity, in particular the vertical transmissibility, can have a big impact on the storage efficiency.

To examine the impact that the geological heterogeneity degree can have on the CO<sub>2</sub> sequestration modeling, [26] constructed a suite of three-dimensional simulation models, with varying net to gross ratios. A radial variogram, with a shale length of 300 m, was used to populate five models of varying degrees of net-sand-to-gross-shale ratios. The models were up-scaled, using flow-based methods, to make the computation feasible. The study concludes that formations containing shale barriers are effective in containing an injected CO<sub>2</sub> plume within the formation and that heterogeneity serves to limit the reliance of the formation seal as the only mechanism for containment.

## 1.5.2 Geological parameters

From the flow modeling perspective, sources of geological uncertainty can manifest themselves in the rock parameters, such as permeability and porosity, that go in the flow equation. However, to represent the geological uncertainty, it is not enough to randomize these parameters. This approach might work in simple geological models, but it can fail to give plausible results for the realistic heterogeneous problems with uncertain structural and depositional descriptions.

In response to the EU priorities of reducing time to first oil and of improving overall hydrocarbon recovery efficiency, the interdisciplinary SAIGUP study was initiated to increase the understanding of the influence of geological uncertainties in oil field recoveries. SAIGUP stands for 'sensitivity analysis of the impact of geological uncertainties on production forecasting in clastic hydrocarbon reservoirs'. The context in SAIGUP is defined for shallow-marine depositional systems. The main objective of the SAIGUP project has been to perform a quantitative sensitivity analysis to measure the impact of sedimentological and structural variations within geological descriptions on oilfield recovery estimates [38, 47, 48]. Herein, we will use six different rock types to investigate the impact of geological heterogeneities on CO<sub>2</sub> sequestration. The rock properties within each facies are populated based on real data. Variations are considered in a horizontal-vertical matrix in three levels of heterogeneities, low, medium, and high, as illustrated in Figure 1.5. The design focused on special considerations; for example, making complex enough heterogeneities to be a plausible representative of realistic models, and producing large enough number of realizations with sufficient overlapping to be able to perform a quantitative sensitivity analysis.

Sedimentological variability is modeled in small and large scales and combined to provide realistic variations of reservoir heterogeneities. All models are considered in a progradational sedimentary environment. A regular grid is used for all of the realizations in two gridding resolutions, fine and coarse, and the total bulk volume is the same in all cases. Each geological realization contains about 1.5 million cells in the fine model. Figure 1.6 shows the fine grid model for a selected realization with medium level of heterogeneity. A major fault in the model breaks the structure and makes large vertical depth difference in the two parts of the model (from about 1500 m to 3000 m). Thickness of the model is much smaller than these depth differences. To make it easier to see the property variations on the grid in the vertical direction, we map the properties on a flat uniform geometry (Figure 1.7).

Figure 1.8 shows the spatial distribution of the six modelled facies in the selected realization, and Figure 1.9 shows the histogram of lateral transmissibility within each facies in the logarithmic scale. Each facies is modeled separately in some levels of upscaling starting from the lamina scales, before populating on the fine grid. Flow based upscaling techniques are used, and the suitability of the methods depends on the balance of forces. When the medium is conductive due to high permeability, the viscous dominated steady state method is used. In the rocks with lower transmissibility where the capillary forces are dominant, the capillary equilibrium is assumed [47].

On the last step, the fine populated grid is mapped on to the coarse grid that is to be used for the flow solver. Since the grid size in the fine model is too expensive computationally for flow simulations,

Table 1.1: Grid specifications for fine and coarse scales in the SAIGUP modeling process.

Parameter	Fine Scale	Coarse Scale
Number of cells in the x direction	80	40
Number of cells in the y direction	240	120
Number of cells in the z direction	80	20
Number of total cells	1,500,000	96,000
Number of active cells	1,500,000	79,000
Model x dimension	<i>3 km</i>	<i>3 km</i>
Model y dimension	<i>9 km</i>	<i>9 km</i>
Model z dimension	<i>80 m</i>	<i>80 m</i>

the lateral dimension is doubled in each cell while every four layers are lumped into one layer in the vertical direction. Figure 1.10 shows the top view of lateral transmissibility in logarithmic scale for four consecutive layers of a selected case, and their corresponding upscaled layer in the coarse grid. Table 1.1 shows the grid specifications in the coarse and fine SAIGUP models.

A detailed discussion about the upscaling of the sedimentological and structural parameters for SAIGUP simulation models can be found at [47].

Structural aspects are modeled via fault modeling. Within the SAIGIP setup, faults are considered with different levels of intensity, orientation, and transmissibility. The orientations may vary in both lateral directions, and we consider a grid that contains faults in both directions (Figure 1.11).

Although these models were designed to study the impact of geological heterogeneity on oil recovery, they may also be used to model a scenario in which CO<sub>2</sub> is injected into an abandoned reservoir. Therefore, we have selected five parameters from the setup and varied these parameters by combining different levels for our CO<sub>2</sub> storage study. These features are lobosity, barriers, aggradation angle, progradation, and fault. In the following, we describe each feature briefly.

**Lobosity:** Lobosity is a metric for describing the interplay between fluvial and wave processes in a shallow-marine depositional system. As a river enters the mouth of the sea, the shore-line shapes where the river flux crashes with the waves from sea. The balance between the sediment supply from rivers and the available accommodation space in the shallow sea defines the shore-line shape. Sea waves smear out the shore-line, while fluvial flux from river makes branches into the sea. Less wave effect produces more pronounced lobe shapes around the river entrance into the sea.

The channels made into the sea mouth by fluvial supplies contain good quality rocks with relatively higher porosity and permeability. Poor quality rock types are located between the conductive branches. Reservoir quality decreases with distance from the shore-face. Lobosity variation can influence the CO<sub>2</sub> injection operation and plume distribution in the aquifer. In this study, models of three levels of lobosity are used: flat shoreline, one lobe and two lobes, see Fig. 1.12.

**Barriers:** Barriers are mud-draped surfaces sitting between reservoir sections that are caused by periodic floods in a shallow-marine depositional system. Mud-drapes extend in both vertical and lateral directions and are potential significant barriers to flow. In the SAIGUP domain used here, these barriers were modeled by defining areas between layers with zero transmissibility multipliers. This areal coverage was designed in three levels: low (10%), medium (50%), and high (90%). We use the same variations in this study, see Fig. 1.13.

**Aggradation angle:** In shallow-marine systems, the sediment supply from rivers deposits in a spectrum of large size grains in the land side toward fine grains deep in the basin. Amount of deposition supplied by the river compared to the accommodation space that the sea provides defines the transition of different rock-types between the river and the sea. If the river flux or sea level fluctuates, the equilibrium changes into a new bedding shape based on the balance of these factors.

When the river flux increases, it shifts the whole depositional system into the sea causing an angle

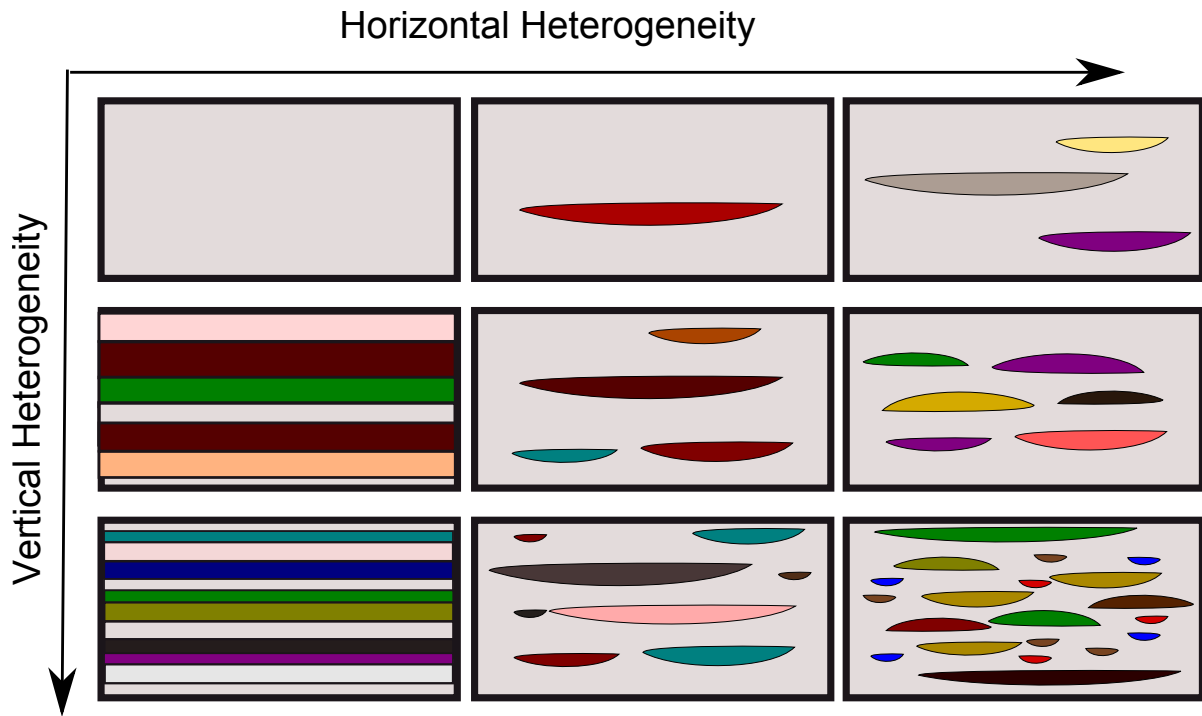


Figure 1.5: Stratigraphic heterogeneity levels in lateral and vertical directions. Arrows direction indicates the increase in the heterogeneity level. Modified from [47].

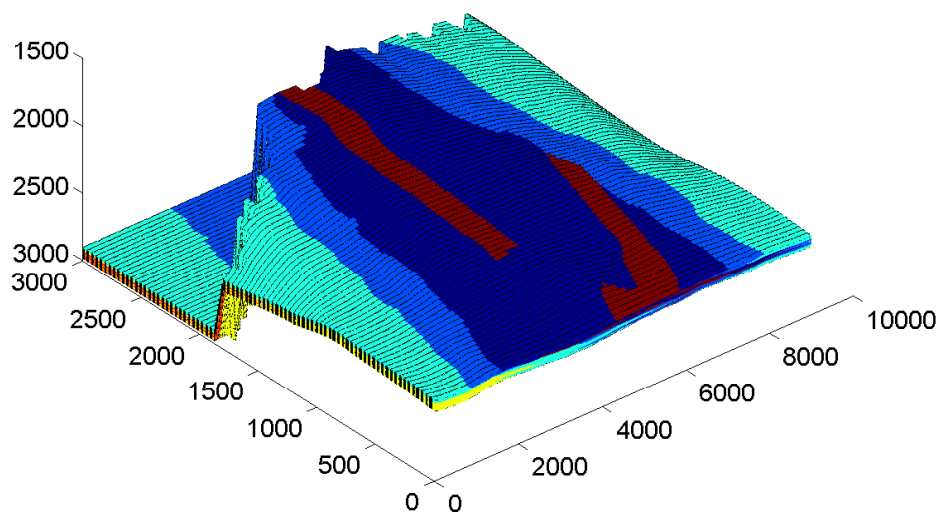


Figure 1.6: Fine grid perspective view. Colors depict rock types; see Figures 1.7 and 1.8. The geological structure is divided in two parts due to a faulting process. The eleveated part is considered in the study.

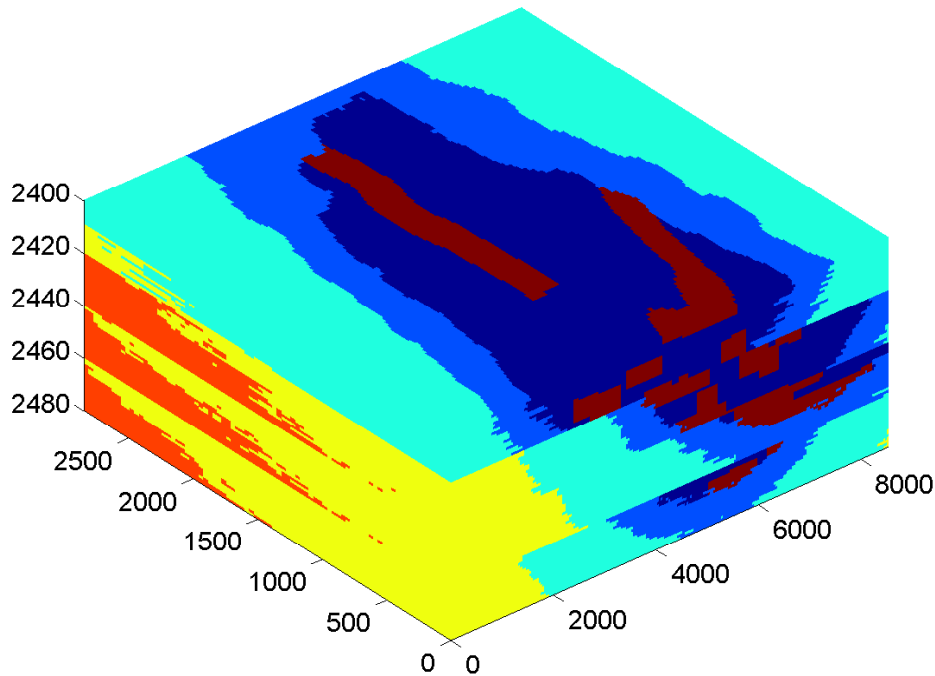


Figure 1.7: Perspective view of the rock type variations for a selected case mapped on a uniform grid.

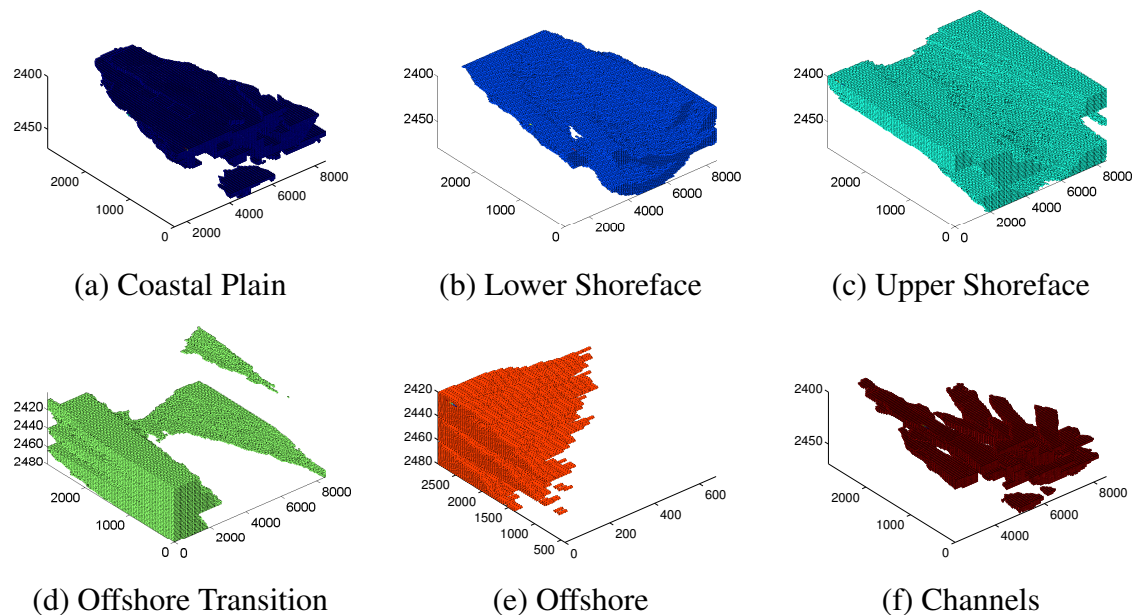


Figure 1.8: Six different rock types used in modeling the stratigraphic heterogeneities. Compare with Figure 1.7

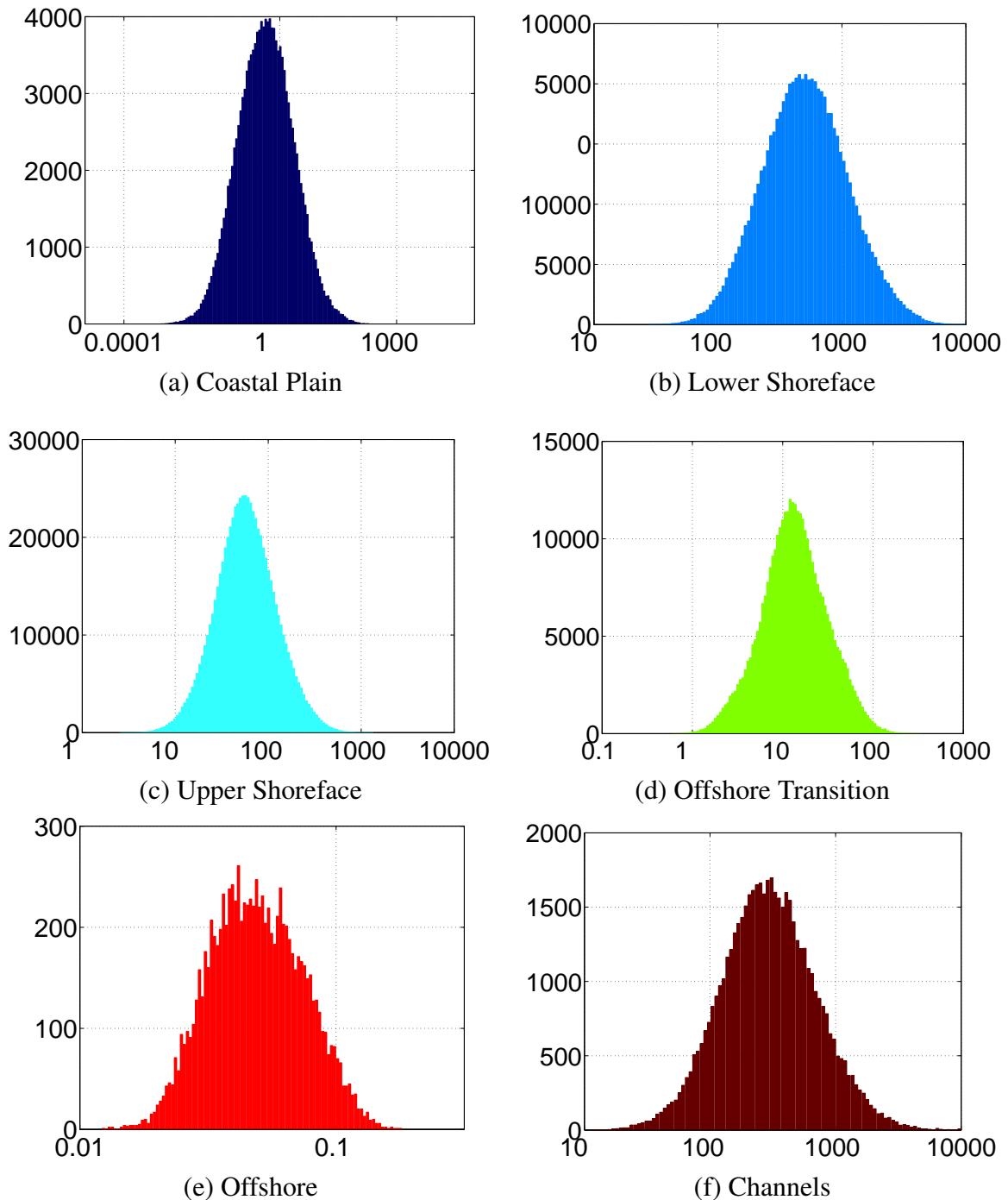


Figure 1.9: Histogram of lateral transmissibility for different facies in a selected case. Scales are logarithmic in units  $\text{cP} \cdot \text{m}^3/\text{day}/\text{bar}$ . Only the x-axis is logarithmic.

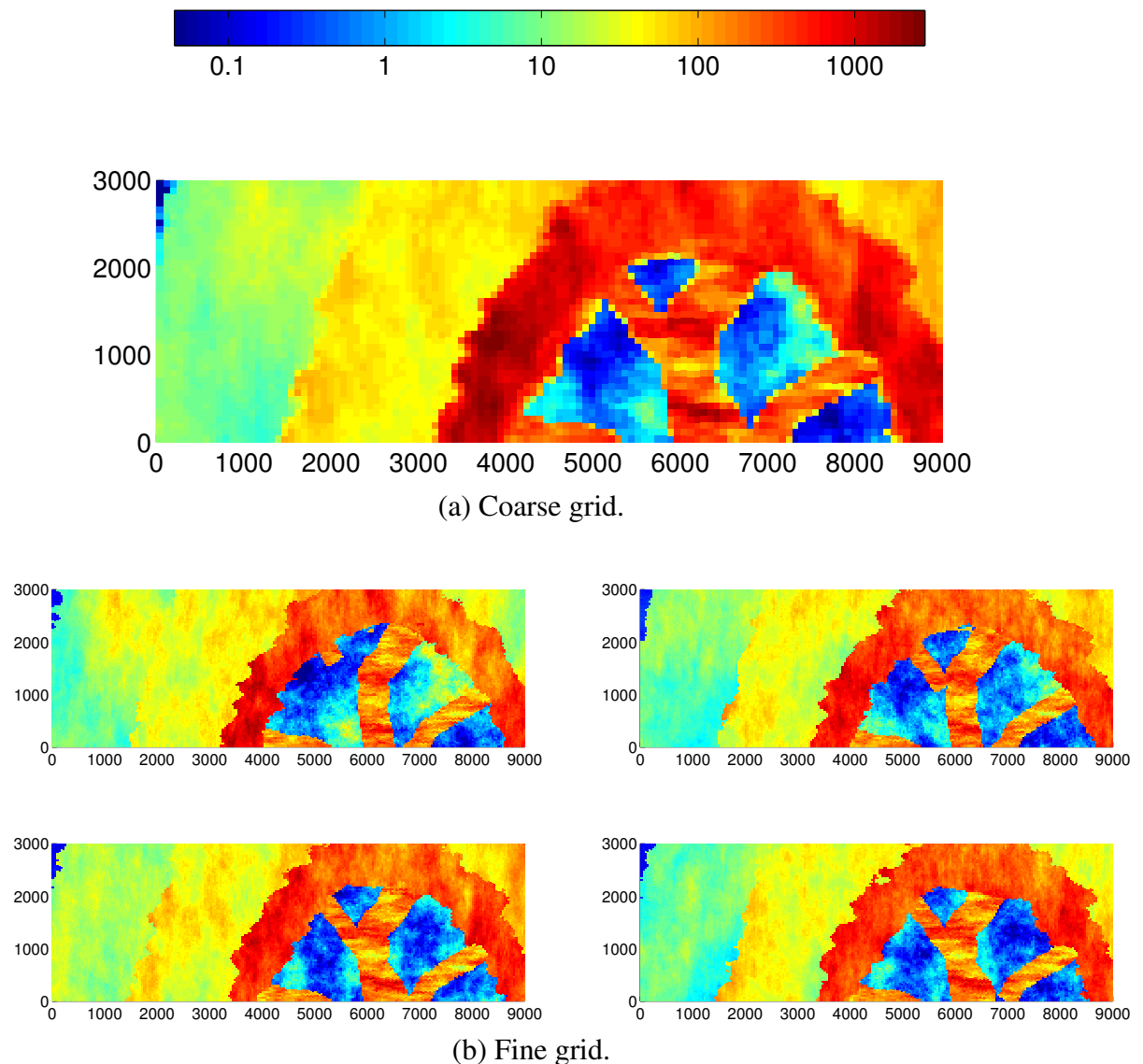


Figure 1.10: Logarithmic of lateral transmissibility plotted for four layers in fine grid versus their representative layer in the coarse grid. The top view is plotted in all figures and units are  $\text{cP} \cdot \text{m}^3/\text{day}/\text{bar}$ .

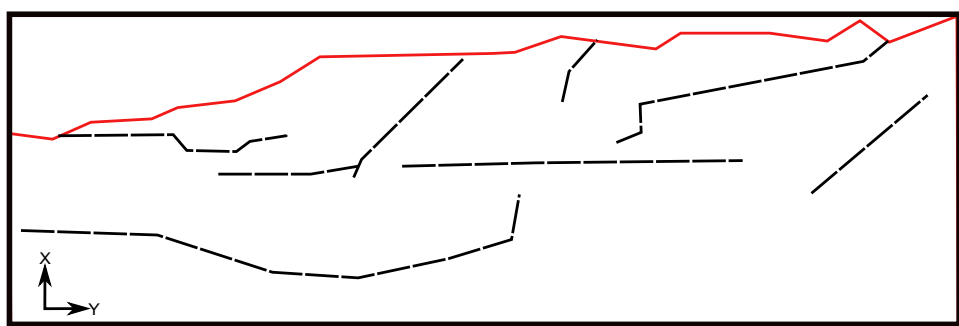


Figure 1.11: Top view illustration of faults used in the faulted grids. The fault plotted in red divides the medium in two parts (compare with Figure 1.6) and only the part below the red line in the top view is considered in the study.

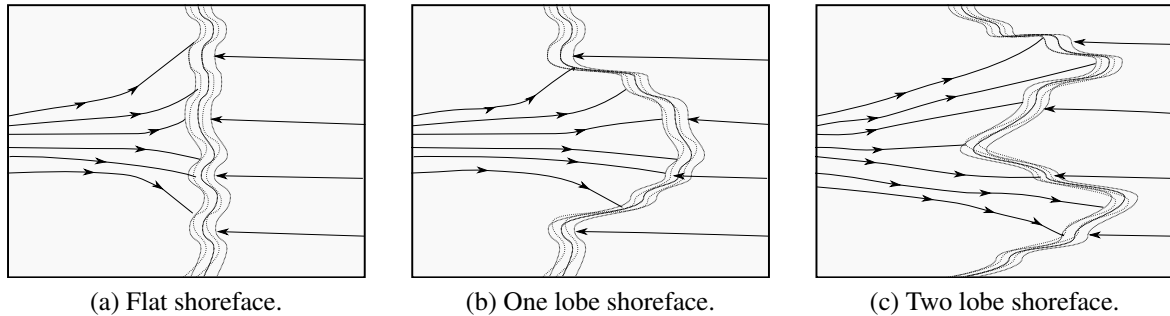


Figure 1.12: Lobosity levels are defined based on the shoreline shape, which is caused by the interplay between fluvial and wave forces. From Figure (a) to (c) the system changes from wave to fluvial dominated.

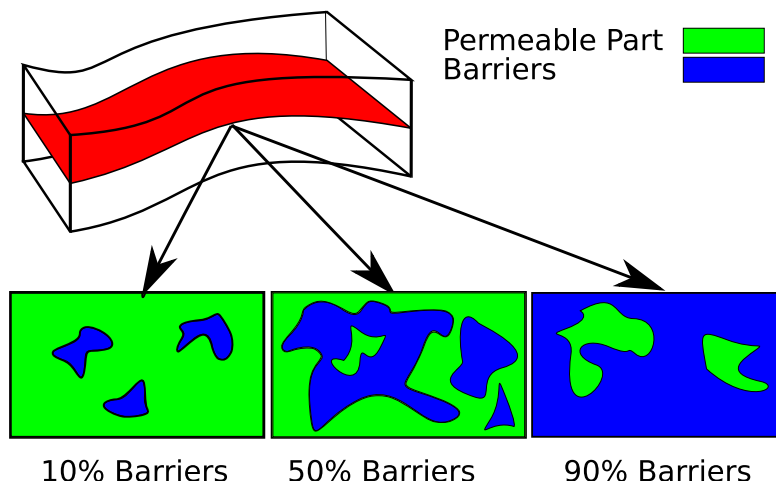


Figure 1.13: Periodic floods and fluctuations in fluvial system can result in shale draped surfaces. These surfaces act as barriers to flow in both vertical and horizontal directions. The barriers are modeled in the SAIGUP study by modifying the transmissibility of cells across the barrier (red surface in the plot). Barrier level variations are specified by areal coverage of zero transmissibility multipliers (indicated by blue color).

between transitional deposits that are stacked on each other because of this shifting. This angle is called aggradation angle. Three levels of aggradation are modeled here: low, medium and high (Fig. 1.14). As we will see later, aggradation can have a major role in influencing the CO<sub>2</sub> flow direction in the medium.

**Progradation:** Progradation is the depositional-dip direction between sea and river. Two types are considered here: up and down the dominant structural dip. Progradation combined with lobosity can influence the plume development in the medium, as the injected CO<sub>2</sub> plume migrates upward to the crest goes through heterogeneities (Fig. 1.15).

For more information about the geological modeling, see the special issue of the Petroleum Geosciences that is devoted to the SAIGUP study [48]. One selected realization of the SAIGUP models is available for download [65] and this model is used as an example in MATLAB Reservoir Simulation Toolbox (MRST) [66].

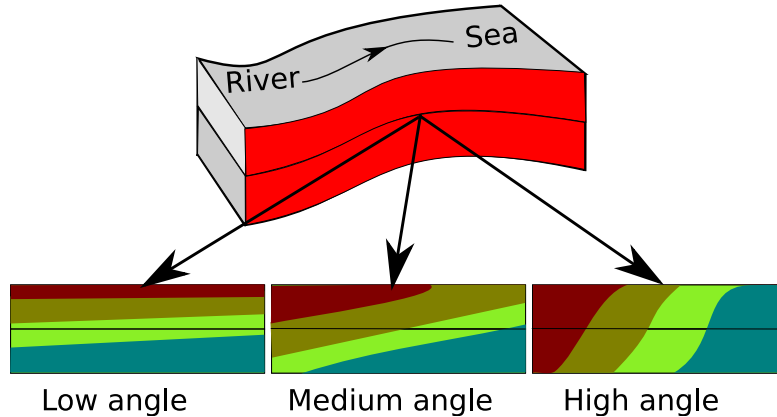


Figure 1.14: The change in the fluvial flux results in a shift in the depositional rock types from the river to the sea. The shift varies from very extensive in amount resulting in near horizontal layers of facies stacked on top of each other (low aggradation angles) to slight shifts resulting in near vertical rock type patterns (high aggradation angles).

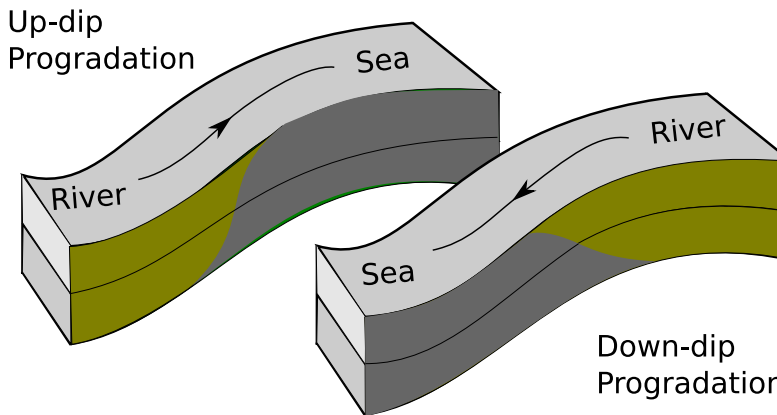


Figure 1.15: Tectonic activities in shallow marine systems can result in various orientations of river to sea depositions that is considered as progradation direction in the SAIGUP study.

## 1.6 Flow equations

After introducing the parameters that make our geological model, we need to define the flow problem. In this section we discuss various formulations of the governing equations describing single and two phase flow in porous medium. Solution to this type of equations is implemented in the ECLIPSE black-oil simulator that we use to model the flow. We introduce the functionalities and axillary equations required to close the flow equation system. This section also includes a brief mathematical discussion on the flow equations. We discuss various flow regimes in the medium in the next section.

### 1.6.1 Single phase flow

Assume a porous domain  $\Omega$  with boundary  $\Gamma$  as shown in Figure 1.16. We write the continuity equation in general form for a single phase flowing in the domain:

$$\text{Accumulation} + \text{In-Out Flux} = \text{Source/Sink} \quad (1.1)$$

$$\frac{d}{dt} \int_{\Omega} \phi \rho d\tau + \int_{\Gamma} \rho v \cdot n d\sigma = \int_{\Omega} q d\tau \quad (1.2)$$

In Equation 1.2,  $\phi$  is the rock porosity,  $\rho$  is the fluid density,  $v$  is the Darcy flux, and  $n$  is the normal vector to the boundary. The term  $q$  denotes the mass source or sink in the system. Integrations are taken over arbitrary domain  $\Omega$  with boundary  $\Gamma$  (Figure 1.16). Flow velocity is considered at the representative elementary volume (REV) scale for porous media [7].

The resistance of a porous medium against flow results in a velocity that can be calculated from pressure and gravity gradient and fluid properties in the medium. This is governed by Darcy's law for incompressible single phase flow:

$$v = -\frac{K\rho g}{\mu} \cdot \nabla \left( \frac{P}{\rho g} + Z \right). \quad (1.3)$$

In Equation 1.3,  $K$  is the permeability of the medium.  $Z$  is the elevation in vertical direction and  $g$  is the gravitational acceleration. Here, we assume that the third coordinate axis aligns with the vertical direction; otherwise the equation should be modified to honor the gravitational acceleration vector projection on the coordinate axes (see [13]). Permeability is a function of pore size distribution and connectivity and in the macro scale, it is a measure of medium conductivity when a fluid is flowing through the medium (Figure 1.17). In general, density varies with pressure and Darcy equation takes the following form:

$$v = -\frac{K}{\mu} \cdot (\nabla P + \rho g \nabla Z). \quad (1.4)$$

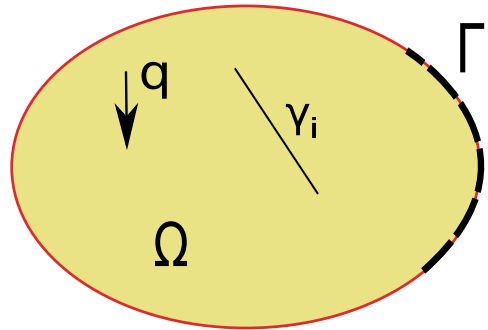


Figure 1.16: The flow problem is solved over domain  $\Omega$  that is bounded by  $\Gamma_i$ . The injection well is modeled as source point  $q$ . Geological heterogeneities can be in the form of discontinuity  $\gamma_i$ .

Substituting  $v$  from Equation 1.4 into Equation 1.2 gives:

$$\frac{d}{dt} \int_{\Omega} \phi \rho d\tau - \int_{\Gamma} \rho \left( \frac{K}{\mu} \cdot (\nabla P + \rho g \nabla Z) \right) \cdot n d\sigma = \int_{\Omega} q d\tau. \quad (1.5)$$

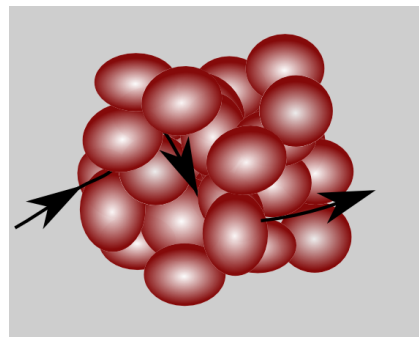


Figure 1.17: Permeability is an indication of how easy it is for the fluids to flow through the medium.

As a primary unknown in Equation 1.5, the pressure depends upon the boundary conditions (as the second term in the left hand side of Equation 1.5 is an integration over the boundaries of the domain). Also, any geological discontinuities in the medium ( $\gamma_i$  in Figure 1.16) appears in Equation 1.5 through the  $K$  tensor and can influence pressure behavior in the domain.

We assume that  $(\phi\rho)$  satisfies the Leibniz integration rule conditions. Then, the derivative in the first term of Equation 1.2 can enter the integral. The second term in Equation 1.2 can be converted into an integration over domain  $\Omega$ , using divergence theorem resulting in the following:

$$\int_{\Omega} \left[ \frac{\partial}{\partial t} (\phi\rho) + \nabla \cdot (\rho v) \right] d\tau = \int_{\Omega} q d\tau. \quad (1.6)$$

Equation 1.6 is valid for arbitrary domain  $\Omega$ , hence the equality is valid for the integrands *almost everywhere* in domain  $\Omega$  in the *general* situation:

$$\frac{\partial}{\partial t} (\phi\rho) + \nabla \cdot (\rho v) = q. \quad (1.7)$$

Fluid and rock change in volume with pressure variations. These dependencies are defined by a parameter called total compressibility, which is approximated by a combination of rock and fluid compressibilities:

$$C_T \approx C_{rock} + C_{fluid}, \quad (1.8)$$

where

$$C_{rock} = \frac{\partial \phi}{\partial P}, \quad (1.9)$$

and

$$C_{fluid} = \frac{1}{\rho} \frac{\partial \rho}{\partial P}. \quad (1.10)$$

In Equation 1.9,  $C_{rock}$  can be assumed constant in moderate pressure changes depicting a linear relation between pressure and porosity. Assuming slight compression gives [62]:

$$\rho \simeq \rho_0 + C_{fluid} \rho_0 (P - P_0). \quad (1.11)$$

By substituting from Equations 1.8, 1.10, 1.9, and Equation 1.4 into Equation 1.7, assuming the spatial density variation to be zero (i.e.,  $\nabla\rho = 0$ ), and by defining volumetric source/sink  $\eta$ , we have the single-phase diffusivity equation:

$$C_T \frac{\partial P}{\partial t} - \nabla \cdot \left[ \frac{K}{\mu} (\nabla P - \rho g \nabla Z) \right] = \eta. \quad (1.12)$$

## 1.6.2 Two-phase flow

In a two-phase flow of CO<sub>2</sub> and water within porous media, interactions between phases lead to loss of energy. This introduces specific phenomena occurring in the pore scale that have impact on the macro scale flow performance. More complicated equations appear in modeling the two-phase flow compared to the single-phase problem. First, we describe some of the conceptual two-phase phenomena in the pore scale and then we will continue by deriving the flow equations for two phases in the system, i.e., CO<sub>2</sub> and water.

When CO<sub>2</sub> and water get in contact at the pore scale, an interface forms between them such that the energy in the system is minimized. Water and CO<sub>2</sub> are also in contact with the porous medium and the interface between them forms an angle from the solid phase in the water phase (shown by  $\theta$  in Figure 1.18) that depends on their ability for wetting the rock. This is called wettability and the phase with the preference of wetting the solid phase is called the wetting phase. The other phase is called the non-wetting phase. Conventionally,  $\theta$  is measured inside the denser fluid. If  $\theta < \frac{\pi}{2}$  then the denser phase is the wetting phase. Wettability in a porous medium depends on the fluids and the rock. It can have

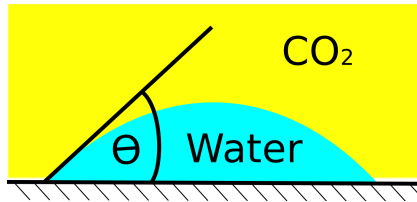


Figure 1.18: In a multiphase system, phases wet the medium with different degrees of preference. Wettability is defined by the angle between two phases' interface and the solid surface ( $\Theta$ ). The wetting phase makes an acute angle with the solid phase. Water is the wetting phase in this example.

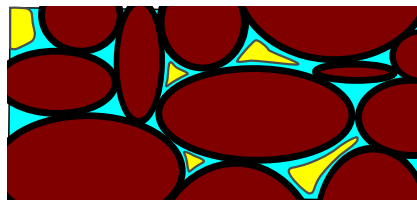


Figure 1.19: The  $\text{CO}_2$  (yellow parts) is the non-wetting phase and it flows through the water (blue parts) that wets the rock grains (brown parts) easier than  $\text{CO}_2$ . The cross section of the medium is illustrated here.

a significant influence in the phase displacement within the medium. For water- $\text{CO}_2$  system, normally water is the wetting phase.

At very low water saturations, the water phase forms molecular films surrounding the rock grains. In this situation, the water phase is immobile and can not make a continuous phase moving through the porous medium. As water saturation in the medium increases, the layers covering the rock grains grow in size until the saturation exceeds the critical level, above which the water phase is able to flow in the medium. This saturation is called the critical or connate water saturation. In a water-wet rock, once the critical water saturation is reached (for example, during the first deposition of sediments), it can not go below that level by being displaced via a non-wetting phase. Therefore, when we inject  $\text{CO}_2$  into an aquifer, there will always be some residual water saturation in the regions invaded by  $\text{CO}_2$ .

As a non-wetting phase,  $\text{CO}_2$  flows in the middle part of the pore space as shown in Figure 1.19. If  $\text{CO}_2$  saturation decreases in the medium, it reaches a critical level under which it can not make a continuous phase flowing through the pore-network. Tiny drops of  $\text{CO}_2$  are trapped in the middle of the pore space and only very large pressure difference across the pore can move them out of the pore. This level of  $\text{CO}_2$  saturation is called the residual saturation. Higher residual saturation is more interesting for the purpose of immobilizing more volumes of injected  $\text{CO}_2$  in the aquifer, which reduces the risk of  $\text{CO}_2$  leaking through any breakings in the geological formation and channeling toward surface.

Relative ease for the phase to flow within the medium is described by the relative permeability parameter. Relative permeability is a function of wettability and phase saturation. High phase saturation indicates a higher space available for the phase to flow through that space. A sample of  $\text{CO}_2$ -water relative permeability functions are shown in Figure 1.20. A library of relative permeability curves for  $\text{CO}_2$ -water system for various rock-types is available at [8].

The difference in surface tension between water and  $\text{CO}_2$  causes a pressure acting on the interface of the two fluids. This pressure is called capillary pressure. In addition, capillary pressure depends on the geometry of pores. Since the pore geometry is very irregular, it is more convenient to use simpler geometry to derive the concept of capillary pressure. Therefore, experimental work in the laboratory is required to specify the capillary pressure functionality in a special case.

Assuming a geometry of pipe to represent a pore structure, after balancing the forces in the pore-system capillary pressure can be written in the following form:

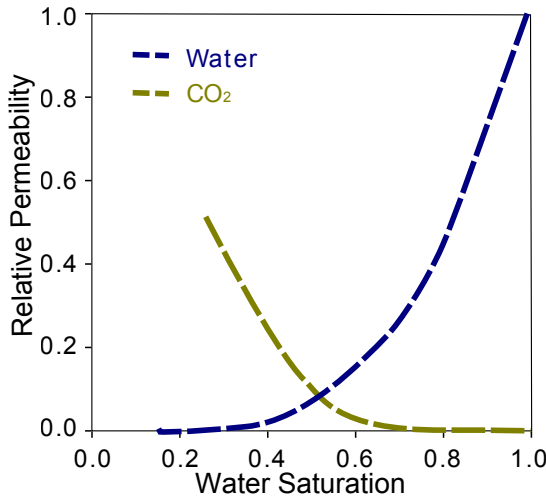


Figure 1.20: Relative permeability is an indication of how easy it is for the two phases to flow together through the medium. Relative permeability depends on the wettability of phases and the relative volumes occupied by each phase (phase saturation).

$$P_c = \frac{2\sigma}{r} \cos\theta, \quad (1.13)$$

where  $\sigma$  is the interfacial tension,  $\theta$  is the angle between the interface and the solid phase, and  $r$  is the radius of the pore.

Capillary pressure is a jump in phase pressure across the interface of the two phases. Therefore, we can relate it to the phase pressures:

$$P_c = P_{nw} - P_w. \quad (1.14)$$

Here,  $P_{nw}$  is the non-wetting phase pressure and  $P_w$  is the wetting phase pressure.

Capillary pressure can be expressed in an empirical relation as a function of wetting phase saturation. Lower capillary pressure is expected for higher wetting saturation, and capillary pressure value goes up for lower wetting saturation (Figure 1.21).

Assume hydrostatic equilibrium for a porous domain in which water and CO<sub>2</sub> are segregated due to buoyancy effect. If capillary forces are considerable in the domain, the sharp interface between water and CO<sub>2</sub> in the macro scale will be replaced by a transition zone with a spectrum of saturations between phases (Figure 1.23). Due to the hydrostatic equilibrium, phase pressure at each depth can be related to the hydrostatic pressure of that phase:

$$P_w = \rho_w g z, \quad (1.15)$$

$$P_{CO_2} = \rho_{CO_2} g z. \quad (1.16)$$

Having the phase pressure, capillary pressure can be calculated by Equation 1.14. As capillary pressure is a function of wetting saturation, the phase saturations can be back-calculated from this functionality and the phase saturation distribution over the medium can be found (Figure 1.22):

$$S_w = P_c^{-1}(S_w). \quad (1.17)$$

We can derive mass and momentum balance for two-phase flow, similar to what we have seen for single-phase flow. The equations must be written for each phase. In Equation 1.5, the accumulation term must be considered only for one phase mass calculated by multiplying the total accumulation mass by phase saturation ( $S_\alpha$ ). Also the velocity is the phase velocity  $v_\alpha$ , and the source/sink term must be written for the phase mass rate  $q_\alpha$ .

For phase  $\alpha = \{w \text{ for water, } CO_2\}$ , we have:

$$\frac{d}{dt} \int_{\Omega} \phi \rho_\alpha S_\alpha d\tau + \int_{\Gamma} \rho_\alpha v_\alpha \cdot n d\sigma = \int_{\Omega} q d\tau. \quad (1.18)$$

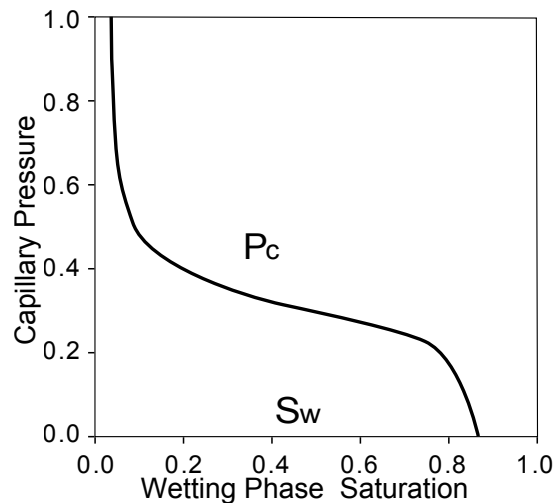


Figure 1.21: Capillary pressure can be expressed as a function of wetting saturation. The plot shows a typical Van Genuchten curve for capillary pressure. The scale in the vertical axis is only for demonstration. For application, see for example [46] and [40].

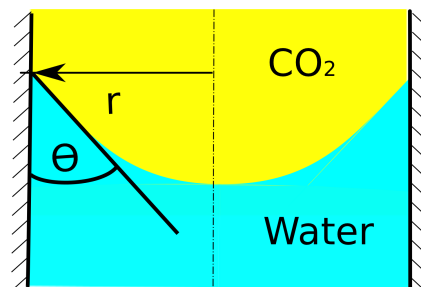


Figure 1.22: Capillary force is caused by the interaction of fluid phases with the pore walls. Capillary pressure is calculated from the force balance at the interface and depends on the curvature of the interface and the pore radius.

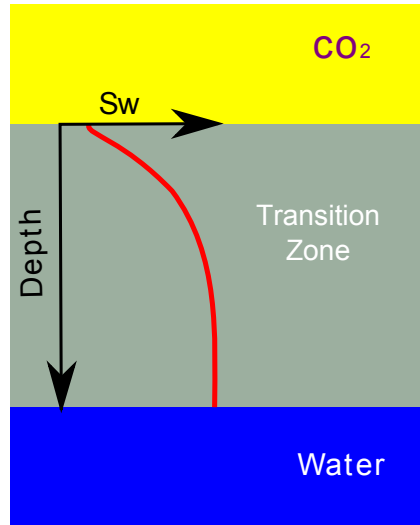


Figure 1.23: Water saturation ( $S_w$ ) distribution in the capillary transition zone. In the hydrostatic equilibrium condition, phases exist at different depths with saturations that depend on the balance between capillary and gravity forces.

Darcy equation for two phases  $\alpha = \{w \text{ for water}, \text{CO}_2\}$  can be written in the following form:

$$v_\alpha = -\frac{K_{e\alpha}}{\mu_\alpha} \cdot (\nabla P_\alpha + \rho_\alpha g \nabla Z). \quad (1.19)$$

Here,  $K_{e\alpha}$  is the effective permeability for phase  $\alpha$  and can be calculated from:

$$K_{e\alpha} = K_{abs} K_{r\alpha}, \quad (1.20)$$

where  $K_{abs}$  is the absolute rock permeability and  $K_{r\alpha}$  is the relative permeability of phase  $\alpha$ .  $P_\alpha$  is the phase pressure,  $\rho_\alpha$  is the phase density,  $g$  is the gravitational acceleration, and  $Z$  is the elevation.

Similar to Equation 1.7, differential form of mass balance equation for each of phases  $\alpha = \{w \text{ for water}, \text{CO}_2\}$  is as follows:

$$\frac{\partial}{\partial t}(\phi \rho_\alpha S_\alpha) + \nabla \cdot (\rho_\alpha v_\alpha) = q_\alpha. \quad (1.21)$$

In this equation,  $q_\alpha$  is the source/sink mass rate for phase  $\alpha$ .

The phase saturations are related by the following equation:

$$S_w + S_{co_2} = 1. \quad (1.22)$$

Fluid properties change by pressure and temperature. Density is mainly a function of pressure and viscosity depends upon temperature. These functions, called by convention equation of state (EOS), must be coupled to the system to honor fluid attribute variability [18, 31].

Mass exchange between phases may happen leading to change in composition. That also influences the fluid properties. In the immiscible fluids, the mass exchange can be in small order leading to slight changes in fluid properties. That can be modeled as a linear function with respect to pressure and temperature.

Extensive mass exchange between phases results in more nonlinear fluid property variations that require a detailed equation of state. Also for highly miscible fluids and high mass transfer between phases, it is better to write mass and momentum balance equations for components within phases in addition to phase equations.

There are a number of approaches to formulate the primary unknowns in the system of flow equations. The direct way is to replace phase velocities from Equation 1.19 into Equation 1.21, leaving the

phase pressures and water saturation as the primary unknowns. This ends in a set of strongly coupled equations.

A popular approach for formulating the set of flow equations is the fractional flow method [10]. In this method the total multiphase flow problem is treated as a single-phase flux of multiphase mixture. Therefore, individual phases are described as a function of total flow. This leads to separate equations for pressure and saturation.

Pressure is defined for the total flow either globally or pseudo-globally and relates to the phase pressure and saturation with auxiliary equations. The fractional flow approach keeps the governing equations in the form of single flow equations, and numerical schemes for single-phase flow can be revised into efficient schemes for multiphase problems.

Pressure and saturation equations have different mathematical nature: pressure has a diffusive character of an elliptical nature, which is numerically more stable than the saturation equation. Saturation equation is of convection-diffusion form with hyperbolic character in the convection part. The convection operator in saturation equation can be highly non-linear due to strong coupling of saturation and phase velocity. This nonlinearity can lead to shocks and discontinuities in the saturation solution.

As an example of fractional flow formulation, global pressure  $P_t$  is defined based on phase pressures:

$$P_t = \frac{1}{2}(P_w + P_{CO_2}) - \int_{S_w|P_c=0}^{S_w} (f_w - \frac{1}{2}) P'_c(S_w) dS_w, \quad (1.23)$$

where water fractional flow  $f_w$  is defined as:

$$f_w(S_w) = \frac{\frac{K_{rw}}{\mu_w}}{\frac{K_{rw}}{\mu_{co_2}} + \frac{K_{rc_{co_2}}}{\mu_{co_2}}}. \quad (1.24)$$

The total velocity is defined as:

$$v_t = v_w + v_{co_2}. \quad (1.25)$$

If capillary and gravity effects are negligible, saturation equation can be solved analytically, e.g. via Buckley-Leverett technique, or method of characteristics.

## 1.7 Flow regimes

A major part of our studies includes modeling physical phenomena occurring within flow through porous media. Various phenomena occurs during a complete sequence of CO<sub>2</sub> sequestration. During injection, the forces imposed by the injector dominate the flow behavior in the region around the injector. When CO<sub>2</sub> plumes develop in a thin layer moving along the stratigraphical structure, the large interface between water and CO<sub>2</sub> enhances the diffusion phenomena and lets more CO<sub>2</sub> be dissolved into water. Convection of water with dissolved CO<sub>2</sub> leads to complicated flow regimes.

The injected CO<sub>2</sub> undergoes various stages until it is stored underground. We consider two stages in our studies: injection and early migration. Many forces act on flow within medium, each of which requires a set of modeling parameters. Simplifying assumptions for flow modeling can be justified at each stage with relevance to dominating forces in the medium.

The following can be recognized as forces acting on the medium at the scale at which Darcy velocity is defined:

- Forces due to pressure gradients, mostly imposed by injectors (and/or producing wells).
- Buoyancy due to density contrasts between flowing phases. Gravity acts in the vertical direction.
- Capillary forces due to inter-facial tensions.
- Hysteresis due to sequencing of imbibition and drainage during flow in the porous medium.

- Convection forces due to gradients of density within one phase.
- Diffusion due to concentration gradients of one component.
- Reaction due to chemical reactions between phases and rock.

Modeling all forces acting on a porous medium is not practical, and we need to look at each flow regime separately by neglecting some forces that have a minor role. Herein, we discuss the main forces during injection and within long term migration.

### 1.7.1 Injection and early migration

Injection of CO<sub>2</sub> in the underground happens by forcing CO<sub>2</sub> mass through an injector into the medium. This poses a pressure gradient around the injector causing flow within the near bore region. Some authors call the force due to pressure difference ‘viscous force’, since viscosity has an important role in transferring the stress due to pressure difference in the porous medium resulting in fluid mobility. We use the same term throughout this thesis.

Viscous and gravity forces are the two major forces acting on the region around the injector during injection. Depending on fluid properties and distance from injection point, force balance changes. Gravity causes rapid phase separation resulting in upward movement of CO<sub>2</sub>. Gravity forces dominate two-phase regions far from the injector with lower viscous flow velocity compared to near well locations, where the flow velocity is high. At each position in the medium, a force balance results in a total force vector that may cause flow in a particular direction (Figure 1.24a).

Attempts in the literature on evaluating force interplay during a multiphase flow regime incorporating injection in the porous medium, employ sensitivity analysis on flow attributes such as flow velocity and pressure. There a number of publications that discusses reducing a complicated flow problem into a simplified problem by taking plausible assumptions [9, 15, 17, 24, 25, 54, 58, 71, 72]. Utilizing analytical solutions gives the flexibility of examining a wide range of parameter variations within the model, enjoying a fast evaluation of the corresponding flow behavior. Semi-analytical and numerical sensitivity analysis are also practiced in the literature to involve more physical modeling features in the flow performance evaluations[2, 3, 61].

The flow equations can be normalized to a dimensionless version that is used in many studies discussing the capillary and gravity influence on the flow. Herein, we give the method reported in [25]. If we assume incompressible flow (i.e., constant phase density) and medium (i.e., constant porosity) in a one-dimensional domain  $\Omega$  without any source/sink, Equation 1.21 reduces to the following for the wetting phase:

$$\phi \frac{\partial s_w}{\partial t} + \frac{\partial v_w}{\partial x} = 0, \quad (1.26)$$

and Darcy equation for one dimension flow becomes:

$$v_w = -K \frac{k_{rw}}{\mu_w} \left( \frac{\partial P_w}{\partial x} + \rho_w g z \right). \quad (1.27)$$

Here,  $x$  is the spatial direction in domain  $\Omega$ ,  $z$  is the vertical elevation and  $g$  is the gravitational acceleration. The system is closed by Equations 1.22 and 1.14 . We can define the dimensionless variables as follows:

$$X^* = \frac{x}{L}; T^* = \frac{t v_t}{L \phi}; \text{ and } P_c^* = \frac{P_c}{\pi_c}, \quad (1.28)$$

where  $L$  is a length constant in the problem,  $v_t$  is the total flux, and  $\pi_c$  is a capillary pressure normalizing constant. For incompressible fluids and a constant total flow rate, the total flux  $v_t$  equals the summation of phase fluxes:

$$v_t = v_w + v_{nw}. \quad (1.29)$$

After reformulating Equation 1.26, fractional flow can be written in the following form:

$$f_w = G(S_w) + C(S_w) \frac{\partial S_w}{\partial X^*}, \quad (1.30)$$

where  $S_w$  is the normalized wetting phase saturation,  $G$  is the gravity contribution, and  $C$  is the capillary contribution to the flow. The gravity and capillary contributions,  $G$  and  $C$ , are expressed by quantities relative to the viscous force [33] and we have:

$$G(S_w) = F_w(1 - N_G k_{rnw}), \quad (1.31)$$

$$C(S_w) = N_C F_w k_{rnw} \frac{\partial P_c}{\partial S_w}, \quad (1.32)$$

wherein:

$$F_w = \frac{\lambda_w}{\lambda_w + \lambda_{nw}}, \quad (1.33)$$

$$N_C = \frac{K \pi_c}{\mu_{nw} L v_t}, \quad (1.34)$$

and

$$N_G = \frac{K(\rho_w - \rho_{nw}) g z}{\mu_{nw} v_t}. \quad (1.35)$$

Here,

$$\lambda_w = \frac{k_{rw}}{\mu_w}, \quad (1.36)$$

and

$$\lambda_{nw} = \frac{k_{rnw}}{\mu_{nw}}. \quad (1.37)$$

Having these definitions, Equation 1.26 reshapes into:

$$\frac{\partial S_w}{\partial T^*} + \frac{\partial G(S_w)}{\partial S_w} \frac{\partial S_w}{\partial X^*} + \frac{\partial}{\partial X^*} \left( C(S_w) \frac{\partial S_w}{\partial X^*} \right) = 0. \quad (1.38)$$

Applying specific type of capillary pressure and relative permeability function may lead to simplified forms of Equation 1.38 with the possibility of having an analytical solution [72].

Some important conclusions in the literature [9, 17, 25, 61, 72] from sensitivity studies on capillary, gravity and viscous forces are summarized here and inferred for CO<sub>2</sub> injection application:

- Gravity and capillary pressure will only influence the flow speed significantly for slow displacement rates. Therefore, around the injection point where normally fluids are flowing with a relatively high speed, viscous forces are dominant.
- If capillary is of any significance, ignoring capillary forces in modeling the injection of CO<sub>2</sub> results in a pessimistic CO<sub>2</sub> sweep efficiency. Capillary helps in the spreading of CO<sub>2</sub> in the frontal CO<sub>2</sub>-water interface.
- Less capillary forces in the porous medium allows more space for CO<sub>2</sub>. This enhances the density segregation due to gravity forces.

The main focus in the series of work in this thesis has been to assess the flow influence by heterogeneity during injection time and early CO<sub>2</sub> migration. For CO<sub>2</sub> injection problems, one objective is to maximize the rate of injection and aligned with that we use relatively high injection rates in our studies. Therefore, we did not include capillarity forces for modeling the high displacement rates within heterogeneities, which can be justified by the results in the literature.

Table 1.2: Spatial scales for CO<sub>2</sub> storage. Ranges are extracted from [13].

Feature	Spatial scale
Capillary fringe	10cm->10m
Plume radius	10km->100km
Pressure perturbation	50km->500km
Migration distance	50km->500+km

Table 1.3: Temporal scales for CO<sub>2</sub> storage. Ranges are extracted from [13, 32].

Feature	Temporal scale
Density segregation	1 month->5+ years
Capillary segregation	1 year->50 years
Injection period	5 years->50 years
Convective mixing	20 years->1000 years
Plume migration	few hundred years->1000 years
Mineral reaction	500 years->100000 years

### 1.7.2 Long term migration

The injected CO<sub>2</sub> volume in the geological formation will travel below the sealing cap by buoyancy forces due to the density difference between water and CO<sub>2</sub>. The mobile CO<sub>2</sub> is at risk of leaking through any imperfections in the sealing layers and abandoned wells. Molecular diffusion occurs at the interface of water and CO<sub>2</sub> and this mass transfer from the CO<sub>2</sub> plume into water increases the water density. Transition of CO<sub>2</sub> from mobile phase into water with dissolved CO<sub>2</sub> is helping the safe storage of CO<sub>2</sub>: the heavier water with dissolved CO<sub>2</sub> has the tendency of moving downward. Time scale for this convective mixing is of the order of several hundreds years (Table 1.3). Yet, this is not the end and the dissolved CO<sub>2</sub> can react with the porous medium ending up in a solid phase and it can be stored permanently in a process called mineral trapping. This is an extremely slow process and it can take thousands of years [32].

Mixing of CO<sub>2</sub> and water in the long-term happens through phases with various time scales and physical phenomena. Diffusion of CO<sub>2</sub> in water continues and layer of water with dissolved CO<sub>2</sub> builds up below the CO<sub>2</sub> plume until it forms heavy parts convecting in the form of unstable fingers, as shown in Figure 1.24b.

The onset time for the convective mixing is important in terms of storage safety. This time depends on the Rayleigh number in the medium:

$$Ra = \frac{Kg\Delta\rho H}{D_c\phi\mu}. \quad (1.39)$$

Here,  $\Delta\rho$  is the density difference between the water and CO<sub>2</sub> phases,  $H$  is the formation thickness, and  $D_c$  is the molecular diffusion coefficient of CO<sub>2</sub> into water phase. The higher density sitting on top of lower density makes an unstable system and the medium must have a minimum Rayleigh number to have a growing instability for a small perturbation in the medium. Heterogeneities in the medium can initiate perturbations, reducing the instability onset time [20, 34]. Therefore, heterogeneity is an important factor that must be considered when we are choosing an aquifer for CO<sub>2</sub> storage.

Capillary fringe in the plume can enhance the onset of the convective mixing. It can speed up the process up to five times [22].

The flow equations for convective mixing are a set of mass and momentum balances for component  $c = \{\text{Water}, \text{CO}_2\}$  within phase  $\alpha = \{\text{Wetting}, \text{Non-Wetting}\}$ :

$$\frac{\partial}{\partial t} \sum_{\alpha} \phi S_{\alpha} \rho_{\alpha} X_{\alpha}^c + \nabla \cdot \sum_{\alpha} \rho_{\alpha} X_{\alpha}^c v_{\alpha} = 0, \quad (1.40)$$

and

$$v_\alpha = -\frac{k_{r\alpha} K}{\mu_\alpha} [\nabla P_\alpha - \rho_\alpha g z] \quad (1.41)$$

where  $X_\alpha^c$  is the mole fraction of component c in phase  $\alpha$  and  $v_\alpha$  is the flux of phase  $\alpha$  [21].

## 1.8 Flow modeling

We use a standard porous media simulator [64] to solve the flow equations in the medium. The simulator is based on finite volume method and the following assumptions are made:

- Two compressible phases are considered in the medium: water and super critical  $CO_2$ .
- No mass exchange occurs between the two phases.
- No heat exchange is considered.

### 1.8.1 Numerical scheme

The simulator uses a standard two-point finite difference scheme to solve Equation 1.21 on a corner-point grid. The Darcy equation for two-phase flow can be expressed based on algebraic difference terms. The equation governing the flow into cell  $a$  from the neighboring cell  $b$  is as follows:

$$F_{ab\alpha} = T_{ab} M_{a\alpha} \Delta \psi_\alpha. \quad (1.42)$$

Here,  $T_{ab}$  is the transmissibility of the medium between the two cells.  $M_{a\alpha}$  is the mobility of phase  $\alpha$  that is taken upstream of the flow from cell  $a$  and  $\Delta \psi_\alpha$  is the potential term difference between two cell centers.

Transmissibility for two neighboring cells (i.e., sharing a face area, see Figure 1.25) is calculated by harmonic average of transmissibilities from the center of each cell to the center of the common face between the two cells:

$$T_{ab} = \left( \frac{1}{T_a} + \frac{1}{T_b} \right)^{-1}. \quad (1.43)$$

Each half transmissibility, for example  $T_a$ , is calculated by an inner product between the permeability of the cell  $K_a$ , the mutual area  $A_{ab}$  between cells, and the distance from cell center to the mutual face center  $d_a$ :

$$T_a = K_a \cdot d_a \cdot A_{ab}. \quad (1.44)$$

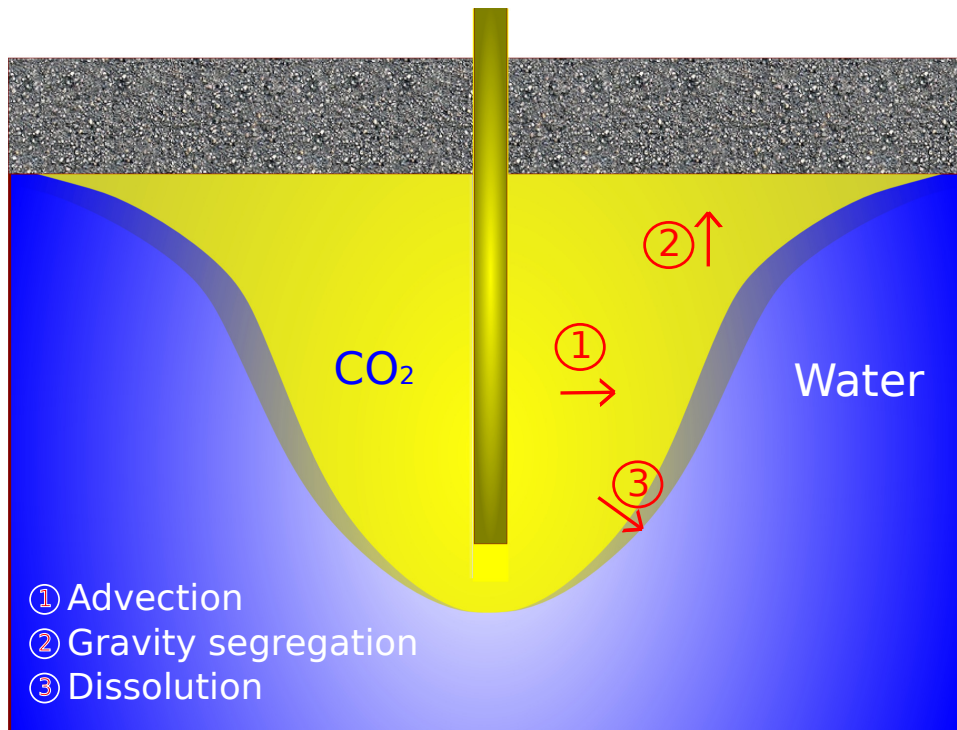
The mobility term in Equation 1.42 is defined as follows:

$$M_{a\alpha} = \frac{k_{r\alpha}}{B_\alpha \mu_\alpha}, \quad (1.45)$$

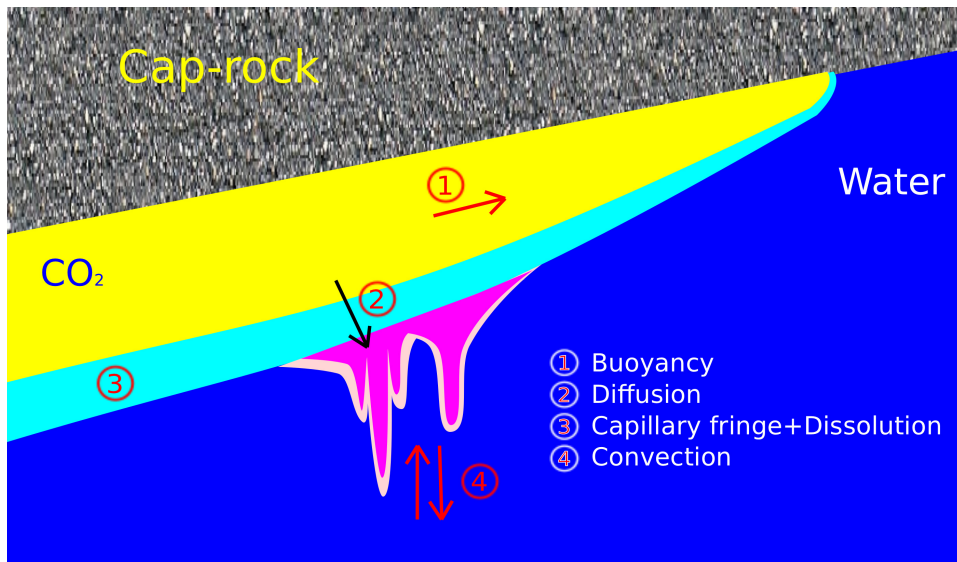
where  $k_{r\alpha}$  is the relative permeability of phase  $\alpha$ ,  $\mu_\alpha$  is the viscosity of phase  $\alpha$ , and  $B_\alpha$  is the formation volume factor of phase  $\alpha$ , which is defined as :

$$B_\alpha = \frac{\text{Volume at surface condition}}{\text{Volume at formation condition}} = \frac{V_{s\alpha}}{V_{r\alpha}}. \quad (1.46)$$

This definition is connected to compressibility of the fluid, i.e., to changes in volume at the surface and at the geological formation condition. It is defined in this way in the simulator to consider cases where a fluid, such as oil, loses its dissolved gas while being produced at surface pressure. Since we assume no mass exchange between phases in our study, here the formation volume factor works like



(a) Injection and early migration flow regime.



(b) Long-term migration flow regime.

Figure 1.24: Flow regimes in geological CO<sub>2</sub> storage; (a) During injection, the main physical processes are the flow advection due to the imposed pressure by the injection, the gravity segregation due to the phase density differences, and the dissolution of CO<sub>2</sub> into water. (b) During the long-term CO<sub>2</sub> migration, the main physical processes in the medium are the gravity segregation, the molecular diffusion, the CO<sub>2</sub> dissolution in water, the water capillary imbibition, and the convection mixing due to gravity instabilities.

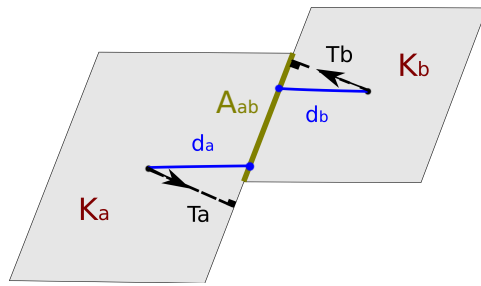


Figure 1.25: Transmissibility between two cells a and b depends on the interface area perpendicular to the flow ( $A_{ab}$ ) and transmissibilities between the center and the cell side within each cell ( $T_a$  and  $T_b$ ).

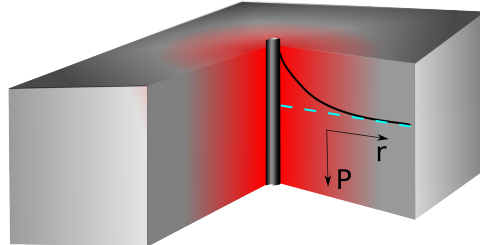


Figure 1.26: Injection operation causes pressure increase near the well-bore. The red color in the figure demonstrates the regions with pressure build-up. The well-bore pressure is calculated by a relation that models the pressure distribution around the well. The black curve in the figure shows a schematic incline of the pressure near the injector.

compressibility of the fluid. Formation volume factor is a function of pressure. Slight compressibility is considered for phases in our study, and phase density is defined as a function of pressure:

$$\rho_\alpha(P) = \frac{\rho_{0\alpha}}{B_\alpha(P)}. \quad (1.47)$$

Here,  $\rho_{0\alpha}$  is the density of phase  $\alpha$  at reference conditions.

Wells are defined as sources or sinks in Equation 1.21. In reality, wells are a void space drilled in the porous medium and the flow into the well-bore and up to the surface for production wells (and vice-versa for injectors) goes through a pressure change that must be modeled separately from the porous medium.

Figure 1.26 shows a schematic pressure distribution around the injector. The well radius is much smaller than the simulation cell containing the well and the pressure in the bottom-hole is different than the cell pressure. The well bottom-hole pressure can be related to the cell pressure containing the well by a separate approximation that can be coupled with flow equations in the grid model. Flow equation for phase  $\alpha$  between the cell center and the well for an injector is written as follows:

$$\eta_\alpha = T_w \cdot M_\alpha \cdot [P_w - P_i]. \quad (1.48)$$

Here,  $\eta_\alpha$  is the volumetric injection rate of phase  $\alpha$ ,  $P_w$  is the injector bottom-hole pressure,  $P_i$  is the cell pressure,  $T_w$  is the transmissibility between the cell and the injection well-bore, and  $M_\alpha$  is the mobility of injection flow into the cell.

A region can be assumed by radius  $r_e$  at which the pressure is equal to the cell pressure. By approximating the flow near the well-bore using Equation 1.12, the transmissibility for this region can be found from the analytical solution of Equation 1.12:

$$T_w = \frac{K \cdot h}{\ln(\frac{r_e}{r_w})}, \quad (1.49)$$

where  $h$  is the medium thickness,  $K$  is the medium rock permeability, and  $r_w$  is the well radius. Here, we assume that the well is completed and connected in the entire thickness  $h$  of the cell and there is no skin effect in the well. The Equation 1.49 can be extended to model wells with partial completions and skins. The effective radius  $r_e$  in Equation 1.49 is estimated from the Peaceman formula and can be related to the cell geometry:

$$r_e = 0.28 \frac{\left[ \delta_x^2 \left( \frac{K_y}{K_x} \right)^{\frac{1}{2}} + \delta_y^2 \left( \frac{K_x}{K_y} \right)^{\frac{1}{2}} \right]^{\frac{1}{2}}}{\left( \frac{K_y}{K_x} \right)^{\frac{1}{4}} + \left( \frac{K_x}{K_y} \right)^{\frac{1}{4}}}. \quad (1.50)$$

Here,  $K_x$  and  $K_y$  are the permeabilities in  $x$  and  $y$  directions and  $\delta_x$  and  $\delta_y$  are the cell sizes in these directions. This equation assumes a vertical well and a diagonal permeability tensor. It can be modified for more general cases.

## 1.8.2 Flow scenarios

All of the SAIGUP realizations have dimensions of 3 km  $\times$  9 km  $\times$  80 m. The model spatial scales capture the typical geological features in a shallow-marine system, such as shore-line shape and aggradation angle variations. Various scales of heterogeneity can considerably impact the flow behavior. The lateral extent of the model is smaller than the scales used for CO<sub>2</sub> storage studies. In some storage sites, the lateral extent that the CO<sub>2</sub> travels can go to hundreds of kilometers. This makes our study limited in the spatial domain around the injector. For the same reason, in the temporal scale, we are more focused on injection and early migration time. We examine a number of injection scenarios to study the spatial distribution of CO<sub>2</sub> in the medium during injection and early migration periods.

The study of pressure is essential for injection operations. A detailed pressure study requires larger scales than what are used here. We choose open boundaries for the model to compensate for the actual large extents of a typical storage location (Figure 1.27). The choice of open boundary is not valid in domains that are bounded by structural seals. In fact, for the closed and semi-closed domains the pressure is a major control on the storage capacity along with other parameters. The results of our pressure study can change significantly by choosing different boundary conditions.

We model the boundary by large pore volumes on the outer closed cells. This makes the pressure to relax earlier than it does in a large domain. Even with such artifact, the effect of heterogeneities is clearly seen in a considerable fraction of cases with an extreme pressure build-up. We investigate the operational concerns related to pressure build-up for a typical injection scenario. Our pressure study can be used for devising mitigation plans by defining operational constraints for injectors. We perform an extensive probabilistic analysis on the CO<sub>2</sub> pressure behavior in the medium that can be applied in further studies with specific concerns about the pressure analysis.

We consider the injection of 20% of the total pore volume of the model(excluding the large volumes at the boundaries), which amounts to 40 MM m<sup>3</sup>. This volume is injected into all realizations in three different scenarios. In the first scenario, the injection is forced to finish in 30 years and an unlimitted pressure rise in the system is permitted. Linear relative permeability functions are considered in this scenario. The purpose of the first scenario is to examine the flow distribution in the medium influenced by geological heterogeneity. Linear assumption for relative permeabilities is taken to speed up the flow within the medium. We have used quadratic relative permeability function in the second scenario. This scenario has shown a considerable increase in the pressure responses for many cases during CO<sub>2</sub> injection into the aquifer. This is mainly due to lower CO<sub>2</sub> mobility at low saturations compared to the linear relative permeability. Albeit, the CO<sub>2</sub> moving under a cap-rock will effectively have a linear relative permeability.

The third injection scenario is similar to the first scenario, except that the injector is controlled by pressure rather than volumetric rate. Thus, injection time is variable depending on the injectivity of the medium.

Only one injector is considered in the study. With one injector, it is easier to study the flow behavior and the plume development within the medium. The injector is located in the flank and to increase the

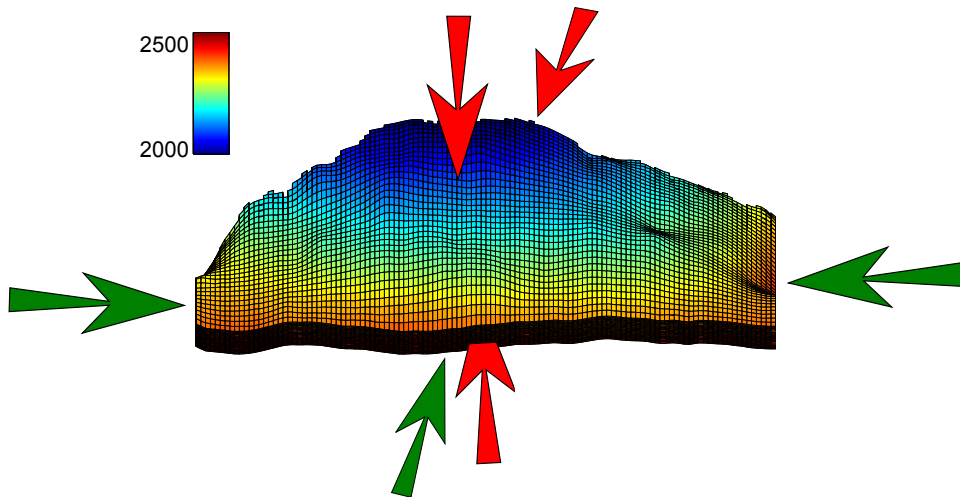


Figure 1.27: In the models used for flow simulation, the top, bottom, and upper side boundaries are closed and the rest are open to the flow. Arrows point to the boundaries and their color indicates if the boundary is open (green) or closed (red). Colors on the grid show the depth of different locations.

sweep efficiency for the up-moving CO<sub>2</sub> plume, the injector is connected to the medium (completed) only in the lower part of the aquifer. The injector location and the completed layers are fixed for all of the realizations. The studies here aim to identify the influence of uncertainty on injectivity and fixing a place for injection helps in achieving this goal. As mentioned earlier, injectivity is a big player in the success of the operations. Uncertainty might be less near the well-bore region than in the larger scale in the domain, but requires costly operation data acquisition. Fixing the location of the well serves to specify the probability of having a feasible injectivity in different heterogeneities.

There are few locations of distorted geometries in the faulted realizations that may be considered as structural traps for the injected CO<sub>2</sub>. The topography in the SAIGUP realizations is simple and does not cover the variational space to be used in a sensitivity analysis. The slight inclination in the structural geometry of the medium, from the flank up to the crest, leads the injected CO<sub>2</sub> to accumulate in the crest and below the faulted side of the aquifer. The structural trapping due to variational morphology is studied in IGEMS, which is a sister project to MatMora (for example, see [67]).

In a homogeneous medium, we expect the CO<sub>2</sub> to accumulate under the cap-rock. A small fraction of the injected CO<sub>2</sub> will escape through the open boundary near the injection well and the rest of it will stay within the medium in two forms that we refer to as mobile and residual volumes. As the CO<sub>2</sub> moves through the rock, part of it stays in the smaller pores due to the capillary trapping process and cannot be discharged by brine. The other parts move through the larger pores and can be displaced by water in an imbibition process. This volume is called mobile. As we are interested in storing the CO<sub>2</sub> permanently and safely, increasing the trapped volume is in line with the objective of minimizing the leakage risk and maximizing the storage capacity. Likewise, the more mobile volume of CO<sub>2</sub> exists in the medium, the higher will be the risk of leakage.

Defining the boundary conditions of the aquifer of interest can influence flow behavior in the system. Computational costs make it more feasible to model the flow locally and in the part of the aquifer that is going through more pronounced changes in flow behavior. Therefore, we can choose the boundaries of the model inside the aquifer in a volume that is containing the injection wells and the areas affected by them. Hydrostatic open boundary condition is a choice for the system boundaries to include the aquifer parts that fall outside the boundaries (Fig. 1.28).

The underground network of aquifer systems can be connected via geological channeling and conductive features. Some aquifers might be active and connected to the surface and expand in volume by variations in water influx due to seasonal rains. This can impose an external force on the system bound-

aries considered in the storage problems. Fig. 1.28 shows the water influx through the boundaries of the system due to external aquifer activities. We consider the external support by imposing a higher pressure than the hydrostatic pressure on the boundary of the model.

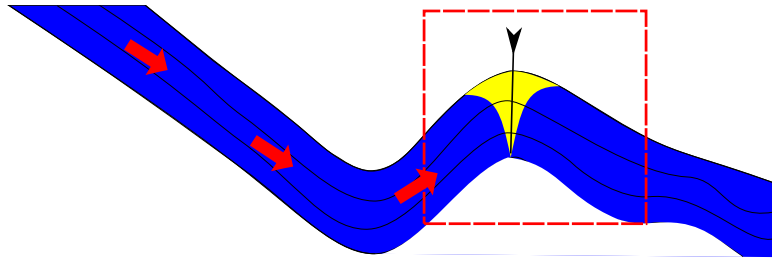


Figure 1.28: The aquifer can be connected to neighboring aquifer systems and the flow from those aquifers (red arrows in the plot) is modeled by imposing external pressure on the open sides of the model. The dotted box in the figure schematically indicates a domain considered for study. Aquifer layers outside the frame are considered external. The yellow color demonstrates the injected  $\text{CO}_2$  in the aquifer.

### 1.8.3 Flow responses

The primary unknowns in the flow model are the  $\text{CO}_2$  pressure and the saturation distribution at different times. From the simulation output, we can derive quantities that address the feasibility of  $\text{CO}_2$  injection. These quantities include a number of flow responses related to the  $\text{CO}_2$  injection and migration problems. Each of these responses are directly or indirectly a measure of success for the operation within a specific realization. In the following, we give a brief description of each of them:

**Total mobile and residual  $\text{CO}_2$  volume:** If the  $\text{CO}_2$  saturation is below the critical value, it will be immobile in the bulk flow, although not in the molecular sense. Less mobile  $\text{CO}_2$  means less risk of leakage. A more efficient volume sweep of  $\text{CO}_2$  plumes can result in larger residual volumes (with saturations less than the critical). We use critical saturation value of 0.2 for both water and  $\text{CO}_2$ . During injection time the flow process is mainly drainage but after injection, imbibition also happens and increases the residual trapped  $\text{CO}_2$ .

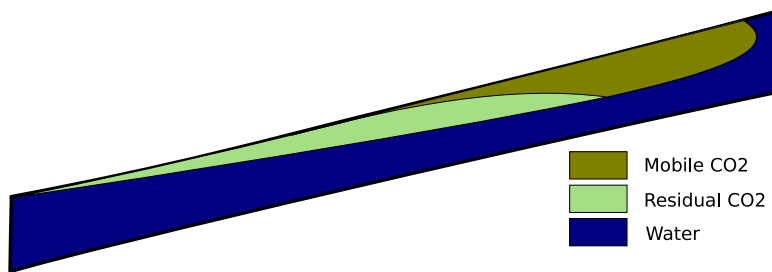


Figure 1.29: Mobile and residual  $\text{CO}_2$  volumes; the injected  $\text{CO}_2$  plume travels upward within the geological formation and leaves behind a volume of residual  $\text{CO}_2$  that is trapped due to capillarity.

**Total number of  $\text{CO}_2$  plumes and largest plume:** To estimate the risk of leakage from the cap-rock, we assume that all mobile  $\text{CO}_2$  connected to a leakage point will escape out of the reservoir. Hence, it is preferable if the total mobile  $\text{CO}_2$  volume is split into smaller plumes rather than forming a big mobile plume. We looked at the largest plume size, the number of plumes, and other statistical parameters.

**Average aquifer pressure:** This is one of the most important responses to be considered. The pressure response in general shows a sharp jump at the start of injection and a declining trend during the injection and plume migration.

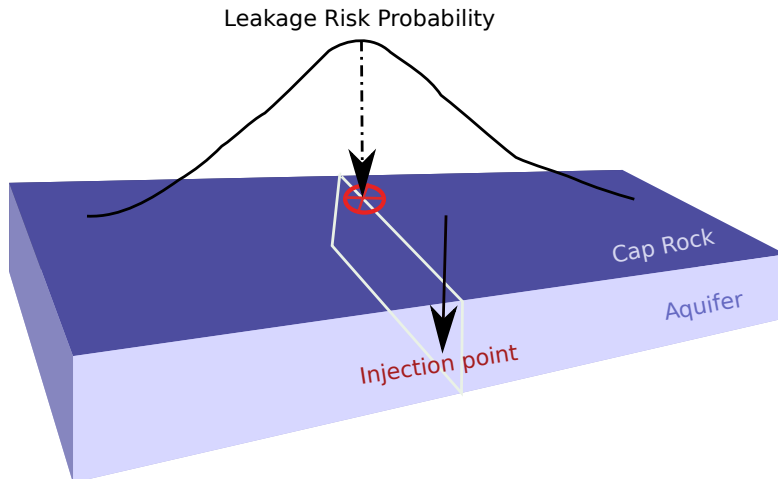


Figure 1.30: We use a 2D Gaussian distribution for leakage probability on the cap-rock.

As soon as the injection starts, a pulse of pressure goes through the medium, introducing a pressure buildup in the aquifer. When the pressure wave reaches the open boundary, the aquifer pressure starts declining to a level maintained by the injector. When the injection operation stops, the pressure support will be removed and the pressure drops and declines until it reaches equilibrium.

**Leakage risk:** During injection operation the foremost important issue is the aquifer pressure, which as discussed earlier, may lead to fractures in the cap-rock. On the other hand, the cap-rock break depends on lithology and sealing thickness and differs from point to point. Some weaker locations can be the most probable to break and start leaking if any mobile CO<sub>2</sub> exists there.

An uncertainty assessment process consisting of geo-mechanical modeling of aquifer combined with flow modeling can cost a large amount of computations. To avoid expensive computations, the idea in this thesis is to model the possible breakings on the cap-rock (considering the stress stream in the medium) by introducing a probability measure on the cap-rock. This measure can be used to evaluate different cases for their risk of leakage, considering the CO<sub>2</sub> distribution under the cap-rock.

Here, we define the probability of leakage as a measure on the cap-rock that assigns a value to each point of the cap-rock, modeling the relative weakness of the cap-rock and the medium at that point. If for example both the cap-rock and the aquifer are continuous homogeneous layers with constant thickness, then the point of cap-rock that sits on the highest point of the injection slice can be the most probable place for leakage in the case of dramatic pressure increase in the well; the stress stream is more in the injection slice and the CO<sub>2</sub> accumulation occurs on the topmost part of the aforementioned slice. Then one may consider a 2D-Gaussian probability distribution on the cap-rock, centered above the injection slice.

If the medium is heterogeneous or tilted, the injected CO<sub>2</sub> may be distributed in different number and sizes of plumes below the cap-rock. Therefore, in addition to the probability of breaking for each point of cap-rock, one must consider the CO<sub>2</sub> connected volume that is attached to that point.

Since we have neither the cap-rock model nor the geo-mechanical properties of the SAIGUP models, we use a simple 2D-Gaussian leakage probability distribution centered at a point on the crest which is in the same slice as the injection point (Fig. 1.30). We calculate the probability of each cell in the top layer and using the simulation results for the case, we weight it by the CO<sub>2</sub> saturation of that cell and the plume size that the cell is attached to. Summing up the values of the topmost cells, we assign a single number to the case, which we call leakage risk of the case. One may weight the case risk value with the average pressure in the system, such that higher pressure gives a bigger weight.

Results are discussed by comparing all cases in plots. However, the conclusions are made based on detailed flow study in some picked cases. For example, Figures 1.31 to 1.35 show the rock properties and CO<sub>2</sub> distribution in the domain at end of injection and end of simulation in two different cases. The

Table 1.4: Geological heterogeneities for two selected cases.

Case	Fault	Lobosity	Barrier	Aggradation Angle	Progradation Direction
A	unfaulted	one lobe	50%	45°	down-dip
B	unfaulted	two lobe	50%	10°	up-dip

heterogeneity description of the selected cases, called A and B, is given in Table 1.4.

CO<sub>2</sub> distribution in Figures 1.33 and 1.34 show that heterogeneity in case B has enhanced the lateral flow compared to case A. Direction of the flow can be seen in Figure 1.35. It is clear that heterogeneity can influence the imbibition and drainage process during and after injection. This, in turn, impacts the residual trapping process.

Figure 1.36 demonstrates the plume evolution during simulation in two different cases, i.e., case A and B. The mobile CO<sub>2</sub> is plotted here and it shows that the injected CO<sub>2</sub> moves more in the vertical direction in case A, ending up in a big mass accumulated under the cap-rock. On the contrary, the heterogeneity in case B enhances the lateral movement of the plume, resulting in a laterally spread plume within the medium.

Figure 1.37 shows the development of pressure in the same cases. We see that injection in case B causes a dramatic pressure build-up due to the poor vertical transmissibility. The pressure build-up spreads out within the medium in case A, while it is trapped in the injection layers for case B.

One way to report the described responses and their relations to the uncertain parameters in one graph is to use scatter plots. Each case will then be represented by a marker sign with attributes dedicated to the set of geological parameter levels used in that case. Figure 1.38 shows some of the codes used in the study. This will be used later in the thesis and in the papers reporting our study.

## 1.8.4 ECLIPSE input file

In this section, important parts of the ECLIPSE input files that are used in modeling the flow are given. We will go through different sections of the ECLIPSE input file. It is assumed that the reader is familiar with the syntax and terminology used in the ECLIPSE simulation. See [64] for more information about ECLIPSE keywords. We use the version 2009 of ECLIPSE-100 black-oil module.

Several flow scenarios were examined before concluding in a few number of scenarios to be used in the study. Two main scenarios are considered that differ mainly in defining the well operational specifications. We will explain more about these cases in the SCHEDULE section. Only the important parts of the input file are given such that it is possible to reproduce the runs.

The model starts by specifying the general simulation settings: grid dimensions, phases involved in the study, simulation start date, and so on. We consider no mass exchange between water and CO<sub>2</sub>. Therefore, it is enough to represent the flow by oil-water system where oil represents the CO<sub>2</sub> phase. We use CO<sub>2</sub> properties for oil:

```
RUNSPEC
DIMENS —Grid dimensions
40 120 20 /
—Two-phase flow problem with no mass exchange
WATER
OIL —CO2 is treated as OIL and CO2 properties used for it.
METRIC —Metric unit system
START —Simulation start date
1 'JAN' 2000 /
```

Then, the grid information are given for each realization. The set of keywords generated in the SAIGUP study are included in the input file. Each included file contains data for a specific keyword. Each file is named after the keyword name it includes with the extension 'INC'. For example, 'PORO.INC' contains the PORO keyword, which contains the porosity value for each cell in the model. Only two

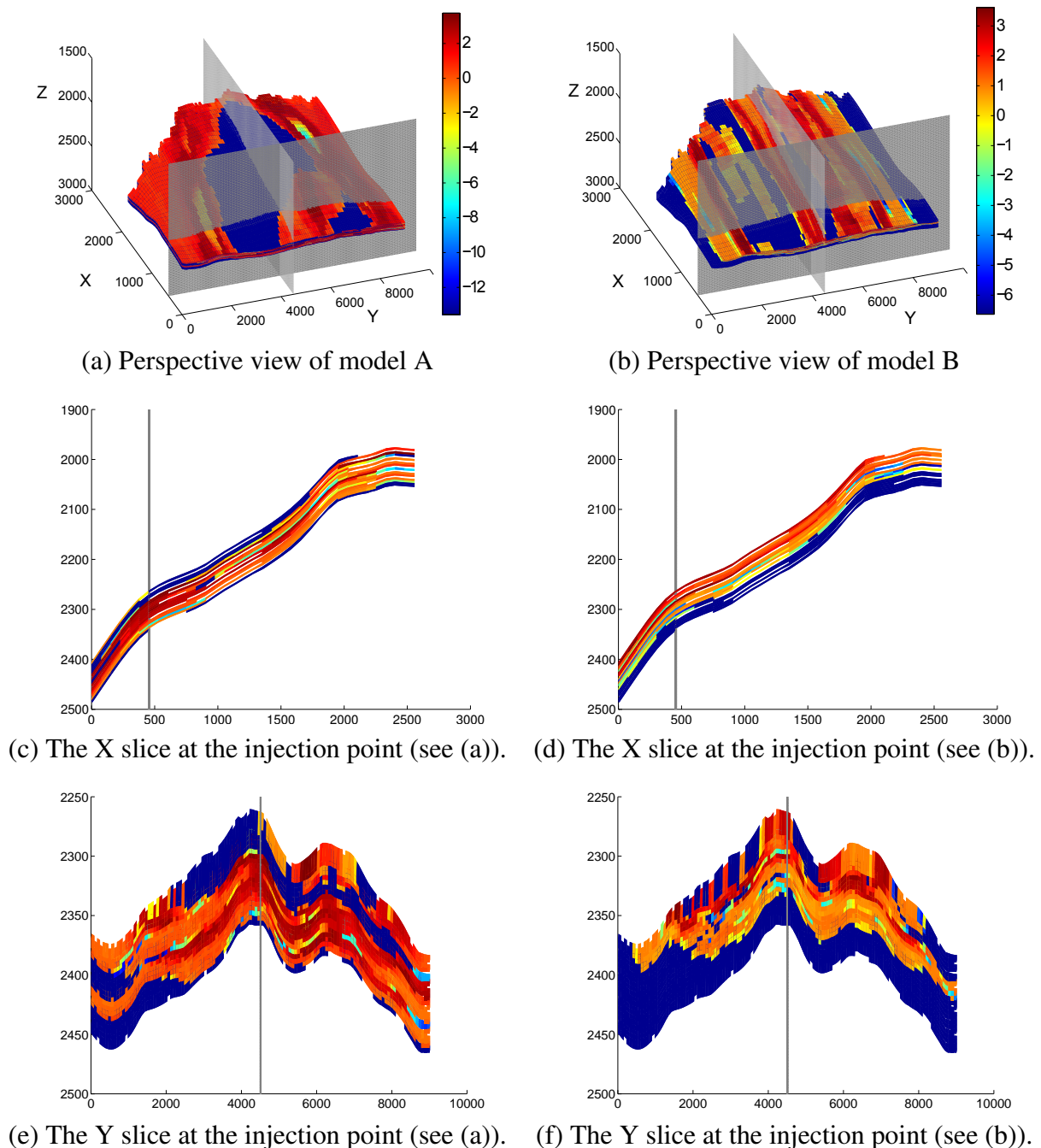


Figure 1.31: Transmissibility in the vertical direction for two selected cases. The left plots correspond to case A in Table 1.4, and the right plots belong to case B. Colors are in log scale and the scale in Figures (a) and (b) are powers of ten in  $\text{cP} \cdot \text{m}^3/\text{day}/\text{bar}$  units.

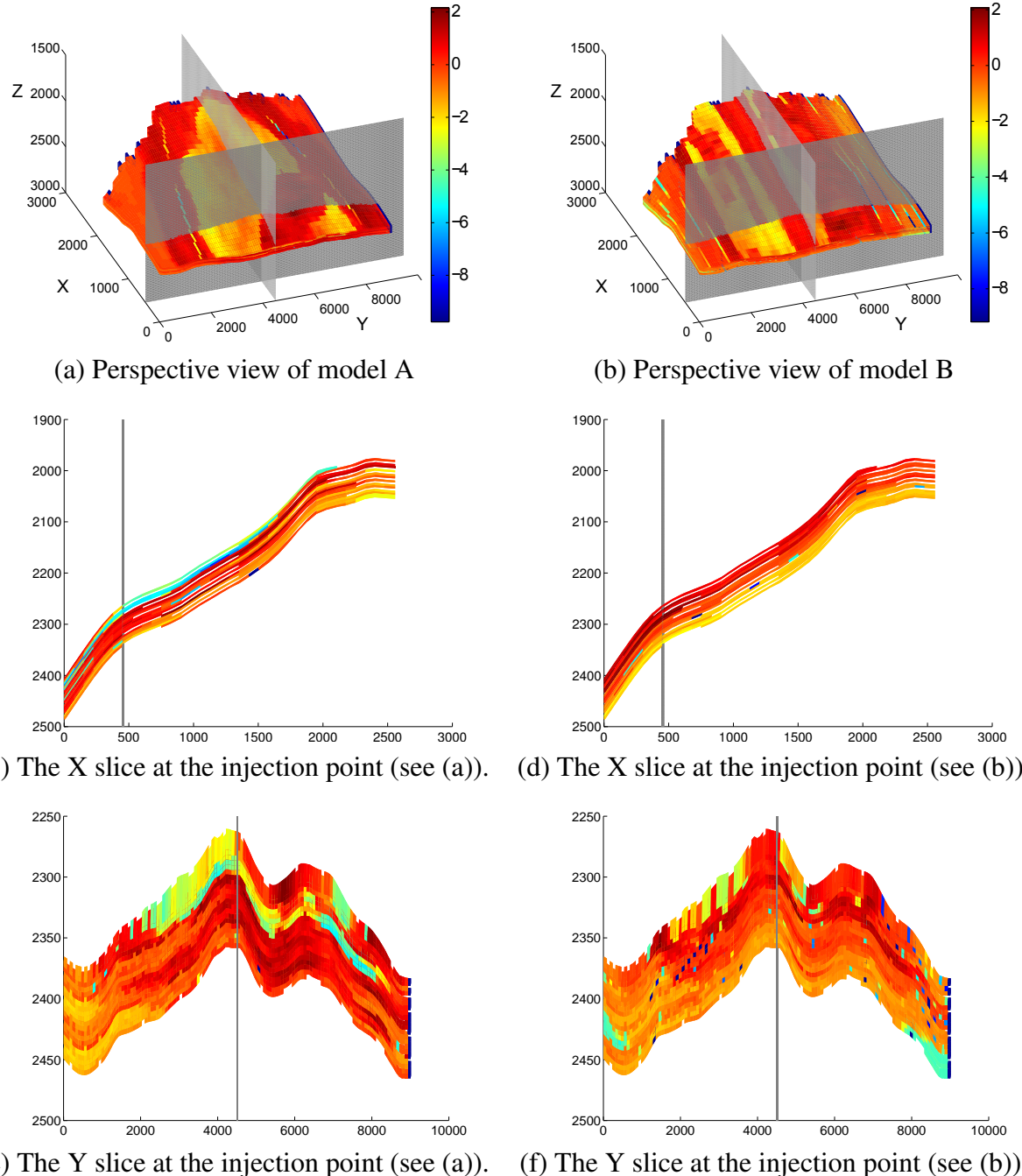


Figure 1.32: Transmissibility in the lateral direction for two selected cases. The left plots correspond to case A in Table 1.4, and the right plots belong to case B. Colors are in log scale and the scale in Figures (a) and (b) are powers of ten in  $\text{cP} \cdot \text{m}^3/\text{day}/\text{bar}$  units.

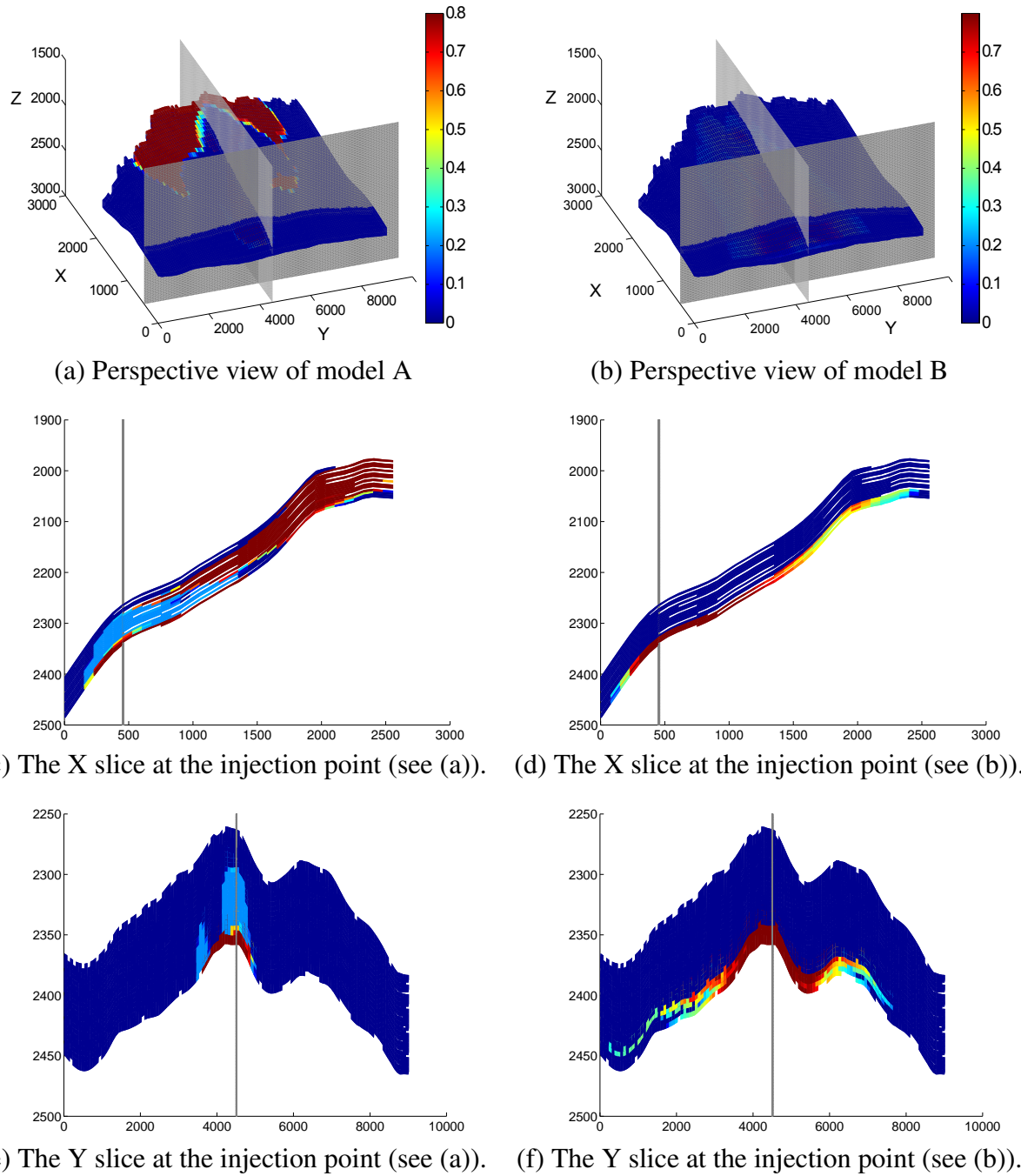


Figure 1.33:  $\text{CO}_2$  distribution at the end of injection for two selected cases. The left plots correspond to case A in Table 1.4, and the right plots belong to case B.

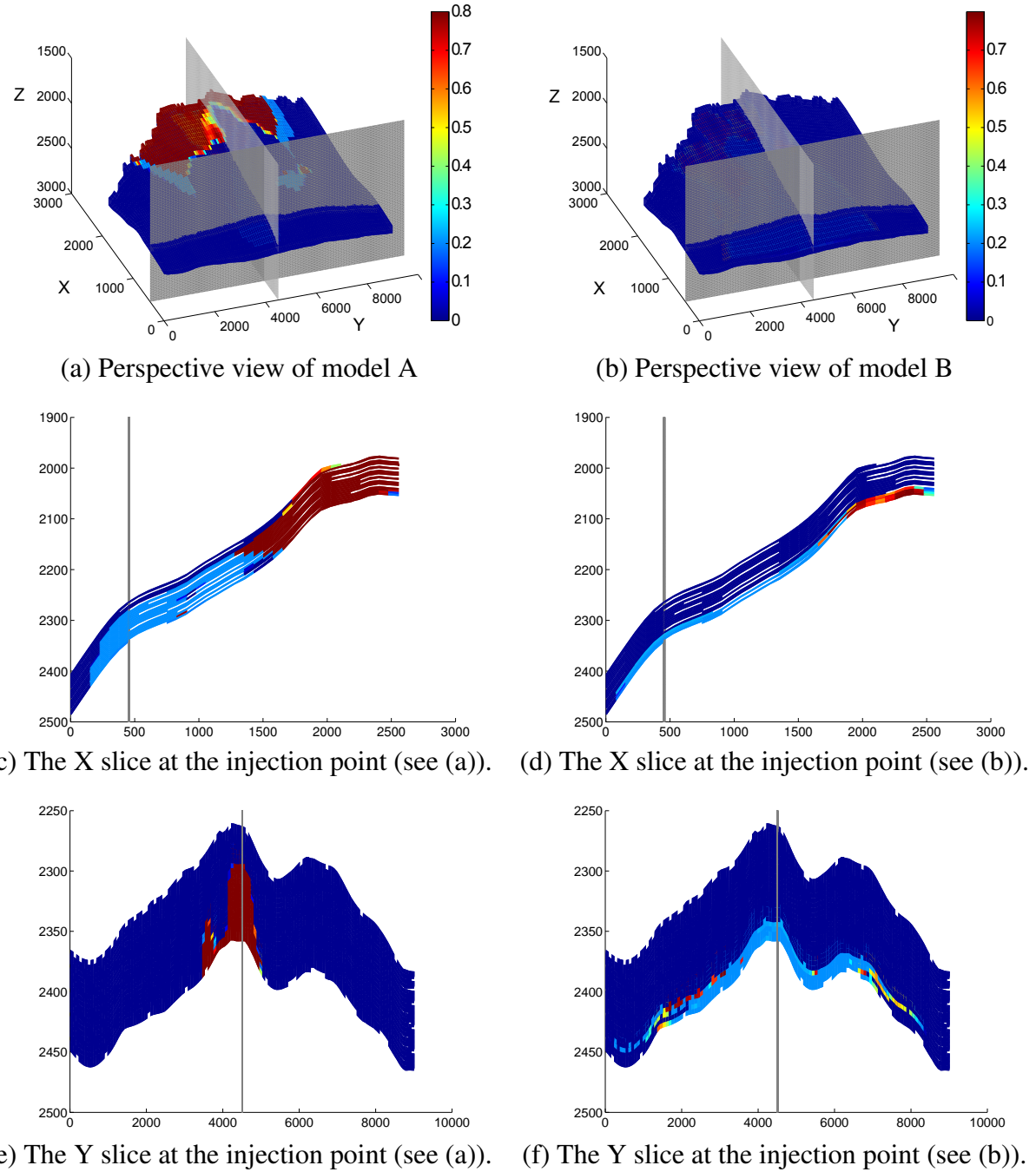


Figure 1.34: CO<sub>2</sub> distribution at the end of simulation for two selected cases. The left plots correspond to case A in Table 1.4, and the right plots belong to case B.

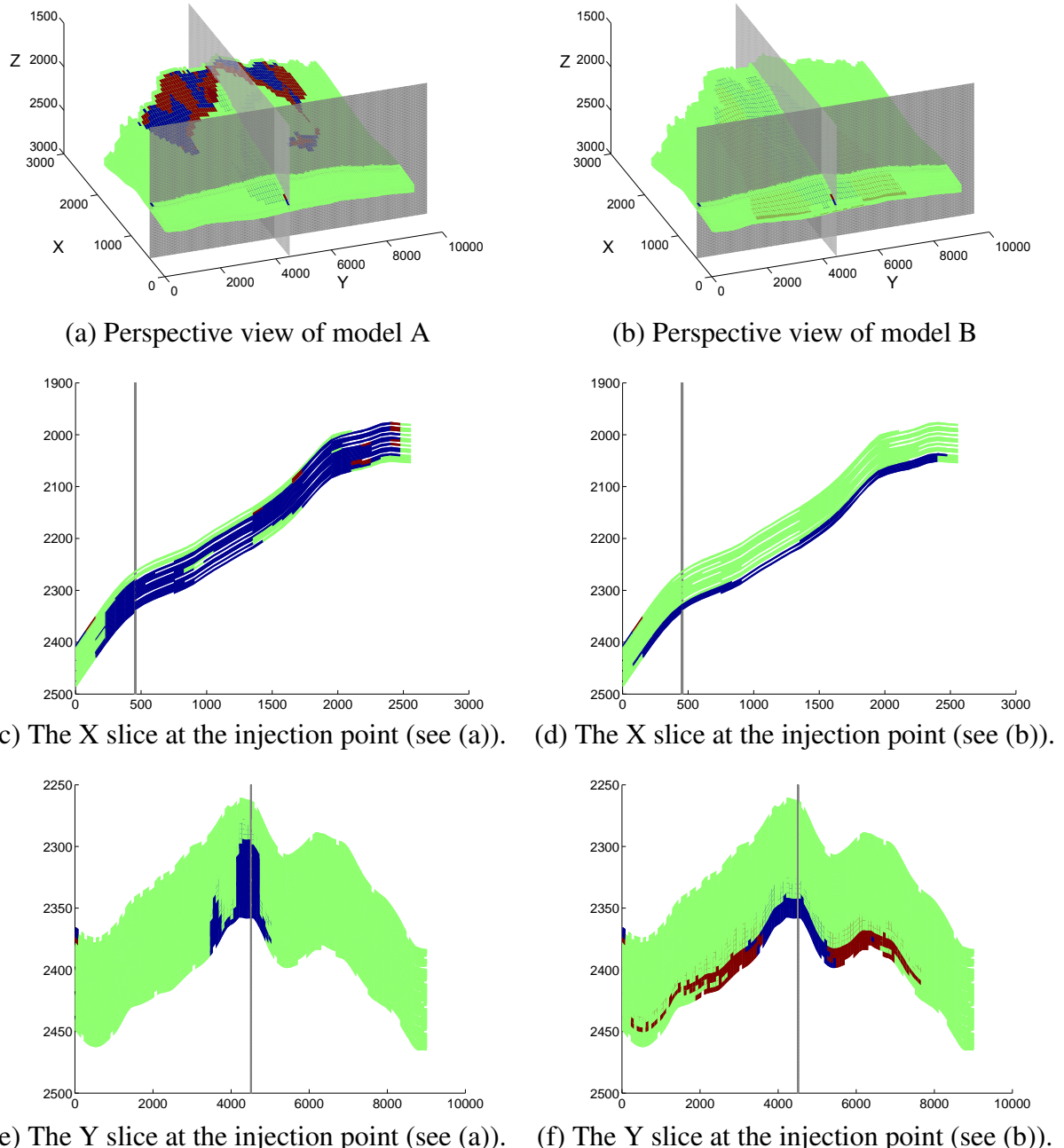


Figure 1.35: Flow sign in the Y direction at the end of injection for two selected cases. The left plots correspond to case A in Table 1.4, and the right plots belong to case B. Blue color corresponds to down-dip direction, red to up-dip direction, and green represents the stagnant fluid.

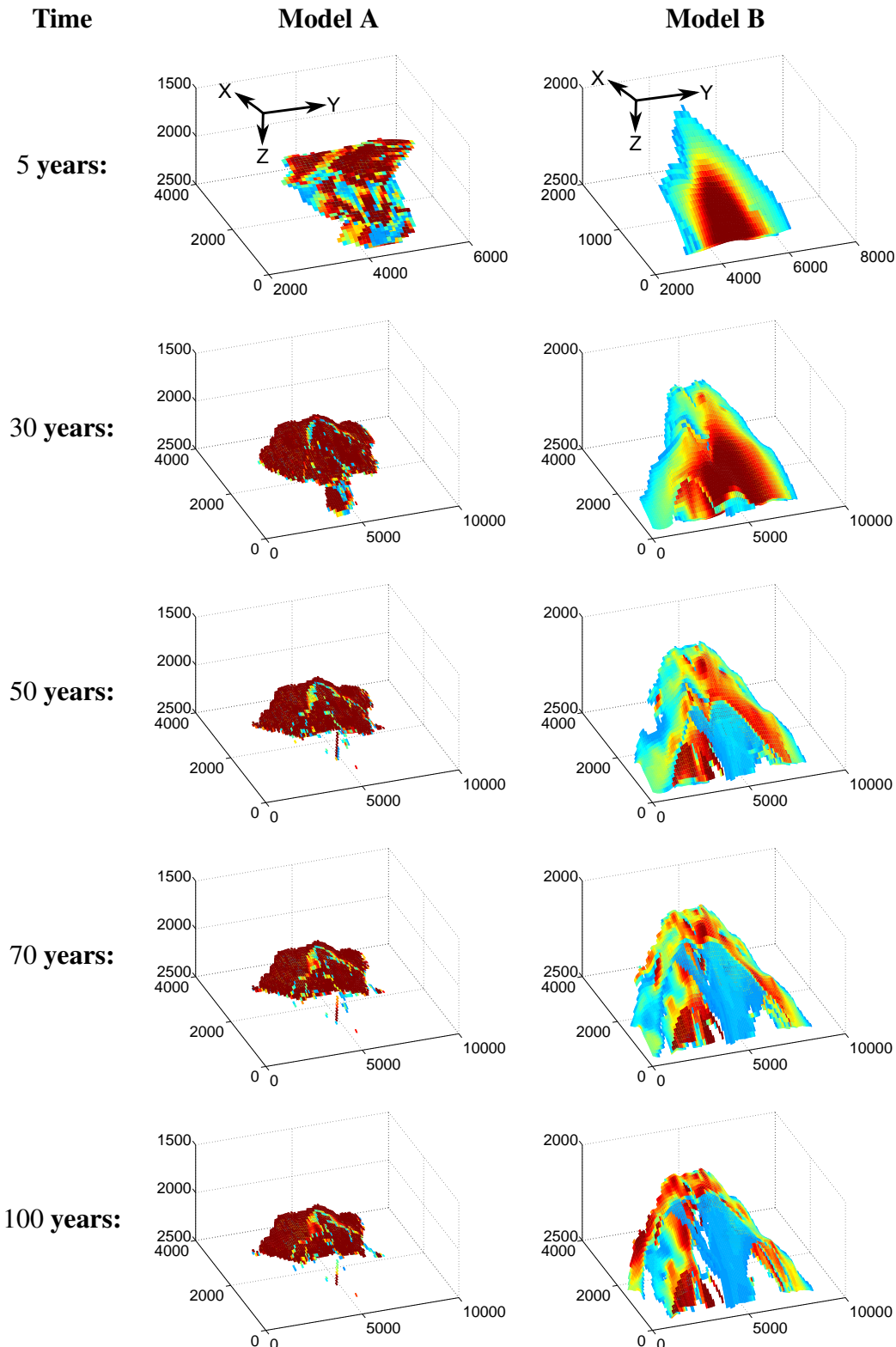


Figure 1.36: Mobile CO<sub>2</sub> distribution at different times for two selected cases. Cases A and B are described in Table 1.4. Compare with Figures 1.31 and 1.32 for transmissibility values in different directions. Colors represent the same ranges shown in Figure 1.34.

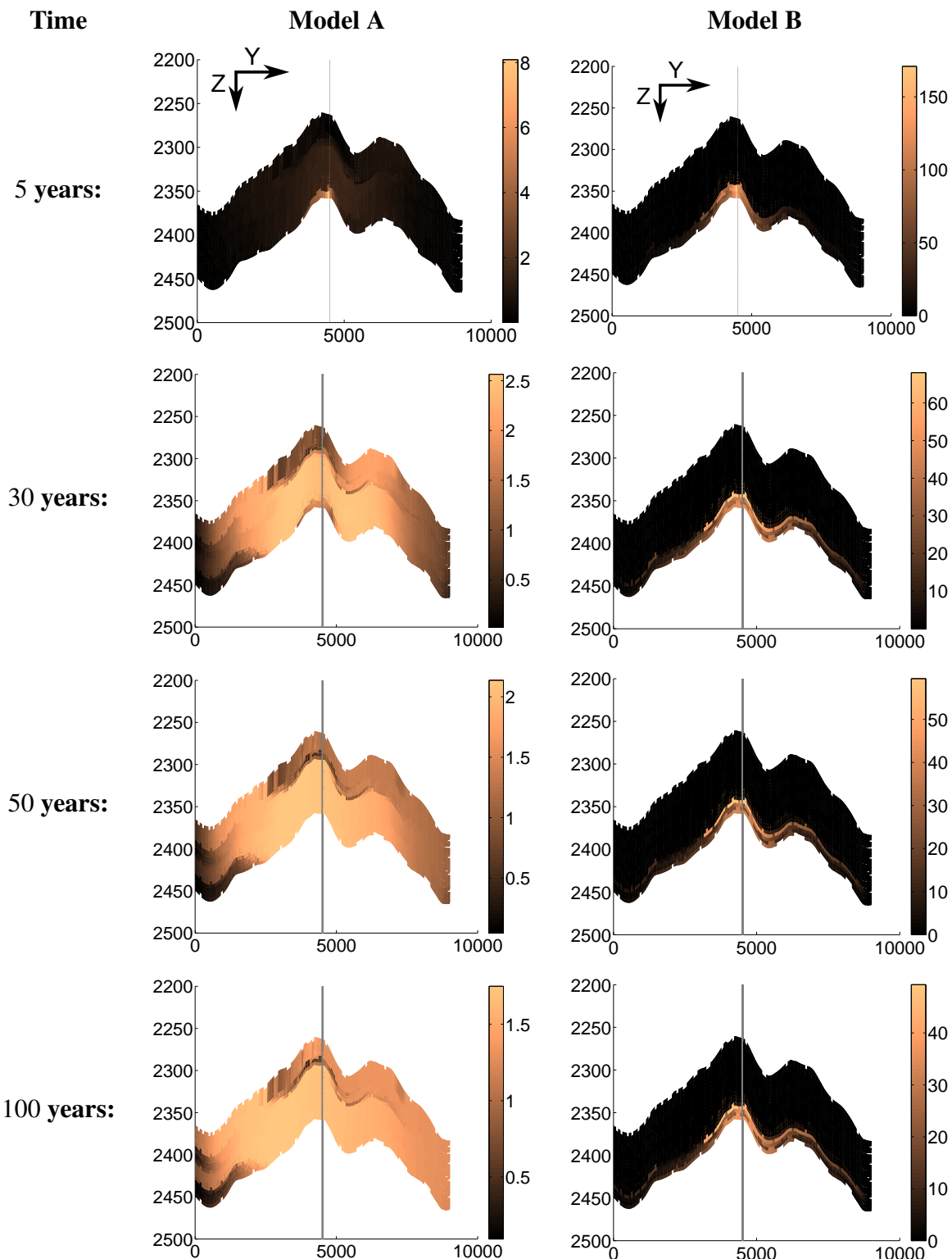


Figure 1.37: Pressure development during injection and early migration. Pressure differences from hydrostatic pressure are shown for two selected cases. Values are in bar. Cases A and B are described in Table 1.4. Compare with Figures 1.31 and 1.32 for transmissibility values in different directions.

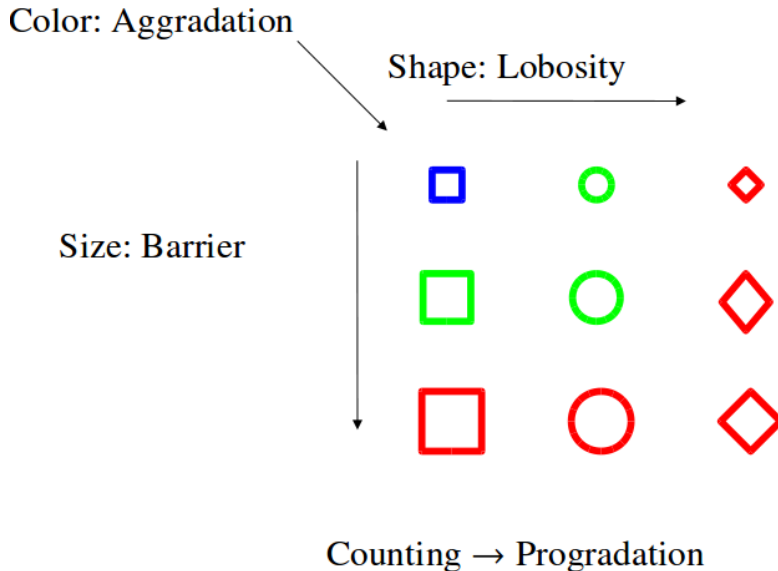


Figure 1.38: Marker codes used to plot the simulation results of all cases together. Aggradation is shown by different colors. Faults are shown by marker thickness; the thickest marker shows a case with close fault, medium thickness represents a case with open faults, and the thin markers indicate a case with no faults. All cases plotted in triples for the three degrees of faults. Therefore, plots contain 54 number of cases in the x-axis. The first 27 case numbers represent the up-dip progradation, and case numbers 28 to 54 have down-dip progradation.

INCLUDE keywords are printed here to improve the readability of the code. In the second INCLUDE we provide the pore volume multipliers for the cells on the boundary of the model. This is used to represent hydrostatic open boundaries for three sides of the model.

```
GRID
INCLUDE — Rock properties are included for each realization
'COORD.INC' / 'ZCORN.INC' / 'ACTNUM.INC' / 'NTG.INC' / 'PORO.INC' /
'PERMX.INC' / 'PERMY.INC' / 'PERMZ.INC' /
'MULTX.INC' / 'MULTY.INC' / 'MULTZ.INC' /
INCLUDE — Pore volume multipliers for the cells in the boundary
'MULTPV.INC' / —1e6 and 1e3 values are used in different parts of the boundary.
```

In the EDIT section, we provide the fault transmissibility multipliers for each faulted case.

```
EDIT
INCLUDE
'EDITNNC.INC' /
```

In the PROPS section the relative permeability data are provided in two sets of tables with two different endpoints for CO<sub>2</sub> to consider the hysteresis effect. In the SOLUTION section, we use the first table to initialize the model with 100% water everywhere, and in the SCHEDULE section we use the second table to consider the residual CO<sub>2</sub> in a drainage process followed by an imbibition. In the presented scenario, linear relative permeabilities are used. Another scenario contains quadratic relative permeabilities that are given to the model similarly. Zero capillary pressure is used here. PVT data for CO<sub>2</sub> (modeled by OIL) and water phases, fluid viscosities, densities, and the rock-fluid compressibility models are provided here.

```
PROPS
SWFN
— Sw      Krw      Pcow
  0.2     0.0      0
  1       1.0      0
```

```

/ —First table is used for time step zero
  0.2    0.0      0
  0.8    1.0      0
/ —Second table is used for the simulation
SOF2
— So   Kro
  0.000 0.0000
  0.800 1.0000
/ —First table is used for time step zero
  0.200 0.0000
  0.800 1.0000
/ —Second table is used for the simulation

PVTW —Water PVT model
  200.0  1.0  3.03E-06  0.4  0.0 /
PVDO — CO2 PVT model
  0.0    1.1    0.04
  400.0  0.95   0.04
/
ROCK —rock-fluid compressibility model
  400.0  0.30E-06 /
DENSITY —Phase densities
  700  1033  0.044/

```

In the REGIONS section we define different domains in the model. We specify the main domain that excludes the cells considered to represent the open boundaries. This is later used in the calculations of flow responses. Also, the saturation table is assigned here to be used in the initialization of the model as explained earlier.

```

REGIONS
INCLUDE
'LRGNS.INC'
SATNUM
96000*1/

```

The model is initialized here for the first time step by considering the hydrostatic equilibrium in the medium prior to CO<sub>2</sub> injection.

```

SOLUTION
— DATUMz Pi@DATUM WOC Pe@WOC GOC Pe@GOC
EQUIL
  2000     250     100      0      0      0      /

```

In the SUMMARY section we specify the output vectors to be used in our analysis.

```

SUMMARY
— FIELD DATA
FPR
FOIP
FWIP
— REGION DATA
ROIP
/
RWIP
/
RWSAT
/
RPR
/
— WELL DATA
WBHP
/
WOIR
/
WVIR

```

/

Finally, in the main part of the model, we define the simulation scenario by providing the injector completion specifications and injection plan for the well. Here we see the SCHEDULE section that is considered for fixed injection rate over 30 years, followed by 70 years of early migration.

```
SCHEDULE
SATNUM —The second saturation table is assigned here to consider the hysteresis effects.
96000*2/
WELSPCS —Well drilling information
'I' 'G' 6 60 1* 'OIL' /
/
COMPDAT —Well completion information
'I' 6 60 17 20 'OPEN' 0 .0 0.1/
/
WCONINJE —Well injection plan
'I' 'OIL' 'OPEN' 'RESV' 1* 3650.0 /
/
RPTRST
BASIC = 3 FREQ=1 FLOWS / — FLOWS produces cell flux values for three directions.
TSTEP
0.1/
TSTEP
120*90 /
WCONINJE —Well is shut-in after 30 years
'I' 'OIL' 'SHUT' 'RESV' 1* 0.0 /
/
TSTEP
280*90 /
END
```

In the other scenario we control the well by pressure constraint and we continue the injection until the aimed total CO<sub>2</sub> volume is injected in the aquifer, or the simulation time reaches 100 years:

```
SCHEDULE
SATNUM —The second saturation table is assigned here to consider the hysteresis effects.
96000*2/
WELSPCS —Well drilling information
'I' 'G' 6 60 1* 'OIL' /
/
COMPDAT —Well completion information
'I' 6 60 17 20 'OPEN' 3 .0 0.1/
/
WCONINJE —The injector is set to inject conditioned by a pressure lower than 400 bar
'I' 'OIL' 'OPEN' 'RESV' 1* 3650.0 400/
/
RPTRST
BASIC = 3 FREQ=8 FLOWS /
ACTION —Stop the well as soon as the total injected volume is 40000000 m3
STPINJ FOIT > 40000000 /
WCONINJE
'I' 'OIL' 'SHUT' 'RESV' 1* 0.0 /
/
ENDACTIO
TSTEP
0.1/
TSTEP —The simulation continues for a total 100 years
120*90 /
RPTRST
BASIC=3 FREQ=8/
TSTEP
280*90 /
END
```

We used a similar approach to the first scenario presented here with small modifications for the stochastic analysis that we will introduce in the next section.

## 1.9 Sensitivity and risk analysis

The process of developing mathematical models to approximate the injected CO<sub>2</sub> in the storage sites consist of several steps. This includes the determination of most influential parameters on the model outputs. Sensitivity analysis can serve as a guide to any further use of the model.

In the initial sensitivity analysis performed on geological uncertain parameters of our studies, we use a large number of detailed flow simulations and measure the variability of model responses with respect to each level of the uncertain parameters.

We can obtain histograms of response  $\Gamma$  for three different levels of parameter  $\alpha$  (i.e., low, medium, and high) by performing simulations over all geological realizations. Measuring the mean response value on each histogram results in an average for all cases with a fixed level for parameter  $\alpha$ . With three average points for low, medium, and high levels of parameter  $\alpha$ , a line can be fitted to those points that approximates the trend of variations of response  $\Gamma$  versus the increase in values of parameter  $\alpha$ .

With an equal probability for each level, the model output variations are examined by looking at each response at two important simulation times, i.e., end of injection and end of simulation. We need a fast flow modeler to assess the uncertainty with input variations over a relatively high resolution. We use a response surface method that is explained in the next section in details.

### 1.9.1 Stochastic analysis

Phenomenon for which variables are uncertain can be modeled as a stochastic process. Uncertainty reduction in different parts of the modeling requires a better understanding and description of input parameters and dependency rules within the system. Parameters can be ranked for their influence on the model output. To know the most influential parameters helps in treating the stochastic nature of the process. Sensitivity analysis serves in identification and evaluation of important model parameters.

As discussed in the earlier sections, various sources of uncertainties are embedded within CO<sub>2</sub> storage modeling and operations. The focus of our research has been on geological uncertainty and its consequences. The procedure used here to identify the relative importance of uncertain geological parameters via sensitivity analysis and the corresponding risk assessment is a general work-flow that can be applied to any type of uncertainties in the model inputs.

### 1.9.2 Arbitrary polynomial chaos expansion

Our research continues by employing stochastic response surface method that approximates the flow responses by projecting them on high-dimensional polynomials. In particular, we use arbitrary polynomial chaos (aPC) expansions, which consists of orthogonal polynomial basis that are constructed according to the uncertainties in the input parameters. The approach is flexible with respect to the quantification of probabilities for uncertain parameters and can be applied in studies with limited knowledge of probabilities.

The reduced model approximated by aPC is considerably faster than the original detailed one, thus provides a promising start point for global sensitivity analysis and probabilistic risk assessment. Variance-based global-sensitivity analysis methods have shown success in non-linear and complex problems [59]. The system can be decomposed into approximating functions of input parameters, and this makes it easy to implement methods based on variance. The bottleneck of variance-based approaches can be their computational costs. In our case, the variance in output responses can be set equal to the variance of polynomial components calculated for each input parameter. Polynomials are inexpensive to evaluate compared with full simulation. This makes it efficient to implement a variance based sensitivity analysis using polynomial approximation. Furthermore, the approach has been significantly simplified by the fact that the polynomial properties of the response surface are known. The speed of polynomial approximation makes it feasible to perform an intensive probabilistic risk assessment via a Monte Carlo process over a high-resolution input variation.

Statistical accuracy of a Monte Carlo process is highly sensitive to the resolution of variational inputs. The response surface method assisting the Monte Carlo procedure must be constructed on a dense Cartesian grid, which will be computationally demanding. As a result, we explore an alternative method, which is a polynomial chaos expansion (PCE). This method only requires a minimum number of model evaluations to construct the approximating response surface. The approach we use is based on the aPC as described in [55]. The main idea is to construct the approximating response surface by projecting the response on orthogonal polynomial basis within the uncertain parameter space. Therefore, uncertainty in input parameters is involved in the process from the initial steps of the work-flow. This approach is an advanced statistical regression method that offers an efficient and accurate way of including nonlinear effects in stochastic analysis [23, 27, 73]. One attractive feature of PCE is the high-order approximation of error propagation as well as its computational speed [56] when compared to Monte Carlo processes.

Earlier PCE techniques put the restriction of specified types of uncertainty distribution functions to be used in the work-flow. In contrast, the arbitrary polynomial chaos (aPC) is flexible enough to accommodate a wide range of data distribution [55]. The aPC can even work in cases with limited uncertainty information reduced to a few statistical moments of samples. They can be specified either analytically as probability density, or cumulative distribution functions, numerically as histograms, or as raw data sets. In terms of performance, the aPC approach shows an improved convergence when applied to input distributions that fall outside the range of classical PCE.

In general, an approximation of system response  $\Gamma$  can be written as a function of uncertain input parameters  $\Theta$ :

$$\Gamma \approx \Upsilon(\Theta). \quad (1.51)$$

Uncertainty of input parameters  $\Theta$  can be represented by mapping  $h$  from random variable space  $\xi$  to random input space  $\Theta$

$$\Theta = h(\xi). \quad (1.52)$$

As discussed earlier,  $h$  can have an analytical or numerical representation.

The response of the system can be expanded into the space of approximating polynomial basis. This expression is specified by constant coefficients  $c_i$ :

$$\Gamma \approx \sum_{i=1}^{n_c} c_i \Pi_i(\Theta). \quad (1.53)$$

Here,  $n_c$  is the number of expansion terms,  $c_i$  are the expansion coefficients, and  $\Pi_i$  are the multi-dimensional polynomials for the variables  $\Theta = [\theta_1, \dots, \theta_n]$ . The number  $n_c$  of unknown coefficients  $c_i$  depends on the degree  $d$  of the approximating polynomial, and the number of considered parameters  $n$ :

$$n_c = \frac{(d+n)!}{d! \times n!}. \quad (1.54)$$

For simplicity, we proceed with describing the procedure for one dimensional orthogonal basis. The high-dimensional basis can be obtained using tensor products on one-dimensional basis. Therefore, we consider the polynomial  $P^{(k)}$  of degree  $k$  in the random variable  $\theta$ :

$$P^{(k)}(\theta) = \sum_{j=0}^k p_j^{(k)} \theta^j. \quad (1.55)$$

where  $k$  can vary between 0 and  $d$ . Polynomials  $P^{(k)}$  are orthogonal, if every pair of them fulfill the following condition:

$$\int_{I \in \Omega} P^{(l)} P^{(m)} d\tau(\theta) = \delta_{lm}, \quad (1.56)$$

where  $\delta$  is the Kronecker delta function and  $\tau$  is the measure for input variable space. If we modify the polynomials  $P^{(k)}$  such that the coefficient of leading terms with the highest degree becomes one (i.e.,  $p_k^{(k)} = 1$ ), the orthogonal polynomial basis satisfying Equation (1.56) can be obtained from the solution of the following linear system of equations [55]:

$$\begin{bmatrix} \mu_0 & \mu_1 & \dots & \mu_k \\ \mu_1 & \mu_2 & \dots & \mu_{k+1} \\ \dots & \dots & \dots & \dots \\ \mu_{k-1} & \mu_k & \dots & \mu_{2k-1} \\ 0 & 0 & \dots & 1 \end{bmatrix} \begin{bmatrix} P_0^{(k)} \\ P_1^{(k)} \\ \dots \\ P_{k-1}^{(k)} \\ P_k^{(k)} \end{bmatrix} = \begin{bmatrix} 0 \\ 0 \\ \dots \\ 0 \\ 1 \end{bmatrix}. \quad (1.57)$$

Here,  $\mu_k$  is the  $k^{\text{th}}$  non-central (raw) statistical moment of the random input variable, which is defined as:

$$\mu_k = \int_{\theta \in \Omega} \theta^k d\tau(\theta). \quad (1.58)$$

Thus, arbitrary polynomial chaos expansion based on Equation 1.57 only demands the existence of a finite number of moments, and does not require the exact knowledge or even existence of probability density functions. If the moments of  $\theta$  are evaluated directly from a data set of limited size or from a discrete probability distribution featuring a finite number of possible outcomes, there need to be  $k$  or more distinct values in the data set or distribution. An interesting aspect is that only moments up to twice the order of the expansion are important. This means that there is no need for any kind of assumption for data probability distribution leading to subjectivity artifacts as discussed earlier.

The PCE techniques are divided into intrusive [30, 49, 70] and non-intrusive [41, 43, 44, 56] approaches. Intrusive techniques require modification of the system of governing equations (e.g., the flow model system). In some cases, this can end up in semi-analytical methods that are used for simpler stochastic analysis studies (e.g., stochastic Galerkin method). However, the intrusive approaches can be very complex and analytically cumbersome and cannot be implemented for industrial applications. In contrast to intrusive techniques, the non-intrusive methods are vastly used in practical studies. These methods do not require any symbolic manipulations of the governing equations. The sparse quadrature and the probabilistic collocation method (PCM, [44, 56]) are among the non-intrusive techniques. In a simple sense, PCM can be considered as a mathematically optimized interpolation of model output for various parameter sets. The polynomial interpolation is based on minimal model evaluations in an optimally chosen set of parameter locations that are called collocation points. Hence, the challenge in these techniques is to find a balance between accuracy and speed to evaluate the uncertainty in the physical processes.

The collocation formulation has the advantage of treating the model as a black-box. This formulation requires the corresponding output to be known in the collocation set of input parameters.

According to [69], the optimal choice of collocation points corresponds to the roots of the polynomial of one degree higher ( $d + 1$ ) than the order used in the chaos expansion ( $d$ ). This strategy is based on the theory of Gaussian integration (e.g., [1]).

For multi-parameter analysis, the full tensor grid of available points from the original integration rule is  $(d + 1)^n$ , which is larger than the necessary number  $M$  of collocation points. This might be used for low-order (1<sup>st</sup>, 2<sup>nd</sup>) analysis of limited number of parameters. However, for a large number of parameters and high order of polynomial approximations, the full grid becomes computationally cumbersome. In the collocation approach, the minimal set of points is chosen from the most probable regions based on the parameter uncertainty information (See [44, 55, 56]).

We implement the probabilistic collocation method for computing the coefficients  $c_i$  in Equation 1.53. The weighted-residual method in the random space is defined as [44]:

$$\int \left[ \Gamma - \sum_{i=1}^{n_c} c_i \Pi_i(\Theta) w(\Theta) p(\Theta) \right] d\tau = 0, \quad (1.59)$$

where  $w(\Theta)$  is the weighting function and  $p(\Theta)$  is the joint probability density function of  $\Theta$ . By substituting the weight function in Equation 1.59 with Delta function, the equation reduces to

$$\Gamma_c - \sum_{i=1}^{n_c} c_i \Pi_i(\Theta_c) = 0. \quad (1.60)$$

In this equation,  $\Gamma_c$  and  $\Theta_c$  are the responses and input parameters in the collocation points. If we have  $\Theta_c$  chosen based on the probability distribution of input parameters, and  $\Gamma_c$  from the minimal model evaluations on  $\Theta_c$ , we can solve Equation 1.60 and find the coefficients  $c_i$ .

### 1.9.3 Sensitivity analysis

Sensitivity analysis helps in understanding the degree of dependency of system responses to input parameters. When the value of the input parameters is uncertain, the model prediction will consist of uncertainties that must be eliminated for a robust and precise prediction. Therefore, sensitivity analysis can be useful both in optimizing the system performance and in studying the variation in performance coming from the stochastic nature of the system.

Global sensitivity analysis covers the entire variational space for uncertain parameters, while other methods, like the gradient-based methods, are limited to the parameters' scope of influence.

Variance-based methods are very popular among different types of sensitivity analysis methods. Variance-based methods provide global sensitivity and are suitable for general non-linear problems. When the response is decomposed into simpler components (for instance, polynomial basis), it is easier to decompose the unconditional variance in the output into terms due to individual parameters and the interaction between them. It is possible then to rank the input parameters based on their contribution to the output variance [59, 63].

Following the linear sensitivity analysis initially performed in the study about the extensive detailed simulations, we tackle the global sensitivity analysis based on the aPC technique. This approach is well described in [55, 57]. Morris method [52] considers a uniform importance of input parameters within predefined intervals. We use a weighted global sensitivity in a more flexible approach accounting for arbitrary bounds and parameters with different importance defined by weighting functions. The big advantage of aPC-based sensitivity method is its low computational costs for obtaining global sensitivity analysis. The aPC based-method places the parameter sets for model evaluation at optimized spacing in parameter space. This can be interpreted as fitting polynomials to the model response. These polynomials approximate the model over the entire parameter space in weighted least-square sense. This is beneficial to compute tangent or local second derivatives (compare FORM, SORM methods, e.g., [42]) that approximate the model well just around one point in the parameter space.

As an advantage, in variance based methods one can work with arbitrary system as a black-box and perform the calculations based on inputs and outputs only. More recent works are concerned about expediting calculation pace [16, 55, 57]. The idea is to replace the system with an approximating function which gives benefits in sensitivity calculations, because it is easy to relate the output variances to the input variables.

We expand the variance of output solution into components. Assume that we break the system output into components:

$$\Gamma = \Gamma_0 + \sum_i \Gamma_i + \sum_{i < j} \Gamma_{ij} + \dots \quad (1.61)$$

A single index shows dependency to a specific input variable, whereas more than one index shows interaction of input variables. If we consider input vector  $\Theta$  to be of  $n$  components  $\theta_i$  for  $i = 1, \dots, n$ , then  $\Gamma_i = f_i(\theta_i)$  and  $\Gamma_{ij} = f_{ij}(\theta_i, \theta_j)$ . In practice, we consider a finite number of terms in Equation (1.61). The first order sensitivity index, so called Sobol index, is defined as follows [63]:

$$S_i = \frac{V[E(\Gamma | \theta_i)]}{V(\Gamma)}, \quad (1.62)$$

where  $E(\Gamma | \theta_i)$  is the conditional expectation of output  $\Gamma$  given  $\theta_i$  and  $V$  is the variance operator. Since  $\theta_i$  can be fixed at any value in its uncertainty interval, each of those values produce a distinct expectation  $E(\Gamma | \theta_i)$ . Equation 1.62 is a measure for variation of these expectations, which indicates the direct contribution of parameter  $\theta_i$  in the output variance. For more than one index, a higher-order Sobol index can be defined as:

$$S_{ij} = \frac{V[E(\Gamma | \theta_i, \theta_j)] - V[E(\Gamma | \theta_i)] - V[E(\Gamma | \theta_j)]}{V(\Gamma)}. \quad (1.63)$$

Here,  $V[E(\Gamma | \theta_i, \theta_j)]$  is the variance of output expectations after fixing  $\theta_i$  and  $\theta_j$ . This index represents significance of variation in output generated from uncertainty in input variables together, i.e., the interaction of uncertain parameters. If we add all indices that contain variable  $\theta_i$ , the sum is called the total Sobol index:

$$S_{Ti} = S_i + \sum_{j \neq i} S_{ij} + \sum_{j \neq i} \sum_{k \neq i} S_{ijk} + \dots \quad (1.64)$$

To clarify the subject, we go through a simple analytical example given in [4]. Suppose that the exact expression for response  $\Gamma$  is known and can be written as a polynomial with parameters  $\theta_1$ ,  $\theta_2$ , and  $\theta_3$ :

$$\Gamma(\theta_1, \theta_2, \theta_3) = \theta_1^2 + \theta_2^4 + \theta_1 \theta_2 + \theta_2 \theta_3^4. \quad (1.65)$$

The Sobol indices can be calculated from functions  $F$  that are defined based on orthogonality condition used to decompose the solution and for  $n$ -dimensional input with Gaussian distribution  $\Phi_n$  in uncertainty domain  $R^n$ . They are as follows:

$$F_0 = \int_{R^n} \Gamma(\Theta) \Phi_n(\Theta) d\Theta, \quad (1.66)$$

$$F_i = \frac{\int_{R^{n-1}} \Gamma|_{\theta_i} \Phi_{n-1}(\theta_{\sim i}) d\theta_{\sim i}}{\Phi_1(\theta_i)} - F_0, \quad (1.67)$$

$$F_{i,j} = \frac{\int_{R^{n-2}} \Gamma|_{\theta_i, \theta_j} \Phi_{n-2}(\theta_{\sim i}, \theta_{\sim j}) d\theta_{\sim i} d\theta_{\sim j}}{\Phi_2(\theta_i, \theta_j)} - F_0 - F_i(\theta_i) - F_j(\theta_j). \quad (1.68)$$

$\Gamma|_{\theta_i}$  and  $\Gamma|_{\theta_i, \theta_j}$  are the  $\Gamma$  values at fixed  $\theta_i$  and  $\{\theta_i, \theta_j\}$  respectively.  $\theta_{\sim i}$  is the vector of dummy variables corresponding to all but the component  $\theta_i$  of uncertain parameters  $\Theta$ .

Let us denote the variances by  $D$ :

$$D = V[F(\Theta)] = \int_{R^n} F^2(\Theta) d\Theta - F_0^2, \quad (1.69)$$

that can be decomposed into:

$$D_i = \int_{R^1} F_i^2(\theta_i) d\theta_i, \quad (1.70)$$

and

$$D_{i,j} = \int_{R^2} F_{i,j}^2(\theta_i, \theta_j) d\theta_i d\theta_j. \quad (1.71)$$

Then the Sobol indices can be found from:

$$S_i = \frac{D_i}{D}, \quad (1.72)$$

$$S_{i,j} = \frac{D_{i,j}}{D}. \quad (1.73)$$

Finally, the total Sobol index can be found from Equation 1.64. When we perform the calculations of Equations 1.66 to 1.71 for our example (i.e., the expression in Equation 1.65) we can obtain the following Sobol indices, assuming Gaussian distributions for the parameters over the interval  $[0, 1]$ :

$$\begin{aligned} S_1 &= 0.0005 & S_2 &= 0.4281 & S_3 &= 0.0000 \\ S_{12} &= 0.0007 & S_{13} &= 0.0000 & S_{23} &= 0.5708 \\ S_{123} &= 0.0000 \end{aligned}$$

and the total sobol indices are:

$$S_{T1} = 0.0012 \quad S_{T2} = 0.9996 \quad S_{T3} = 0.5708 .$$

The total Sobol index can be used as a sensitivity measure to rank parameters for their influence on the results variation. In this example, we can see the ranking that the total Sobol indices suggests is consistent with what can be inferred directly from the simple expression in Equation 1.65:  $\theta_2$  is the most influential parameter, because it appears in three terms, and in one of them with a forth degree. Interactions are represented by two indices, and  $S_{13}$  is zero, because there exist no term in Equation 1.65 that contains both  $\theta_1$  and  $\theta_3$ .

With known polynomial coefficients, Sobol indices are easy to calculate. When the number of parameters is large, it is possible to do initial sensitivity analysis with lower degree polynomial to filter out pertinent parameters. Then the analysis continues on the filtered parameters with a higher degree polynomial approximation.

#### 1.9.4 Risk analysis

The risk is the impact of uncertainty on objectives. Quantifying the risk requires calculating this impact, which consist of two parts: quantification of the uncertainty and evaluation of the system consequences. Risk  $R$  of a process is quantitatively defined as the consequence  $C$  caused by the process multiplied by the probability  $P$  of that consequence to happen:

$$R = P \times C. \quad (1.74)$$

In the case of CO<sub>2</sub> injection into deep aquifers, the amount of CO<sub>2</sub> which stays mobile and undissolved in the medium for a time after injection can be considered as a consequence, bearing the potential of leakage up to the surface if exposed to a geological leakage point. The risk could be the expected amount of CO<sub>2</sub> that will leak through ill-plugged abandoned wells or cracks in the sealing rocks.

We consider looking at responses and the probability of them to happen. We initially examine this probability by drawing the histogram of response values obtained from detailed simulations on large number of realizations at end of injection and end of simulation. Yet larger number of points in the uncertain parameter space are studied employing the data-driven aPC method, which requires a considerably shorter time for evaluating the responses than what takes for a full simulation. This way it is possible to perform an intensive Monte Carlo process in a full tensor grid of input parameter variational space, resulting in a high resolution output probability distribution.

## 1.10 General summary

The work objectives were as follows:

- Assessing the significance of geological modeling in early stages of CO<sub>2</sub> storage operations.
- Applying a mathematical tool to perform global sensitivity analysis and probabilistic risk assessment for geological CO<sub>2</sub> storage.
- Introducing a framework for extensive realistic sensitivity analysis and risk assessment of geological CO<sub>2</sub> storage.

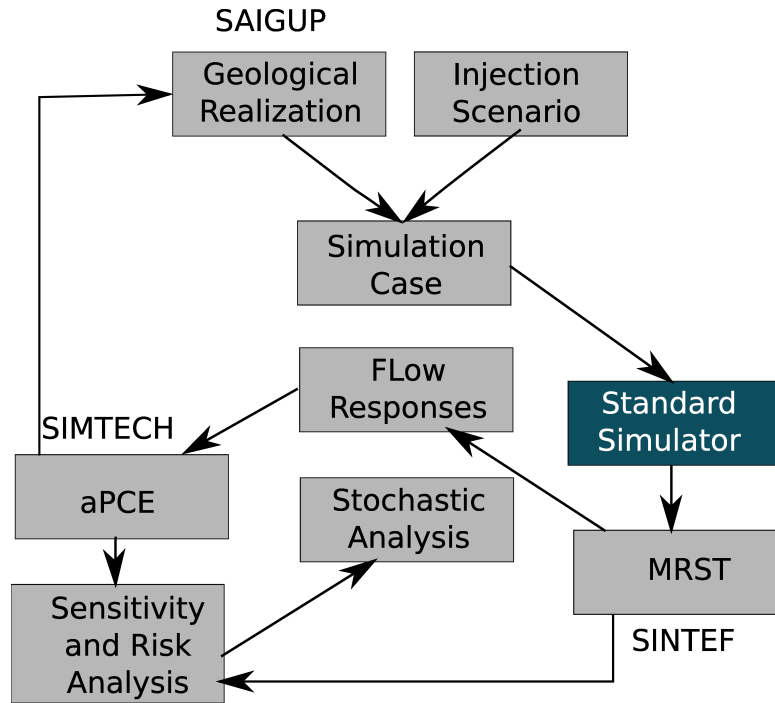


Figure 1.39: Flowchart of workflow implemented in an automated procedure.

The significance of geological uncertainty is examined through an extensive study of CO<sub>2</sub> flow in different geological models. Sensitivity analysis and risk assessment provided a ranking of the studied geological parameters for various flow responses in the chosen medium. The workflow implemented in this study is a stepwise procedure that can be generalized for use in any similar large-scale analysis.

### 1.10.1 Implementation of the work-flow

This thesis incorporated working with a large number of realizations, various flow scenarios, and different procedures and software. While the study was in progress, new ideas and challenges required the manipulation of new steps in the workflow. To achieve the defined goals of the research, an automated workflow was designed that connected different parts of the study. This enhanced the efficiency of performing necessary modifications to the workflow.

The MATLAB programming language is used for implementing the workflow in this research. The main reason for this choice, apart from the rich facilities available within the MATLAB toolboxes, is to utilize the numerous functions within the MATLAB Reservoir Simulation Toolbox (MRST) that is available as free and open-source software. For flow simulations, commercial software is used, which is a standard simulator for the oil and gas industry and research.

Figure 1.39 shows the workflow elements implemented using numerous MATLAB functions. Functions from MRST at SINTEF and the stochastic tools from the SIMTECH group at Stuttgart University are utilized and merged into the workflow. The workflow design is constructed to be flexible and general. Some research at SINTEF has been performed by replacing the commercial simulator with in-house simulators. However, the main study is performed using a commercial standard simulator.

### 1.10.2 Generic application of results

We rank the most influential geological parameters for early stages of CO<sub>2</sub> storage operations. The demonstrated workflow can be used in any study concerning the site selection and early stages of geological CO<sub>2</sub> storage. However, there are some limitations in our presentation of the workflow that must be considered when this work is applied in similar studies.

The first limitation is the SAIGUP model size. CO<sub>2</sub> storage studies require large models that can cover the CO<sub>2</sub> spatial traveling extent within the aquifer. Therefore, our study is limited to the domain around the injector.

An over-pressurized injection can introduce breakings in the sealing cap-rock that is used for structural CO<sub>2</sub> trapping. It is more feasible to use a minimum number of wells to minimize the project costs and the risk of CO<sub>2</sub> leakage through abandoned wells. Therefore, a typical injection scenario includes a few injectors with no production well to balance the injection pressure. The elliptic nature of the pressure equation and the small compressibility of the medium produce a large area influenced by the injection pressure. Therefore, pressure-related studies require a large model domain to study the effect of the impulse imposed by the injector on the entire region connected to the impulse.

To overcome this limitation in the SAIGUP models, we exaggerated the cell volumes at the model boundaries that are supposed to be open. The large pore volumes on the boundaries avoid extreme pressure build-up caused by injecting into a closed system. However, the study is limited to the region near the well. Because the high pressures occur near the injector, it is more interesting to study pressure build-up around the well rather than examining the entire region influenced by the injection pressure.

The pressure behavior is very sensitive to the way the boundaries are defined. In reality, there are different aquifer systems. Some aquifers are large with very large pore volumes. To model these aquifers, we can use smaller model domains with open boundaries. However, some aquifers are medium and small in size. To model these aquifers, we can assume semi-closed and closed boundaries. For any aquifer system, we can define the boundary by exaggerating the pore volume of the cells along the model boundaries. The transmissibilities of the boundary cells can also be modified to represent the size of the aquifer system, controlling the amount of pressure relaxation in the medium through the boundaries. If CO<sub>2</sub> exists in the boundaries, relative permeability function at the boundary can be modified in addition to the transmissibilities.

The open boundaries in our study are considered completely open. This assumption allows pressure to relax through the boundaries. However, the results of our pressure study are influenced by this choice. While we have observed many cases with extreme pressures due to heterogeneity effects, the pressures reported in our study are moderate compared to partially closed boundaries. The sensitivity analysis is based on comparing the pressure values of the different cases. Therefore, the outcome of the sensitivity analysis should be valid regardless of the boundary choices. The size limitation in the SAIGUP models resulted in an extension to the current study, which is called IGEMS [67].

The IGEMS models are larger compared to the SAIGUP models. There is only one major structural trap in the SAIGUP models that allows for most of the injected CO<sub>2</sub> to accumulate under the cap-rock. This is not sufficient for studying the effect of variations in the top-surface topography on CO<sub>2</sub> movement in the medium. The IGEMS study has focused on the structural trapping due to deformations in the top-surface morphology and faults. The results show that structural trapping can be important in controlling the extent of CO<sub>2</sub> storage due to structural trapping and controlling the speed of the plume migrating under the top sealing cap-rock.

In the vertical direction, the SAIGUP models can be improved with a higher grid resolution. Variations in the vertical direction exist at considerably smaller scales than in the horizontal. In particular, this is more important for the long-term CO<sub>2</sub> migration in which a thin plume of CO<sub>2</sub> migrates beneath a sealing layer due to buoyancy forces.

Another issue to be mentioned is the geological uncertainty assumption used in the stochastic analysis. We consider nearly uniform distributions for the probabilities of uncertain parameter values. While there is no loss of generality, there are two comments that could improve our analysis:

- In general, the uncertainty probability may not directly follow a uniform distribution. Actually, this information is very case dependent and can change from one location to another.
- One advantage of the aPC method is its flexibility to be applied for arbitrary forms of uncertainty data. Choosing various distributions for the geological parameters would better demonstrate the strength of the aPC method.

Because we are limited to the SAIGUP models that are based on equally probable values for the geological parameters, uniform uncertainty distributions are chosen. A general stochastic process using the aPC must be considered in the following steps:

- Use the techniques from the aPC method to derive appropriate sample points for the geological parameters.
- Construct geological models at these sample points.
- Perform flow simulations for each sample point.
- Construct the proxy model.
- Perform global sensitivity analysis using the Sobol indexes method and the proxy model.
- Perform the Monte Carlo simulations using the aPC study to assess the uncertainty and risk.

The link between designing geological realizations and the implementation of the aPCE method is depicted in Figure 1.39. The sensitivity analysis and risk assessment procedure must start from the 'aPCE' box in Figure 1.39. The collocation points from the given geological uncertainty are first found, and then, based on those collocation points, we design the geological realizations. However, due to the availability of a large set of SAIGUP realizations generated before this study, our starting point was from the 'Geological Realization' box in Figure 1.39. This change resulted in assuming a given geological uncertainty knowledge that suits the SAIGUP geological design. Nevertheless, we practice the procedure in a geological modeling and flow analysis scope that is novel and can be consulted for further extensive studies.

## **Chapter 2**

**Introduction to the papers**

## 2.1 Introduction

The main scientific part of this thesis consists of three papers. They come in a sequence to show the research progress within this PhD program. Paper I includes a detailed study of how variations in geological parameters impact the evolution of the injected CO<sub>2</sub> plume. Knowing the migration path of the plume is essential if one wants to assess the risk for CO<sub>2</sub> leaving the aquifer through imperfections in the caprock or through open lateral boundaries. Second, to determine the feasibility of the injection process and reduce the potential for introducing fracturing during the injection process, it is crucial to know the pressure buildup. Likewise, it is important to know how far pressure pulses induced during injection propagate beyond the zones invaded by the injected CO<sub>2</sub>. Therefore, a special study is dedicated to pressure analysis in the system. This is reported in Paper II, which is submitted to the International Journal of Greenhouse Gas Control (IJGGC). Finally, Paper III reports modern stochastic techniques used to perform detailed quantitative sensitivity analysis and probabilistic risk assessments. This paper is accepted for publication in the IJGGC. This paper was submitted for publication earlier than the second paper.

## 2.2 Summary of papers

**Paper I:** *Impact of geological heterogeneity on early-stage CO<sub>2</sub> plume migration: CO<sub>2</sub> spatial distribution sensitivity study*

### Summary:

We use a set of SAIGUP realizations selected to cover the variability of five sedimentological and structural geological parameters. The selected parameters are lobosity, barriers, aggradation angle, progradation direction, and faults. Each of these parameters varies over three levels, except the progradation direction, which includes up-dip and down-dip directions. Combining the available parameters makes 162 realizations. However, two cases were missing in the original setup. Therefor, 160 geological realizations are used here.

30 years of injection and 70 years of early migration of CO<sub>2</sub> are simulated and flow responses related to the storage capacity and leakage risk objectives are defined and calculated from the simulation results. The responses are reported in scatter plots at the end of injection and at the end of early migration time.

This work is specific in examining how heterogeneity influences flow behavior by using a number of geological realizations. Flow responses defined in this work are specific to CO<sub>2</sub> studies and differ from the responses used in the original SAIGUP project to study oil recovery. We simulate the aquifer average pressure, residual and mobile CO<sub>2</sub> saturation, and spatial distribution of connected CO<sub>2</sub> volumes. These responses can be considered to evaluate the site storage capacity and risk of CO<sub>2</sub> leakage to surface.

The injector is controlled by a constant rate and no pressure constraint is set to allow for all ranges of pressure, including those that are unrealistic. Moreover, we define an additional model output that is related to the risk of CO<sub>2</sub> leakage through any breakings in the cap-rock.

Finally, we perform a quantitative sensitivity analysis by using the flow simulation results. The sensitivity analysis results suggest that aggradation angle, fault criteria, and progradation direction are the most influential geological parameter in our study.

In this work, we clearly see the range of variations in the flow responses that demonstrates how important it is to model the geological features accurately.

**Comments:** This work initially was presented at the ACM conference in Edinburgh, 2010. More details of the work are reported in proceedings for the CMWR conference in Barcelona, 2010 (Section A.1) and in the ECMOR conference in Oxford, 2010 (Section A.2). The final version is submitted to the Groundwater.

The following comments are important to be considered here:

- *The SAIGUP realizations*

Topography is a major player in the gravity dominated flow behavior. The SAIGUP realizations include variability in topography of the geological layering via structural changes due to faults and also barriers in the model. These are good enough for early migration when the CO<sub>2</sub> and water segregate and plumes accumulate below cap-rock and start the longer migration. In the long-term migration, top surface geometry is an important geological parameter and larger models than the SAIGUP models with a better resolution of the top surface are needed to get good predictions of the long-term migration phase. This was considered in the next generation of geological studies performed following this study [53, 67] under the IGEMS research project.

- *Physical assumptions*

The work concentrates on how geological heterogeneity impacts the flow performance. We need to measure the volumetric sweep efficiency of CO<sub>2</sub> plumes to evaluate the residual trapping. Including more physics in the modeling will add the computational costs specially when the flow modeling is used in a sensitivity analysis or risk assessment process. Therefore, we used simple fluid models for PVT.

- *Uncertainty considerations*

Our main motivation for using the SAIGUP data was the extensive work that was put into building realistic geological realizations. The geological parameters are changed in value between low and high levels. These values are assumed with the same probability. In general, this probability might not be uniform, depending to the regional geology of the storage site.

Within one geological realization, injection location can dramatically impact the injectivity of the well. In fact, this is an uncertain parameter in the CO<sub>2</sub> storage operations. Choosing to inject in the river channels or in the permeable homogeneous parts near the shore will enhance the injectivity and the CO<sub>2</sub> sweep efficiency in the medium. On the other hand, injecting in locations with low permeabilities and pore-volumes can significantly increase the injection pressure, while limiting the transport of CO<sub>2</sub> in the medium. Studying the impact of injection location can be performed by injecting in many different points in one realization and comparing the corresponding flow responses. However, this will considerably increase the number of detailed simulations in the study.

For the allowed time, we limited our study to a fixed point by injecting via one well in the flank part of the SAIGUP models. This location is selected after qualitative analysis of a detailed study on a homogeneous case. There, we aimed to fulfill the criterion of maximizing the CO<sub>2</sub> storage capacity via increasing the vertical travel path toward the structural trap location under the cap-rock. One mitigating strategy for minimizing the effect of injection location can be to inject via several wells in different locations in the medium.

Similar argument applies to the leakage risk study reported here. We use a leakage probability over the cap-rock that can dramatically influence the calculated leakage risk. We take this assumption to simplify the way we introduce the method.

### **Contribution of the candidate:**

The idea of using realizations from the SAIGUP project to study how variations in geological parameters impact the injection and early-stage migration of CO<sub>2</sub> was first suggested by the main supervisor of this thesis. The conceptual design of the injection scenario, as well as the measured reservoir responses were developed jointly with the co-authors of the paper. The candidate was solely responsible for working out the details of the simulation setup, developing a work-flow, performing simulations, post-processing results, and developing the first analysis of the results. The candidate then collaborated with the co-authors to refine the analysis and write the paper.

**Paper II: Geological storage of CO<sub>2</sub>: heterogeneity impact on pressure behavior**

**Summary:**

Pressure build-up is an important criterion that can determine the success and failure of CO<sub>2</sub> storage operations. Over-pressurized injections can induce new fractures and open the existing faults and fractures that increases the risk of leakage for the mobile CO<sub>2</sub> in the domain. On the other hand, the pressure disturbance imposed on the system travels within the domain beyond the scales of CO<sub>2</sub> distribution. If the CO<sub>2</sub> is injected into a saline aquifer connected to fresh water aquifers, the pressure pulse may result in fresh water contaminations by the brine far from the injection point. We define specific pressure responses to examine the pressure disturbance in the system during injection.

Two injection scenarios are examined for the same 160 geological realizations setup. In the first scenario, the injector is set to a fixed volumetric rate to inject the CO<sub>2</sub> volume in 30 years into the domain, allowing for an unlimited pressure build-up. In the second scenario, a pressure constraint is set on the injector that results in various rate of injection in different geological realizations to inject the same amount of CO<sub>2</sub> volume considered in the first injection scenario.

Pressure response sensitivity study with respect to different geological features indicates the significance of aggradation angle, progradation direction, and faults during injection. A probabilistic pressure analysis is also performed based on the 160 simulations on the available realizations.

**Comments:**

The results reported in this paper can vary by choosing different boundary conditions for the model and different model size. We choose open boundaries on three sides of the model. In general, pressure values can be larger than those that are simulated here.

Well location is chosen to be fixed in our study. Choosing different location of injection in the model can result in a dramatically different pressure behavior. We use one injector in the study to simplify the pressure analysis. To investigate the effect of well location on the results, one can inject via many injectors. Other option is to study the impact of changing the well location in a single injector model.

Finally, the early pressure build up that happens around the well is due to the low CO<sub>2</sub> saturations existing near the injector in the beginning of injection. This build-up is sensitive to the grid resolution around the injector. The simulated pressures can be less if we use finer grid near the injector. In some experiments that is not reported in the paper, we concluded that, with the grid used in our study, this difference is not very dramatic.

**Paper III: Geological storage of CO<sub>2</sub>: global sensitivity analysis and risk assessment using the arbitrary polynomial chaos expansion**

**Summary:**

In this paper, we perform a stochastic sensitivity and risk analysis. We obtain a high resolution global sensitivity and probabilistic study on the flow responses that are defined and discussed in the previous papers. We choose barriers, aggradation angle, and faults from the SAIGUP geological parameters. Faults are considered by changing the transmissibility value across them, which is a continuous parameter. One more parameter is added to the study which is common in the literature and models the external pressure support from other aquifers attached to the model (regional groundwater effect).

Flow simulation on high resolution variational geology demands a huge computational costs. To enhance the calculation speed, we use a data-driven method that does not need to solve the full physical flow equations. We approximate the flow solver by a response surface method that is a polynomial and relates the system output to the input with a minimal computational cost. We use the arbitrary polynomial chaos expansion (aPC) to approximate the flow responses. The aPC method considers the uncertainty in the input variables.

A global sensitivity analysis is performed by employing Sobol indices that are based on variances of

responses. The method is shown to be robust in problems of high levels of complexity and non-linearity.

And finally, we perform a Monte-Carlo process using the approximating polynomial on a high resolution input variations. This makes it possible to perform a high resolution probabilistic study on the flow responses. This way, extreme cases can be identified by probability of occurrence.

### Comments:

This work was presented in the proceedings of the European Geosciences Union (EGU) General Assembly 2012, April, Vienna, Austria, Geophysical Research Abstracts., Vol. 14, EGU2012-9243. The detailed report is accepted for publication in the International Journal of Greenhouse Gas Control (IJGGC), in May 2013, <http://dx.doi.org/10.1016/j.ijggc.2013.03.023>.

To implement our stochastic technique, we choose geological parameters in this study that can be interpolated between two levels of their values. For example, it makes sense to use barriers coverage level of 25% between the low (10%) and medium (50%) levels used in the previous studies. Some of the geological parameters are discrete and can not be interpolated between two values. For instance, lobosity can only be varied over three points and we can not define a 1.5-lobe.

Having a large number of points in the input values interval requires intensive geological modelings to be used in the flow simulations. Using the data-driven polynomial, the approach only needs evaluating the polynomial in the defined values, and there is no need for full geological modeling except in the collocation points, i.e., point values that the polynomial coefficients must be calculated.

The work reported here is to demonstrate the work-flow of using the aPC for global sensitivity analysis and probabilistic risk assessment. A normal work-flow starts by defining the uncertainties in the input parameters and follows by building the geological models for the aPC collocation points that are based on those uncertainties. To perform this study on the SAIGUP models that are consistent with a uniform uncertainty in the geological parameters, with no loss of generality, we used uniform uncertainty distributions for our study. However, the aPC method is not limited to uniform uncertainty descriptions.

Geological features are ranked based on the sensitivity analysis results. The results are in agreement with dynamics of the flow in the aquifer. Aggradation angle is the most influential parameter, while the regional groundwater has the least influence in the model responses. The study is not limited to the assumed uncertainty of input parameters and the conclusion may change for a very different uncertainty description.

### Contribution of the candidate:

The study was a joint work between the candidate and the co-authors on the following steps:

- Defining the problem.
- Designing the simulation scenarios.
- Designing the work-flow.
- Integrating the aPC MATLAB code into the work-flow.
- Performing the runs and processing the results.
- Performing the global sensitivity analysis.
- Performing the risk assessment.
- Analyzing the results and preparing plots.
- Writing the report.

The candidate had a solid and major contribution in every step, and in particular, integrating the aPC code into the work-flow, running the simulations, performing the sensitivity and risk analysis, and processing the results. The report has gone through extensive reviews.

# **Chapter 3**

## **Scientific results**



# Paper I

## 3.1 Impact of geological heterogeneity on early-stage CO<sub>2</sub> plume migration: Sensitivity study

M. Ashraf, K. A. Lie, H. M. Nilsen & A. Skorstad

Submitted to *Groundwater*



# Impact of Geological Heterogeneity on Early-Stage CO<sub>2</sub>-Plume Migration: Sensitivity Study

Meisam Ashraf      Knut-Andreas Lie      Halvor M. Nilsen      Arne Skorstad

November 10, 2013

## 1 Introduction

Sedimentary basins consist of thick piles of lithified sediments that provide large volumes that can be used to store carbon dioxide produced from localized sources as a possible means to reduce the rate of anthropogenic emission into the atmosphere [25, 18]. Sedimentary basins contain fluids (mostly brine) whose flow is controlled by high-permeable strata through which the fluids can flow and low-permeable strata which inhibit fluid flow. How efficient the geological storage of CO<sub>2</sub> will be, is determined by how the low and high permeability strata are stacked inside the sedimentary basin [24]. Carbon dioxide injected deep in a sedimentary basin will form a plume that has a lower density than the formation brine and hence will migrate upward by buoyancy forces. The most secure type of geological storage is therefore provided in depleted petroleum reservoirs that contain stratigraphic and structural traps that have held hydrocarbons for million of years. Unfortunately, oil and gas reservoirs do not contain sufficient pore volumes to store the large amounts of CO<sub>2</sub> that are required to significantly reduce current and future carbon emissions. A more viable solution is to use saline aquifers that have very slow flow rates and offer large volumes of pore space. Aquifers are typically connected to the surface through permeable strata, and the injected CO<sub>2</sub> may therefore in principle travel in the up-dip direction and eventually leak out through sedimentary outcrops. In practice, this process will take millions of years because of the long distances involved. Moreover, as the plume migrates upward, some of the CO<sub>2</sub> will be trapped as small droplets between rock grains (residual trapping), some of it will dissolve into the formation water (dissolution trapping), and some of it will react with rock minerals and become permanently trapped. In general, the flow of CO<sub>2</sub> in subsurface rocks is governed very complex interactions between physical forces acting on the reservoir fluids and properties of the reservoir rock itself. It is therefore necessary to develop effective (numerical) models that can be used to accurately describe the pertinent flow dynamics and provide a detailed inventory of injected volumes. Numerical models must also properly account for geological heterogeneity—i.e., variations in hydraulic conductivity and fluid storage—and how this heterogeneity influences the flow dynamics.

The main concern for policy makers and the general public is the operational safety and the risk of leakage, i.e., how likely it is that the injected carbon dioxide (or highly saline brine) will migrate into water resources, into active petroleum reservoirs, or back to the surface through ill-plugged wells [43], through caprocks broken by the high pressure imposed to the system during the injection operation, or via conductive features like fractures and faults. Likewise, there is a concern about pressure buildup, which may extend much further than the injected CO<sub>2</sub> plume (the effluent of CO<sub>2</sub> into brine). In other words, the operator of a potential injection site needs to maximize storage volumes while minimizing leakage risks and effects on areas surrounding the injection point. Over the last two decades, there have been a large number of simulation studies of CO<sub>2</sub> sequestration, including in particular, studies of pilot projects like Sleipner [13, 7, 12, 40, 9], In Salah [8, 11, 46], Ketzin [21, 34, 29, 30, 45], or Johansen [2, 6, 19, 17, 52]).

Geological heterogeneity is recognized in many studies as a major control mechanism that influences flow from small laminated scales to large global scales. Stratigraphic heterogeneity, for instance, is dependent on the depositional environment, and affects the geometry and spatial distribution of depositional facies as well as the spatial permeability distribution within facies. Practically, including all details of every scale into flow simulation model is impossible. Moreover, the understanding of the geology of a specific reservoir or aquifer is typically (surprisingly) limited: experience from the

petroleum industry shows that drilling new wells into mature reservoirs typically reveal structural and stratigraphic details that were not visible in state-of-the-art 3D/4D seismic surveys. The description of the geological heterogeneity will therefore have large uncertainties attached. Deep saline aquifers that have been identified as potential storage sites are typically much less characterized: the aquifer has typically been penetrated by a small number of wells, if any, and 3D seismic surveys often have limited coverage. If flow simulations are to be used to assess risks associated with a storage operation, the numerical flow model must properly account for the impact of uncertainty in the geological description. Yet, most studies of CO<sub>2</sub> injection commonly employ simplified or conceptualized reservoir descriptions, in which the medium is considered (nearly) homogeneous, or use a single petrophysical realization, and instead focus on developing complex models of the flow physics, discretization schemes, and solvers.

Early studies of the impact of heterogeneity consider 2D models with geostatistically populated permeabilities [33, 51]. Likewise, a layered heterogeneity is examined in [37]. Later, Hovorka et al. [26] studied the impact of heterogeneities in the Frio formation from the Texas Gulf Coast, including stratigraphic heterogeneities resulting from transitions between rocks deposited in sand and mud-dominated depositional facies and structural heterogeneity from growth faults, folds, and salt diapirs. The heterogeneities were parametrized and used as input to a solver to assess the effectiveness of CO<sub>2</sub> storage and its sensitivity to these parameters. Likewise, Obi and Blunt [44] investigate the heterogeneity in an oil field in the North Sea including fluvial and a prograding depositional environment. Flett et al. [20] constructed a suite of 3D models, in which a radial variogram was used to populate five models with varying net-to-gross ratios, and concluded that formations containing shale barriers are effective in containing an injected CO<sub>2</sub> plume within the formation and that heterogeneity serves to limit the reliance of the formation seal as the only mechanism for containment. Nilsen et al. [41, 50] considered a large set of high-resolution models of the top surface and concluded that uncertainty in morphology effects at a small scale may have a significant impact on (large-scale) estimates of the non-trivial interplay between structural and residual trapping. The opposite case, with a single top-surface topology and multiple property realizations, was considered by Goater et al. [23].

The most comprehensive study geological uncertainty to day, however, was conducted in the SAIGUP project, which focused on how geological uncertainty impacts reserve estimates and production forecasts [38, 27, 39]. Here, an ensemble of synthetic but realistic models of shallow-marine reservoirs were generated and several thousand cases were run for different production scenarios. The results showed that realistic variations in the structural and sedimentological description have a strong influence on production responses. In general, one cannot expect that knowledge of how geological heterogeneity impacts flow predictions of oil-water systems can be carried directly over to CO<sub>2</sub>-brine systems relevant for CO<sub>2</sub> injection scenarios, which involve temporal and spatial scales and density ratios that are quite different from those encountered in oil recovery. Potential storage sites may also have geological characteristics that differ from those seen in producible oil reservoirs. Nevertheless, we will herein try to leverage the comprehensive geomodeling effort from SAIGUP. To this end, we consider a scenario in which CO<sub>2</sub> is injected into an abandoned shallow-marine reservoir and use geological realizations generated as part of the SAIGUP project—which, geologically speaking, represent a viable storage site—to study the impact of geological heterogeneity on the short to medium term predictive modeling of CO<sub>2</sub> plume formation and migration. How heterogeneity impacts the injection operation will be studied in a separate work, in which we also discuss more realistic pressure constraints on injection well.

The outline of the paper is as follows: We start by describing the geological realizations, the underlying parameters, and the flow model in Section 2. In Section 3, we introduce a set of flow responses that we will use to describe the feasibility of the storage operation and the variations in the resulting flow patterns. Section 4 analyzes how the various geological parameters impact the formation and early-stage migration of the CO<sub>2</sub>plume. In Section 5, we discuss how the contact between the CO<sub>2</sub> plume(s) and the caprock, and hence the leakage risk, is influenced by the geological parameters. Finally, some concluding remarks are given in Section 6.

## 2 Model Setup

Sedimentary basins are formed by superposition of high and low permeable strata that control the lateral and vertical flow of the fluids in the medium. Aquifers consist of layers with high permeability and therefore usually have pressure distributions that are (almost) hydrostatic. Lower-permeable parts of the basin are called aquitards, and here the flow will be orders of magnitude slower than in aquifers. However, the area exposed to flow may be very large, which consequently enables large volumes to flow across bedding between two adjacent aquifers. Aquifers and aquitards can be covered by evaporitic beds that are almost impermeable (aquitrudes) [24].

The flow in aquifers generally depend on the balance between viscous, capillarity, and segregation forces. Viscous forces act because of the pressure change imposed by wells or background flow within the medium. In regions with slow velocities, capillary forces will dominate and in high permeability regions, gravity segregation can be considerably dominant. Any of these forces can be important for the movement of the injected CO<sub>2</sub>. Herein, we consider the injection and early migration phase for a storage operation in which supercritical CO<sub>2</sub> is injected into a shallow-marine reservoir underneath a sealing cap-rock that forms a type of structural trap that is often seen in petroleum reservoirs. This means that we can expect viscous dominance during injection and gravity dominance during the subsequent migration phase.

To represent the aquifer geology, we use an ensemble of synthetic models developed in the SAIGUP study [38]. The SAIGUP models were originally designed to encompass the sedimentological architectures and fault structures of European clastic oil reservoirs, with a focus on shoreface reservoirs. Here, the deposition of sediments is due to variations in sea levels so that facies are forming belts in systematic patterns (curved belts for river deposits, parallel belts for wave deposits, etc). Sediments are deposited when the sea level is increasing, whereas barriers may be formed when the sea level is decreasing. Shoreface reservoirs are bounded by faults and geological horizons.

To derive an objective geological parametrization, the SAIGUP project indexed a broad suite of shallow-marine reservoir to continuously varying anisotropy and heterogeneity levels, structural complexity ranges from unfaulted to compartmentalized, and fault types from transmissive to sealing. From this, a set of geological realizations were created with sedimentary heterogeneity changing in different levels of heterogeneity in lateral and vertical directions. Structural heterogeneity was represented by variations of the fault orientations, intensity, and the transmissibility across the fault. Particular care was taken to ensure that the number of realizations was sufficient to form a basis for sensitivity analysis and that there was enough overlap in the geological parameter variations between realizations to allow for quantitative assessment of the contribution of each geological parameter. Although models are synthetic, each realization should be complex enough to represent a plausible geology suitable for realistic flow modeling.

The geological realizations were built within a sequence stratigraphic framework for progradational shallow-marine sedimentary environments. A regular grid was used to model the sedimentological parameters, with structural modeling added to the models afterwards. The depositional modeling started by population of six facies associations, each with internal heterogeneity on a fine grid. Lamina-scale models (meter-scale) were built to capture the lamina-scale effects on flow through each facies. Some of these facies were modeled in three dimensions to account for anisotropy; some were modeled deterministically, while other facies were populated stochastically. Figure 1 shows an illustration of the modeled facies for a specific case. Next, the facies produced at appropriate lamina scales were upscaled by geo-pseudo methods in different intermediate steps and finally mapped onto a geological grid. This grid was considered too fine for the flow simulation and was upscaled in a last step to a coarse grid (Figure 2). Each grid-block in the coarse simulation model were represented by values of porosity, net-to-gross ratio (shale content), directional permeabilities, and an index to the facies contained in the grid-block. Specifications of the fine and coarse grids are given in Table 1.

In our study, we have selected the following five parameters that altogether give 160 realizations:

**Lobosity** – is defined by the plan-view shape of the shoreline. As a varying parameter, lobosity indicates the level at which the shallow-marine system is dominated by each of the main depositional processes. Two depositional processes are considered in the SAIGUP study: fluvial and wave processes. The higher the amount of sediment supply provided from rivers is relative to the available accommodation space in the shallow sea, the more fluvial dominant the process

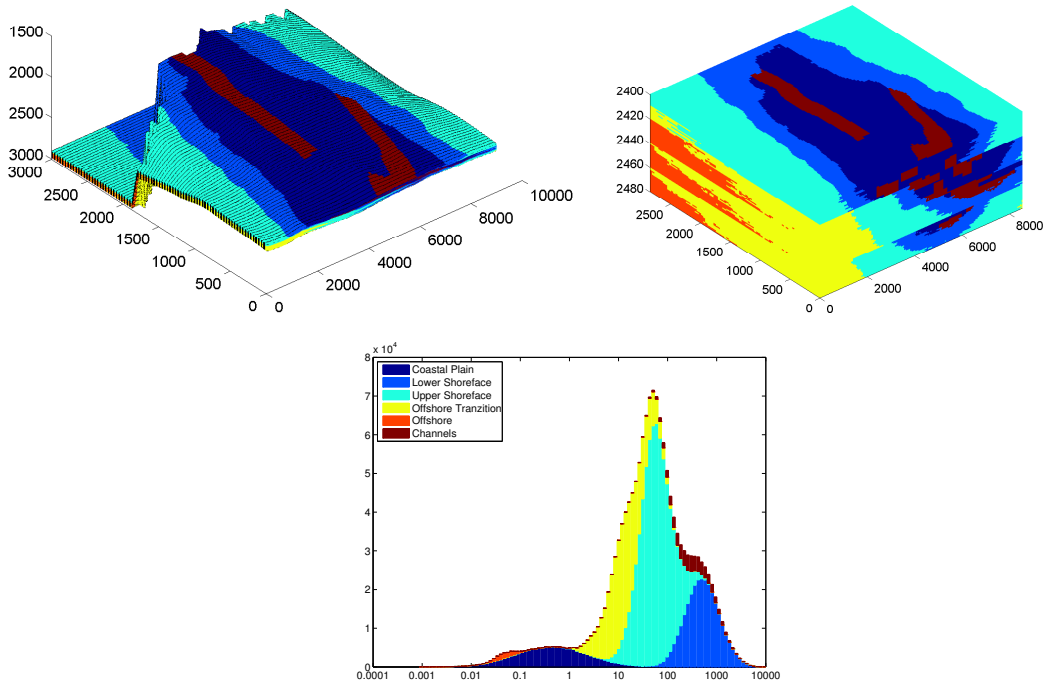


Figure 1: Facies variations for a selected fine model, with colors corresponding to different rock types. The upper-left plot shows a perspective view of the actual grid, whereas the rock types have been mapped to a uniform grid for a better visualization to the upper right. The lower plot shows a histogram of the logarithm of the lateral permeability (unit:  $\text{cP m}^3/\text{day}/\text{bar}$ ).

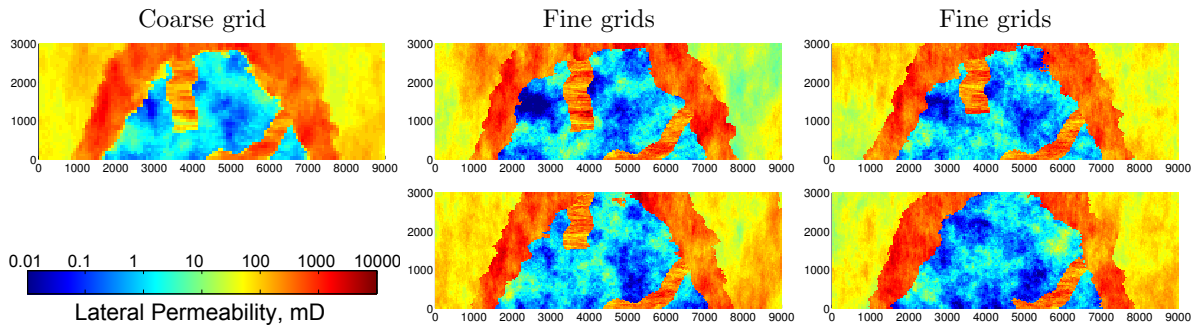


Figure 2: Top view of the logarithm of the lateral permeability plotted for the first four layers of the fine grid versus their representative layer in the coarse grid.

Table 1: Specifications for the fine and coarse grids used in the SAIGUP modeling process.

Parameter	Fine scale	Coarse scale
Grid spacing ( $x$ -direction)	37.5 m	75 m
Grid spacing ( $x$ -direction)	37.5 m	75 m
Grid spacing ( $x$ -direction)	1 m	4 m
Total number of cells	1,500,000	96,000
Number of active cells	1,500,000	79,000
Lateral extent ( $x$ -direction)	6 km	6 km
Lateral extent ( $y$ -direction)	9 km	9 km
Vertical extent ( $z$ -direction)	80 m	80 m

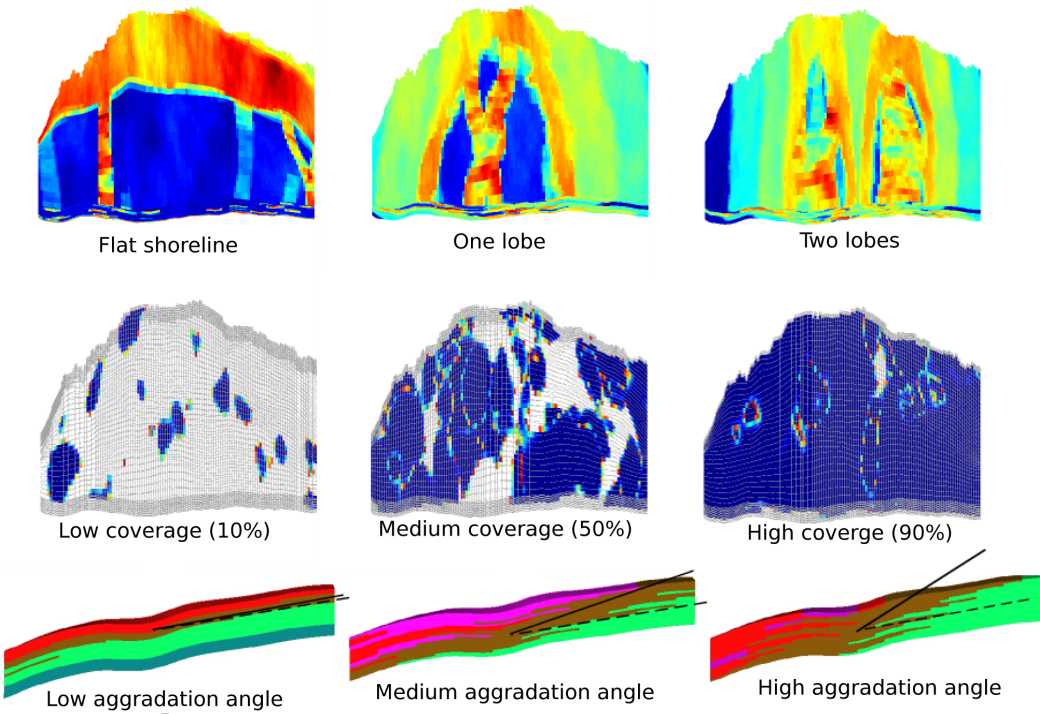


Figure 3: Illustration of geological parameters from the SAIGUP study: the top row shows three different lobosities for up-dip progradation (if the lobes flip over the long axis, we will have down-dip progradation); the middle row shows barriers representing different degrees of mud-draped coverage; and the bottom row shows aggradational angle.

will be. As the river enters the mouth of the sea, it can divide into different lobes and branches. Wave processes from the sea-side smear this effect and flatten the shoreline shape. Less wave effect produces more pronounced lobe shapes around the river mouths. Very high permeability and porosity can be found in the channeling branches, while dense rock with low permeability fills the space between them. Reservoir quality decreases with distance from the shore-face. We expect that the level of lobosity can have a considerable effect on the CO<sub>2</sub> injection and plume size in the aquifer. Models of three levels of lobosity are used herein: flat shoreline, one lobe, and two lobes, as illustrated in the upper row of Figure 3.

**Barriers** – Periodic floods result in a sheet of sandstone that dips, thins, and fines in a seaward direction. In the lower front, thin sheets of sandstone are interbedded with mud-stones deposited from suspension. These mud-draped surfaces will potentially act as significant barriers to both horizontal and vertical flow, and are modeled by transmissibility multipliers corresponding to three levels of coverage for the barrier sheet: low (10%), medium (50%), and high (90%), as illustrated in the middle row of Figure 3.

**Aggradational angle** – In shallow-marine systems, two main factors control the shape of the transition zone between river and basin: amount of deposition supplied by the river and the accommodation space that the sea provides for these depositional masses. One can imagine a constant situation in which the river is entering the sea and the flow slows down until stagnation. The deposition happens in a spectrum from larger grains depositing at the river mouth to fine deposits in the deep basin. If the river flux or sea level fluctuates, the equilibrium changes into a new bedding shape based on the balance of these factors. The SAIGUP data models cases in which, for instance, the river flux increases and shifts the whole depositional system into the sea. The angle at which the transitional deposits are stacked on each-other because of this shifting, is called aggradational angle. Three levels of aggradational angle are modeled here: low, medium, and high angles. The three parameter choices are illustrated in the bottom row of Figure 3, where we in particular notice how a low aggradational angle gives continuous facies layering parallel to the dip

Table 2: Geological parameters from the SAIGUP project included in this study. The last column reports markers used to distinguish different parameters in the plots.

Parameter	Levels	Marker
Lobosity	flat, one-lobe, two-lobe	square, circle, diamond
Barrier	low(10%), medium(50%), high(90%)	small, medium, large
Aggradation	low(parallel layering), medium, high	blue, green, red
Progradation	up-dip, down-dip	first half, second half
Fault	unfaulted, open faults, closed faults	thin, medium, thick

direction of the model.

**Progradation** – denotes the direction of the depositional dip. Two types are considered here: up and down the dominant structural dip. Because the model is tilted a little, this corresponds to the lobe direction from flank to crest or vice versa.

**Fault** – are represented by three different parameters in the SAIGUP study: fault type, intensity, and transmissibility. Herein, we limit our study to compartment faults of medium intensity and consider three parameter choices: no faults, open faults, and closed faults.

Table 2 lists the markers (shape, size, color, thickness) that will be used to signify different parameter values in plots of simulation results later in the paper.

We will consider storage of forty million cubic meters of supercritical CO<sub>2</sub>, which amounts to approximately 20% of the total pore volume in the aquifer. The CO<sub>2</sub> will be injected from a single well over a period of thirty years, and after the injection period, seventy years of plume migration is simulated for all cases. Hydrostatic boundary conditions are imposed on the sides, except at the faulted side on the crest, and no-flow boundary conditions are imposed on the top and bottom surfaces.

If the medium was homogeneous and of sufficient permeability, one would expect that the injection would create one big plume that moves upward because of the gravity force until it accumulates under the structural trap of the cap-rock, i.e., migrating from the injection point and upward to the crest of the aquifer. The idea is therefore to inject as deep as possible to increase the travel path and the volume swept by the plume before it reaches the crest. To this end, the injector is placed down in the flank and only completed in the three lowest layers of the aquifer. The formation and early migration of the plume will crucially depend on the complex interaction between the injected CO<sub>2</sub> and the heterogeneity inside the reservoir; that is, whether the CO<sub>2</sub> encounters low permeability rocks in the vicinity of the well bore, or whether high permeability pathways are available to enable plume migration away from the injection point. The fixed well position was chosen manually based on a number preprocessing simulation runs and held fixed for all model realizations. This way, we avoid introducing an additional parameter into the simulation study. On the other hand, we may also introduce certain artifacts, like exaggerated pressure responses if the well hits a low-permeable area, that would have been avoided if the well position was optimized for each realization. A more comprehensive study should, of course, also have investigated possible effects and impacts of different well positions and completion strategies to increase the robustness of the observations.

The injected CO<sub>2</sub> is assumed to be a supercritical fluid with density 700 kg/m<sup>3</sup> and viscosity 0.04 cP. The supercritical fluid is modeled as a dead oil with a formation factor of 1.1 at 0 bar and 0.95 at 400 bar. (The assumption of (almost) constant properties is reasonable since pressure and temperature effects will typically counteract each other at relevant depth ranges.) Brine is assumed to be slightly compressible ( $3.03 \cdot 10^{-6}$  psi<sup>-1</sup>) with density 1033 kg/m<sup>3</sup> and viscosity 0.4 cP. The rock compressibility is set to  $3 \cdot 10^{-7}$ . For both fluids, we will use Corey-type relative permeability functions

$$k_{rCO_2} = (1 - S)^\alpha, \quad k_{rw} = S^\alpha, \quad \alpha = 1, 2$$

where  $S$  denotes the saturation of brine normalized for end points 0.2 and 0.8.

Relative permeabilities for CO<sub>2</sub>-brine systems have been thoroughly discussed in the literature; [4, 5, 22] summarize 35 experiments on sandstone and carbonate rocks and more experiments can be found in [1, 47, 53]. There are also papers that analyze the impact of the relative permeability (e.g., [10, 31, 32]), and investigate the endpoint and hysteresis effects, see e.g., [49, 28]. In many

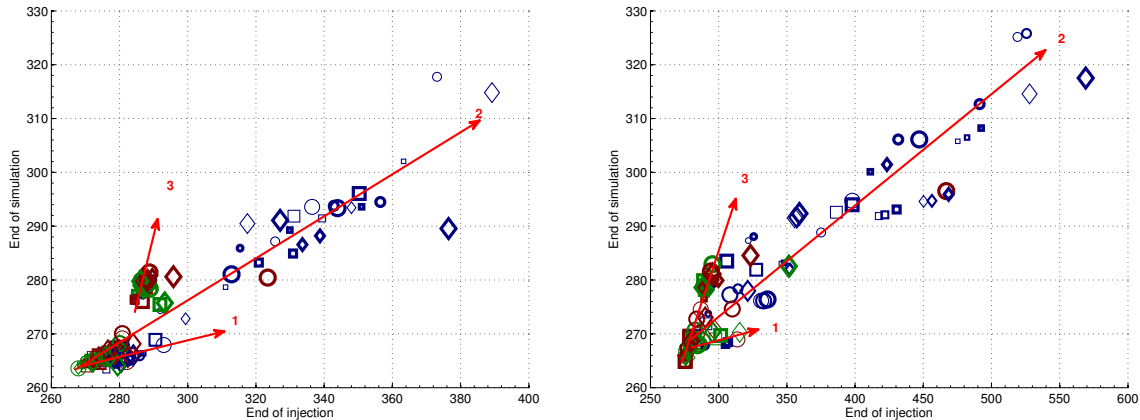


Figure 4: Cross-plot of average aquifer pressure at the end of simulation versus at the end of injection for linear (left) and quadratic (right) relative permeabilities.

storage scenarios, however, the segregation of supercritical CO<sub>2</sub> and brine will typically take place in the rock with high permeability. This is the basis for the popularity of so-called vertical-equilibrium models [42] for investigating CO<sub>2</sub> sequestration. The effective relative permeability after segregation has occurred is linear if capillary effects are small, and if nonlinear relative permeabilities are used, large errors will occur in cells in which segregation should have occurred and the saturation is low, as demonstrated in [36]. Sensitivity to vertical grid resolution is also observed by Wei and Saaf [52]. In the following, we will therefore primarily use linear relative permeabilities, even though this choice is not necessarily representative on the small scale. Introducing linear relative permeabilities can be viewed as using the pseudo-relative permeabilities that are least influenced by the vertical grid resolution and best represent the flow of the system for large grid blocks. In addition, using linear relative permeabilities not only simplifies and speeds up the flow simulations, but also accentuates and accelerates the flow effects we study. For completeness, however, we also report results using nonlinear relative permeabilities.

### 3 Basic Flow Responses

In this section we will give a qualitative discussion of how some basic flow responses like the wave speeds of the plume migration, average aquifer pressure, mobile and residually trapped volumes, and plume sizes are affected by variations in the geological parameters.

#### 3.1 Pressure responses

The average aquifer pressure in general shows a sharp jump at the start of injection and a declining trend during injection and plume migration caused by pressure release through the open boundaries. (Specifying different boundary conditions would have resulted in different pressure trends). Figure 4 shows cross-plots of the average aquifer pressure at the end of injection and end of simulation for our two different choices of relative permeability functions. In both plots, one can recognize three different trends which have been indicated by three straight lines. The first trend, which has the gentlest slope, represents cases with large pressure variation during injection and small range of pressure variation during the migration phase after the end of injection. In these cases, the heterogeneity of the medium forms channels toward the open boundaries through which the injection pressure is released, resulting in low aquifer pressure at the end of simulation. The second trend, represents cases in which the heterogeneity affects injection, gravity segregation, and flow through open boundaries. In particular, we observe that most cases that have high injection pressure correspond to a low aggradation angle, for which low vertical permeability forces the injected CO<sub>2</sub> plume to move relatively slow in the lowest, poor-quality layers before migrating up toward the cap-rock, see Figure 5. This increases the pressure in the domain during injection and keeps a higher pressure gradient to the open boundaries. In the third trend, which includes scenarios with closed faults, the heterogeneity makes chambers and

Table 3: Geological parameters for four different cases selected for visualization.

Case	Faulted	Lobosity	Barrier	Aggradation	Progradation
Case 1	no	one-lobe	medium	medium	down-dip
Case 2	no	two-lobe	medium	low	up-dip
Case 3	no	one-lobe	high	high	up-dip
Case 4	no	one-lobe	high	high	down-dip

compartments in which the pressure increases during injection and then remains high. Heterogeneity also affects the gravity segregation process more than in the other two trends because of faults and a high barrier coverage.

We also see the effect of curvature in the relative permeabilities by comparing the two plots in Figure 4. Higher range of pressure variations is observed during injection for the nonlinear relative permeability runs. Moreover, nonlinear relative permeability gives lower mobility which leads to higher pressure build-up during injection. This means that longer time is required for the pressure to be released through the open boundaries after injection and more cases therefore follow the second and third trend. More details about the bottom-hole pressure are given in a companion paper [3], which also discusses more realistic constraints on the injection operation.

### 3.2 Plume migration

The direction in which the CO<sub>2</sub> plume moves in the medium will primarily impact the amount of residual (and structural) trapping, but as we will see later, also significantly change the extent to which the plume contacts the caprock, which again affects the risk for leakage through breaches and holes in the caprock. When evaluating the safety of a long-term storage operation, there are several potentially conflicting aspects that need to be considered with regard to plume migration. On one hand, we prefer the plume to spread out laterally to enhance residual trapping and mixing of CO<sub>2</sub> and brine; the amount of residual trapping is positively correlated with the sweep efficiency of the CO<sub>2</sub> plume, i.e., the percentage of the aquifer volume that has been in contact with CO<sub>2</sub>. On the other hand, one typically wants to confine the plume to the smallest volume possible to simplify monitoring operations, minimize the contact with potential leakage points, and minimize the risk of leakage and contamination into other aquifers. However, if a big movable plume connects with a leakage pathway through the caprock, large volumes of CO<sub>2</sub> may escape, and for this reason, it may be better if the injected CO<sub>2</sub> splits into many small plumes. To investigate these aspects, we will study the number of plumes and their volumes.

#### 3.2.1 Boundary fluxes

Because we have chosen to inject a relatively large amount of CO<sub>2</sub> corresponding to one fifth of the aquifer's pore volume, it is to be expected that the pressure and saturation fields will interact strongly with the model boundaries, which in some cases will lead to substantial loss of CO<sub>2</sub> across the boundaries. The model has open boundaries on three sides, which are modeled by imposing huge pore-volume multipliers in the outer cells, while no-flow boundary conditions are imposed along the top faulted side. Using large pore-volume multipliers to represent open boundaries enables volumes of CO<sub>2</sub> to leave and later re-enter the aquifer. (In addition, this method will contribute to eliminate effects from Dirichlet type boundary conditions). The flux out of the open boundaries can be considered as a measure of the lateral movement of the plume, and reflects the relative difficulty of forcing the injected CO<sub>2</sub> up-dip towards the crest compared with driving it down-dip through the nearby open boundaries.

The lower boundary is closest to the injection point and hence the most likely place where injected CO<sub>2</sub> volumes will escape. Figure 6 shows plots of the CO<sub>2</sub> flow across this boundary at the end of injection versus the flow across the boundary at the end of simulation. Toward the end of injection, most cases have positive flux values, which means that parts of the main plume connected to the injection point have been forced to leave the domain in the down-dip direction by the increased injection pressure. However, after injection stops, many cases have small negative fluxes, which means that a small volume of CO<sub>2</sub> reenters the domain. Once again, we observe that cases with low aggradation

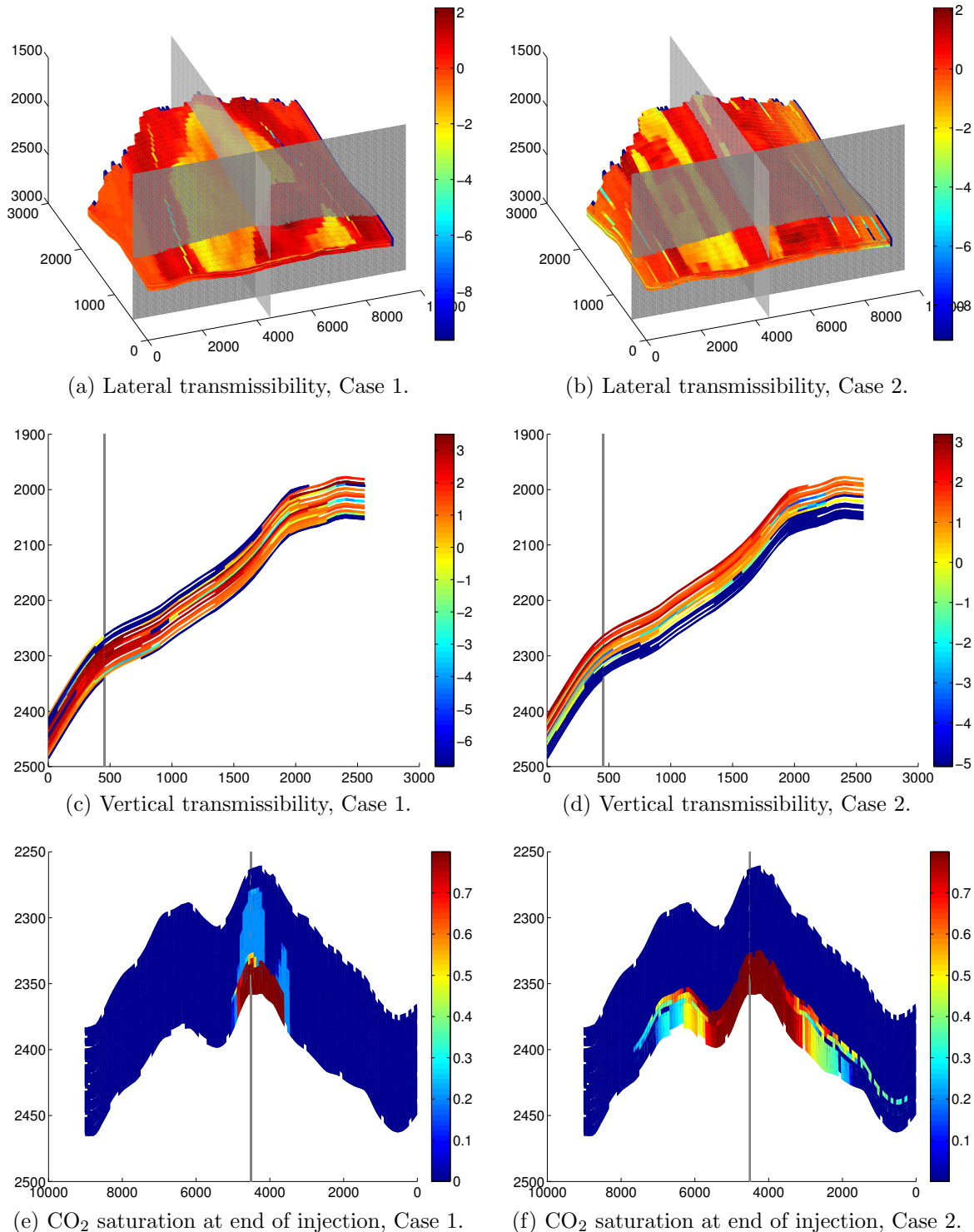


Figure 5: Impact of heterogeneity on CO<sub>2</sub> flow for Cases 1 and 2 in Table 3. The slice planes used to create the side views in (c) to (f) are shown as in gray in the perspective views in (a) and (b).

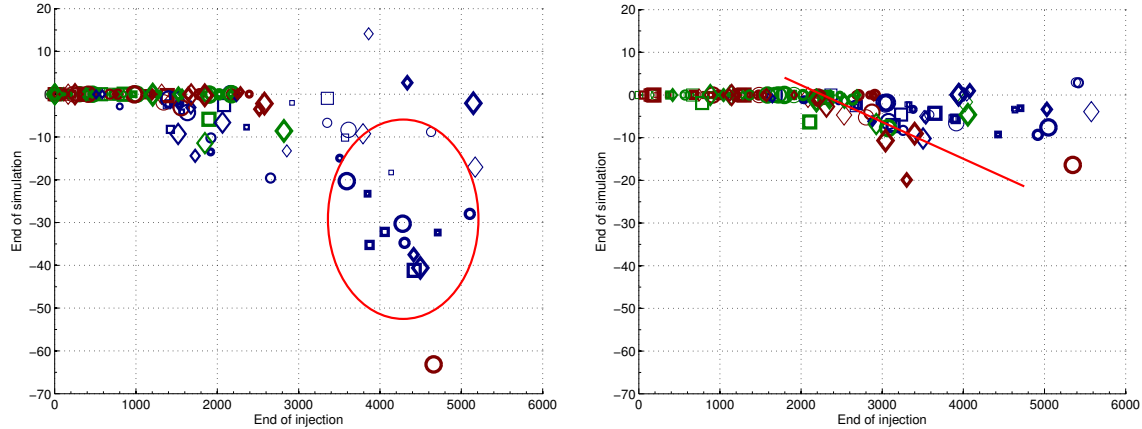


Figure 6: Cross-plot of  $\text{CO}_2$  flux out over the down-dip boundary for linear (left) and quadratic (right) relative permeabilities. Positive values represent outward fluxes and negative values represent inward fluxes.

angle stand out from the rest. In these cases, the injected plume is almost entirely confined to the bottom of the model because of poor vertical communication (see Figures 5 and 7). Hence, a large portion of the injected volume will be forced out of the domain in the down-dip direction. After the end of injection, gravity forces will gradually cause some of these lost volumes to move up-dip again and reenter the domain. We notice that cases with closed faults (shown is the red circle in the left plot of Figure 6) show a relatively higher return flux for the linear relative permeability function. With nonlinear relative permeability function, some of the cases follow a linear trend (shown by the red line in the right-hand plot), in which the return flux is proportional to the outward flux.

### 3.2.2 Total mobile/residual $\text{CO}_2$

Residual trapping occurs when the  $\text{CO}_2$  saturation is below the residual saturation value of 0.2. Although the residually trapped  $\text{CO}_2$  is free to move in a molecular sense on the microscale, the corresponding bulk volume is considered immobile on the macro scale. To reduce the risk of leakage, it is therefore important to obtain an efficient volumetric sweep that will maximize the residual volumes and minimize the mobile volumes. Herein, we will define residually trapped volumes as volumes in which the  $\text{CO}_2$  saturation is below the residual value of 0.2. Notice that with this definition, all mobile volumes (in which the saturation exceeds 0.2) will contain a residual portion of  $\text{CO}_2$  that is not free to escape. This portion will eventually become residually trapped if the saturation of the mobile  $\text{CO}_2$  decreases to the residual value.

Figure 9 shows cross-plots of the total residual volume at the end of injection versus the residual volume at the end of simulation. Drainage is the dominant flow process during injection. When injection ceases, the plume migration turns into an imbibition-dominated process which increases the residual trapping of  $\text{CO}_2$ . With linear relative permeability, the imbibition process takes place relatively fast and the residual volume increases significantly in the post-injection phase. Once again, low-aggradation cases form notable exceptions that have small amounts of residual trapping. The reason is primarily that significant volumes have been lost over the down-dip boundary, and secondarily that the (vertical) sweep is limited because the  $\text{CO}_2$  plume is confined to the lower layers of the reservoir during most of the simulation time.

With quadratic relative permeabilities, the predicted migration process is significantly slower and many cases have almost the same residual volume at the end of injection and end of simulation. As already discussed on page 7, the prediction of the gravity segregation of  $\text{CO}_2$  and brine is strongly affected by vertical grid resolution for nonlinear relative permeabilities and may severely under-predict segregation in low-saturation regions. On the other hand, the curvature of the relative permeability function does not have a considerable influence on the flow path (compare the streamline paths in Figure 10 for a selected case). Compared with the results in the left right plot of Figure 9, we therefore ultimately expect a significant increase in residual trapping before the plume settles; this prognos-

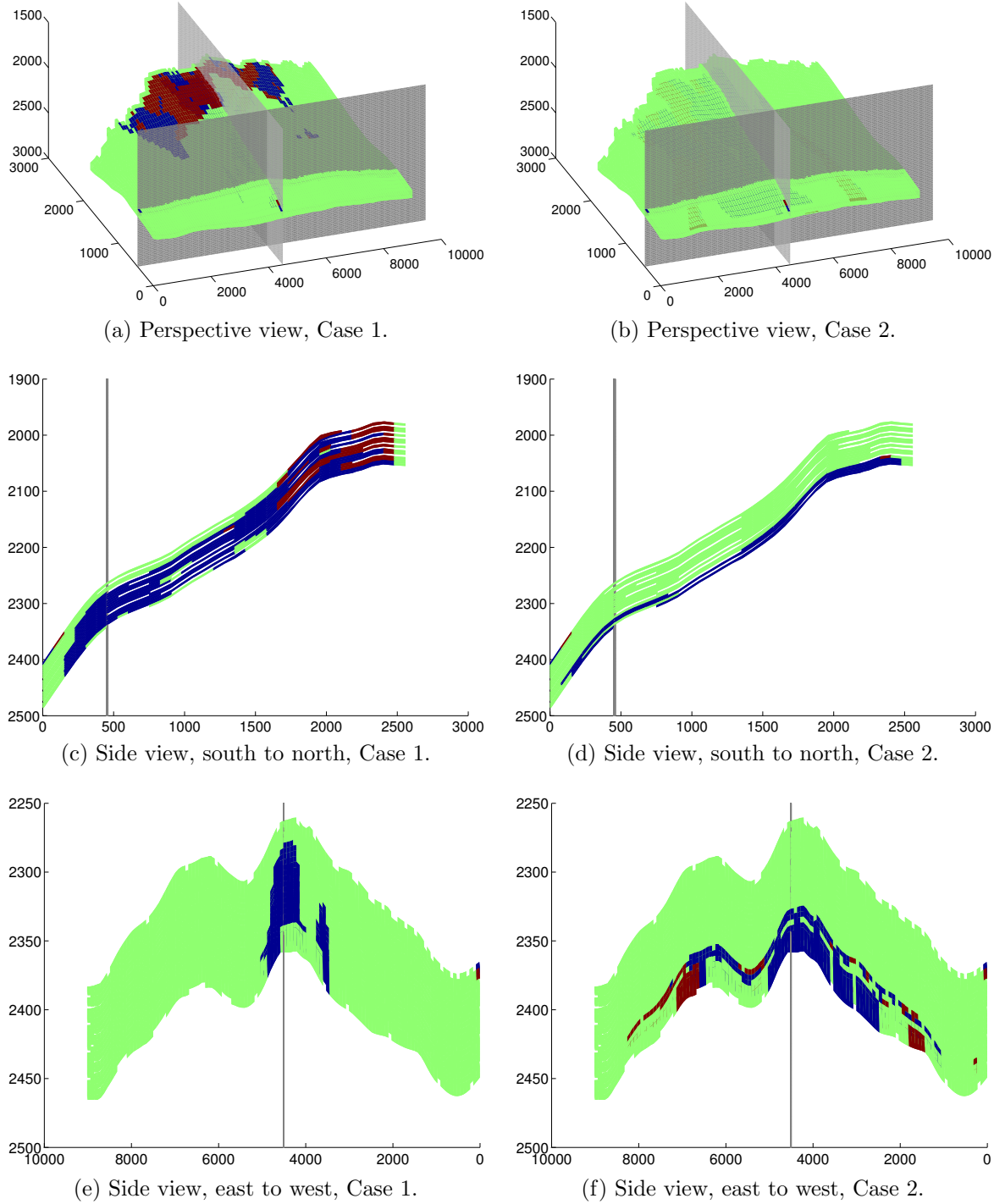


Figure 7: CO<sub>2</sub> flow in the dip direction at the end of simulation for Cases 1 and 2 from Table 3. Blue color shows the flow up-dip, red color the flow down-dip, and the green areas with no CO<sub>2</sub> flow.

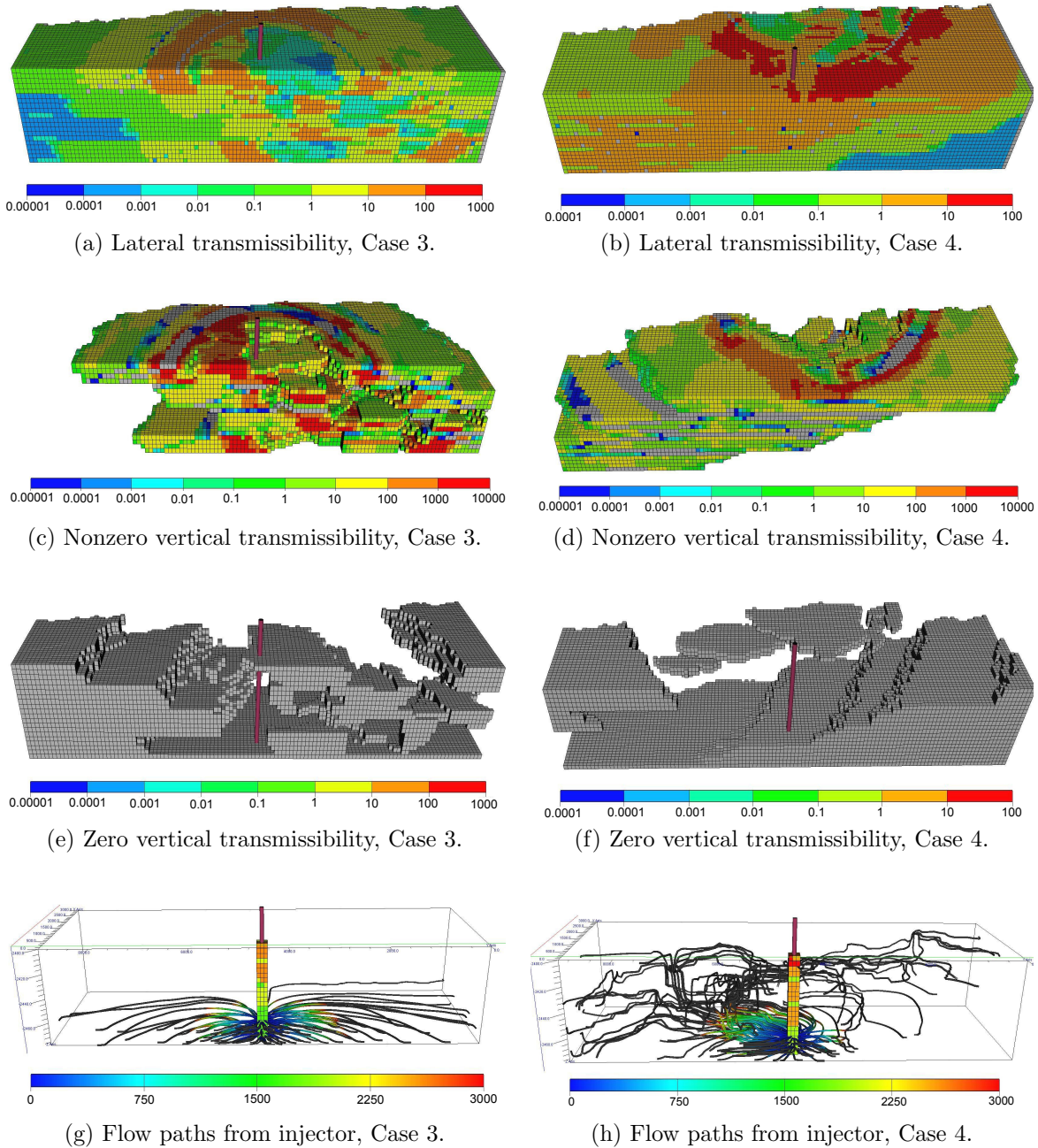


Figure 8: Effect of heterogeneity on CO<sub>2</sub> flow for Cases 3 and 4 from Table 3. The two cases differ in progradation direction, and lateral flow is enhanced in the down-dip case (Case 4).

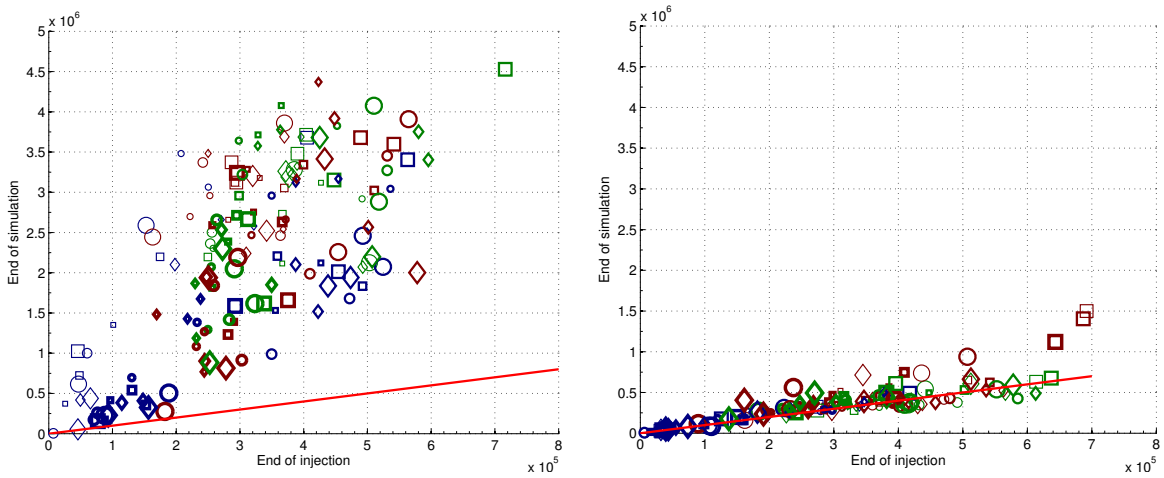


Figure 9: Residually trapped volumes for linear (left) and quadratic (right) relative permeabilities. Cases on the red lines have the same values at the end of injection and end of simulation.

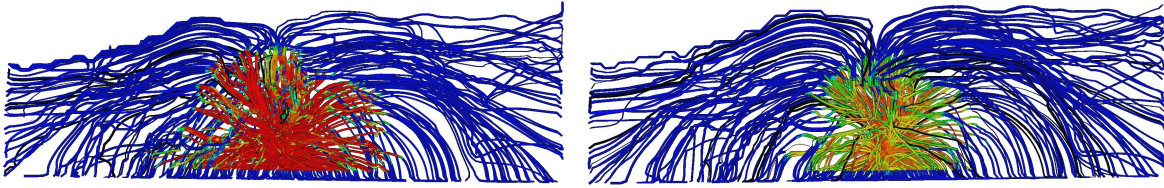


Figure 10: Top view of CO<sub>2</sub> saturation plotted on streamlines for linear relative permeabilities (left) and quadratic permeabilities (right). Red color corresponds to the mobile CO<sub>2</sub> and blue represents the water phase.

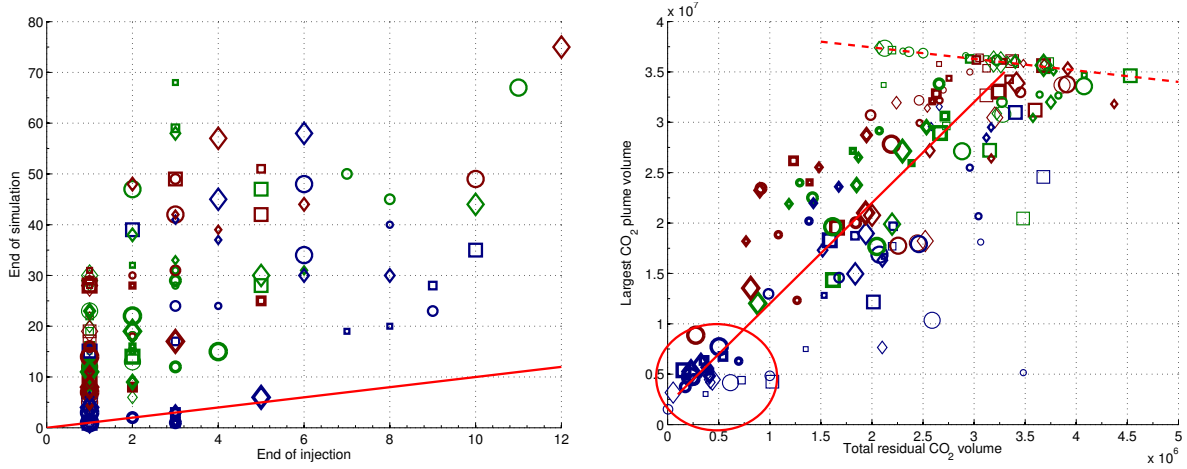


Figure 11: The cross-plot to the left shows the number of CO<sub>2</sub> plumes at the end of simulation versus the number of plumes at the end of injection for linear relative permeability function. The right plot shows the volume of the largest CO<sub>2</sub> plume versus the volume of residual CO<sub>2</sub> at the end of simulation.

tication has been confirmed for a few (arbitrary selected) cases by computing the plume migration for more than ten thousand years. We also observe that in some cases the residual volumes *decrease* after injection ceases. This is an artifact and is caused by mobile CO<sub>2</sub> invading zones of residual CO<sub>2</sub>, thereby turning residual volumes into mobile volumes according to the definition of residual trapping used herein. These cases are therefore likely to be influenced by hysteresis effects [1, 28, 49], which for simplicity have been disregarded in this study.

### 3.2.3 Connected CO<sub>2</sub> volumes

In the next section, we will study the risk of leakage through the caprock. To this end, we will use a simplistic model which assumes that all mobile CO<sub>2</sub> connected to a leakage point will escape through that point. Hence, it is preferable if the total mobile CO<sub>2</sub> volume is split into smaller plumes rather than forming a big mobile plume. Moreover, the surface area per volume increases by splitting the plume (assuming constant plume shape) and this helps residual trapping (and mixing of brine and CO<sub>2</sub>).

During injection, the flow support from the well builds a connected mass of CO<sub>2</sub> shaping one or a few big plumes. When the injection ceases, the CO<sub>2</sub> starts distributing in the medium and plumes may split because of branches in the flow paths created by heterogeneity. The plot to the left in Figure 11 shows how the number of plumes increases significantly in most cases during the migration phase, except for a few low-aggradation cases for which the injected plumes stay intact or reform into a single plume.

The right plot in Figure 11 shows the volume of the largest CO<sub>2</sub> plume versus the residual trapping. Here, we see two major trends indicated by a solid and a dashed line. The solid line, having a positive slope, represents cases that loose CO<sub>2</sub> through the open boundaries, mainly through the one closest to the injection point. As a consequence, less CO<sub>2</sub> volume exists in the system and the size of the largest plume will be smaller. Hence, less volume will be swept while the plume migrates upward (if it does), which again means that less CO<sub>2</sub> is residually trapped. In particular, we notice the cases inside the ellipse which are the same cases that had large CO<sub>2</sub> volumes escaping through the down-dip boundary as shown in Figure 6. The dashed line with negative slope corresponds to cases for which almost all of the injected CO<sub>2</sub> stays inside the domain. These cases show a small range of variation for the largest plume size and are reflecting the effect of different heterogeneity features on the residual trapping process. Because equal volumes of CO<sub>2</sub> are injected in all cases, we notice that the bigger the main plume is, the smaller the residual volume will be (mainly because the fraction of CO<sub>2</sub> that corresponds to saturation below 0.2 inside the movable plume is not considered to be residually trapped according to the definition used herein).

## 4 Analysis of Parameter Impact

The main purpose of the current study is to investigate how geological heterogeneity impacts the formation of a CO<sub>2</sub> plume during injection and during the early-stage migration after injection ceases. In this section, we will therefore perform a simple 'sensitivity analysis' that will tell us something of how the different geological parameters impact the flow responses discussed in the previous section. The five geological parameters impact the flow responses to different degrees; some parameters are more influential during injection, others take effect when the migration starts after injection has ceased, and some are influential both during injection and migration. Comparing the relative impact of the different parameters will indicate which of the parameters are most important to represent accurately when modeling a specific aquifer of the type considered herein.

To quantify the relative impact of each geological parameter, we will define normalized sensitivities that measure how much each of the basic flow responses discussed in the previous section change due to a unit change in a normalized geological parameter. We emphasize that these sensitivities cannot be interpreted as gradients in the strict mathematical sense. We will use barriers as an example to explain the analysis. There are three levels of barriers: low, medium and high. Suppose that we want to calculate the sensitivity of the number of plumes with respect to the level of coverage for the barrier sheets. We do this in two steps: first we average the number of plumes for cases of the same level of barriers. Having three levels of barrier, this results in three averaged plume numbers corresponding to each level of barriers. In the next step, we fit a line through these three points and calculate the

slope of this line, which thus represents how the number of plumes increases if the barrier parameter increases one level. For other parameters like fault and lobosity, we follow the same procedure. We use three levels for each parameter and fit a trend through these three points. For example, the first level of fault criteria relates to unfaulted cases, the second relates to open faults, and the third represents cases with closed faults.

Figure 12 shows the sensitivity for three different flow responses. In the upper row, we see that during injection the average aquifer pressure is most influenced by aggradation, while at the end of simulation the most influential parameter is the fault specification. The lack of good vertical communication for low aggradation angles means that the CO<sub>2</sub> is confined to the lower (poor quality) layers and relatively high pressures must be imposed to inject the required amount of CO<sub>2</sub> into the aquifer. For higher angles, the CO<sub>2</sub> can flow more easily upward through channels with higher permeabilities and less pressure support is required. Hence, the negative sensitivity. After the injection ceases, the dominating force is gravity, the main flow direction is vertical, and the pressure is now mostly affected by faults. If the faults are closed, they will prevent the release of pressure through the open boundaries. We also observe that the effect of progradation switches from positive to negative after the injection is stopped: Injecting in the up-dip direction is easier than injecting down-dip, while a down-dip deposition opens up more conductive medium in front of the plume as it migrates toward the crest.

The second row in Figure 12 shows the sensitivity in the number of CO<sub>2</sub> plumes. During injection, the barrier coverage is the most influential parameter, because mud-draped surfaces enhance the lateral flow and force the plume to split rather than migrating toward and accumulating at the crest. Aggradation has a similar effect: the lower the angle is, the more the injected CO<sub>2</sub> spreads out laterally. At the end of simulation, progradation and aggradation are the dominant effects. In particular, higher aggradation angle improves the segregation across layers and thus increases the splitting of plumes through heterogeneities. The impact of the faults is more significant than the figure shows: open faults contribute to split plumes, while the unfaulted cases and the cases with closed faults introduce a small number of plumes. In average, the positive and negative contributions cancel out to almost zero. Finally, the bottom row in Figure 12 reports sensitivities for the total residual volume. Here, aggradation is the most influential parameter during injection and faults the most important parameter during the migration phase.

The discussion is based on the overall trend averaged over all realizations and one should therefore be careful to draw general conclusions. For example, pressure sensitivity values with respect to progradation dip direction are based on only two points: the average over all cases with up-dip progradation and the average over all cases with down-dip direction. In Figure 12, we see that the progradation sensitivity changes polarity from the end of injection to the end of simulation. Squeezing the information of about 80 cases in one point makes it more difficult to make a general conclusion from this result. Figure 13 shows that some cases do not follow the trend shown in Figure 12. While there is a slight increase in the average level of pressure values from Figure 13a to Figure 13b, the average pressure level is decreasing when we compare Figure 13c to Figure 13d.

Similar analyzes have been conducted for other flow responses as well. Altogether, our sensitivity study shows that aggradation is the parameter that has most impact on the flow responses we have studied. Aggradation has either the largest or the second largest sensitivity during both injection and migration for almost all responses. The faulting has the second highest impact. Mostly effected by closed fault, the fault parameter influences the storage capacity and the extent to which a CO<sub>2</sub> plume accumulates under the caprock. Barriers play a dominating role for the splitting of plumes during injection, whereas the progradation affects the gravity segregation through conductive channels during the migration phase and the volume available to flow in the dip direction. Finally, lobosity has small impact compared to the other parameters and can therefore likely be ignored for the fluid responses considered above. However, lobosity has a considerable effect on the lateral movement and splitting of plumes during the migration period and may therefore have a more significant impact on the estimates of point leakage.

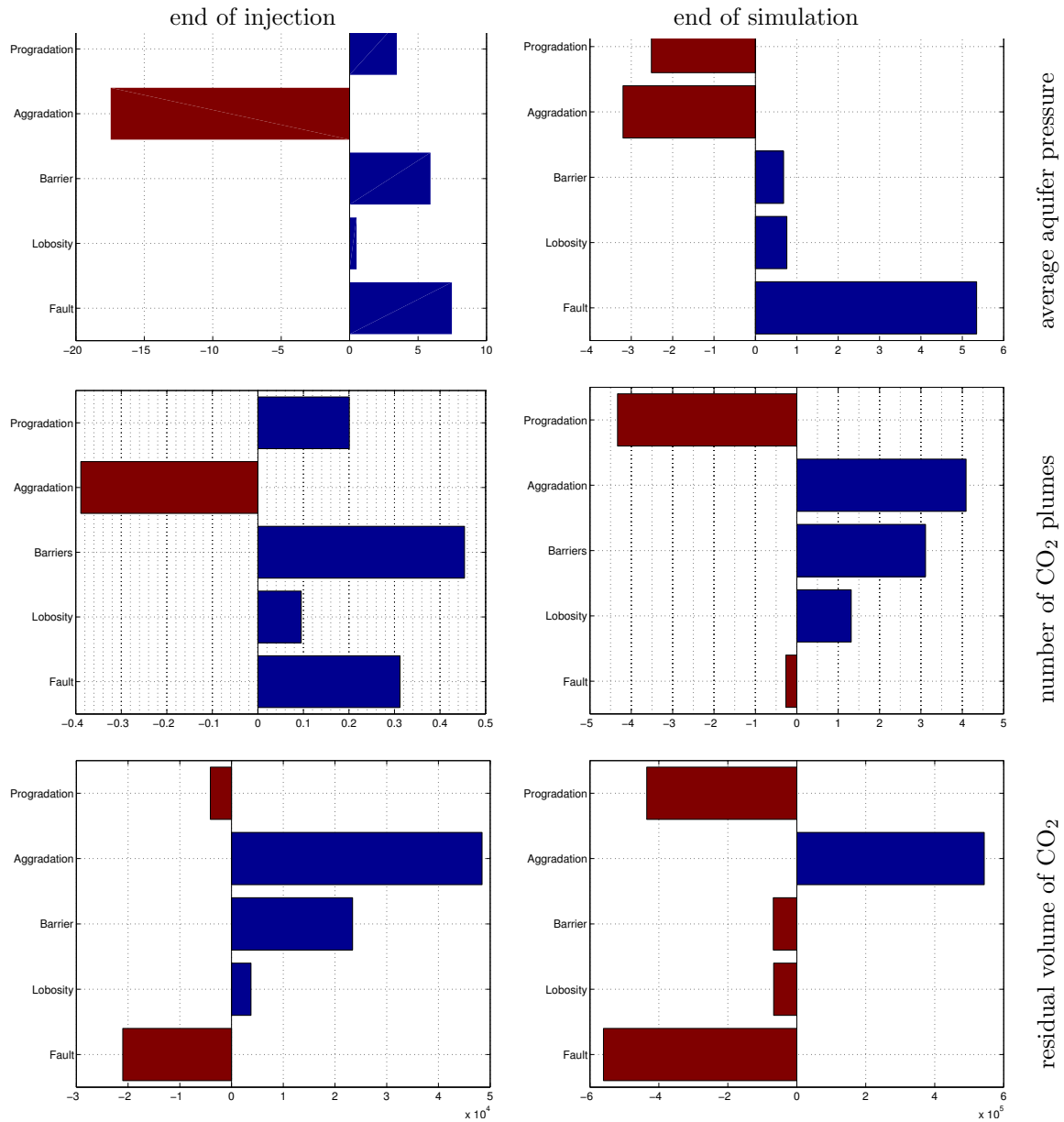


Figure 12: Sensitivities to different geological parameters at end of injection and end of simulation for the average aquifer pressure, number of CO<sub>2</sub> plumes, and residual volume of CO<sub>2</sub>.

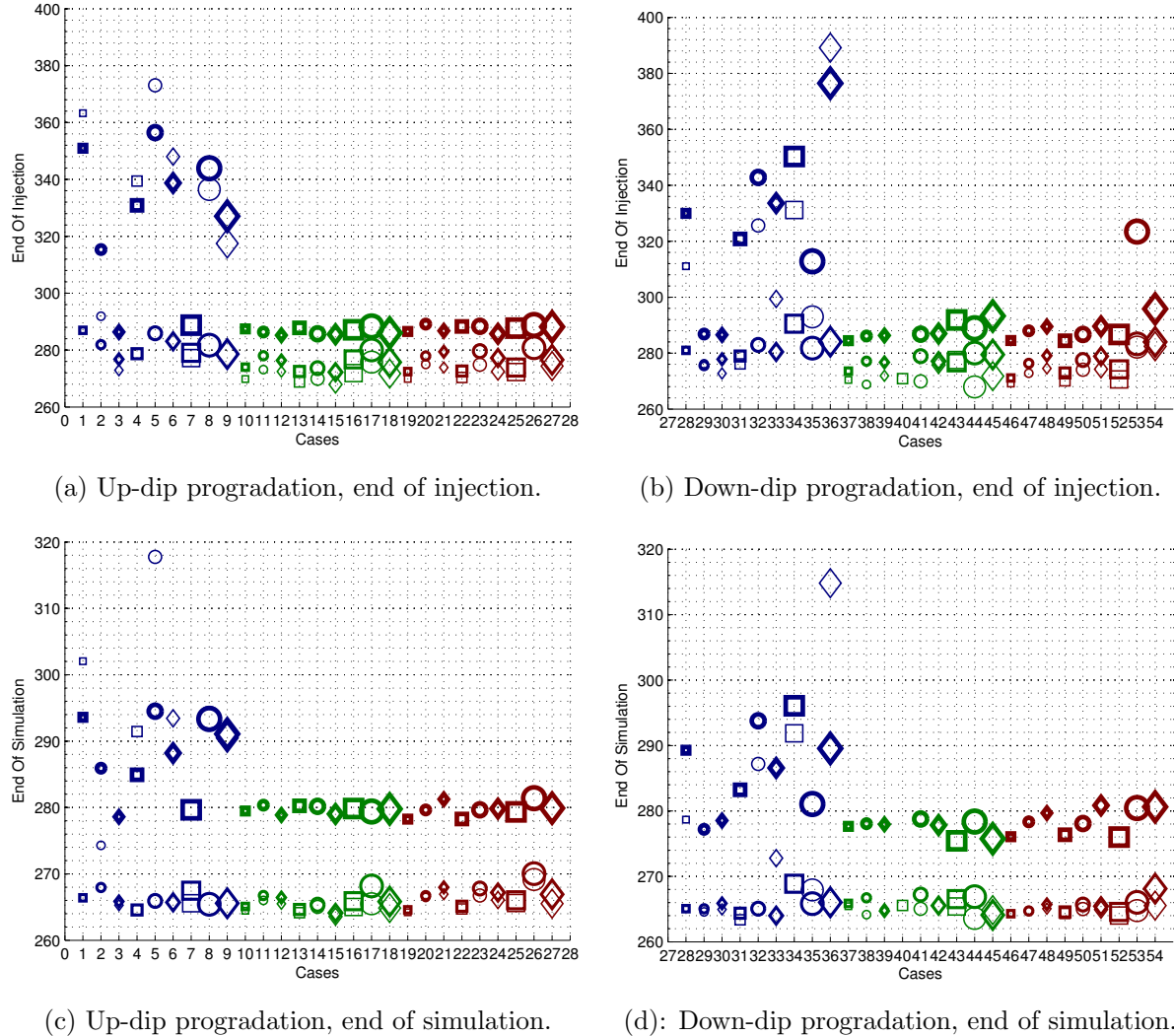


Figure 13: Effect of progradation on the pressure response.

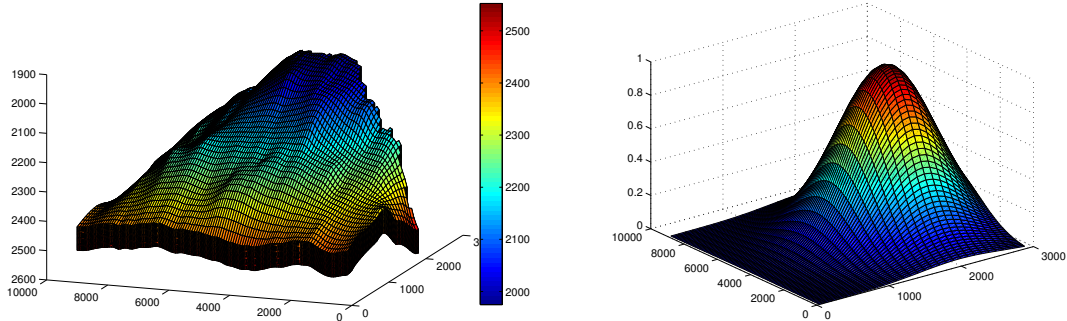


Figure 14: The left plot shows a sample grid geometry with depth values shown in meters. The right plot shows the Gaussian probability distribution for point leakage through the caprock. The distribution is centered at a point on the crest which is in the same slice as the injection point.

## 5 Risk for Point-Leakage

The capillary-sealing potential of the caprock is typically expressed in terms of the maximum over-pressure that the brine-saturated caprock can sustain, and leakage will only take place if the pressure of the CO<sub>2</sub> column exceeds this capillary entry pressure. The entry pressure is controlled by the interfacial tension between brine and CO<sub>2</sub>, the water-wettability of caprock minerals, and the pore size distribution within the caprock [35, 15, 16, 14, 48]. The water-wettability is altered in the presence of CO<sub>2</sub> under pressure conditions that are typical for a storage site. Pore-size distribution is due to depositional factors.

The SAIGUP study does not supply any information about the caprock and its geomechanical properties (including breaches and other regions of “high permeability” that may form potential leakage paths). We are therefore only able to conduct a conceptual study of the risk associated with point leakage through imperfections in the caprock. To this end, we assume that each point on the top surface has a prescribed probability for being a leakage point. In lack of any useful information, we will simply assume that the probability for point leakage follows a standard 2D Gaussian distribution centered at a given point on the crest, see Figure 14. This is physically unrealistic, but simple to treat mathematically. Moreover, we will also disregard the effects of capillary entry pressure and wettability alterations, which contribute to reduce potential leakage rates, and simply assume that all mobile CO<sub>2</sub> (except for the residual portion) will escape through the caprock if a plume comes in contact with a leakage point. We have seen above that the heterogeneity and tilt of the medium will cause the injected CO<sub>2</sub> to be distributed under the caprock as a number of plumes with variable sizes. For each cell along the top surface, we now define the risk as the probability of point leakage weighted by the volume of the CO<sub>2</sub> plume that the cell is part of. We then sum the values for all the topmost cells, normalize this sum, and use the resulting single number as a measure of leakage risk. The worst possible case would be if all the injected CO<sub>2</sub> volume forms a mobile plume that contacts every point along the top surface; this gives a risk value equal to one. For all reasonable cases, however, the risk value will be less than one because not all of the CO<sub>2</sub> will be mobile (because of residual trapping and loss of volumes across the open boundaries), because the mobile volume may form more than one plume, or because not all the mobile volume has reached the top due to reduced vertical mobility.

Figure 15 shows the resulting leakage risk for all cases at the end of simulation computed using linear relative permeabilities. Similarly, the left plot in Figure 16 shows how the risk changes during the seventy year period from the end of injection to the end of simulation, whereas the right plot shows a cross-plot of the leakage risk versus the total volume of mobile CO<sub>2</sub>. The plots lead to the rather obvious conclusion that improved vertical connection will increase the risk of mobile CO<sub>2</sub> migrating upward to connect a potential breach in the caprock, and hence that there is a positive correlation between the volume of mobile CO<sub>2</sub> in the system and leakage risk. However, we also observe that there are cases which have zero risk for leakage through the caprock. These are cases with low aggradation, for which the flow stays in the injected layers and moves laterally toward the open boundaries, resulting in a low amount of mobile CO<sub>2</sub> in the system. Furthermore, these cases have

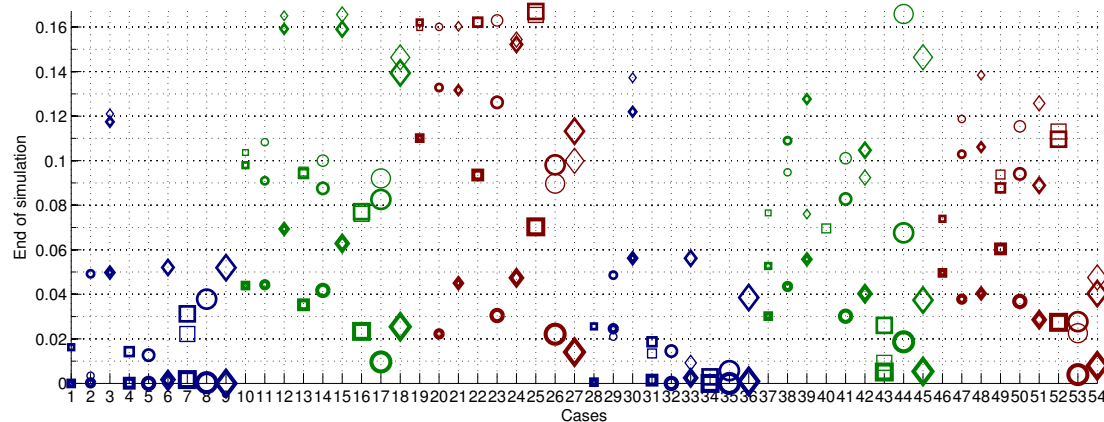


Figure 15: Leakage risk at the end of simulation for linear relative permeabilities.

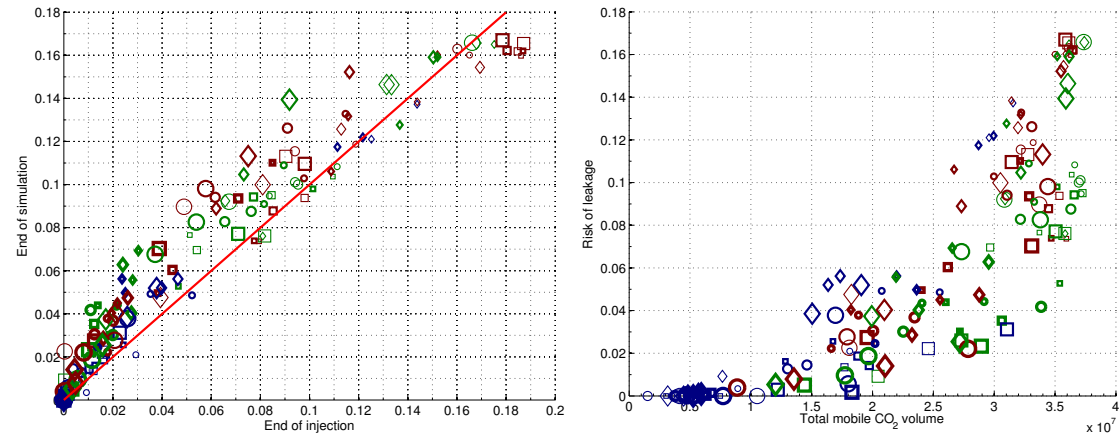


Figure 16: The left plot shows a cross-plot of leakage risk for linear relative permeability function. The right plot shows mobile CO<sub>2</sub> volume versus leakage risk at the end of simulation.

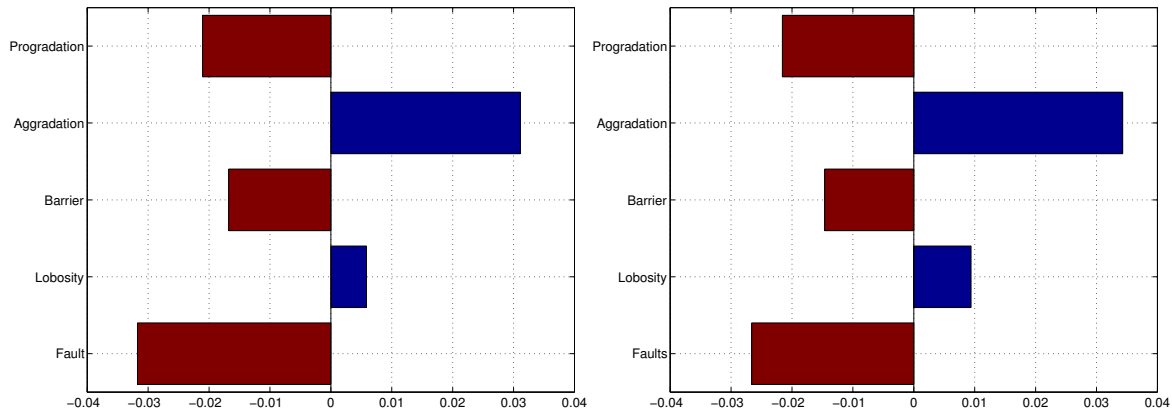


Figure 17: Sensitivity of the leakage risk with respect to the five geological parameters at the end of injection (left) and at the end of simulation (right).

(almost) no cross-layered CO<sub>2</sub> movement, which means that (almost) no CO<sub>2</sub> reaches the top surface. In other words, the low-aggradation cases, which have seemed to be unfavorable in our discussion in the previous two sections because of high injection pressure, larger lateral spread, and loss of volumes through the open boundaries, here appear as the most favorable with respect to potential leakage through imperfections the caprock.

Figure 17 shows sensitivities for the leakage risk. Because the total injected volume of CO<sub>2</sub> corresponds to 20% of the available pore volume, a major plume will in a majority of the cases have migrated to the crest of the reservoir already during the injection phase. Hence, the leakage-risk sensitivity shows almost the same profile at the end of injection and the end of simulation. This can also be observed in Figure 16. The sensitivity is slightly less during injection compared to at the end of simulation, because more CO<sub>2</sub> will accumulated below the caprock at the end of simulation. This overtakes the effect of the reduction in mobile volumes because of residual trapping and the increase in the number of plumes at end of simulation, which both result in less risk of leakage.

Once again, aggradation angle and fault criteria are the two most influential parameters. Increasing the aggradation angle improves the vertical communication and contributes to enhance the formation of CO<sub>2</sub> plumes below the caprock. Closed faults limit the movement of the plume and result in less accumulation below the caprock, whereas open faults generally increase the upward migration of plumes.

## 6 Conclusions

We have presented a study of how various geological parameters influence the injection and early-stage migration of CO<sub>2</sub> in progradational shallow-marine systems. One hundred and sixty equally probable realizations were considered and several flow responses related to storage capacity and risk of point leakage were calculated at the end of injection and after seventy years of gravity-dominated plume migration based on simulations using both linear and nonlinear relative permeabilities. We believe that linear permeabilities are a good starting point when studying the long-term impact of geological heterogeneities when this impact can be considered a first-order effect as herein. Flow predictions using nonlinear relative permeabilities are more sensitive to vertical grid resolution and can lead to severe under-prediction of gravity segregation effects in low-saturation regions if this resolution is not chosen sufficiently fine (see e.g., [36]). A more comprehensive study should therefore investigate the need for vertical (and lateral) grid refinement as in [52]. Vertical grid refinement will typically result in a CO<sub>2</sub> plume that is thinner vertically and has a much larger areal extent. If the segregated plume only fills the upper fraction of the grid cells, the movement of the plume will effectively be governed by linear permeabilities if capillary effects are small. For these reasons, we have herein primarily used linear permeabilities, which give significantly higher wave speeds and lead to earlier accumulation of CO<sub>2</sub> under the caprock and hence provide more pessimistic estimates of the plume migration and the risk associated with point leakage after a prescribed number of years than what is obtained by (possibly under-resolved) simulations with nonlinear relative permeabilities.

Altogether, we have demonstrated and discussed how the heterogeneity induced by different geological parameters give large variations in flow responses. Each geological parameter will influence the flow behavior and can result in local/global pressure build-up or pressure drop, enhance the flow direction, hinder the flow in the medium, or lead to loss of injected volumes over the open boundaries, and may induce different effects during the injection and plume migration. Specifically, we have demonstrated how variation in aggradation angle, fault criteria, and progradation direction significantly change the flow direction within the medium and hence impact the residual trapping and formation of movable CO<sub>2</sub> plumes under the caprock. Barriers are important during injection and must be modeled more carefully if the study focuses on injection operations. The large variations observed herein—e.g., for the reservoir pressure—are of course somewhat exaggerated by the fact that we consider a fixed injection point without regard to whether this point is favorable or not for each specific model realization. Despite this, we believe that our study shows that geological heterogeneity has a major impact on the injection and formation of a CO<sub>2</sub> plume and the subsequent early-stage migration of this plume. Any predictive study should therefore incorporate a realistic and detailed description of the geological heterogeneity as well as estimates of geological uncertainty to provide reliable forecasts of operational risks and the long-term fate of injected CO<sub>2</sub>.

## References

- [1] M. Akbarabadi and M. Piri. Relative permeability hysteresis and capillary trapping characteristics of supercritical CO<sub>2</sub>/brine systems: an experimental study at reservoir conditions. *Advances in Water Resources*, 2012.
- [2] I. Akervoll and P. Bergmo. A study of Johansen formation located offshore Mongstad as a candidate for permanent CO<sub>2</sub> storage. In *European Conference on CCS Research, Development and Demonstration. 10–11 February 2009, Oslo, Norway*, 2009.
- [3] M. Ashraf. Impact of geological heterogeneity on early-stage CO<sub>2</sub> plume migration: pressure sensitivity study. *Submitted*, 2013.
- [4] B. Bennion and S. Bachu. Drainage and imbibition relative permeability relationships for supercritical CO<sub>2</sub>/brine and H<sub>2</sub>S/brine systems in intergranular sandstone, carbonate, shale, and anhydrite rocks. *SPE Reservoir Evaluation & Engineering*, 11(3):487–496, 2008.
- [5] B. Bennion and S. Bachu. Drainage and imbibition CO<sub>2</sub>/brine relative permeability curves at reservoir conditions for carbonate formations, spe 134028. In *SPE Annual technical conference and exhibition, Florence, Italy, Society of Petroleum Engineers*, 2010.
- [6] P. E. S. Bergmo, E. G. Lindeberg, F. Riis, and W. T. Johansen. Exploring geological storage sites for CO<sub>2</sub> from Norwegian gas power plants: Johansen formation. *Energy Procedia*, 1(1):2945–2952, 2009.
- [7] M. Bickle, A. Chadwick, H. E. Huppert, M. Hallworth, and S. Lyle. Modelling carbon dioxide accumulation at Sleipner: Implications for underground carbon storage. *Earth and Planetary Science Letters*, 255:164–176, 2007.
- [8] R. Bissell, D. Vasco, M. Atbi, M. Hamdani, M. Okwelegbe, and M. Goldwater. A full field simulation of the In Salah gas production and CO<sub>2</sub> storage project using a coupled geo-mechanical and thermal fluid flow simulator. *Energy Procedia*, 4(0):3290–3297, 2011.
- [9] F. C. Boait, N. J. White, M. J. Bickle, R. A. Chadwick, J. A. Neufeld, and H. E. Huppert. Spatial and temporal evolution of injected CO<sub>2</sub> at the Sleipner Field, North Sea. *Journal of Geophysical Research: Solid Earth*, 117(B3), 2012.
- [10] M. Burton, N. Kumar, and S. L. Bryant. CO<sub>2</sub> injectivity into brine aquifers: Why relative permeability matters as much as absolute permeability. *Energy Procedia*, 1(1):3091–3098, 2009.
- [11] A. Cavanagh and P. Ringrose. Simulation of CO<sub>2</sub> distribution at the In Salah storage site using high-resolution field-scale models. *Energy Procedia*, 4(0):3730 – 3737, 2011.
- [12] R. A. Chadwick and D. J. Noy. History-matching flow simulations and time-lapse seismic data from the Sleipner CO<sub>2</sub> plume. *Geological Society, London, Petroleum Geology Conference series*, 7:1171–1182, 2010.
- [13] R. A. Chadwick, P. Zweigel, U. Gregersen, G. A. Kirby, S. Holloway, and P. N. Johannessen. Geological reservoir characterization of a CO<sub>2</sub> storage site: The Utsira Sand, Sleipner, northern North Sea. *Energy*, 29(9–10):1371–1381, 2004. 6th International Conference on Greenhouse Gas Control Technologies.
- [14] C. Chalbaud, M. Robin, J. Lombard, F. Martin, P. Egermann, and H. Bertin. Interfacial tension measurements and wettability evaluation for geological CO<sub>2</sub> storage. *Advances in Water Resources*, 32(1):98–109, 2009.
- [15] P. Chiquet, D. Broseta, and S. Thibeau. Capillary alteration of shaly caprocks by carbon dioxide. In *SPE Europec/EAGE Annual Conference*, 2005.
- [16] P. Chiquet, D. Broseta, and S. Thibeau. Wettability alteration of caprock minerals by carbon dioxide. *Geofluids*, 7(2):112–122, 2007.

- [17] H. Class et al. A benchmark study on problems related to CO<sub>2</sub> storage in geologic formations. *Comput. Geosci.*, 13(4):409–434, 2009.
- [18] P. J. Cook, A. Rigg, and J. Bradshaw. Putting it back where it came from: Is geological disposal of carbon dioxide an option for Australia. *Australian Petroleum Production and Exploration Association Journal*, 1, 2000.
- [19] G. T. Eigestad, H. K. Dahle, B. Hellevang, F. Riis, W. T. Johansen, and E. Øian. Geological modeling and simulation of CO<sub>2</sub> injection in the Johansen formation. *Computational Geosciences*, 13(4):435–450, 2009.
- [20] M. Flett, R. Gurton, and G. Weir. Heterogeneous saline formations for carbon dioxide disposal: Impact of varying heterogeneity on containment and trapping. *Journal of Petroleum Science and Engineering*, 57(1-2):106–118, 2007.
- [21] A. Förster, B. Norden, K. Zinck-Jørgensen, P. Frykman, J. Kulenkampff, E. Spangenberg, J. Erzinger, M. Zimmer, J. Kopp, G. Borm, et al. Baseline characterization of the CO<sub>2</sub>SINK geological storage site at Ketzin, Germany. *Environmental Geosciences*, 13(3):145–161, 2006.
- [22] O. Gharbi, B. Bijeljic, E. Boek, and M. J. Blunt. Changes in pore structure and connectivity induced by CO<sub>2</sub> injection in carbonates: a combined pore-scale approach. In *Proceedings of the international conference on greenhouse gas technologies (GHGT)*, volume 11, 2012.
- [23] A. L. Goater, B. Bijeljic, and M. J. Blunt. Dipping open aquifers—the effect of top-surface topography and heterogeneity on CO<sub>2</sub> storage efficiency. *International Journal of Greenhouse Gas Control*, 17:318–331, 2013.
- [24] W. D. Gunter, S. Bachu, and S. Benson. The role of hydrogeological and geochemical trapping in sedimentary basins for secure geological storage of carbon dioxide. *Geological Society, London, Special Publications*, 233(1):129–145, 2004.
- [25] B. Hitchon. *Aquifer disposal of carbon dioxide: hydrodynamic and mineral trapping: proof of concept*. Geoscience Pub., 1996.
- [26] S. D. Hovorka, C. Doughty, S. M. Benson, K. Pruess, and P. R. Knox. The impact of geological heterogeneity on CO<sub>2</sub> storage in brine formations: a case study from the Texas Gulf Coast. *Geological Society, London, Special Publications*, 233(1):147–163, 2004.
- [27] J. A. Howell, A. Skorstad, A. MacDonald, A. Fordham, S. Flint, B. Fjellvoll, and T. Manzocchi. Sedimentological parameterization of shallow-marine reservoirs. *Petroleum Geoscience*, 14(1):17–34, 2008.
- [28] R. Juanes, E. J. Spiteri, F. M. Orr Jr, and M. J. Blunt. Impact of relative permeability hysteresis on geological CO<sub>2</sub> storage. *Water Resources Research*, 42:W12418, 2006.
- [29] T. Kempka, H. Class, U.-J. Görke, B. Norden, O. Kolditz, M. Kühn, L. Walter, W. Wang, and B. Zehner. A dynamic flow simulation code intercomparison based on the revised static model of the Ketzin pilot site. *Energy Procedia*, 40(0):418–427, 2013.
- [30] T. Kempka, M. Kühn, H. Class, P. Frykman, A. Kopp, C. Nielsen, and P. Probst. Modelling of CO<sub>2</sub> arrival time at Ketzin—Part I. *International Journal of Greenhouse Gas Control*, 4(6):1007–1015, 2010.
- [31] A. Kopp, H. Class, and R. Helmig. Investigations on CO<sub>2</sub> storage capacity in saline aquifers: Part 1. dimensional analysis of flow processes and reservoir characteristics. *International Journal of Greenhouse Gas Control*, 3(3):263–276, 2009.
- [32] S. Krevor, R. Pini, L. Zuo, and S. M. Benson. Relative permeability and trapping of CO<sub>2</sub> and water in sandstone rocks at reservoir conditions. *Water Resources Research*, 48(2), 2012.
- [33] H. Law and S. Bachu. Hydrological and numerical analysis of CO<sub>2</sub> disposal in deep aquifer systems in the Alberta sedimentary basin. *Ener. Convers. Mgmt*, 37(6-8):1167–1174, 1996.

- [34] U. Lengler, M. D. Lucia, and M. Kühn. The impact of heterogeneity on the distribution of CO<sub>2</sub>: Numerical simulation of CO<sub>2</sub> storage at Ketzin. *International Journal of Greenhouse Gas Control*, 4(6):1016–1025, 2010.
- [35] S. Li, M. Dong, Z. Li, S. Huang, H. Qing, and E. Nickel. Gas breakthrough pressure for hydrocarbon reservoir seal rocks: implications for the security of long-term CO<sub>2</sub> storage in the weyburn field. *Geofluids*, 5(4):326–334, 2005.
- [36] I. S. Ligaarden and H. M. Nilsen. Numerical aspects of using vertical equilibrium models for simulating CO<sub>2</sub> sequestration. In *Proceedings of ECMOR XII–12th European Conference on the Mathematics of Oil Recovery*, Oxford, UK, 6–9 September 2010. EAGE.
- [37] E. Lindeberg. Escape of CO<sub>2</sub> from aquifers. *Energy Conversion and Management*, 38:S235–S240, 1997.
- [38] T. Manzocchi et al. Sensitivity of the impact of geological uncertainty on production from faulted and unfaulted shallow-marine oil reservoirs: objectives and methods. *Petroleum Geoscience*, 14(1):3–15, 2008.
- [39] J. D. Matthews, J. N. Carter, K. D. Stephen, R. W. Zimmerman, A. Skorstad, T. Manzocchi, and J. A. Howell. Assessing the effect of geological uncertainty on recovery estimates in shallow-marine reservoirs: the application of reservoir engineering to the saigup project. *Petroleum Geoscience*, 14(1):35–44, 2008.
- [40] H. M. Nilsen, P. A. Herrera, M. Ashraf, I. Ligaarden, M. Iding, C. Hermanrud, K.-A. Lie, J. M. Nordbotten, H. K. Dahle, and E. Keilegavlen. Field-case simulation of CO<sub>2</sub>-plume migration using vertical-equilibrium models. *Energy Procedia*, 4(0):3801–3808, 2011. 10th International Conference on Greenhouse Gas Control Technologies.
- [41] H. M. Nilsen, A. R. Syversveen, K.-A. Lie, J. Tveranger, and J. M. Nordbotten. Impact of top-surface morphology on CO<sub>2</sub> storage capacity. *International Journal of Greenhouse Gas Control*, 11(0):221–235, 2012.
- [42] J. M. Nordbotten and M. A. Celia. *Geological Storage of CO<sub>2</sub>: Modeling Approaches for Large-Scale Simulation*. John Wiley & Sons, Hoboken, New Jersey, 2012.
- [43] J. M. Nordbotten, D. Kavetski, M. A. Celia, and S. Bachu. A semi-analytical model estimating leakage associated with CO<sub>2</sub> storage in large-scale multi-layered geological systems with multiple leaky wells. *Under Review at: Environmental Science and Technology*, 2008.
- [44] E.-O. I. Obi and M. J. Blunt. Streamline-based simulation of carbon dioxide storage in a North Sea aquifer. *Water Resources Research*, 42(3), 2006.
- [45] Y. Pamukcu, S. Hurter, P. Frykman, and F. Moeller. Dynamic simulation and history matching at Ketzin (CO<sub>2</sub>SINK). *Energy Procedia*, 4(0):4433–4441, 2011.
- [46] Y. Pamukcu, S. Hurter, L. Jammes, D. Vu-Hoang, and L. Pekot. Characterizing and predicting short term performance for the In Salah Krechba field CCS joint industry project. *Energy Procedia*, 4(0):3371–3378, 2011.
- [47] J.-C. Perrin and S. Benson. An experimental study on the influence of sub-core scale heterogeneities on CO<sub>2</sub> distribution in reservoir rocks. *Transport in porous media*, 82(1):93–109, 2010.
- [48] H. Shao, J. R. Ray, and Y.-S. Jun. Dissolution and precipitation of clay minerals under geo-logic CO<sub>2</sub> sequestration conditions: CO<sub>2</sub>–brine–phlogopite interactions. *Environmental science & technology*, 44(15):5999–6005, 2010.
- [49] E. Spiteri, R. Juanes, M. Blunt, and F. Orr. Relative-permeability hysteresis: Trapping models and application to geological CO<sub>2</sub> sequestration. In *SPE Annual Technical Conference and Exhibition*, 2005.

- [50] A. R. Syversveen, H. M. Nilsen, K.-A. Lie, J. Tveranger, and P. Abrahamsen. A study on how top-surface morphology influences the storage capacity of CO<sub>2</sub> in saline aquifers. In P. Abrahamsen, R. Hauge, and O. Kolbjørnsen, editors, *Geostatistics Oslo 2012*, volume 17 of *Quantitative Geology and Geostatistics*, pages 481–492. Springer Netherlands, 2012.
- [51] L. Van der Meer. The CO<sub>2</sub> storage efficiency of aquifers. *Energy Conversion and Management*, 36(6):513–518, 1995.
- [52] L. Wei and F. Saaf. Estimate CO<sub>2</sub> storage capacity of the Johansen formation: numerical investigations beyond the benchmarking exercise. *Computational Geosciences*, 13(4):451–467, 2009.
- [53] L. Zuo, S. Krevor, R. W. Falta, and S. M. Benson. An experimental study of CO<sub>2</sub> exsolution and relative permeability measurements during CO<sub>2</sub> saturated water depressurization. *Transport in porous media*, 91(2):459–478, 2012.

# Paper II

## 3.2 Geological storage of CO<sub>2</sub>: Heterogeneity impact on pressure behavior

M. Ashraf

Submitted to *International Journal of Greenhouse Gas Control (IJGGC)*



# Geological storage of CO<sub>2</sub>: Heterogeneity impact on pressure behavior

Meisam Ashraf

November 23, 2013

## Abstract

Due to the high rates of industrial CO<sub>2</sub> emission, it is an operational objective to maximize CO<sub>2</sub> injection rates into underground geological formations. Forcing high volumetric rates into the injection wells can result in an over-pressurized system, which can cause possible breaches in the formation integrity and can increase the risk of CO<sub>2</sub> leakage.

The goal of this study is to investigate and control the pressure buildup during injection to avoid the uncontrolled development of fractures in the medium. Herein, we study how geological heterogeneity influences the pressure behavior of a typical CO<sub>2</sub> injection operation. Five geological feature variables are considered as inputs for the sensitivity analysis. These features include various degrees of faults, lobosity, flow barriers, aggradational angle, and progradation direction.

Two injection scenarios are examined. In the first scenario, CO<sub>2</sub> is injected through a single well at a constant rate and the pressure in the well and the domain is allowed to build up without limit. In the second scenario, a pressure constraint is set on the well and the target injection rate is reduced to keep the pressure below the safety limit. Model responses related to pressure buildup and propagation within the system are defined and demonstrated using a single geological realization. Results for all realizations are presented and discussed accordingly. We conclude by ranking aggradational angle, progradation direction, and faults as the most influential geological parameters.

The novelty of this work lies in the use of a large parametrized ensemble of equiprobable and realistic geological realizations to analyze how pressure builds up and propagates through the storage medium. The demonstrated workflow is generic and can be used in any extensive pressure study. Likewise, our investigation reveals several generic patterns in how the different geological parameters influence the pressure buildup in this type of shallow-marine systems, but the relative ranking of which parameters are the most important may, of course, change if one selects a different injection scenario, injection location, number of injector, or set of geological realizations.

## 1 Introduction

The industrial CO<sub>2</sub> emission rate is expected to increase over the next decade if necessary preventive actions are not taken. For example, according to the Energy Information Administration, carbon dioxide emissions in the United States are forecast to reach 6.41 billion tonnes by 2030. The Kyoto Protocol proposed an emission cut that requires a reduction of 1.75 billion tonnes of carbon dioxide [16].

Geological storage of CO<sub>2</sub> is a proposed solution to fight global climate change. Clear operational criteria and policies must be put forward to avert unwanted consequences. Concerns connected to putting large volumes of CO<sub>2</sub> into underground geological formations are not limited to the spatial distribution of the injected fluid. The pressure signals imposed through the injection point can travel beyond the scale of the zones where CO<sub>2</sub> is present. Although geological barriers can hinder the pressure exchange between different regions, pressure can transfer through low-permeable rocks where the CO<sub>2</sub> is trapped by capillarity.

In addition to the depleted oil and gas fields, deep geological aquifers are practical targets for the geological storage of CO<sub>2</sub>. If one is injecting into brine aquifers, the pressure waves can push the brine into connected fresh water aquifers, contaminating them. Brine displacement issues are discussed in [5] by defining open, closed, and semi-closed aquifer boundaries. Brine might also leak through abandoned wells into other zones. Cailly et al. [4] discuss how to design the injection process to prevent any leakage through wells.

Geomechanical deformations are important during the injection period. They can lead to changes in effective permeability and porosity. It is possible that the pressure buildup around injection wells can crack the rock with uncontrolled fractures extending to the structural sealing layers. Faults can be activated due to high pressure in the system, providing a leakage path across layers. In addition to the increased spatial spread of CO<sub>2</sub>, an intensive induced fracture network can result in local earthquakes.

Simplified geological assumptions allow the use of established analytical solution of the flow governing equations. Neuman and Witherspoon [11] presented solutions that are useful for determining the hydraulic properties of leaky confined aquifer systems. They assumed that the aquifer is homogeneous, isotropic, and of uniform thickness. Moreover, they assumed the spatial extent of the aquifer to be infinite. Chabora and Benson [6] used the analytical solution provided in [11] to study the leakage of the stored CO<sub>2</sub> through the caprock by measuring the pressure buildup in the aquifer. They performed sensitivity analysis on the pressure variation by changing the formation parameters and injection criteria. Chabora and Benson found a correlation between the pressure buildup values in the medium and the specifications of aquifer and injection operations. This correlation gives insight in the design and monitoring phases of the storage operations. Such pressure monitoring approaches are based on geological simplifications.

Injection causes pressure evolution in the domain that starts by transient pressure buildup near the injector. As the injection proceeds, the injected CO<sub>2</sub> invades larger region in the domain. The two-phase region grows in size and the injected CO<sub>2</sub> moves in both vertical and horizontal directions within the aquifer. In the vertical direction, the CO<sub>2</sub> moves upward due to the buoyancy forces and in the horizontal direction the influx from the injector pushes the CO<sub>2</sub> through the two-phase zone. When the pressure pulse imposed by the injector reaches the boundaries of the domain, the average pressure in the aquifer increases in a

quasi-steady state trend. Pressure buildup development in the medium, in particular the transient pressure changes, can be influenced dramatically by geological heterogeneities. This study aims to evaluate the importance of sophisticated geological modeling in simulating the pressure variation in the domain.

Spatial pressure distribution in the aquifer depends on the extent of the domain. The available volume for CO<sub>2</sub> storage in closed or semi-closed systems with limited spatial extent is mostly provided by medium compressibility in response to formation pressure buildup. Moreover, the caprock and structural traps that are supposed to be sealing may allow the CO<sub>2</sub> to leak at a rate that depends on the pressure buildup in the aquifer. Birkholzer et al. [3] investigated the influence of domain size on pressure rise in the medium caused by CO<sub>2</sub> injection, assuming a homogeneous aquifer to study the pressure development for various model sizes, ranging from 10 to 100 km. They simulated CO<sub>2</sub> injection over 30 years in 250 m thick formation with a rate of 120 kg/s, and performed sensitivity analysis with focus on the plume migration and the evolution of pressure buildup in the aquifer. In addition to the spatial extent, various hydrological properties were examined to study the impact on CO<sub>2</sub> storage capacity. The results in [3] suggest that the storage capacity in closed and semi-closed aquifers is controlled by the operational pressure constraints and it is much smaller than the capacity of large aquifers. The simulations in [3] show that the region of elevated pressure is much larger than the size of the CO<sub>2</sub> plume. In a 20 km model, a substantial pressure increase of 45 bar from hydrostatic was observed at the model boundaries. They used closed boundary condition in the model that caused a global pressurizing in the medium. A local pressure rise above 60 bar was simulated near the injection well.

In general, constraints must be imposed on the bottom-hole pressure of the injection well to limit the pressure buildup in the aquifer, which will typically reduce the injection rate that is possible to safely achieve. Rock quality within the injection region has a significant impact on pressure buildup and therefore geological uncertainty plays a considerable role in assessing the success and feasibility of the operation. Most of the pressure-related studies in the literature provide either deterministic case studies or generic preventive measures based on theoretical studies [12, 17, 8, 18, 14, 13]. It is important to include realistic geological descriptions in any geological uncertainty study. For example, realistic permeability variation in the grid should be included, possibly in the form of an ensemble of equiprobable realizations.

Within the context of oil recovery, the impact of geological uncertainty on different field-development strategies is thoroughly investigated in the SAIGUP project for shallow-marine depositional systems [7, 9, 10]. Based on several injection/production patterns, the study concludes that geological uncertainty has a dramatic influence on the oil recovery estimates. We have previously used a number of geological realizations from the SAIGUP project to investigate the impact of geological uncertainty on the injection and early migration of CO<sub>2</sub> [2, 1]. The focus in these studies was to use the parametrized ensemble of geological realizations to measure how sensitive the spatial CO<sub>2</sub> distribution is to variations in the geology. Certain structural features were considered and several flow responses were defined to measure the storage capacity, the trapping efficiency, and the leakage risk. The sensitivity of these responses to variations in geological parameters was investigated. The results show that varying the geology gives large variation in responses, and aggradation angle and barrier coverage were found to have the most significant impact on the CO<sub>2</sub> flow behavior [2, 1].

Herein, we will use the same SAIGUP geological realizations to perform detailed analysis of how geological variations impact the pressure buildup and propagation in aquifers. The spatial extent of the SAIGUP models,  $9\text{ km} \times 3\text{ km} \times 80\text{ m}$ , is considerably smaller than the extent of large aquifers. To compensate for the size, we consider open boundary conditions by exaggerating the pore volume of the cells at the boundaries of the model. This choice of boundary modeling results in an early relaxation of the pressure in the medium when the pressure pulse arrives at the boundary. Overall, the pressure values reported in our study can therefore be expected to be higher if they were modeled in a larger model. This study complements [2, 1], in the sense that we herein analyze the sensitivity of pressure to the same geological parameters. In addition to the injection scenario used in [2, 1], we examine a different injection scenario with more realistic well control for the injection operation. Our study shows that details in the geology can have a pronounced effect on the pressure development, which demonstrates the importance of realistic and detailed geological modeling when designing CO<sub>2</sub> storage operations and monitoring the pressure development in the aquifer. To the best of our knowledge, this is the first pressure study in the context of CO<sub>2</sub> storage that considers the geological uncertainty in the form of a parametrized set of structural and sedimentological variables.

## 2 Geological parameters

In the SAIGUP study, six rock types were included to model a shallow-marine system. Each rock type was modeled at appropriate scales to honor the interaction of flow with various heterogeneity types at different spatial scales (Figure 1). Each facies was upscaled in a number of stages and finally all the rock types were mapped on a fine-grid geological model. Some of the meter-scale facies were modeled in three dimensions to capture anisotropy. Variation within each rock type was modeled either deterministically by considering a periodic pattern or modeled internally by stochastic population. Channels were modeled on the fine grid and went through two stages of upscaling. Tests showed that when upscaled, models with different grid resolutions produced similar results. The specifications of the rock types are given in Table 1. For more detail of the SAIGUP sedimentological modeling see [7].

Table 1: The facies used in the SAIGUP geological modeling and their modeling scales.

Facies name	X Scale	Y Scale	Z Scale
Offshore transition zone	0.5 m	0.5 m	0.5 cm
Lower shoreface	0.5 m	0.5 m	0.5–2.0 cm
Upper shoreface	0.5 m	0.5 m	0.2–0.5 cm
Coastal plane	75 m	—	—
Offshore	75 m	—	—
Channels	0.04–1 m	0.04–1 m	0.5 cm

The wave and fluvial depositional processes acting at the shoreline control the plan-view shape, the channel abundance in the delta plain, and the abundance of mud-drapes. These parameters were characterized and summarized as three different types of shorefaces. A wave-dominated deposition produces a straight plan-view shape, very few channels, and no dipping

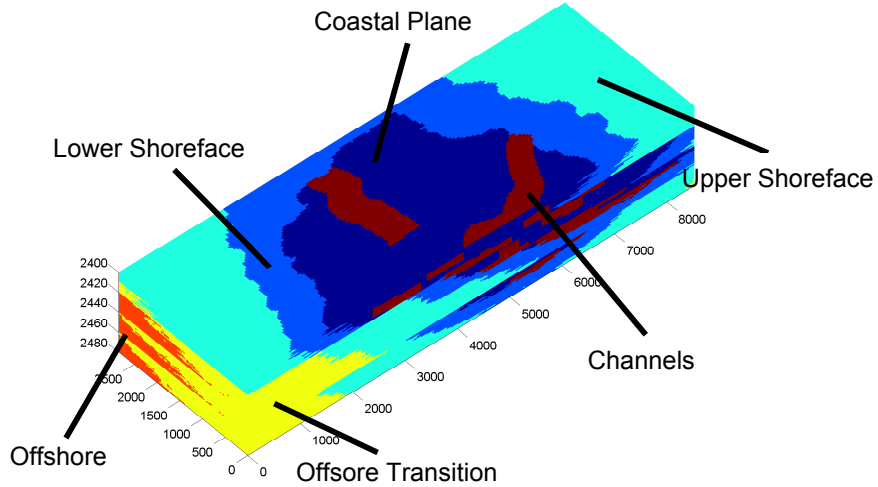


Figure 1: Geological modeling in the SAIGUP realizations contains six facies that represent a shallow-marine system. The rock types are represented by various colors for a selected realization. Axes show the spatial dimension of the model in meter.

Table 2: Specification of geological and simulation models; averaged values are arithmetic averages and belong to the specific geological realization shown in Figure 1.

Parameter	Value
Model dimensions	3 km × 9 km × 80 m
Geological grid resolution	80 × 240 × 80
Simulation grid resolution	40 × 120 × 20
Simulation grid resolution	40 × 120 × 20
Average of lateral permeability	181 mD
Average of Vertical permeability	26.8 mD
Average of porosity	0.145

Table 3: Colors and line and marker types used to signify different values of the geological parameters outlined in Figure 2.

Code	Description	Color/line/marker	Feature values
<b>Thickness</b>	Fault	thin/medium/thick	unfaulted/open/close
<b>Shape</b>	Lobosity	square/circle/diamond	flat/one-lobe/two-lobe
<b>Size</b>	Barriers	small/medium/large	10% / 50% / 90%
<b>Color</b>	Aggradation	blue/green/red	low/medium/high
<b>Case no. counting</b>	Progradation	first half/second half	up-dip / down-dip

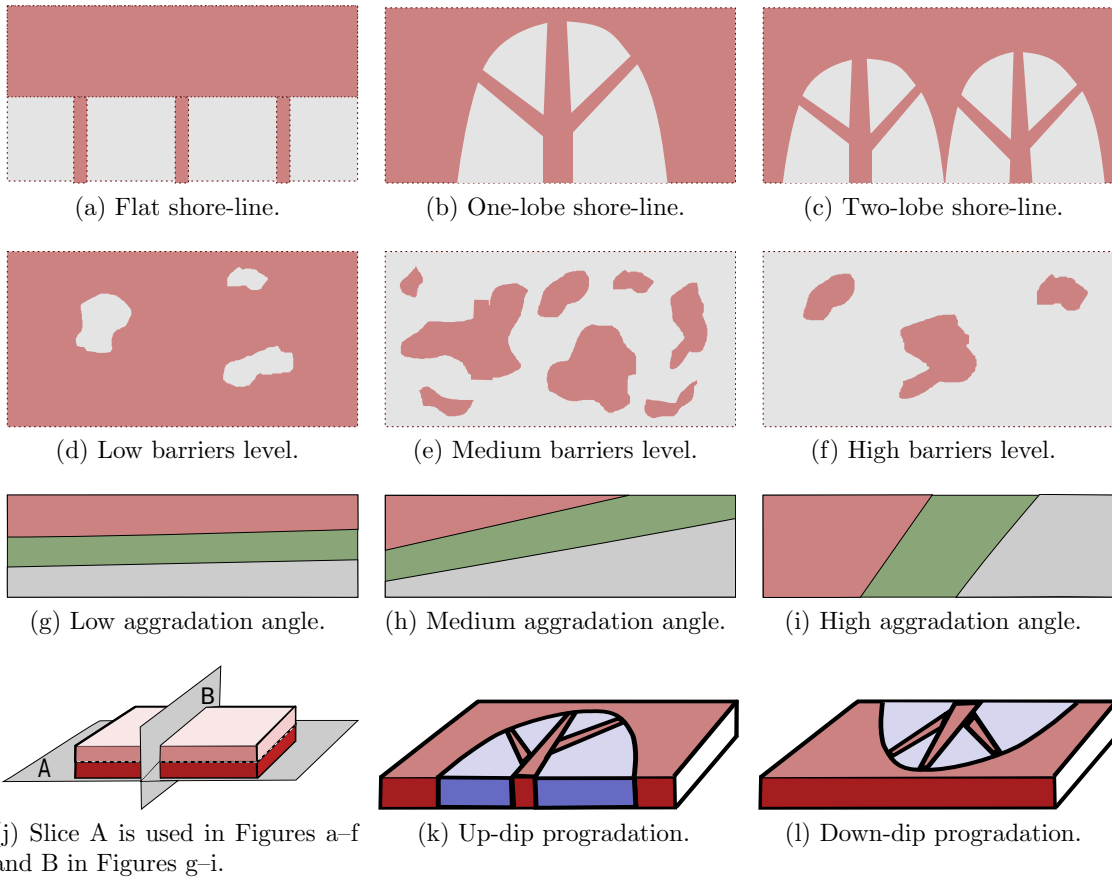


Figure 2: The studied geological features. a–c) Shoreline shape, gray is for poor quality rock and brown color resembles a good quality rock. d–f) Barriers level defined by transmissibility multiplier; gray color is for zero and brown color shows one. g–i) Aggradation angle. k–l) Progradation direction. Figure j shows the slices used in other figures.

barriers. If the river flux is high enough to dominate the wave system in the sea, a lobate shape shoreface generates with a moderate number of channels and some dipping barriers. Higher levels of fluvial domination end up in two-lobe system with numerous channeling and dip barrier surfaces.

Shale-draped surfaces may provide both horizontal and vertical barriers to fluid flow and are common in fluvial-dominated systems. They are the product of very short-term fluctuations in the fluvial systems and periodic floods in the delta. Shore line shape is correlated to the shape of these flow barriers; straight shorelines typically have planar seaward-dipping clinoforms and curved shorelines have clinoforms that resemble top-truncated cones. Within SAIGUP, these barrier surfaces were modeled as stepped transmissibility multipliers on the cell faces. Dipping barriers were not included in the flat shoreline models and in the realizations with lobosity, between one and three barriers were included. For the purpose of SAIGUP, three levels of barrier coverage were modeled for all of the SAIGUP models (10%, 50% and 90% coverage). All levels of coverage were subsequently slightly modified by removing the barriers where the fluvial channel deposits were present, since clinoforms are a feature of the delta front and not formed within a channel setting.

Aggradation angle models the variation of shoreline in a 2D depositional dip-orientated cross-section. Within SAIGUP, the trajectory varies between horizontal progradation and pure vertical aggradation. Aggradation angle is a function of the balance between sediment supply and the rate of accommodation in the sea. When the fluvial flux increases in level, the deposition from the river toward the sea pile toward the sea and makes the aggradation angle.

The final factor varied during the sedimentological modeling was the progradation or depositional-dip direction. Figure 2 shows a schematic of each geological parameter with its variation. The progradation direction is important for CO<sub>2</sub> injection operations because the structural dip controls the injection well position and the direction of CO<sub>2</sub> plume movement during injection. In Figure 3, injecting in high permeability channels enhances the well injectivity and lowers the pressure buildup in the medium.

The faults are modeled as post-depositional with no related changes in facies thickness or shoreline orientations. Faulting process causes layers with different quality to become adjacent (Figure 4). This can enhance the pressure connectivity by breaking sealing layers, or it can produce sealed compartments that are not connected to the rest of the domain.

In the last step of the SAIGUP modeling process, the geological realizations were upscaled via flow-based methods to a coarse grid that was found suitable for detailed flow simulations. Details of geological and simulation grids are given in Table 2.

Herein, we have selected four of the geological parameters from the SAIGUP project (Figure 2) to study the impact of heterogeneity in the petrophysical parameters on the pressure responses in a typical CO<sub>2</sub> injection problem. Altogether, this gives 54 different petrophysical realizations. In addition, we consider three different degrees of faulting in the models: unfaulted, open, and closed faults (Figure 5). Combining all the features and levels makes 162 cases. However, two cases were missing in the original data set and in the following we will therefore consider 160 different models. Each of these models are represented with different colors, line types, and marker types and sizes, as explained in Table 3.

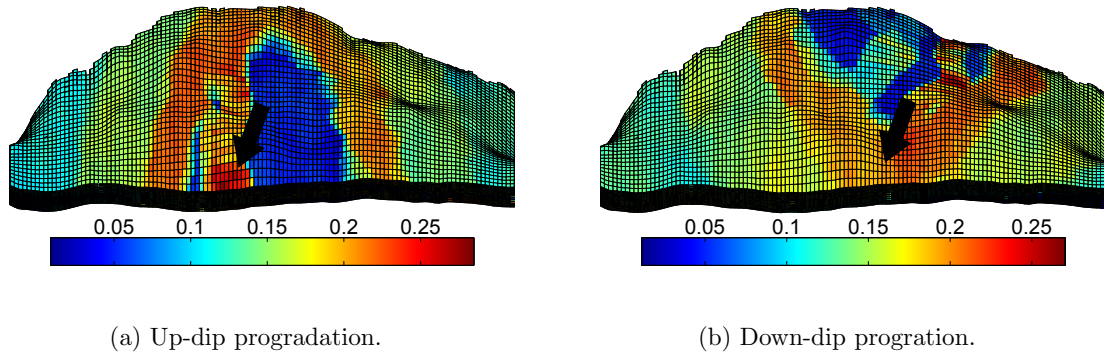


Figure 3: Progradation dip direction shown by porosity for a case with one lobe. Arrows point to injection locations in the flank. Up-dip progradation (left) contains heterogeneities in the form of high contrast channels surrounded by poor quality rocks. The injectivity in this case can be dramatically good or bad, depending on the well location. On the other hand, down-dip progradation (right) provides a lower contrast in the flank that can be low rock quality in general with low injection quality.

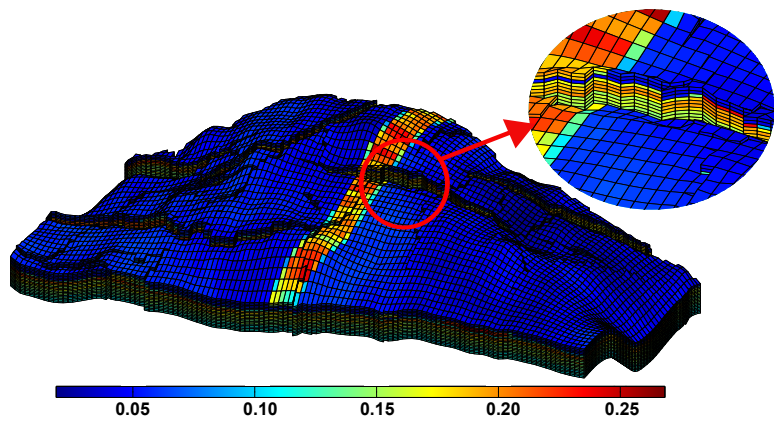


Figure 4: Faults connect layers with different rock types. Porosity is shown ion the grid. Across the fault, layers with low pore volume and permeability (the latter is not shown here) sit next to high pore volume and permeability layers.

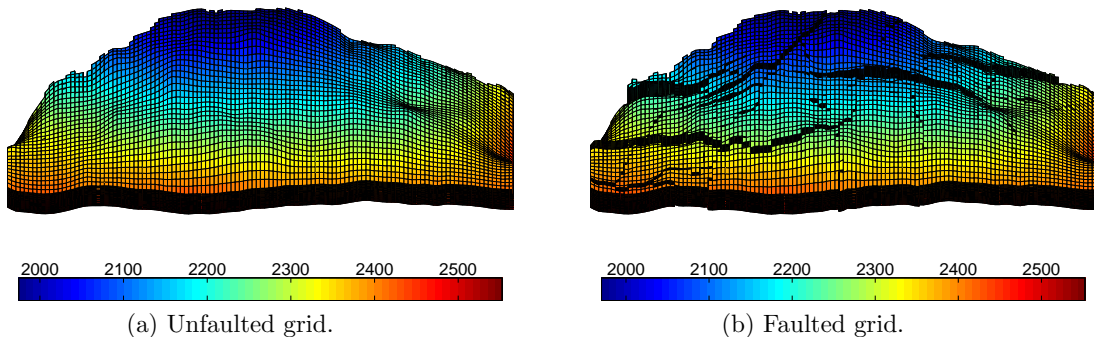


Figure 5: Structural models used in the study. Depth in meter is shown by color. In the faulted structure, faults exist both in the dip and lateral directions.

### 3 Injection scenario

We assume open boundaries on the sides of the simulation model (Figure 6). The spatial dimensions of the model are relatively small ( $9\text{km} \times 3\text{km} \times 80\text{m}$ ). Therefore, assuming closed or semi-closed boundaries results in an unrealistic pressure buildup in the domain due to the injection operation. The open boundaries are modeled by exaggerating the two last cells at the boundaries. The second last cell pore volume is magnified  $10^3$  times and the pore volume of cells at the boundary is multiplied by  $10^6$ . These values are calculated such that no considerable pressure change occurs in the out-most cells at the boundary. No-flow boundary condition is applied on the top and bottom of the model. Moreover, the evaluated side on the crest is located at a large fault displacement and is considered as a close boundary.

The study will be limited to a single injection point so that we can study how the medium responds to the pressure imposed by a vertical injection well, whose position and completions are assumed to be fixed across all realizations. The position and completions were decided by studying a homogeneous model. One big plume will form around the injection point and migrate upward in the domain because of buoyancy forces. To maximize the potential for structural and residual trapping as the plume migrates in the up-dip direction toward the crest of the model, we chose an injection point down in the flank, some distance away from the lower boundary to reduce the possibility of fluids being pushed out through this boundary in the down-dip direction. The well was completed in the four deepest cells corresponding to the lowest layer of the model. Completing the well in the same four cells for all realizations may exaggerate pressure buildup if the well is completed in a low-permeable region, but has the advantage that we keep the comparison between the different realizations as simple as possible and avoid introducing extra parameters in the study. In a real storage operation, one would likely seek to optimize the injection point and complete the well in geological layers that have a satisfactory injectivity. In a more comprehensive study, one should therefore perform simulations for multiple injection locations, but as this would dramatically increase

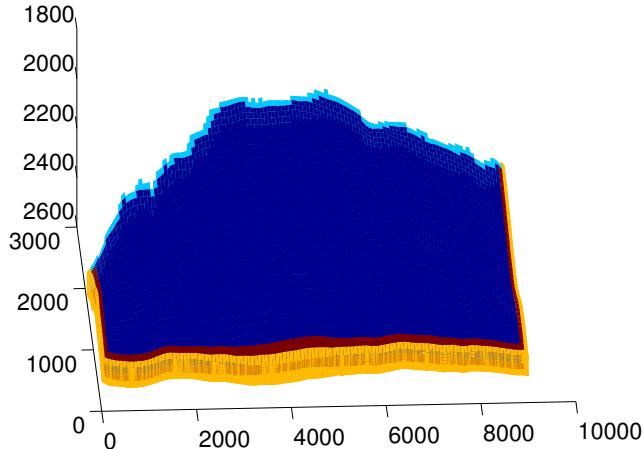


Figure 6: Boundaries in the flow simulation model; the crest boundary (light blue) is considered closed to flow. The pore volume of the cells at the other sides of the model are multiplied by  $10^3$  (red) and  $10^6$  (yellow) to model open boundaries.

the required number of detailed flow simulations, such simulations are not conducted in this study.

Instead, we will consider two strategies for injecting a volume of  $4 \times 10^7 \text{ m}^3$  of supercritical CO<sub>2</sub>, which amounts to 20% of the total pore volume of the models. In the first strategy, which is similar to the one used in [2], the entire CO<sub>2</sub> volume is injected within 30 years using a constant volumetric rate. In the second strategy, the injector operates with the priority of injecting a volumetric rate of  $3650 \text{ m}^3/\text{day}$ . A pressure constraint of 400 bar is set on the injector. If the well bottom-hole pressure goes higher than that, the well priority changes to continue operating at 400 bar by reducing the injection rate until the target CO<sub>2</sub> volume is injected into the medium. As soon as the total injected volume reaches total target, the injector is shut in from the bore-hole and no injection happens for the rest of simulation time up to 100 years.

A standard simulator for multiphase flow in porous medium is used that is based on finite volume method [15]. Two phases (water and supercritical CO<sub>2</sub>) are considered with no mass exchange between them. The fluid compressibility  $C_{fluid}$  is used to model the phase density changes with pressure variation from reference pressure  $P_0$ :

$$\rho = \rho_0 + C_{fluid}\rho_0(P - P_0).$$

Effect of rock compressibility is considered by  $C_{rock}$ :

$$C_{rock} = \frac{\partial \phi}{\partial P}.$$

The water and supercritical CO<sub>2</sub> are assumed to be slightly compressible, with fluid parameters described in Table 4.

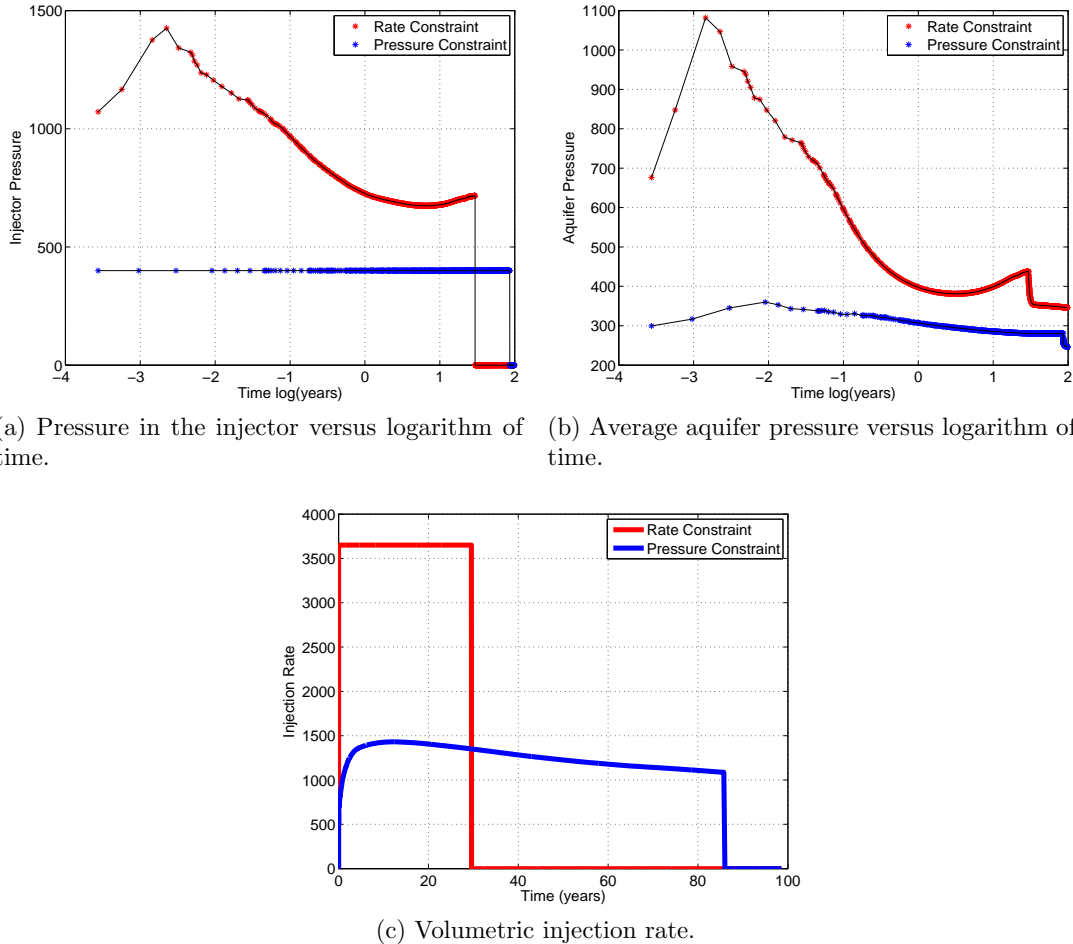


Figure 7: Aquifer and well pressure and injection rate in different injection scenarios shown for a test case.

Table 4: Simulation parameters used in the study.

Parameter	Description	Value
$S_{rw}$	Residual brine saturation	0.2
$S_{rCO_2}$	Residual CO <sub>2</sub> saturation	0.2
$K_{rCO_2}$	CO <sub>2</sub> relative permeability	$(1 - S_{CO_2} - S_{rw})^2$
$K_{rw}$	Brine relative permeability	$(S_w - S_{rCO_2})^2$
$\rho_{CO_2}$	Supercritical CO <sub>2</sub> density at reference pressure	700.15 kg/m <sup>3</sup>
$\rho_w$	Brine density at reference pressure	1033 kg/m <sup>3</sup>
$C_{rock}$	Rock compressibility	$0.3 \times 10^{-6}$ 1/bar
$C_{CO_2}$	CO <sub>2</sub> compressibility	$0.375 \times 10^{-4}$ 1/bar
$C_{water}$	Water compressibility	$0.3 \times 10^{-6}$ 1/bar
$P_0$	Reference pressure	400 bar
$\mu_{CO_2}$	CO <sub>2</sub> viscosity	0.04 cP
$\mu_w$	Brine viscosity	0.4 cP
$q$	Target injection rate	3600 m <sup>3</sup> /day
$P_{cr}$	Critical well pressure	400 bar

## 4 Pressure analysis

We start by discussing the pressure responses for one particular realization. Then, we continue with the full analysis of all the 160 specified realizations made by combining the geological variable levels discussed earlier.

Some of the reported results are chosen at 2.4 hours (0.1 day), because at this time the maximum pressure value is calculated at the injection point compared to other times. In the start of injection, the injected CO<sub>2</sub> has to displace the water. In the start of injection, low CO<sub>2</sub> saturation around the injector causes low mobility for CO<sub>2</sub> and this results in a big pressure build-up (Figure 7).

Four types of responses are considered to compare the different simulation cases. One important question is how fast we can inject a fixed total volume into each realization. Pressure behavior in the system is studied by looking at the average aquifer pressure and the pressure elevation across the well. An overpressure region is defined in which the volumetric spread of over-pressurized locations in the model is measured. Finally, the farthest place from the injection point that a pressure build up has reached is reported for each realization to see the impact of heterogeneity and channels on how the pressure wave travels through the medium.

Figure 8 shows the pressure and saturation responses for the two injection scenarios for a selected simulation case. This realization has one lobe, parallel rock-type stratigraphy (i.e., low aggradation angle), up-dip progradation, high barrier coverage, and is faulted with open faults. The pressure buildup in Figures 8c and 8f tells how heterogeneity impacts the ability to maintain the pressure locally rather than transferring it across the medium. Comparing Figures 8b and 8c with Figures 8e and 8f, we see that imposing a pressure constraint significantly reduces the pressure buildup in the medium (as should be expected). However, the pressure disturbance propagates widely through the system in both cases (Figures 8c and 8f), far beyond the CO<sub>2</sub> invaded zones shown in Figures 8a and 8d.

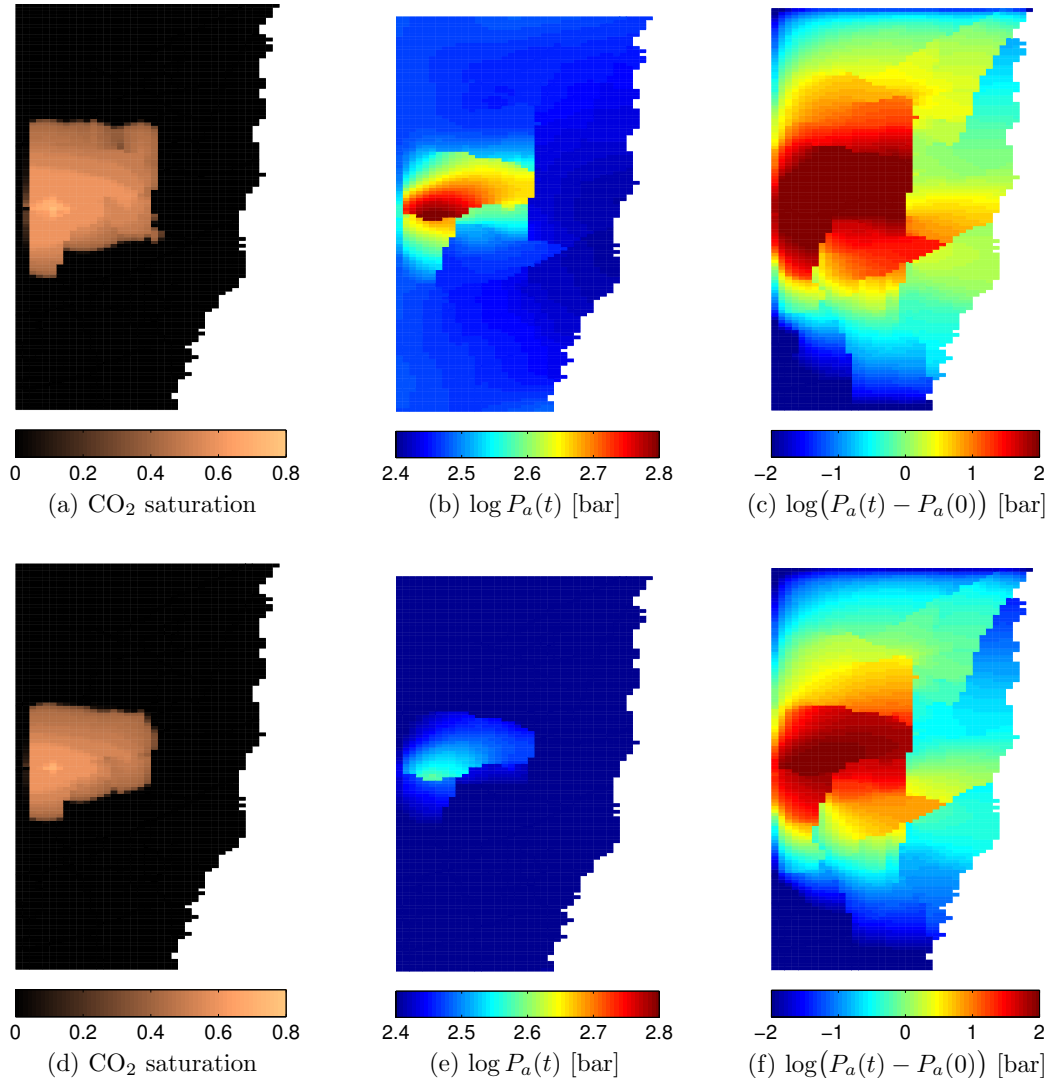


Figure 8: Top view of responses at the middle of the injection period (15 years). The first row corresponds to rate-constrained and the second row belongs to the pressure-constrained injection scenario.

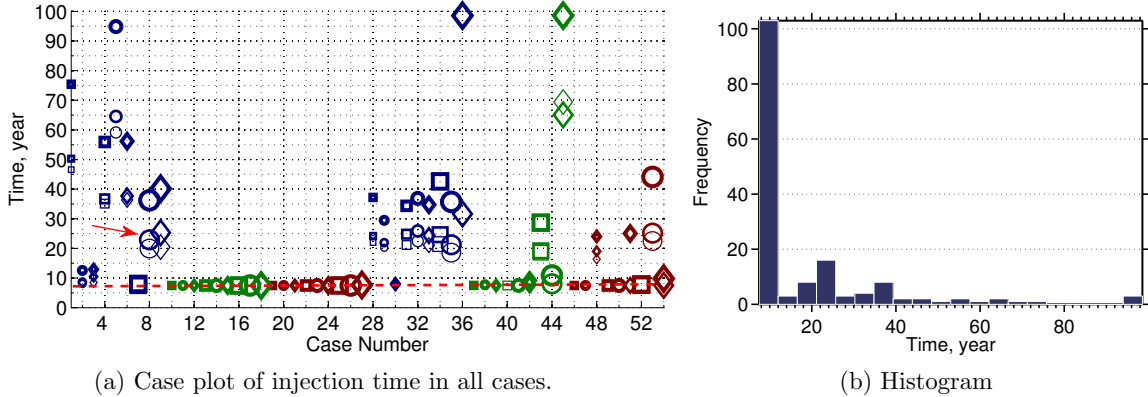


Figure 9: Time to inject a quarter of the total specified  $\text{CO}_2$  volume for all cases in the pressure-constrained scenario. The dashed red line in the left plot denotes the targeted injection time of 7.5 years, and the red arrow points to the case shown in Figure 8. (The case numbers refer to the different petrophysical realizations; in addition, each realization can have three different degrees of faulting. See Table 3.)

#### 4.1 Injection time

In the pressure-constrained scenario, the lower the injectivity of the well is, the longer it will take to inject into the medium, if the pressure is to be kept below the critical limit. In some of the cases it takes longer than 100 years (i.e., longer than the total simulation time) to inject the specified  $\text{CO}_2$  volume. To compare cases, we therefore calculate the time at which a quarter of the targeted volume is injected, which is less than 100 years for all simulation cases.

Figure 9 shows the injection time for all cases in the pressure-constrained scenario. For many cases, the injector keeps the target rate and thus completes the injection within the planned time period of 7.5 years (the dashed red line in the figure). The rest of the cases require longer injection time because of the lower injectivity of the medium. This leads to pressure control in the injector, followed by a decrease in the injection rate. In almost all the realizations with low aggradation angle, shown in blue color (Table 3), the injection rate is reduced below the constant target rate. Also cases with closed faults, denoted by thick markers, have (significantly) longer injection time. The effect of progradation direction is apparent in realizations with higher aggradation angle: for some of the cases colored green and red in the right half of the plot in Figure 9, injection takes longer than the corresponding cases in the left half. Therefore, down-dip progradation, independent of aggradation angle, can result in lower injectivity.

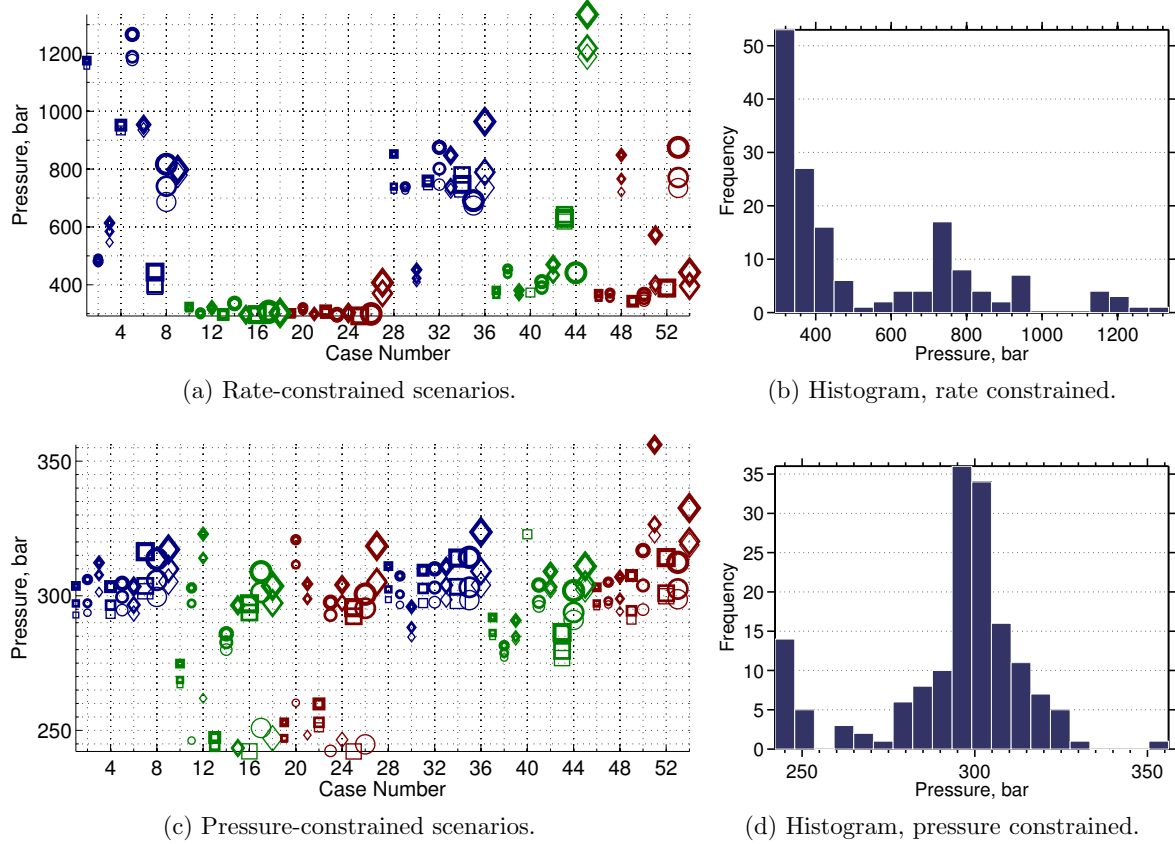


Figure 10: Average aquifer pressure values 2.4 hours after injection started. (The case numbers refer to the different petrophysical realizations; in addition, each realization can have three different degrees of faulting. See Table 3.)

## 4.2 Well and aquifer pressure

To see the overpressure caused by different heterogeneities, we compare cases for their average pressure and well pressure elevation. Average aquifer pressure 2.4 hours after the start of injection is plotted for all cases in Figures 10a and 10c; the corresponding histograms are shown in Figures 10b and 10d. In the rate-constrained scenario, high ranges of average pressure are observed (Figure 10a). Effects of aggradation angle, progradation and faulting are visible in the plot. Three clusters can be identified in the histogram of Figure 10b with medium, high and extreme pressure values. In Figure 10d, a small group of cases show lower pressures, while most of cases are distributed around the mean value ( $\approx 300$  bar).

We define the average elevation in the well pressure at time  $t_c$  as the temporal average of the difference between the bottom-hole pressure  $P_w$  and the average aquifer pressure  $\bar{P}_a$ :

$$\overline{\Delta P} = [\int_0^{t_c} (P_w - \bar{P}_a) dt] / t_c. \quad (1)$$

The average well-pressure elevation is plotted for all cases in Figures 11a and 11c and histograms are shown in Figures 11b and 11d. Higher values imply a poor injectivity of the medium. For the rate-constrained scenarios, we see that maintaining the target rate will in many cases require a huge pressure elevation (up to 1400 bar in the worst cases) that would not be feasible nor possible to obtain. Pressure control on the injector reduces the range of pressure elevation variation below 170 bar.

Two regions can be identified in the medium, the region near the injection point; and the part of aquifer which is far from the injection point. The well-bore pressure is effected directly by heterogeneities in the near well-bore region, while the larger-scale region influences the average aquifer pressure. Pressure elevation variations in Figures 11a and 11b are influenced by the heterogeneity near the well-bore, where the reaction to injecting a fixed amount of CO<sub>2</sub> starts by a local pressure buildup. Heterogeneity on the scale of aquifer plays a considerable role in the range of variations in Figures 11c and 11d. In the pressure-constrained scenario, local pressure is controlled by putting a constraint on the well. Hence, the pressure elevation variations are controlled by the average aquifer pressure.

As we see in Figure 11a, low aggradation angle and down-dip progradation result in a poor injectivity and high pressure buildup in the injector. In particular, vertical transmissibility drops dramatically for low aggradation angles [2]. This restricts the pressure transfer within the injection layer, and therefore the pressure builds up locally around the well. Moreover, in cases with down-dip progradation the low permeability rocks surrounding river branches near the injector result in a local pressure buildup.

A group of cases in Figure 11c have a relatively low pressure elevation of less than 50 bar. These cases have a good injection quality, and the pressure is released through open boundaries easier than other cases. The rest of the cases show higher pressure elevation because of the heterogeneities in the larger scale, far from the injector. These results are obtained for a fixed injection location and one may observe different results, if one chooses to drill and complete the injector in the best formation with highest possible injectivity.

Faults influence both local pressure buildup near the injector as well as the average aquifer pressure. Therefore, they have a visible trend in many cases in Figures 11a and 11c (for example, see the three cases denoted by red circles in the right end of Figure 11a). This is specially more apparent in cases with high level of barriers.

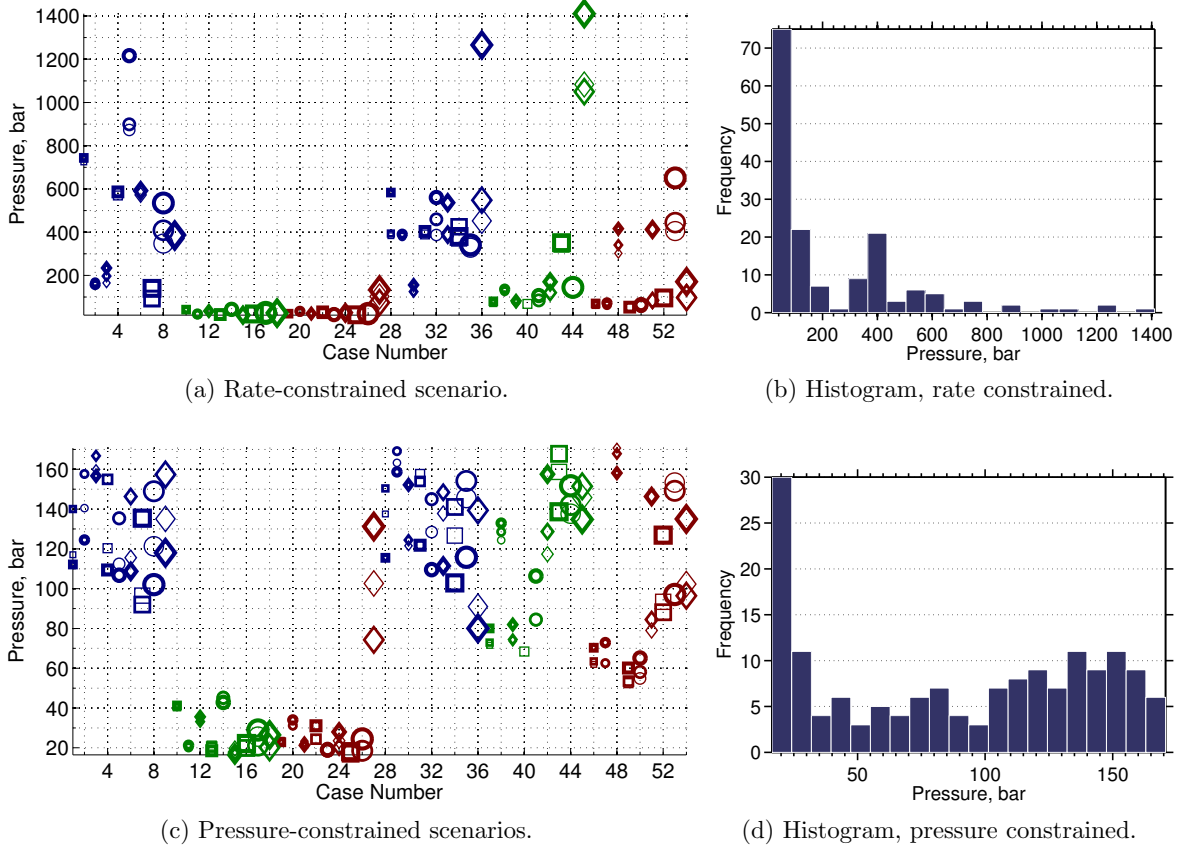


Figure 11: Average elevation in pressure for all cases after 2.4 hours. (The case numbers refer to the different petrophysical realizations; in addition, each realization can have three different degrees of faulting. See Table 3.)

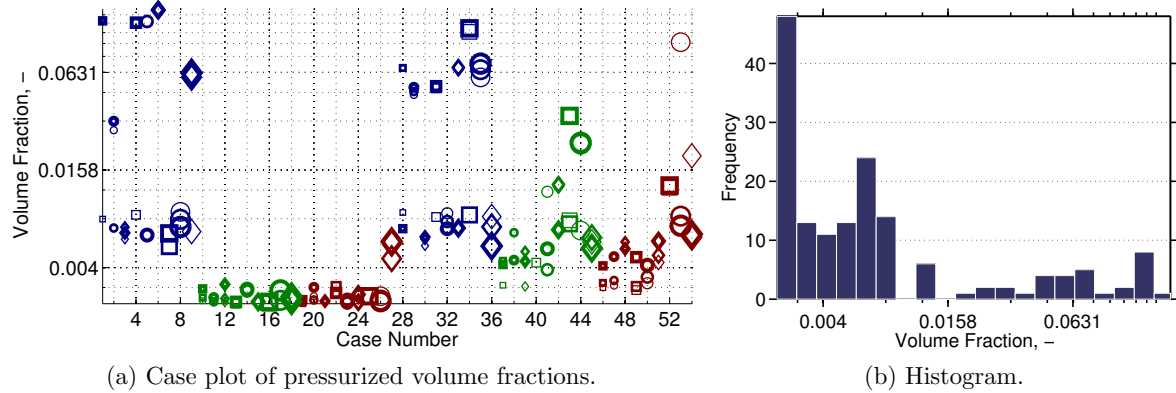


Figure 12: Pressurized volume fraction for all cases in the rate-constrained scenario. (The case numbers refer to the different petrophysical realizations; in addition, each realization can have three different degrees of faulting. See Table 3.)

### 4.3 Pressurized region

Here, we study the overpressure distribution in the medium defined so that all cells with a pressure higher than 300 bar value form a region that is called the pressurized region. Case plots and histogram of the ratio of pressurized volume to the total volume of all active cells in the model at the start of injection are given in Figure 12. Here, we clearly see that low aggradation angle is very influential in the pressure buildup in the injection zone. A group of cases with low aggradation angle have a relatively large pressurized region, but there are also a number of cases with low aggradation angles that have a relatively low pressurized fraction. In these cases, the medium is conductive toward the open boundaries and the heterogeneity in the medium does not cause a major pressure buildup. Other observation in Figure 12a is the progradation effect; down-dip progradation shows a rise in pressurized fraction for higher aggradation angles.

### 4.4 Buildup region

To study the pressure change, and how a pressure disturbance spreads through the medium, we use another metric. We calculate the pressure change by subtracting the initial hydrostatic pressure at each location from the current pressure. Different realizations are compared for the size of a region, which we call the buildup region, in which the pressure has increased from its initial value by 10 bar. The value of 10 bar was chosen to make sure that the region has not reached the boundaries in any of the studied cases. The smaller the buildup region is, the less volume will be exposed to pressure change in the aquifers (Figure 13).

Higher pressure in the medium will obviously cause a larger buildup region. Impact of progradation on the pressure buildup is illustrated in Figure 13a. Up-dip progradation shows a relatively lower pressure buildup compared to down-dip progradation cases. However, this effect is clearly overruled by aggradation, as cases with low aggradation angle show the same pressure buildup for both types of progradation directions (Note the blue colored markers that do not follow the lines in Figure 13a).

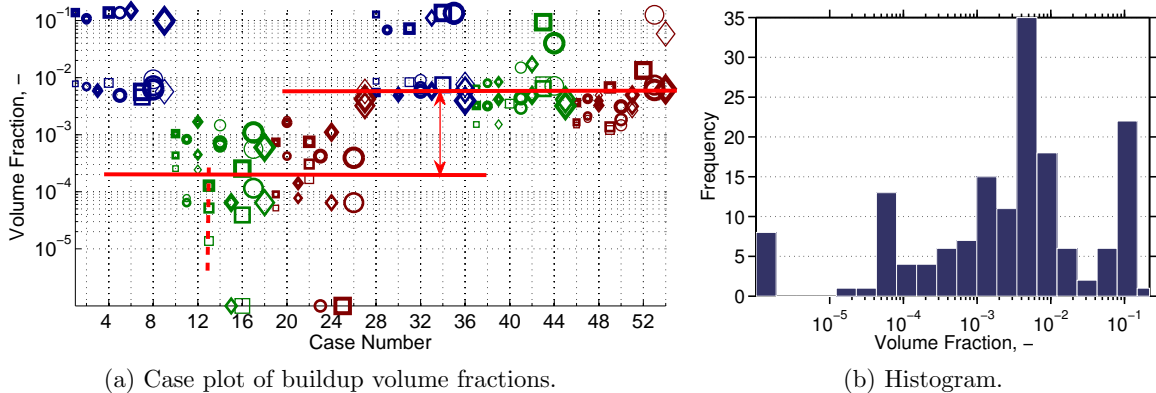


Figure 13: Buildup volume fraction for all cases in the rate-constrained scenario. (The case numbers refer to the different petrophysical realizations; in addition, each realization can have three different degrees of faulting. See Table 3.)

Several cases in Figure 13a show a trend for the fault parameter. The dashed line shows the trend of buildup pressure increase due to fault feature variations in three cases. Faulting changes the geometry of layers and puts different layers adjacent to each other. This enhances the connectivity in the medium. Local heterogeneities and closed faults around the injector make a larger buildup region, because they cause higher pressure buildup in the domain. In these cases, the effect of heterogeneity of different scales, namely on the scale of near injector and far from injector, are combined causing a larger buildup fraction.

#### 4.5 Farthest pulse

As discussed earlier, irregular geometries like faults and unconformities can lead to pressure spread in the domain. Looking at the volume fraction of pressurized and buildup regions helps in comparing cases for their pressure conductivity, but it does not show the extent of pressure spread in the medium. For that reason, we also look at the farthest cell from the injection point that falls within the buildup region defined earlier.

Figure 14 shows the farthest distance from the injector at which pressure buildup is observed for the different injection scenarios. In Figure 14b, three groups of cases can be identified: cases with zero distance of farthest pressure buildup pulse, cases with medium distances, and those with large distances from the injection point. Three specific cases are chosen as samples from each of the groups (see Figure 15 for example). In the first group (Figure 15a), the injector is placed in a permeable region and the medium is conductive toward open boundaries and hence the imposed injection pressure does not build up beyond the 10 bar threshold from its initial value, neither locally around the well nor globally in the aquifer scale. The cases in the second group (Figure 15b) have a medium range of 3–4 km of pressure-propagation distances from the injection point. Heterogeneity in these cases is not making a high pressure buildup around the injector and throughout the medium.

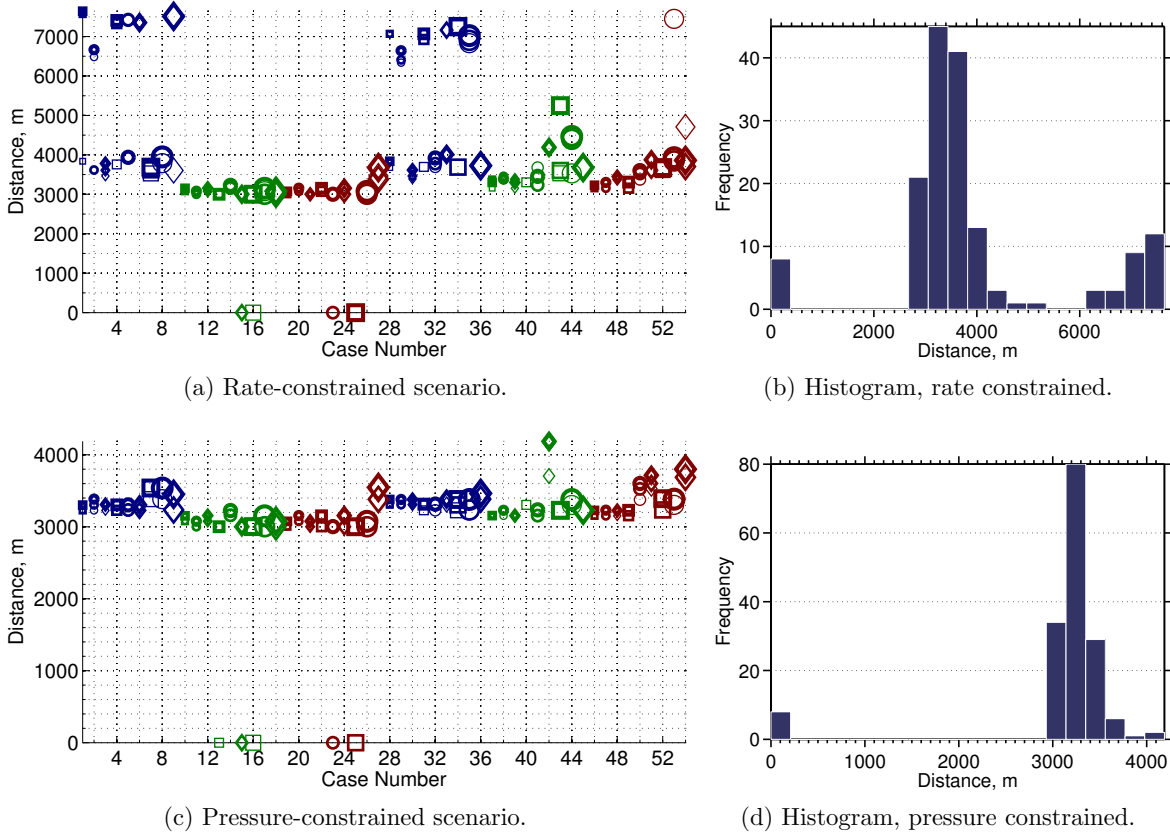


Figure 14: The farthest distance at which a pressure buildup is observed after 2.4 hours after injection start. (The case numbers refer to the different petrophysical realizations; in addition, each realization can have three different degrees of faulting. See Table 3.)

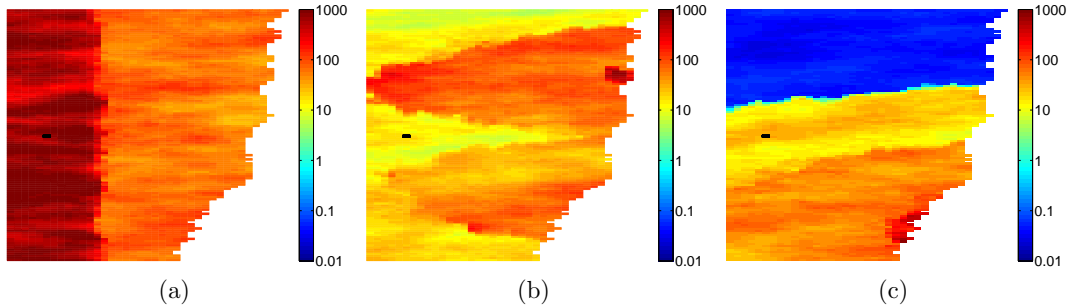


Figure 15: Top view of the permeability for three types of different realizations (in units milli Darcy); the well location is shown with black color in each plot. Heterogeneity can influence the pressure propagation within the medium. From case (a) to (c) the pressure build up shows higher values around the injector with larger propagation distances from the injection point.

In the third group (Figure 15c), low-permeable rocks in the injection layer cause a high pressure buildup around the injection point. If the injector zone is isolated by sealing heterogeneities, the pressure rises in a limited region. However, if the well is connected throughout the medium, and the heterogeneities in the aquifer scale contain relatively low permeability rocks, the pressure build up spreads wider in the aquifer. In Figure 15c, the injection point is located close to a low transmissibility rock. This rises the pressure level in the injector. Other parts of the aquifer are connected with poor quality rocks, resulting in a wide buildup region.

The farthest pulse distance ranges from 8 km to approximately 10 km in the extreme cases. By controlling the injection pressure, the maximum shrinks to slightly above 4 km (Figure 14d).

## 5 Discussion

So far, we reported the model responses that measure the pressure rise and pressure disturbance propagation in the domain. The pressurized volume fraction indicates the actual high pressures that may occur in an injection operation. The buildup volume fraction and the farthest pulse are indicators of how the pressure disturbance is spread in the system. We are interested in limiting both the pressure increase and the distance the elevated pressure propagates into the aquifer.

In most of the results, aggradation angle, progradation direction, and faults play a major role in the pressure behavior. For low aggradation angles, geological layers are made of rock types piled in a parallel stratigraphy. Thus, efficient vertical permeability is the harmonic average of these layers. If any of these layers contain a low-permeability rock, the vertical transmissibility will be low, and injecting into a limited space that is vertically sealed increases the pressure at the injection point.

The progradation direction can dominate the pressure behavior. It is very important to locate the injector in a high permeability zone that is connected to other parts of the domain via permeable channels. Injecting into the riverside of a shallow marine depositional system may result in locating the injection point in low-quality rocks between river branches joining the sea. This fact increases the pressure significantly near the injection point and can result in a high well-bore and aquifer pressure.

Structural deformations due to faulting process can increase the connectivity in the medium. If the overall transmissibility of the aquifer scale is high, the injection pressure releases through the open boundaries. However, if the injection area is surrounded by low-quality medium, the pressure increases in the aquifer and the connectivity enhanced by the fault geometries spreads the buildup region in the domain. On the other hand, sealing faults result in high pressures within closed zones around the injection point, but may also limit the propagation of the pressure disturbance in the domain.

From an operational perspective, pressure limits must be set to keep the operations within safe margins. One approach to study the safety of an operation could be setting critical limits on the pressure responses measured here. These limits should be inferred from realistic operational requirements and can then be used to filter out cases with undesirable/unacceptable pressure behavior. Herein, we assume that the limits are set to be 53 years for the injection

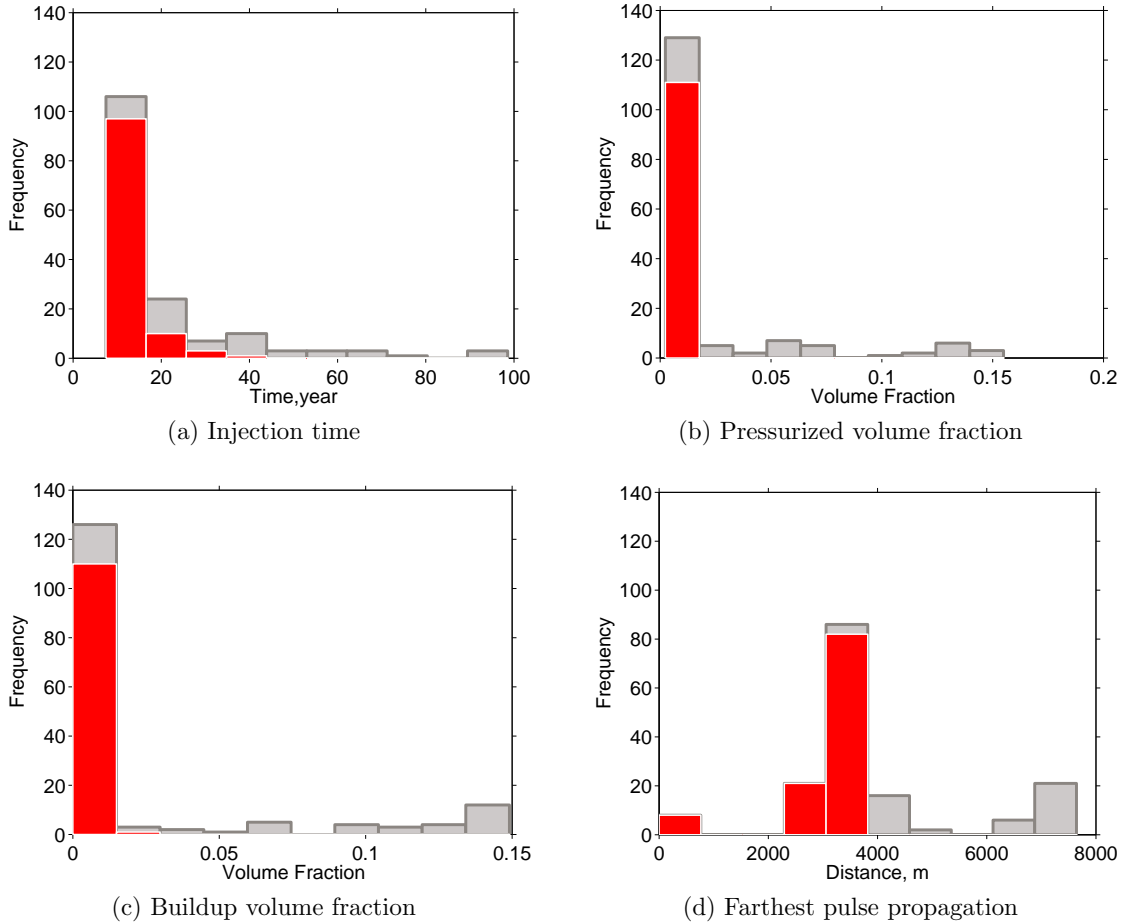


Figure 16: Defined pressure criteria can be used to filter cases that are appropriate for the proposed injection scenario. Figure shows the histogram of filtered cases (red) compared with the histogram of all cases (gray) for different pressure responses.

time, 0.0787 for the pressurized volume fraction, 0.0745 for the buildup volume fraction, and 3822 m for the farthest pulse distance from the injection point. (These values are the mid-points of the range of variations in the results). By these assumptions, 49 cases out of the total number of 160 cases exceed the critical limits. Figure 16 shows the histogram of filtered cases compared with the histogram of all studied cases for each response.

## 6 Conclusions

This work is part of a comprehensive sensitivity study to assess the impact of geological heterogeneity on CO<sub>2</sub> injection and early plume migration. The aim of this study is to determine how different geological parameters impact the pressure buildup and establish which combinations that may potentially lead to buildup of high pressure values and large-distance propagation of elevated pressures. Simulation responses related to the pressure behavior in the system are defined and calculated for two CO<sub>2</sub> injection scenarios. Geological variations

in shallow-marine depositional systems are examined by using a large number of parametrized realizations representing a spectrum of sedimentological and structural scenarios.

The studied responses are most sensitive to aggradation, progradation direction, and faulting. Low aggradation angles inhibit the upward movement of the CO<sub>2</sub> plume and keep the flow restricted to the geological layers in which the CO<sub>2</sub> is injected. In cases with low rock quality in the injection layers, pressure will build up in the well-bore and large volumes may be forced down-dip and out through the lower boundary, as observed in [2]. In the down-dip progradation, the majority of the region around injection point is made of low quality rock and injecting in down-dip progradation normally ends up in a higher pressure buildup and a lower injectivity. Faults change the geometrical structure of the medium and they put different layers in contact. Pressure disturbances can leak through faults to larger distances from the injection point. Closed faults can significantly reduce the injectivity quality.

The workflow of the pressure study demonstrated here can be used in specific studies in the context of geological uncertainty. In particular, the insight of how different geological parameters impact the pressure buildup (and the migration of the CO<sub>2</sub> plume) can be used to predict optimal injection locations for this type of shallow-marine systems. The workflow can also be used for other depositional systems. However, since the study only involved two specific injection strategies, it is possible that one may obtain different outcomes than reported herein if significantly different values are used for the operational limits.

## References

- [1] M. Ashraf, K.-A. Lie, H. M. Nilsen, J. M. Nordbotten, and A. Skorstad. Impact of geological heterogeneity on early-stage CO<sub>2</sub> plume migration. In *CMWR*, 2010.
- [2] M. Ashraf, K. A. Lie, H. M. Nilsen, and A. Skorstad. Impact of geological heterogeneity on early-stage CO<sub>2</sub> plume migration: Sensitivity analysis. In *ready for submission*, 2012.
- [3] J. Birkholzer, Q. Zhou, J. Rutqvist, P. Jordan, K. Zhang, and C.-F. Tsang. Research project on co<sub>2</sub> geological storage and groundwater resources: Large-scale hydrological evaluation and modeling of impact on groundwater systems. Technical report, Lawrence Berkeley National Laboratory, Berkeley, CA, USA, 2008.
- [4] B. Cailly, P. Le Thiez, P. Egermann, A. Audibert, S. Vidal-Gilbert, and X. Longaygue. Geological storage of CO<sub>2</sub>: A state-of-the-art of injection processes and technologies. *Oil & Gas Science and Technology*, 60(3):517–525, 2005.
- [5] A. Cavanagh and N. Wildgust. Pressurization and brine displacement issues for deep saline formation CO<sub>2</sub> storage. *Energy Procedia*, 4:4814–4821, 2011.
- [6] E. R. Chabora and S. M. Benson. Brine displacement and leakage detection using pressure measurements in aquifers overlying co<sub>2</sub> storage reservoirs. *Energy Procedia*, 1(1):2405–2412, 2009.
- [7] J. A. Howell, A. Skorstad, A. MacDonald, A. Fordham, S. Flint, B. Fjellvoll, and T. Manzocchi. Sedimentological parameterization of shallow-marine reservoirs. *Petroleum Geoscience*, 14(1):17–34, 2008.

- [8] T. Le Guenan and J. Rohmer. Corrective measures based on pressure control strategies for CO<sub>2</sub> geological storage in deep aquifers. *International Journal of Greenhouse Gas Control*, 2010.
- [9] T. Manzocchi, J. N. Carter, A. Skorstad, B. Fjellvoll, K. D. Stephen, J. A. Howell, J. D. Matthews, J. J. Walsh, M. Nepveu, C. Bos, et al. Sensitivity of the impact of geological uncertainty on production from faulted and unfaulted shallow-marine oil reservoirs: objectives and methods. *Petroleum Geoscience*, 14(1):3–11, 2008.
- [10] J. D. Matthews, J. N. Carter, K. D. Stephen, R. W. Zimmerman, A. Skorstad, T. Manzocchi, and J. A. Howell. Assessing the effect of geological uncertainty on recovery estimates in shallow-marine reservoirs: the application of reservoir engineering to the SAIGUP project. *Petroleum Geoscience*, 14(1):35–44, 2008.
- [11] S. P. Neuman and P. A. Witherspoon. Theory of flow in a confined two aquifer system. *Water Resources Research*, 5(4):803–816, 1969.
- [12] J. Nicot. Evaluation of large-scale CO<sub>2</sub> storage on fresh-water sections of aquifers: an example from the Texas Gulf Coast Basin. *International Journal of Greenhouse Gas Control*, 2(4):582–593, 2008.
- [13] J. Rutqvist, J. Birkholzer, F. Cappa, and C.-F. Tsang. Estimating maximum sustainable injection pressure during geological sequestration of CO<sub>2</sub> using coupled fluid flow and geomechanical fault-slip analysis. *Energy Conversion and Management*, 48(6):1798–1807, 2007.
- [14] J. Rutqvist and C. F. Tsang. A study of caprock hydromechanical changes associated with CO<sub>2</sub> injection into a brine formation. *Environmental Geology*, 42:296–305, 2002. 10.1007/s00254-001-0499-2.
- [15] Schlumberger. Eclipse technical description manual, 2009.
- [16] S. Solomon, D. Qin, M. Manning, Z. Chen, M. Marquis, K. B. Averyt, M. Tignor, and H. L. Miller, editors. *Climate Change 2007 – The Physical Science Basis: Working Group I Contribution to the Fourth Assessment Report of the IPCC*. Cambridge University Press, Cambridge, UK and New York, NY, USA, Sept. 2007.
- [17] L. G. H. van der Meer. Investigations regarding the storage of carbon dioxide in aquifers in the Netherlands. *Energy Conversion and Management*, 33(5-8):611–618, 1992.
- [18] L. G. H. van der Meer. The conditions limiting CO<sub>2</sub> storage in aquifers. *Energy Conversion and Management*, 34(9-11):959–966, 1993.

# **Paper III**

## **3.3 Geological storage of CO<sub>2</sub>: Application, feasibility and efficiency of global sensitivity analysis and risk assessment using the arbitrary polynomial chaos.**

,  
M. Ashraf, S. Oladyshkin, W. Nowak

Proceedings of the European Geosciences Union (EGU) General Assembly 2012, April, Vienna, Austria, Geophysical Research Abstracts., Vol. 14, EGU2012-9243. Published in International Journal of Greenhouse Gas Control (2013).





Contents lists available at SciVerse ScienceDirect

**International Journal of Greenhouse Gas Control**

journal homepage: [www.elsevier.com/locate/ijggc](http://www.elsevier.com/locate/ijggc)



## Geological storage of CO<sub>2</sub>: Application, feasibility and efficiency of global sensitivity analysis and risk assessment using the arbitrary polynomial chaos

Meisam Ashraf<sup>a,b,\*</sup>, Sergey Oladyshkin<sup>c,1</sup>, Wolfgang Nowak<sup>c,2</sup>

<sup>a</sup> Department of Mathematics, University of Bergen, 5028 Bergen, Norway

<sup>b</sup> SINTEF ICT, Department of Applied Mathematics, P.O. Box 124 Blindern, N-0314 Oslo, Norway

<sup>c</sup> SRC Simulation Technology, Institute for Modelling Hydraulic and Environmental Systems (LH2), University of Stuttgart, Pfaffenwaldring 61, 70569 Stuttgart, Germany

### ARTICLE INFO

#### Article history:

Received 20 July 2012

Received in revised form 1 March 2013

Accepted 23 March 2013

Available online xxxx

#### Keywords:

CO<sub>2</sub> storage

Global sensitivity analysis

Probabilistic risk assessment

Uncertainty quantification

Arbitrary polynomial chaos

Sobol indices

### ABSTRACT

Geological storage of CO<sub>2</sub> is a proposed interim solution for mitigating the climate change. Modeling CO<sub>2</sub> storage is accompanied by huge geological uncertainties and excessive computational demands. However, the considerable costs and potential hazards of the technique require feasibility studies to assess all possible risks. This makes computationally efficient methods for sensitivity analysis, uncertainty quantification and probabilistic risk assessment indispensable.

Our goal is to demonstrate the application and feasibility of the arbitrary polynomial chaos expansion (aPC) for these tasks under realistic conditions. We model a typical CO<sub>2</sub> injection scenario in realistic geological realizations of a shallow marine deposit. Our scenario features uncertain parameters that control the structure of geological heterogeneities, including the density of barriers, the aggradation angle, fault transmissibility and regional groundwater effects. The aPC approximates the models by a polynomial-based response surface to speed up the involved statistical analysis of an otherwise expensive simulation tool.

We demonstrate how such an analysis can guide further exploration and the design process of finding suitable injection rates. Our case study demonstrates clearly that the aPC is an efficient, feasible and hence valuable approach in this context, and we strongly encourage its future use. A key advantage of the aPC over more conventional polynomial chaos methods is the flexibility to work with arbitrary probability distributions of uncertain parameters. From our featured parameters, we found the aggradation angle to be the most and the regional groundwater effect to be the least influential one. To the best of our knowledge, this is the first analysis of structural parameters for geological heterogeneities in the CO<sub>2</sub> context and within a probabilistic setting.

© 2013 Elsevier Ltd. All rights reserved.

### 1. Introduction

In the context of climate change mitigation, geological storage of CO<sub>2</sub> has been proposed as interim solution. The idea has been challenged during the last decades for its costs and potential hazards (Lenzen, 2011; Viebahn et al., 2007). A large number of studies have been performed in the industry and research communities to

evaluate the safety and feasibility of CO<sub>2</sub> storage, addressing issues such as the status and barriers of CO<sub>2</sub> storage (Bachu, 2008), screening and ranking of geological storage sites (Bachu, 2003), large-scale impacts of CO<sub>2</sub> injection in deep saline aquifers (Birkholzer et al., 2009), new solution methodologies for CO<sub>2</sub> leakage (Nordbotten et al., 2005), the capture project (Thomas, 2005), and leakage estimates (Celia et al., 2004). Furthermore, many pilot projects have been installed, like In Salah (Riddiford et al., 2004), Ketzin (Förster et al., 2006), and Johansen (Eigestad et al., 2009). A discussion on the experiences from the existing pilot projects is reported in Michael et al. (2010).

Yet, there is a big demand for studies which demonstrate the appropriateness of the storage operation. Transparent scientific results are required to communicate the facts and evidences about feasibility and possible risks within public and industry. The large involved time and space scales, however, cause substantial

\* Corresponding author at: Department of Mathematics, University of Bergen, 5028 Bergen, Norway. Tel.: +47 9987 2717; fax: +47 7351 4037.

E-mail addresses: meisam@resman.no (M. Ashraf), Sergey.Oladyshevkin@iws.uni-stuttgart.de (S. Oladyshkin), Wolfgang.Nowak@iws.uni-stuttgart.de (W. Nowak).

<sup>1</sup> Tel: +49 711 685 60116; fax: +49 711 685 60430.

<sup>2</sup> Tel: +49 711 685 60113; fax: +49 711 685 60430.

computational issues in such studies (e.g., Class et al., 2009), and the modeling procedure is accompanied by a huge extent of geological uncertainties (e.g., Walton et al., 2004; Brennan et al., 2010; Wilson et al., 2003; Hansson and Bryngelsson, 2009).

In an approach to quantify the impact of geological heterogeneity on model predictions of multiphase flow in geological formations, a large number of shallow marine depositional realizations have been generated and used in the sensitivity analysis of the impact of geological uncertainties on production forecasting (SAIGUP) (see Howell et al., 2008; Manzocchi et al., 2008; Matthews et al., 2008). There, the impact of variable geological parameters has been quantified for oil recovery in different field development scenarios. The main general conclusion of that study is that realistic features of geological uncertainty in modeling (other than typical hydrological parameters) can lead to considerable uncertainties in prediction. Ashraf et al. (2010a,b) used a number of SAIGUP realizations to study the impact of geological heterogeneity on the injection and early migration of CO<sub>2</sub> in a shallow-marine aquifer with a complex, heterogeneous geological structure. That study transferred the significance of some of the geological structural features to the case of CO<sub>2</sub> injection.

In practice, modeling complicated physical phenomena in the subsurface requires stochastic approaches. Uncertainty can exist in different levels, from the formulation of dependency rules in the model to uncertainty about appropriate values for the model input parameters. Uncertainty coming from any source in the modeling procedure propagates through the model to the predicted responses. Ranking the important model parameters based on their influence on the model responses can support a better understanding of the system, and it can result in a better design of subsequent studies on the stochastic nature of the process. Hence, identifying and evaluating the sensitivities and uncertainties of model parameters and their impact on prediction uncertainties and projected risks is a significant task. Sensitivity analysis is known to be the right approach to identify the significance of uncertainty sources within the modeling process (Oladyshkin and Nowak, 2012) and to improve the understanding of model behavior (Sobol, 2001). For example, the European Commission and the United States Environment Protection Agency recommend using sensitivity analysis in the context of extended compact assessment for policy making (Commission, 2002).

Uncertainty sources within the CO<sub>2</sub> storage problem can be classified in different types as geological, physical and operational uncertainties. This work is devoted to geological uncertainties. However the same procedure can be applied to extend the work for other types as well. Here, we use a set of SAIGUP realizations to perform a sensitivity analysis and to assess the risks caused by uncertainties in a choice of parameters that govern the geological structure of the featured shallow-marine deposit.

The goal of this study is to test and demonstrate the applicability of a recent set of methods to a realistic scenario. We choose a stochastic response surface method to project the model response to parameter changes onto high-dimensional polynomials via the arbitrary polynomial chaos expansion (aPC) (Oladyshkin and Nowak, 2012; Oladyshkin et al., 2011). Highly similar ideas to the aPC have also been proposed in other scientific areas (Witteveen et al., 2007; Witteveen and Bijl, 2006; Ghanem and Doostan, 2006; Soize and Ghanem, 2004). As we review in Section 2, the involved orthogonal polynomial basis can be constructed for arbitrary probability distributions of the uncertain parameters. This data-driven approach provides fast convergence (Oladyshkin and Nowak, 2012) in comparison to the classical polynomial chaos expansion (e.g., Wiener, 1938; Ghanem and Spanos, 1991; Le Maître and Knio, 2010). Moreover, it avoids the subjectivity of data treatment that would arise when being forced to fall back onto a limited number of theoretical distributions that can be tolerated with previous

generalized versions of polynomial chaos expansions (Wan and Karniadakis, 2007; Xiu and Karniadakis, 2002). The reduced model represented by the response surface is significantly faster than the original complex one, and thus provides a promising starting point for global sensitivity analysis, uncertainty quantification, and probabilistic risk assessment.

In the current paper, we use global sensitivity analysis rather than a local one, because local analysis fails to cover the non-linear variation of model responses over the entire range of probability distributions of the input parameters. A practical approach in global sensitivity analysis is to work with the impact of uncertain parameters on prediction variances, because this shows a good success in nonlinear problems (Reuter and Liebscher, 2008). In the current study, we use Sobol indices (Sobol, 2001) for sensitivity analysis, which are indeed working with variances. The fact that the aPC based response surface is based on orthonormal polynomials with exploitable known properties (Oladyshkin et al., 2012) substantially simplifies this analysis.

Finally, we perform risk analysis by applying a Monte-Carlo procedure to the response surface. The approximating polynomial is fast enough to be used for a large number of Monte-Carlo realizations. This makes it possible to cover the entire range of variations in the model input described by the assigned probability distributions, and thus provides accurate estimates for the risk in the system. We conclude with a discussion of the results.

The global sensitivity analysis and uncertainty quantification studies for CO<sub>2</sub> storage existing in the literature are concerned with classic hydrological uncertain parameters like porosity, pore volume and permeability as global constants (see for example Brennan et al., 2010; Kovscek and Wang, 2005; Oladyshkin et al., 2011). To the best of our knowledge, the current study is the first one that implements the proposed mathematical analysis tools on realistic geological structural parameters at reservoir scale. The parameters we consider are the level of barriers presence, aggradation angle, fault transmissibility, and regional groundwater effects. The considered features are the structural and depositional features that dictate the distribution of hydrological parameters such as permeability and porosity, both in terms of value and spatial distribution. These are among the most uncertain geological parameters identified with the SAIGUP study (except the regional groundwater effect, which is specific to this study).

## 2. Response surface via arbitrary polynomial chaos expansion

Working with uncertain parameters in complex, non-linear and dynamic systems puts a high demand on stochastic tools to analyze the system and to propagate uncertainties through the system. Conceptually straightforward numerical Monte-Carlo (MC) techniques are computationally demanding since the statistical accuracy of their predictions depends on the number of realizations used. The Monte-Carlo estimation error (measured as standard deviation) for output statistics typically decreases only with the square root of the number of realizations used. Using a stochastic response surface is a promising approach in this respect.

Obviously, a response surface can be constructed in different ways, e.g. it can be constructed directly on a dense Cartesian grid of input parameters at extremely high computational efforts. In the current paper, we apply an alternative methodology which demands only minimum number of model evaluations to construct the response surface. This approach is based on the theory of polynomial chaos expansion (PCE) introduced in Wiener (1938). Generally, all PCE techniques can be viewed as an efficient approximation to full-blown stochastic modeling (e.g., exhaustive MC). The basic idea is to represent the response of a model to changes in

variables through a response surface that is defined with the help of an orthonormal polynomial basis in the parameter space. In simple words, the dependence of model output on all relevant input parameters is approximated by a high-dimensional polynomial. The resulting polynomials are functions of the model parameters. This projection can be interpreted as an advanced approach to statistical regression.

The PCE offers an efficient and accurate high-order way of including non-linear effects in stochastic analysis (e.g., Zhang and Lu, 2004; Foo and Karniadakis, 2010; Fajraoui et al., 2011). One of the attractive features of PCE is the higher-order in uncertainty quantification (e.g., Ghanem and Spanos, 1990, 1991; Le Maître and Knio, 2010), as well as its computational speed when compared to other methods for uncertainty quantification performed on the full model, such as MC (Oladyshkin et al., 2011). Due to its elegant reduction of models to polynomials, it allows performing many tasks analytically on the expansion coefficients. Alternatively, it allows performing excessive MC on the polynomials since they are vastly faster to evaluate than the original model.

Unfortunately, the original PCE concept (Wiener, 1938) is optimal only for Gaussian distributed input parameters. To accommodate for a wide range of data distributions, a recent generalization of PCE is the arbitrary polynomial chaos (aPC Oladyshkin et al., 2011). Compared to earlier PCE techniques, the aPC adapts to arbitrary probability distribution shapes of input parameters and, in addition, can even work with unknown distribution shapes when only a few statistical moments can be inferred from limited data or from expert elicitation. The arbitrary distributions for the framework can be either discrete, continuous, or discretized continuous. They can be specified either analytically (as probability density/cumulative distribution functions), numerically as histogram or as raw data sets. This goes beyond the generalization of PCE in methods such as the generalized polynomial chaos (gPC) or the multi-element gPC (ME-gPC) (Wan and Karniadakis, 2007; Xiu and Karniadakis, 2002). The aPC approach provides improved convergence in comparison to classical PCE techniques, when applied to input distributions that fall outside the range of classical PCE. A more specific discussion and review of involved techniques will follow in Sections 2.1–2.3.

With an introduction to response methods via the aPC, we describe here the theoretical background that we use in our modeling procedure. The related techniques for sensitivity and risk analysis used in this work are explained in Sections 4 and 5.

### 2.1. Definitions and polynomial chaos expansion

Suppose that we approximate a problem by a functional  $\Upsilon$ , which represents the model responses  $\Gamma$  for the input variables  $\Theta$ :

$$\Gamma \approx \Upsilon(\Theta). \quad (1)$$

Like all PCE methods, the aPC is a stochastic approach to approximate the response surface. Considering the uncertainty in the input variables, the aPC constructs a set of polynomial basis function and expands the solution in this basis. Thus, the response vector  $\Gamma$  in Eq. (1) can be approximated by Oladyshkin and Nowak (2012):

$$\Gamma \approx \sum_{i=1}^{n_c} c_i \Pi_i(\Theta). \quad (2)$$

Here,  $n_c$  is the number of expansion terms,  $c_i$  are the expansion coefficients, and  $\Pi_i$  are the multi-dimensional polynomials for the variables  $\Theta = [\theta_1, \dots, \theta_n]$ , and  $n$  is the considered number of modeling parameters. If the model response  $\Gamma(\Theta)$  depends on space and time, then so do the expansion coefficients  $c_i$ .

The number  $n_c$  of unknown coefficients  $c_i$  results from the number of possible polynomials with total degree equal to or less than  $d$ . This number depends on the degree  $d$  of the approximating polynomial, and the number of considered parameters  $n$ :

$$n_c = \frac{(d+n)!}{d!n!}. \quad (3)$$

### 2.2. Data-driven orthonormal basis

All polynomials  $\Pi_i$  in expansion (2) are orthogonal, i.e., they fulfill the following condition:

$$\int_{I \in \Omega} \Pi_l \Pi_m p(\Theta) d(\Theta) = \delta_{lm}, \quad (4)$$

where  $I$  is the support of  $\Omega$ ,  $\delta$  is the Kronecker symbol, and  $p(\Theta)$  is the probability density function for the input parameters. We obtain the orthonormal basis with the moments-based method proposed in Oladyshkin and Nowak (2012) and Oladyshkin et al. (2011). Orthonormality has the advantage that many subsequent analysis steps are accessible to relatively simple analytical solutions.

Knowledge on variability never is so perfect such that we could express the probability of model parameter values in a unique distribution function. Available data are mostly scarce, and fitting a density function to observed frequencies is often biased by subjective choices of the modeler. Oladyshkin et al. (2011) argued that, with aPC, it is possible to use available probabilistic information with no additional formal knowledge requirements for their probability distributions, only based on the statistical moments of the available data. They showed that, it is possible to calculate estimates for the mean, variance, and higher order moments of the model response  $\Gamma(\Theta)$  even with incomplete information on the uncertainty of input data, provided in the form of only a few statistical moments up to some finite order.

### 2.3. Non-intrusive determination of the coefficients

The next task is to compute the coefficients  $c_i$  in Eq. (2). Generally, all PCE techniques can be sub-divided into intrusive (Ghanem and Spanos, 1993; Matthies and Spanos, 2005; Xiu and Karniadakis, 2003) and non-intrusive (Keese and Matthies, 2003; Isukapalli et al., 1998; Li and Zhang, 2007; Oladyshkin et al., 2011) approaches, i.e., methods that require or do not require modifications in the system of governing equations and corresponding changes in simulation codes. The challenge in choosing between the methods is to find a compromise between computational effort for model evaluations and a reasonable approximation of the physical processes by the interpolation.

For our study, we prefer the probabilistic collocation method (PCM: see Oladyshkin et al., 2011, 2011; Li and Zhang, 2007) from the group of non-intrusive approaches like sparse quadrature (Babuška et al., 2007; Xiu and Hesthaven, 2005; Gerstner and Griebel, 2003; Barthelmann et al., 2000). In a simple sense, PCM can be interpreted as a smart (mathematically optimal) interpolation and extrapolation rule of model output between and beyond different input parameter sets. It is based on a minimal and optimally chosen set of model evaluations, each with a defined set of model parameters (called collocation points). For this reason, the collocation approach became more popular in the last years. Also, the collocation formulation does not require any knowledge of the initial model structure. It only requires knowledge on how to obtain the model output for a given set of input parameters, which allows treating the model like a "black-box". The distinctive feature of non-intrusive approaches is that any simulation model can

be considered a "black-box", i.e., commercial software can be used without any modifications required.

According to Villadsen and Michelsen (1978), the optimal choice of collocation points corresponds to the roots of the polynomial of one degree higher ( $d+1$ ) than the order used in the chaos expansion ( $d$ ). This choice adapts the position of collocation points to the involved distribution shape, and is based on the theory of Gaussian integration (e.g., Abramowitz and Stegun, 1965). For one-dimensional problems (i.e., when analyzing only one uncertain model parameter), it allows exact numerical integrations of order  $2d$  given  $d+1$  values of the function to be integrated.

For multi-parameter analysis, the number of available points from the corresponding Gaussian integration rule is  $(d+1)^n$ , which is larger than the necessary number  $M$  of collocation points. The minimum value of  $M$  is equal to the number of coefficients  $n_c$  in Expansion (2), according to Eq. (3). The full tensor grid can be used only for low-order (1st, 2nd) analysis of few parameters. For higher-order analysis of many parameters, the tensor grid suffers from the curse of dimensionality (a full tensor grid in  $n$  dimensions requires  $(d+1)^n$  points, which rises exponentially in  $n$ ) (Nobile et al., 2008). In that case, a smart choice of a sparse subset from the tensor grid becomes necessary. Then, PCM chooses the minimum required number of collocation points, equal to the number of coefficients  $n_c$ , from the full tensor grid according to their probability weight, i.e., according to their importance as specified by the available probability distribution of  $\Theta$ . This simply means to select the collocation points from the most probable regions of the input parameter distribution (see Oladyshkin et al., 2011).

The weighted-residual method in the random space is defined as (Li and Zhang, 2007):

$$\int \left( \Gamma - \sum_{i=1}^{n_c} c_i \Pi_i(\Theta) \right) w(\Theta) p(\Theta) d\tau = 0, \quad (5)$$

where  $w(\Theta)$  is the weighting function and  $p(\Theta)$  is the joint probability density function of  $\Theta$ . Please note that choosing  $w_i = \Pi_i$  in Eq. (5) results in the method discussed by Ghanem and Spanos (1991) and Le Maître and Knio (2010). In PCM, the weighting function is chosen as the delta function:

$$w(\Theta) = \delta(\Theta - \Theta_c). \quad (6)$$

$\Theta_c$  is the set of collocation points. Substituting from Eq. (6) into Eq. (5) gives the following:

$$\Gamma_c - \sum_{i=1}^{n_c} c_i \Pi_i(\Theta_c) = 0, \quad (7)$$

where  $\Gamma_c$  are the response values corresponding to the collocation values  $\Theta_c$ . We solve Eq. (7) to find the coefficients  $c_i$ .

Hence, in total,  $n_c$  detailed runs are required to determine the  $n_c$  unknown coefficients. The roots of the data-driven polynomial basis (see Section 2.2) define the positions of the collocation points specific to the distribution of input parameters at hand and, thus, indicate the optimal parameter sets for model evaluation, using all available information about the input parameters. In our study, we have  $n=4$  uncertain parameters and we use a polynomial of degree  $d=2$ . This means that only  $n_c=15$  detailed runs are necessary to obtain the expansion coefficients and approximate the response surface.

### 3. CO<sub>2</sub> storage problem

Here, we describe the injection scenario for which we analyze sensitivities, uncertainties, and risks in Sections 4 and 5. The same flow responses are studied here as in Ashraf et al. (2010a,b). These are CO<sub>2</sub> pressure, CO<sub>2</sub> mobile and residual volumes and leakage risk

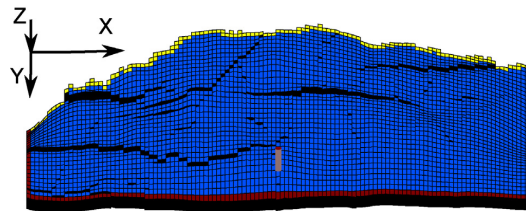


**Fig. 1.** Boundary conditions and the well location in the designed injection scenario. Red color corresponds to the open boundaries and yellow color shows the closed side on the crest. (For interpretation of the references to color in this figure legend, the reader is referred to the web version of the article.)

as described below. Then, we describe the uncertain parameters considered in the study followed by a discussion on the uncertain structural aspects of the considered geological settings.

#### 3.1. Modeling scenario

A typical scenario of CO<sub>2</sub> injection is defined in which a volume of  $40 \times 10^6 \text{ m}^3$  is injected via one well during an injection period of 30 years. This volume corresponds to 20% of the total aquifer pore volume. After stopping injection, simulation continues for 70 years to study the early migration of the CO<sub>2</sub> plume. For brevity, we omit the detailed model equations here and refer the interested reader to Oladyshkin and Nowak (2012) and Oladyshkin et al. (2011).

In our scenario, we feature an aquifer system that is formed by shallow-marine deposits. There is one closed boundary on the top side of the model and the other sides are assumed to be open (Fig. 1). All the open boundaries are modeled as Dirichlet boundaries, two of which with hydrostatic pressure distribution (the right and bottom boundaries in Fig. 1). The remaining left boundary is also hydrostatic, but modified in order to account for the regional groundwater effect (see below).

The cells on the faces of the open boundaries are equipped with a very large pore volume multiplier, such that they numerically represent a much larger volume and effectively enlarge the domain. This helps to minimize the boundary effects of a computational domain that would otherwise be relatively small compared to the injected CO<sub>2</sub> volume (about 20% of the total pore volume, see above). The pore volume multiplier technique allows for a physically reasonable pressure build-up close to the boundary. Moreover, this allows the CO<sub>2</sub> that has left the domain to re-enter by gravity segregation after the injection has stopped.

A summary of the used parameter values is given in Table 1. The hydrological parameters like permeability and porosity vary within individual realizations due to the considered geological structure (see Fig. 2 for the histograms of porosity and permeability in one selected realization). They also differ between the different realizations, as they are changed to represent different geological features. Although the geological realizations of this model vary in some geological features, but the same total pore volume, grid, and fault

**Table 1**  
Aquifer model information.

Parameter	Value	Unit
Number of active cells in the model	78,720	–
Resolution X, Y, Z	40 × 120 × 20	–
Scale X, Y, Z	3000 × 9000 × 80	m
Injection rate	3650	m <sup>3</sup> /day
Initial pressure	266.5	bar
Critical CO <sub>2</sub> and water saturations	0.2	–
CO <sub>2</sub> viscosity	0.04	cp
Water viscosity	0.4	cp
Rock compressibility	0.3e-6	1/bar

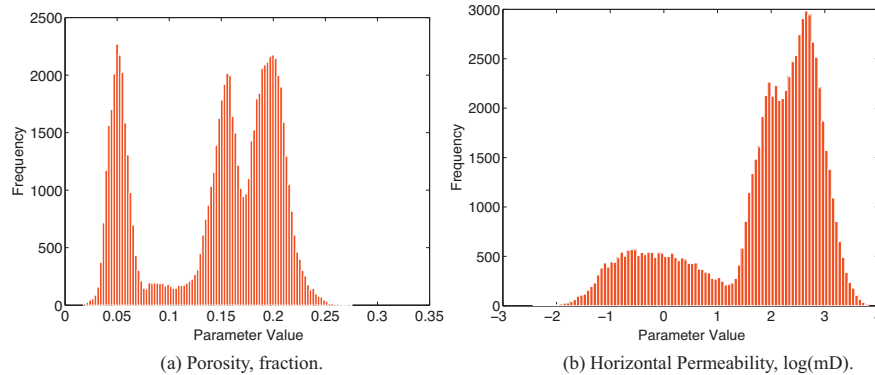


**Fig. 2.** The histograms of hydrological parameters shown for a realization with low levels of heterogeneity. The vertical permeabilities are approximately one order of magnitude lower than the horizontal permeabilities.

geometry is considered. The injection well is screened in the lower part of the model.

### 3.2. Analyzed model predictions

We seek to maximize the CO<sub>2</sub> storage volume and minimize the risk of leakage. These quantities are measured by various simulation outputs that are described in Table 2 and discussed in the following.

CO<sub>2</sub> pressure is considered as the spatial average of the pressure distribution in the entire domain, weighted by the CO<sub>2</sub>-filled pore volume in each model cell. Monitoring or predicting the pressure response within the CO<sub>2</sub> plume is important to avoid over-pressurized injection operations.

Residual CO<sub>2</sub> volume is the volume of trapped CO<sub>2</sub> that is left in the small pores in an imbibition process. This volume is crucial for the long-term storage capacity of reservoirs.

Mobile CO<sub>2</sub> volume is the volume of CO<sub>2</sub> that can move in a continuous phase in the medium. It is considered as one of the important flow responses, because only mobile CO<sub>2</sub> volumes can lead to leakage through any failure in the sealing cap-rock or ill-plugged well.

Finally, we consider leakage risk through cap-rock failure. Cap-rock integrity is a major concern for the safety of CO<sub>2</sub> storage operations. An over-pressurized injection can lead to fractures that may extend up to the cap-rock, penetrate through the cap-rock, or activate pre-existing faults and fractures, and finally lead to CO<sub>2</sub> leakage. In addition, the capillary barrier effect of the cap-rock can be overcome by a local pressure build-up. Thus, the probability of cap-rock failure can depend on the geomechanical properties of the cap-rock and of the medium, on the topography of the cap-rock, and on the pressure build-up resulting from the CO<sub>2</sub> injection and migration. More details about failure mechanisms and failure criteria can be found in the literature (e.g., Zweigle and Heill, 2003; Aker et al., 2013; Rohmer and Seyed, 2010). However, geomechanical modeling and knowledge about pre-existing features that

can be activated during injection would be required to take these processes into account.

Here, we demonstrate how cap-rock integrity can be considered in the workflow of sensitivity analysis and uncertainty assessment in a simplified manner. To avoid detailed studies of multiphase flow coupled with geomechanical simulations and fracture mechanics, we follow a pragmatic approach. The idea is to assign a spatial probability distribution of cap-rock failure over the area of the cap-rock layer, such that each point of the cap-rock has its own failure probability. In principle, this probability could be assigned in correspondence with the current pressure distribution and with geological features such as varying cap-rock thickness, material properties, faults and fractures. For the means of demonstration, we simply assign a spatial Gaussian function as a scenario assumption to provide the cap-rock failure probability for each point of the cap-rock (see Fig. 3). Leakage risk is defined as the probability of leakage (due to cap-rock failure) times the amount of escaping CO<sub>2</sub> in case of leakage. Thus, we spatially integrate the product between cap-rock failure probability and the volume of mobile CO<sub>2</sub> below each point of the cap-rock over the entire area of the cap-rock.

### 3.3. Uncertain parameters

The most apparent uncertainty in CO<sub>2</sub> storage is the lack of geological knowledge. Large geological scales and diversity of rock properties make it impossible to obtain the whole descriptive picture for a study. A geological study will therefore be accompanied

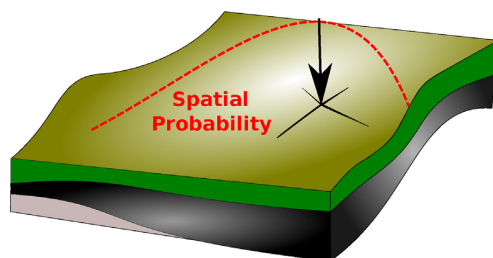


**Fig. 3.** CO<sub>2</sub> leakage risk is computed as the product of a cap-rock failure probability and the amount of mobile CO<sub>2</sub> beneath the cap-rock, integrated over the entire surface area of the cap-rock. Here, we use a Gaussian function as simple scenario assumption for the cap-rock failure probability (indicated schematically by the color shading and the dashed red line with the black coordinate system). (For interpretation of the references to color in this figure legend, the reader is referred to the web version of the article.)

**Table 2**  
Important model responses and their brief description. For more information, see Ashraf et al. (2010a,b).

Response	Description
Average CO <sub>2</sub> pressure	Volume average of pressure, weighted by CO <sub>2</sub> volume
Mobile CO <sub>2</sub>	Volume of CO <sub>2</sub> in places with saturation above critical value
Residual CO <sub>2</sub>	Volume of CO <sub>2</sub> in places with saturation below critical value
Leakage risk	A risk value for the leakage through the cap-rock

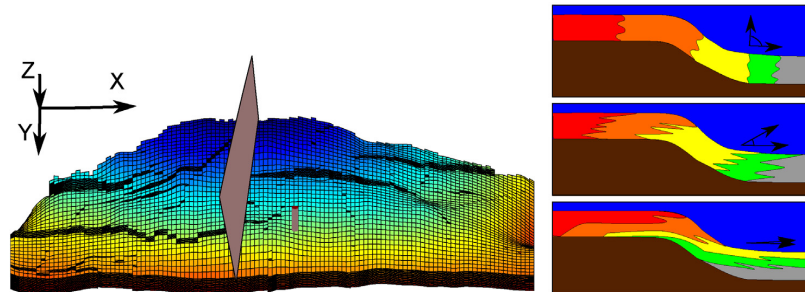


**Fig. 4.** The river flows from left to right toward the sea on the model vertical section shown here (left figure). Aggradation angle is demonstrated in three levels (right figure); from top: low, medium and high aggradation angle. Between deposition and now, the entire system was rotated by tectonic effects such that the original river flow direction is oriented upward, not downward.

by huge levels of uncertainty. Many studies have shown the significance of geological heterogeneity on underground flow performance (e.g., Dutton et al., 2003; Eaton, 2006). To obtain a descriptive image of a feature, like faults and depositional structure, such that uncertainty can be reduced, we must provide adequate data. The process of data collection from underground layers is very costly, therefore it is important to know the ranking of influence each feature has on the flow in order to optimize the cost of data acquisition in modeling.

From the geological parameters that are relevant for shallow-marine deposits used in Ashraf et al. (2010a,b), we pick three parameters: the degree to which barriers may block horizontal and vertical flow, aggradation angle, and fault transmissibility. In addition to these, we consider the regional groundwater effect as an uncertain parameter in our study. Here, we give a brief description on each one, followed by the probabilities assigned to these parameters.

**Barriers:** During the formation of shallow-marine deposits, periodic floods result in a sheet of sandstone that dips, thins, and fines in a seaward direction. In the lower front, thin sheets of sandstone are inter-bedded with the mud-stones deposited from suspension. These mud-draped surfaces are potential significant barriers to both horizontal and vertical flow. In the SAIGUP realizations, these barriers were modeled by transmissibility multipliers in specific layers of the formation. The position of the barriers is generated by creating an elliptic cone-shaped surface that follows the plan-view shoreline shape of the facies, characterized from real world data (Howell et al., 2008). We define the degree of barrier presence by the areal percentage of zero-valued transmissibility multipliers. Fig. 5 shows a medium level of barriers.

**Aggradation angle:** in shallow-marine systems, two main factors control the shape of the transition zone between river and basin: the amount of deposition supplied by the river and the accommodation space that the sea provides for these depositional masses. Deposition happens in a spectrum from larger grains

depositing earlier on the land side, to fine deposits happening in the deep basin. If the river flux or sea level fluctuates, equilibrium changes into new bedding shape based on the balance of these factors. In the SAIGUP study, progradational cases are considered, in which river flux increases and shifts the whole depositional system into the sea. The angle at which transitional deposits are stacked on each other because of this shifting is called the aggradation angle. Three levels of aggradation are shown in Fig. 4: low, medium and high. The study reported in Ashraf et al. (2010a,b) showed that aggradation can have a dramatic influence on the injection and migration process.

**Fault transmissibility:** Huge uncertainties can be involved when modeling the presence of faults. Faults are discrete objects that are modeled by changing the geometry of the simulation grid. The transmissibility for flow across faults changes during the process of faulting. This causes a spectrum of transmissibilities, from a sealing fault with no flow across it, to a fault that has not produced any barriers to the flow within its opening space.

Within a simulation grid, the influence of faults on the local and global flow behavior depends on a number of parameters including fault length, orientation, intensity and transmissibility. The well location with respect to the faults can change the overall behavior of injected CO<sub>2</sub> plume significantly. In the SAIGUP models, different levels of fault orientations, transmissibility, areal intensity, and well patterns are considered. For this study, we consider all fault modeling parameters at their medium level and consider to vary only the fault transmissibility. These variations, however, do not affect the definition of the no-flow boundary, which is motivated by the presence of an impermeable fault.

The used geology realizations contain compartmentalized fault systems comprising approximately equal densities of strike-parallel and strike-perpendicular faults based on a portion of the Gullfaks field (Manzocchi et al., 2008; Howell et al., 2008). Fig. 6 shows the fault pattern and location of the injector considered for the study.

It is shown in Manzocchi et al. (1999) that the transmissibility multiplier provides a numerically more robust representation of faults within reservoir simulation than conventional permeability multipliers. We consider the fault transmissibility multipliers to range between zero and one. A multiplier value of one corresponds to a fault permeability equal to the harmonic average of cell permeabilities across the fault, i.e., to a fault without any influence on flow (Manzocchi et al., 1999).

**Regional groundwater effect:** geological modeling always comes with the uncertainty of how large the aquifer is and how it is connected to other underground aquifers. This is a direct consequence of the need to define boundary conditions to limit the computational domain, which cannot always coincide with meaningful physical boundaries in large-scale systems. However,

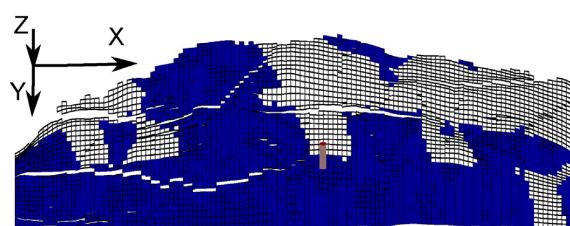


**Fig. 5.** The figure shows 50% of zero transmissibility multipliers in a specific model layer representing a medium level of barriers. One layer of the model is shown in the figure.

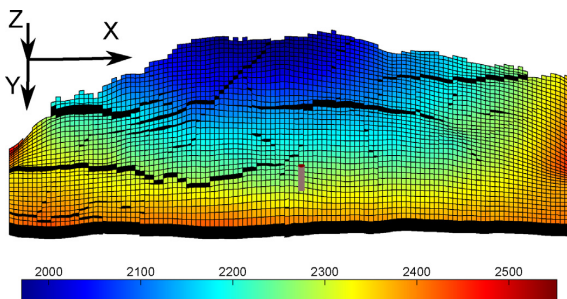


**Fig. 6.** Fault orientation and intensity of the model used in the study. Depth in meter is shown by color on the grid. (For interpretation of the references to color in this figure legend, the reader is referred to the web version of the article.)

connections to active external aquifers can be accounted for by adapting the values for the boundary conditions accordingly. Some connections might even change throughout the year, depending on rainfall. The flux across model boundaries might influence the CO<sub>2</sub> plume dynamics during and after injection. To simulate such effects, we changed the left boundary pressure by adding an uncertain additional pressure value  $\Delta p$  that varies between 0 and 100 bar.

As a scenario assumption, this pressure value is added at the start of injection, i.e., the pressure distribution is not at a steady state when the simulation starts, and this triggers a corresponding transient brine flow. We do so in order to analyze the effect of transient groundwater effects on the system. This may seem an

arbitrary choice, but assuming a steady-state would also be arbitrary to some extent.

The overall process for sensitivity analysis, uncertainty propagation, and risk assessment starts by specifying probability information for the uncertain parameters. Next, one has to design and choose the simulation cases required to obtain the expansion coefficients in the approximating polynomial. However, in our study, we had access to the set of SAIGUP geological realizations and simulation results that had been designed without the considerations possible with the aPC. The computing time for each SAIGUP realization was about 2 h on a 2.4 GHz Intel Xeon CPU, and we decided to recycle these highly expensive simulations in our study. The large computing times are a key motivation to build a cheaper surrogate model for further analysis. Hence, we assume the histograms of uncertain parameters such that they result in collocation points that coincide with the SAIGUP designed values. Therefore, the histograms used in this study are almost uniform, as shown in Fig. 7. In fact, these input distributions could also be handled with the gPC method already mentioned in the introduction, and would correspond to the use of Legendre polynomials. In our case, we use the aPC to avoid the step of modeling the input distributions as exactly uniform. Consequently, the polynomials resulting from the aPC approach are very close to Legendre polynomials. The aPC, however, could be used for any type of histograms and so provides the freedom in other studies to adapt to arbitrary input statistics.

The main concern here is not a unique probability description of the input geological parameters, but rather we perform an uncertainty analysis practice, relying on a scenario assumption of probability distributions. Thus, no general geological conclusion is expected from this study, and results might change by feeding the work-flow with a different probability description.

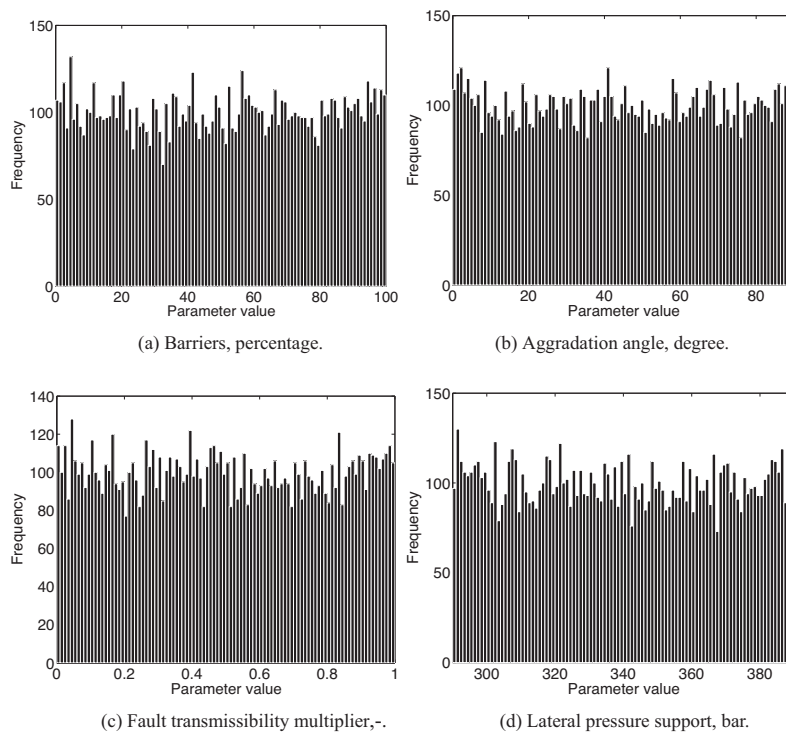


**Fig. 7.** The histograms of geological variables used in this study are sampled from uniform distributions.

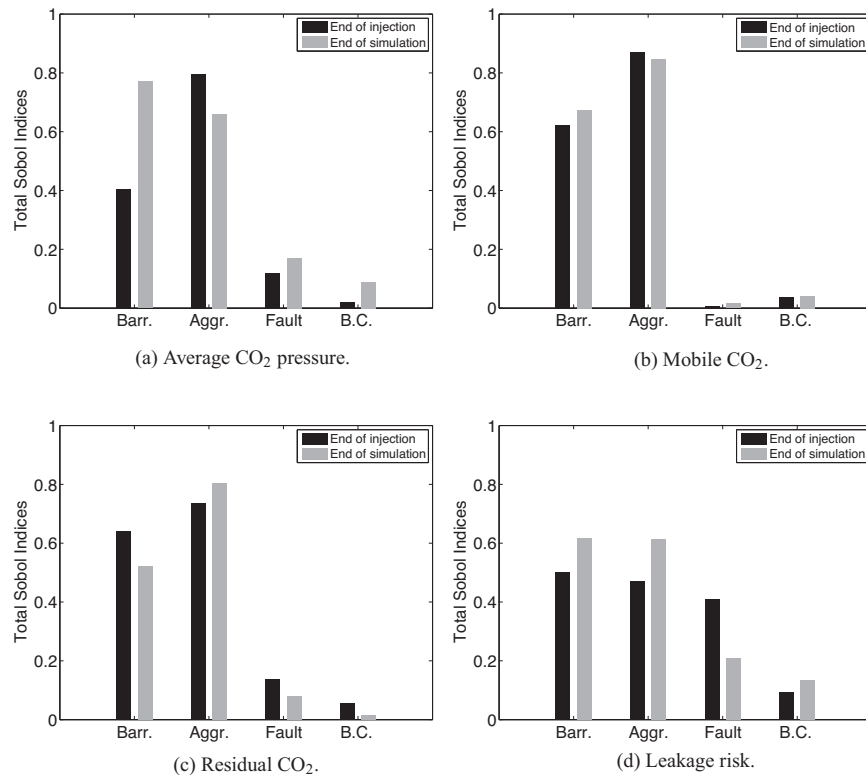


**Fig. 8.** Sensitivity analysis for different responses (a)–(d) with respect to the uncertain parameters. In the figures above, Barr. is for barriers, Aggr. for aggradation angle, Fault for fault transmissibility, and B.C. for regional groundwater effect.

#### 4. Sensitivity analysis

In this section, we tackle global sensitivity analysis with Sobol indices based on the aPC technique, following the line of work on aPC by Oladyshkin and Nowak (2012) and Oladyshkin et al. (2011, 2012). The big advantage of global aPC-based sensitivity analysis is that one can obtain global sensitivity information at computational costs that are hardly larger than those for local analysis. The reason is the following: local methods use infinitesimally small spacing between parameter sets for model evaluation to get numerical derivatives evaluated at a single point. The aPC-based method places the parameter sets for model evaluation at an optimized spacing in parameter space. This can be interpreted as fitting secants (or polynomials for non-linear analysis) to the model response. These secants (polynomials) approximate the model over the entire parameter space in a weighted least-square sense (compare with the best unbiased ensemble linearization approach described by Nowak (2009)). This is more beneficial compared to computing a tangent or local second derivatives (compare FORM, SORM methods, e.g., Jang et al., 1994) that approximate the model well just around one point in the parameter space.

The system featured here is non-linear due to two reasons: First, the involved multi-phase flow equations Oladyshkin et al., 2011 form a coupled system of non-linear partial differential equations, and second, these equations are non-linear in their coefficients. The latter is even more significant if parameters are spatially heterogeneous.

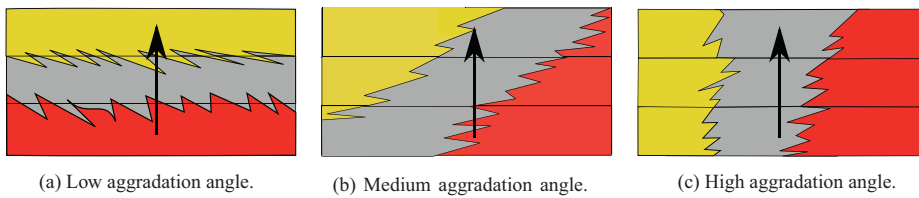
In the following, we briefly summarize the Sobol sensitivity indices technique for quantifying the relative importance of each

individual input parameter in the final prediction. Then, we implement the method for our geological CO<sub>2</sub> storage problem, based on the aPC response surface.

The model responses featured here for global sensitivity analysis (this section) and for the probabilistic risk analysis (see Section 5) are listed in Table 2 and have been discussed in Section 3.1. In the sense of global sensitivity analysis Saltelli (2008), not only should the analysis technique be global, but also should the analyzed quantities be global. In the latter, global refers to the fact that they are relevant for the engineer, are crucial in decision processes, etc. For example, an overall leakage risk is more informative in final decisions than the leakage rate at a specific point, and a total stored volume of CO<sub>2</sub> is more informative for volumetric efficiency considerations of the reservoir than the CO<sub>2</sub> saturation at individual points.

##### 4.1. Sobol sensitivity indices

The method is well described in the literature (Sobol, 2001; Saltelli, 2008, 2010; Reuter and Liebscher, 2008). More recent works are concerned about expediting calculation pace by computing Sobol indices analytically from polynomial chaos expansions (Crestaux et al., 2009; Oladyshkin et al., 2011, 2012; Le Maître and Knio, 2010; Sudret, 2008). The idea behind the combination of PCE techniques with Sobol indices is to replace the analyzed system with an approximating function which leads to mathematical and numerical benefits in the sensitivity analysis.



(a) Low aggradation angle. (b) Medium aggradation angle. (c) High aggradation angle.

**Fig. 9.** Illustration of how the aggradation angle affects the effective vertical conductivity.

Using polynomials for this approximation is convenient, because it is easy to analytically obtain the output variances from the statistics of the input variables of the polynomials. In our case, the solution is approximated by orthogonal polynomials with ascending polynomial degree. We expand the variance of model output into individual components originating from all possible combinations of input parameters. Assume that we break the system output into components as follows:

$$\Gamma = \Gamma_0 + \sum_i \Gamma_i + \sum_i \sum_{j>i} \Gamma_{ij} + \dots \quad (8)$$

A single index (here:  $i$ ) shows dependency to a specific input variable. More than one index (e.g.:  $i$  and  $j$ ) shows interaction of two or more input variables. If we consider the input vector  $\Theta$  to have  $n$  components  $\theta_i$  for  $i = 1, \dots, n$ , then  $\Gamma_i = f_i(\theta_i)$  and  $\Gamma_{ij} = f_{ij}(\theta_i, \theta_j)$ . In practice, we stop at a finite number of terms in Eq. (8). The

first order sensitivity index, the so called Sobol index, is defined statistically as follows (Saltelli, 2008):

$$S_i = \frac{V[E(\Gamma | \theta_i)]}{V(\Gamma)}, \quad (9)$$

where  $E(\Gamma | \theta_i)$  is the conditional expectation of output  $\Gamma$  for a given value of  $\theta_i$  and  $V$  is the variance operator. In plain words,  $S_i$  is the fraction of total variance  $V(\Gamma)$  that can be explained by the parameter  $\theta_i$ . Since  $\theta_i$  can be fixed at any value in its uncertainty interval, each of those values produces a distinct expectation. In Eq. (9), the variance of those expectations is divided by the unconditional variance of output (i.e., with no input variable fixed). For more than one index, a higher-order Sobol index can be defined as:

$$S_{ij} = \frac{V[E(\Gamma | \theta_i, \theta_j)] - V[E(\Gamma | \theta_i)] - V[E(\Gamma | \theta_j)]}{V(\Gamma)}. \quad (10)$$

Here,  $V[E(\Gamma | \theta_i, \theta_j)]$  is the variance of output expectations after fixing  $\theta_i$  and  $\theta_j$ . This index represents the significance of variation in output generated from the joint uncertainty in several input

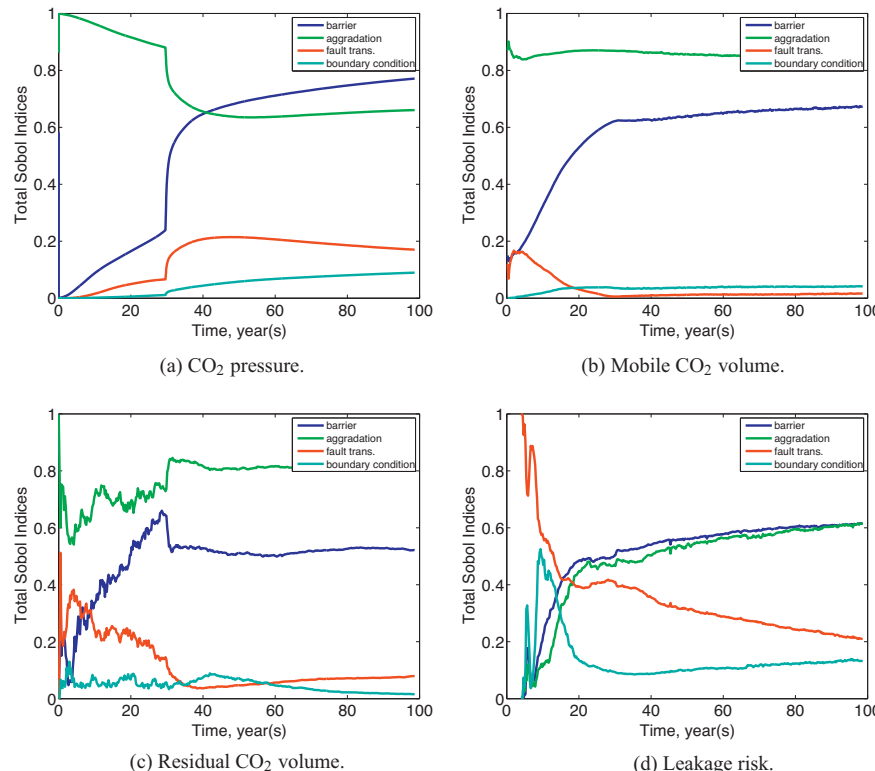


**Fig. 10.** Sensitivities (expressed by total Sobol indices) plotted versus time for different responses.

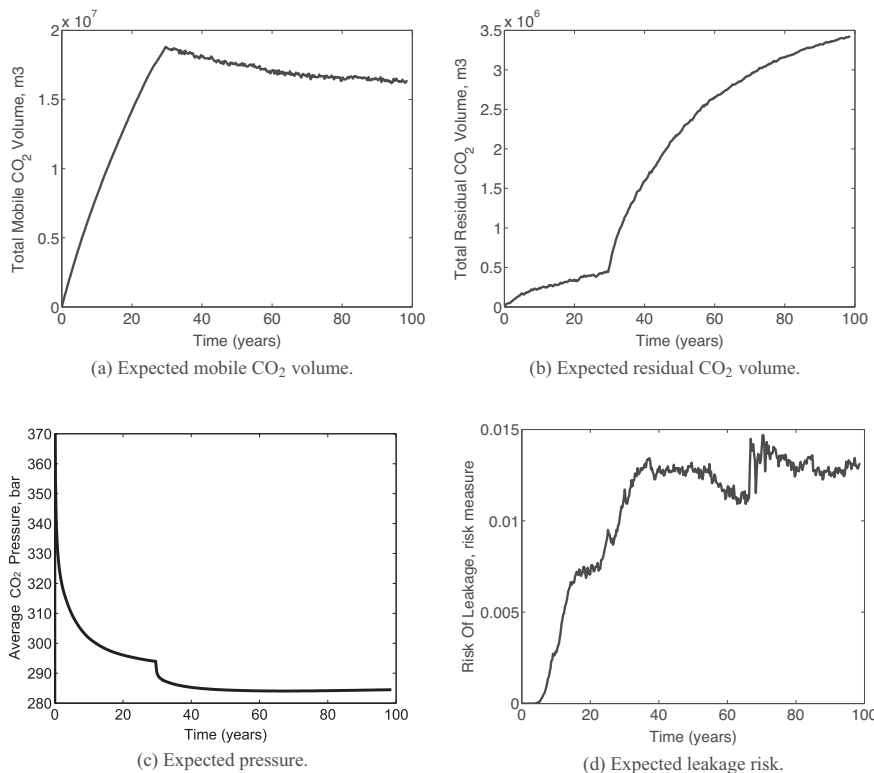


**Fig. 11.** Expectation for response values versus time. The pressure value for initial time step in (c) goes up to 670 bar.

variables, i.e., from the interaction of uncertain parameters. If we add all indices that contain a given variable  $\theta_i$ , the sum is called the total Sobol index:

$$S_{Tl} = S_l + \sum_{j \neq i} S_{lj} + \sum_{j \neq i} \sum_{k \neq i} S_{ljk} + \dots \quad (11)$$

The total Sobol index is a sensitivity measure to rank parameters according to their influence on the model results. When this index is close to zero, the corresponding parameter has a negligible role in the variation of the system response. In that case, the uncertainty in that parameter does not introduce a considerable uncertainty in the response, and the parameter could be omitted from further analyses.

In practice, we evaluate the Sobol indices analytically from the expansion coefficients of the aPC as described by Oladyshkin et al. (2012).

#### 4.2. Sensitivity analysis

We calculate the total Sobol indices for the geological CO<sub>2</sub> storage problem that is described earlier. The results are based on an aPC expansion of order two that is obtained by fifteen detailed simulations. The choice of order two is supported by the results of Oladyshkin et al. (2011), where the authors found in a similar CO<sub>2</sub> storage problem that second order may be the cheapest non-linear expansion, but still sufficiently accurate for this type of purpose. Recently, Oladyshkin et al. (2012) provided the results of a numerical convergence analysis for aPC-based Sobol analysis. They report that increasing the expansion order beyond 2 introduces only small changes to the sensitivity values for their considered system, and

does not change the ranking of the analyzed parameters anymore. A study similar to the current study without aPC needed one hundred and sixty runs to perform a sensitivity analysis with a different method (Ashraf et al., 2010b). The pattern of sensitivity reported here is similar to what is produced in that study, but at dramatically reduced costs.

#### 4.3. Results

The flow behavior in the domain is influenced by the type and intensity of different heterogeneities. This influence can be traced in the CO<sub>2</sub> pressure and saturation distributions over time. During injection, viscous forces imposed by the injector dominate the force balance. Viscous forces act in the form of spatial pressure gradients in all directions. After 30 years, the injection stops, and gravity starts playing the major role in the flow dynamics, acting in the vertical direction (Ashraf et al., 2010a,b).

Barriers and aggradational angle have different impacts on the flow during each flow regime, i.e., injection or after injection. Low fault transmissibility hinders the flow and keeps the pressure in compartments. Geometry distortion in the geological layers because of the faulting processes plays a considerable role in the splitting of CO<sub>2</sub> plumes within the domain. Water flux from lateral boundaries due to the regional groundwater effect enhances the spread of CO<sub>2</sub> and leads the mass of CO<sub>2</sub> toward the other open boundaries.

Fig. 8 shows the sensitivity of different responses to the uncertain parameters. Total Sobol indices are plotted at specific times. End of simulation refers to the year 100, i.e., 70 years after injection stops. This time duration is long enough for the flow to

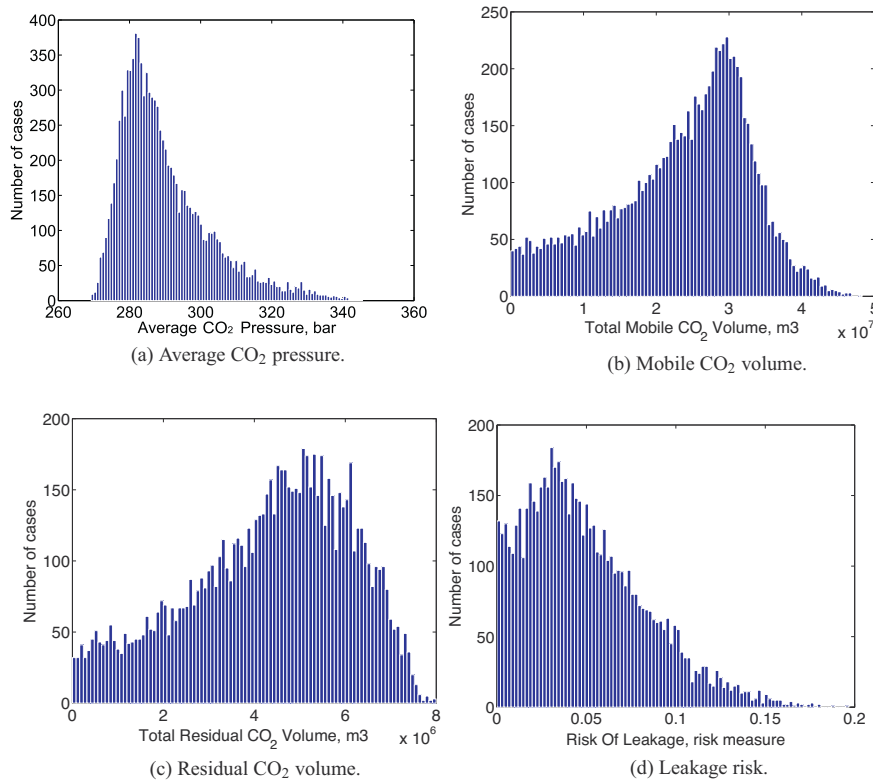


**Fig. 12.** Histograms of selected response values at end of injection.

stabilize at a stationary condition for the majority of the model runs.

As already observed in Ashraf et al. (2010a,b), the aggradation angle plays a significant role in the flow behavior. In cases with low aggradation angle, the stratigraphy of rock types is a pattern of parallel layering. For higher aggradation angles, rock-types are distributed between more modeling layers. The effective vertical permeability changes from the harmonic average (in Fig. 9a) toward the arithmetic average (in Fig. 9c), as the aggradation angle increases from 0 to 90°. The harmonic average might be much smaller than the arithmetic average, in particular when there are vertically impermeable rock-types in the medium. The shallow marine depositional system contains some rock-types with almost zero transmissibility in the vertical direction. Therefore, a low aggradation angle can hinder the flow from traveling upward across layers in the domain and force it to stay trapped in some lower layers, as seen for many of the low aggradation angle realizations in our study. The relatively large sensitivities to the level of barrier presence are based on the same effects.

Our results show a relatively weak sensitivity of responses with respect to the water influx from one side of the model. This sensitivity is in particular low during injection, when the high pressure imposed from the well dominates the dynamics of flow in the medium (Fig. 8a). The sensitivity patterns for the mobile and residual CO<sub>2</sub> volume are similar in Fig. 8b and c, because the mobile and residual CO<sub>2</sub> volume add up to the total injected CO<sub>2</sub> volume, with the exception of the CO<sub>2</sub> volume that has left the domain. Hence, they are highly dependent on each other. More detailed results are shown in Fig. 10a-d. Total Sobol indices are plotted for each response during the entire time interval. When the flow regime

switches from injection to a gravity-dominated system, we observe a jump or sharp drop in some of the sensitivity plots (Fig. 10a and c at 30 years).

The sensitivity of the CO<sub>2</sub> pressure with respect to the presence of barriers jumps up, right after stopping the injection. This happens because barriers slow down the pressure release through open boundaries, resulting in local pressure build-ups.

The sensitivity of the residual CO<sub>2</sub> volume with respect to barriers presence drops soon after injection. This is reasonable since the residual trapped volume is more a function of lateral flow in the medium, compared to the vertical flow in the relatively small thickness of the aquifer.

## 5. Risk analysis

The risk  $R$  of a process is quantitatively defined as the extent of consequence  $C$  caused by the process, multiplied by the probability  $P$  of that consequence to happen:

$$R = P \times C. \quad (12)$$

The consequence can be defined by direct measures in the simulation responses, or it can be related to consequences caused in the environment outside the considered system. For example, in the case of CO<sub>2</sub> injection into deep aquifers, the amount of CO<sub>2</sub> which stays mobile and undissolved in the medium for a time after injection can be considered as a consequence, bearing the potential of leakage up to the surface if exposed to a geological leakage point. The consequence could also be defined by a criterion for external consequences, like the rate of climate change (either locally or globally) due to CO<sub>2</sub> leakage, the costs of pumping CO<sub>2</sub> that does not

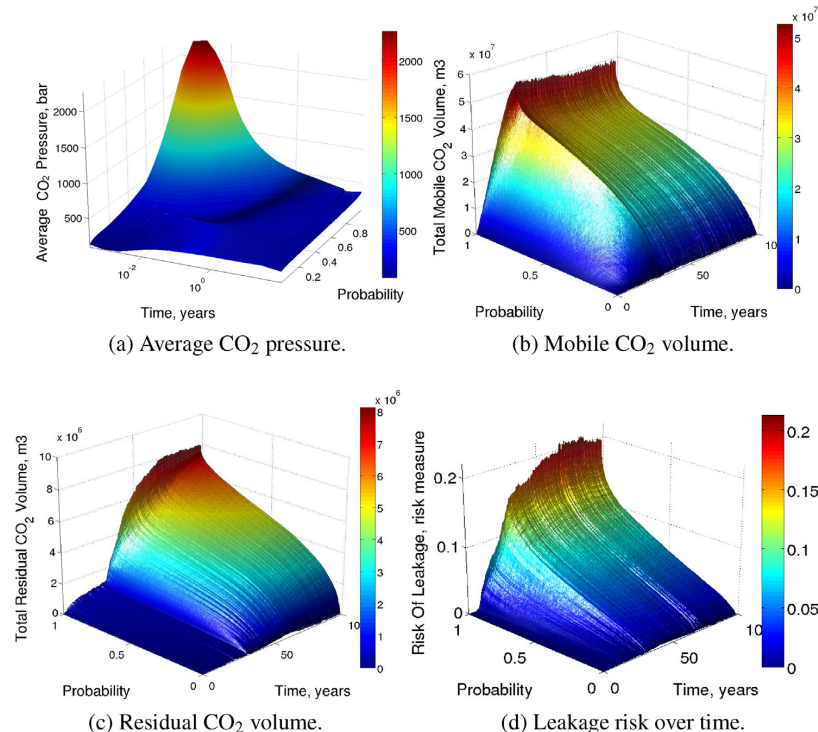


**Fig. 13.** Evolution of the cumulative distribution function of different response values over time.

remain in the subsurface, or via the related costs for CO<sub>2</sub> emission certificates.

The other part is the probability of these consequences to happen. This depends on the stochastic behavior of the process which results in the respective outcomes.

We use the polynomial-based reduced model for risk analysis, because it is fast enough to perform a Monte-Carlo analysis with a large number (here: 10,000) of realizations on the polynomials. Thanks to the higher-order approximation via the aPC, the principal non-linear physical behavior of CO<sub>2</sub> storage is included in the analysis, and detailed probabilistic risk assessment becomes feasible. We analyze here the same quantities as in Section 4, i.e., average CO<sub>2</sub> pressure, the volume of mobile or immobile CO<sub>2</sub>, and leakage risk. For definitions, see Section 3.1.

#### 5.1. Quantification of expected values in CO<sub>2</sub> storage

Average response values can be calculated analytically from the polynomial (e.g., Oladyshkin et al., 2011) or via the Monte-Carlo post-process as mentioned above. Fig. 14a-d shows some of the calculated expectations as functions of time. In Fig. 11a, the mobile CO<sub>2</sub> volume increases linearly in the medium because of the constant injection rate during the first thirty years. After injection, the mobile volume of CO<sub>2</sub> is reduced due to the trapped volume in residual form and the migration of CO<sub>2</sub> across open boundaries.

Fig. 11b shows the expected values for the volume of residually trapped CO<sub>2</sub> as a function of time. The plot shows the significance of imbibition during the plume migration period, when water replaces CO<sub>2</sub> that is moving upward because of gravity segregation. During injection, CO<sub>2</sub> invades the aquifer and drainage is dominant. Therefore, the expected residual CO<sub>2</sub> plot shows a smaller slope during injection than what it shows later in time.

When injection starts, a pressure pulse travels through the medium at a finite velocity because of the slight compressibility of brine. The initially built-up pressure releases through open boundaries over time and the average pressure drops in the aquifer (Fig. 11c). The large pressure build-up in the very early time steps occurs because large pressure values have to be exceeded in the injection cell before CO<sub>2</sub> becomes mobile at saturations above the residual value. During this period, the CO<sub>2</sub> pressure is defined almost only by the pressure in the injection cell (compare the definition of CO<sub>2</sub> pressure in Section 3.2). Under realistic injection settings, a pressure rise of up to 400 bars (from 270 to 670 bar in the first simulation time step, not visible in Fig. 11c) would be very unrealistic and would not be allowed to occur. At the end of Section 5.2, we will investigate this issue in more detail.

Also, during early injection time, the pressure is larger than at the end of injection. There are a few realizations where the contributions from the external aquifer support, a dense barrier system close to 100% areal coverage, an adverse aggradation angle of the formation and extremely low fault transmissibilities interact to effectively block the CO<sub>2</sub> flow close to the well. This has strong effects on pressure when the rock at the injector position happens to be poorly permeable, leading to a very poor injectivity. An adapted CO<sub>2</sub> injection strategy would react by lowering the injection rate, by choosing a different injection position, or by even abandoning the entire site.

Based on the results of the current study, it is possible to identify such adverse combinations and guide site investigation strategies to pay attention to such situations. In a follow-up study (ready for submission), we are currently investigating an active injection strategy controlled by an upper allowable pressure limit.

However, the initial sharp pressure increase is released very quickly. This happens, when first parts of the CO<sub>2</sub> plume have found

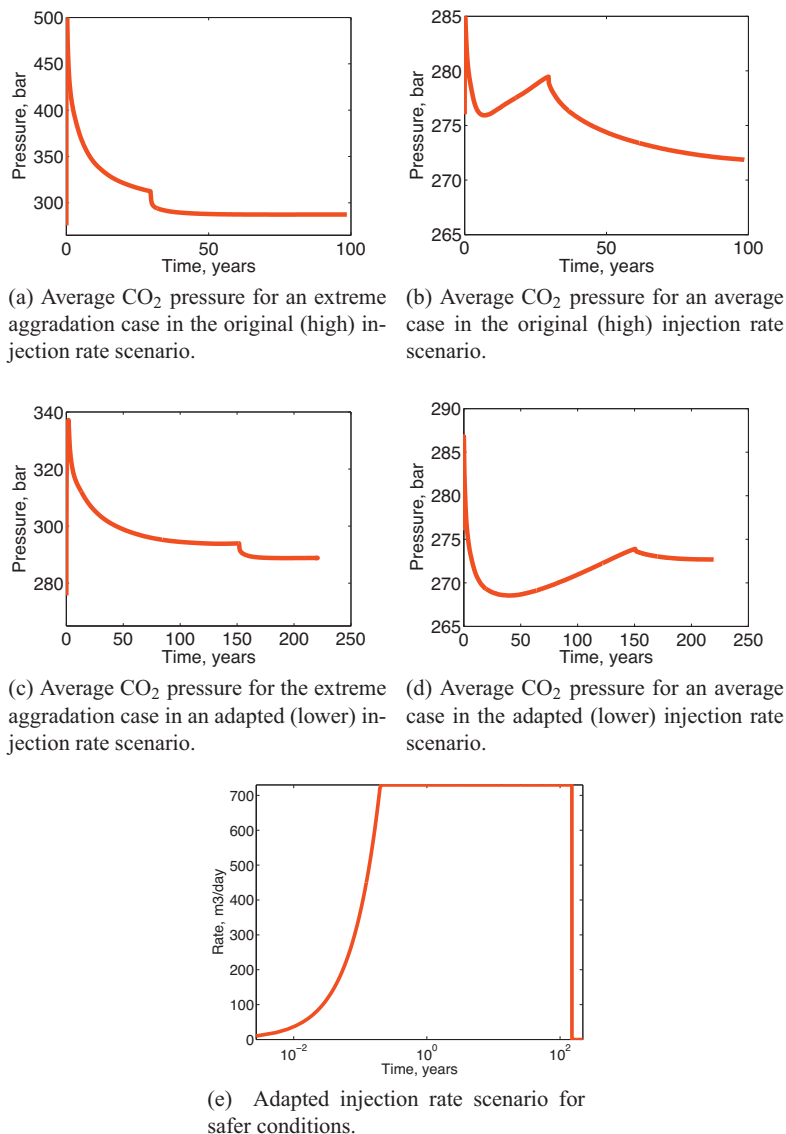


**Fig. 14.** Average CO<sub>2</sub> pressure values versus time for two selected cases. The initial pressure peak values in the first time step have been truncated in the plots (a), (b) and (c). They go up to 1680, 334 and 338 bar respectively.

flow pathways into regions with better rock properties, providing the possibility to relax the pressure build-up, and also to let the CO<sub>2</sub> escape towards the boundaries.

The expected leakage risk is plotted in Fig. 11d, and increases in value as the injected CO<sub>2</sub> travels upward and accumulates beneath the sealing cap-rock.

### 5.2. Results of CO<sub>2</sub> storage risk assessment

In this section, the probability distributions (rather than expected values) of system responses during and after injection are studied. Results from the MC analysis of the response surface

are given as histograms of output values and also as cumulative distribution functions (CDF) for probabilities (Figs. 12 and 13).

Fig. 12a–c shows the histograms of responses obtained from the Monte-Carlo process at the end of injection. A long tail is observed for lower mobile and residual CO<sub>2</sub> values in Fig. 12b and c. The long tail means a large range of possible low values. Pressure shows a long tail for higher values. This means that even high critical values still have substantial probabilities to be exceeded, indicating that the possibility of geomechanical damage to sealing layers will have to receive a large attention. We observe an issue of mass conservation in Fig. 12b, where a few realizations show more mobile CO<sub>2</sub> in the domain than the total injected volume (which is about  $40 \times 10^6$  m<sup>3</sup>). This is a typical issue for a large class of statistical

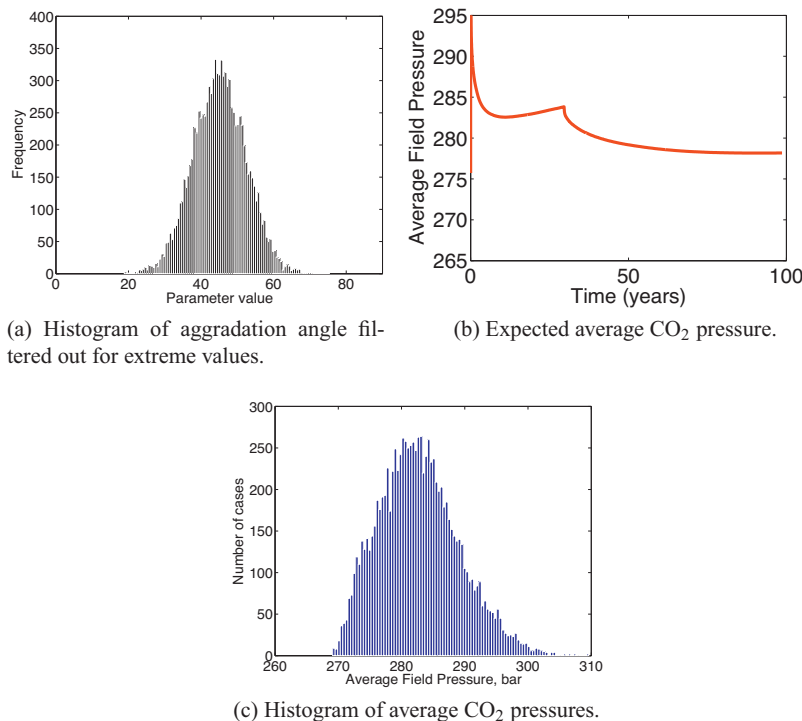


**Fig. 15.** Extreme aggradation angle values can result in impractical injection operations. Filtering out the extreme aggradation cases (e.g., by geophysical screening) leads to more favorable conditions. (a) More narrow distribution of aggradation. (b) New expected value for CO<sub>2</sub> field-average pressure under more narrow aggradation range. (c) New distribution of CO<sub>2</sub> field-average pressure at end of injection. The initial pressure peak in (b) reached 341 bar, and is truncated here.

methods that interpolate or extrapolate simulation results in the parameter space, because their setup is not based on the mass conservation equation. In this specific case, the mass conservation issue is caused by approximating the response surface via polynomials, with vanishing residuals only at the collocation points. The polynomials are evaluated at many randomly chosen parameter sets drawn from the histograms shown in Fig. 7, which do not coincide with the collocation points.

Finally, we report how the corresponding probabilities change over time in Fig. 13a–c. High pressure buildup is considerable during the early injection time, and it is negligible after injection during plume migration (Fig. 13a). An over-pressurized injection can induce fracturing in the medium, extending to the sealing layers. Any fractures caused in the structural traps can expose the mobile CO<sub>2</sub> to leakage paths. Therefore, higher pressure values can be interpreted as high risk in early time.

The presented framework for risk assessment indicates that the pressure in the reservoir is unacceptably large (see Section 5.1 and Fig. 11c) and can be too high. In the following, we use our method to investigate this critical issue. Fig. 14a and b shows the predicted time evolution of field-average CO<sub>2</sub> pressure for a collocation point with adverse and well-suitable values of the aggradation angle, respectively. It becomes apparent, that the unacceptable pressure values arise only under extreme values of the aggradation angle. Reacting to this insight, we see and discuss two possible options in the following.

The first option is to lower the injection rate, so that we keep the pressure values in a safe region, even under the probability that the reservoir might have an adverse aggradation angle. Fig. 14e shows the injection rate for a safe scenario: the injection rate ramps up over a year from zero to one fifth of the level used

before. The corresponding pressure behavior for the adverse and the well-suitable cases is shown in Fig. 14c and d. Please note that the case with the less extreme aggradation angle shows the typical rise in CO<sub>2</sub> pressure up to the end of injection (Fig. 14b and d), following just after the initial pressure peak due to first entry.

The second option is to improve our understanding about the properties of the analyzed storage site. In particular, some additional exploration actions could help to reduce the uncertainty in the aggradation angle. In the previous analysis we considered that all values of aggradation angle between zero and ninety degrees are equiprobable, which is a very conservative assumption on the initial state of knowledge. As a scenario variation, we will now assume that further exploration decreased the probability of the extreme aggradation values. Fig. 15a shows the modified assumption on the aggradation distribution, where the extreme values have low probability values in comparison to the initial assumption. The present aPC framework allows estimating the influence of such an uncertainty reduction onto the model output without expensive computational costs. Technically, the Monte-Carlo process can be performed on the response surface under the new assumption on uncertainty. Fig. 15b and c shows the new expected field-average CO<sub>2</sub> pressure and the histogram of average CO<sub>2</sub> pressure at the end of injection, respectively. The new pressure statistics indicate a feasible reservoir operation, even with the original (large) injection rate.

## 6. Conclusion

In this paper, we used the arbitrary polynomial chaos expansion (aPC) method in a sensitivity analysis and risk assessment process.

The goal was to demonstrate the application and feasibility of aPC-based methods in the context of realistic CO<sub>2</sub> injection scenarios. We implemented this method for a typical CO<sub>2</sub> storage problem. Four uncertain parameters with assumed uncertainty distributions are considered. Injection and early migration of CO<sub>2</sub> is studied. The flow sensitivity to geological heterogeneity is evaluated and quantified using Sobol indices. Risk analysis is performed on the defined problem. Flow dynamics are discussed and corresponding interpretations and explanations of the sensitivity and risk results are provided.

The performance of the aPC method has been satisfactory. It is very fast, compared to other stochastic methods for low-parametric systems, and this speed-up allows us to perform an extensive Monte-Carlo process on the aPC-based response surface to calculate the probability of response values throughout simulation time. This study was a first-time application of the aPC to study a realistically complex type of geological structural uncertainty. Based on our assessment of aPC feasibility, we can strongly encourage the use of aPC for sensitivity and risk analysis in complex situations.

The results have shown that the most influential parameter for most of the responses is the aggradation angle of deposition layers of the considered shallow-marine aquifer. The least relevant parameter is the regional groundwater effect, especially during injection time. We re-iterate that the aim of this study was to demonstrate a practice of using arbitrary polynomial chaos expansion for the sensitivity and risk analysis of a typical CO<sub>2</sub> storage problem. Since, in general, the levels of involved input uncertainty are not unique, the physical and geological conclusions of this study are restricted to the probability assumptions taken here and should not be generalized to systems that are very different.

### Acknowledgements

The authors would like to acknowledge the sponsors of the MatMora project defined in the University of Bergen in partnership with SINTEF-ICT and the University of Stuttgart, and the German Research Foundation (DFG) for financial support of the project within the Cluster of Excellence in Simulation Technology (EXC 310/1) at the University of Stuttgart. We would also like to thank the three anonymous reviewers for their constructive comments.

### References

- Abramowitz, M., Stegun, A.I., 1965. *Handbook of Mathematical Functions with Formulas, Graphs, and Mathematical Tables*. Dover, New York.
- E. Aker, E. Skurtveit, L. Grande, F. Cuisiat, Ø. Johnsen, M. Soldal, B. Bohloli, Experimental methods for characterization of cap rock properties for CO<sub>2</sub> storage, Multiphysical Testing of Soils and Shales, pp. 303–308.
- Ashraf, M., Lie, K., Nilsen, H., Nordbotten, J., Skorstad, A., 2010a. Impact of geological heterogeneity on early-stage CO<sub>2</sub> plume migration. In: CMWR.
- Ashraf, M., Lie, K.-A., Nilsen, H.M., Skorstad, A., 2010b. Impact of geological heterogeneity on early-stage CO<sub>2</sub> plume migration: sensitivity study. In: Proceedings of ECMOR XII.
- Babuška, I., Nobile, F., Tempone, R., 2007. A stochastic collocation method for elliptic partial differential equations with random input data. *SIAM Journal on Numerical Analysis* 45 (3), 1005–1034.
- Bachu, S., 2003. Screening and ranking of sedimentary basins for sequestration of CO<sub>2</sub> in geological media in response to climate change. *Environmental Geology* 44 (3), 277–289.
- Bachu, S., 2008. CO<sub>2</sub> storage in geological media: role, means, status and barriers to deployment. *Progress in Energy and Combustion Science* 34 (2), 254–273.
- Barthelmann, V., Novak, E., Ritter, K., 2000. High dimensional polynomial interpolation on sparse grids. *Advances in Computational Mathematics* 12 (4), 273–288.
- Birkholzer, J., Zhou, Q., Tsang, C., 2009. Large-scale impact of CO<sub>2</sub> storage in deep saline aquifers: a sensitivity study on pressure response in stratified systems. *International Journal of Greenhouse Gas Control* 3 (2), 181–194.
- Brennan, S., Burruss, R., Merrill, M., Freeman, P., Ruppert, L., 2010. A probabilistic assessment methodology for the evaluation of geologic carbon dioxide storage. US Geological Survey Open-File Report 1127, 31.
- Celia, M., Bachu, S., Nordbotten, J., Gasda, S., Dahle, H., 2004. Quantitative estimation of CO<sub>2</sub> leakage from geological storage: analytical models, numerical models and data needs. In: Proceedings of 7th International Conference on Greenhouse Gas Control Technologies (GHGT-7).
- Class, H., Ebigbo, A., Helmig, R., Dahle, H., Nordbotten, J., Celia, M., Audigane, P., Darcis, M., Ennis-King, J., Fan, Y., et al., 2009. A benchmark study on problems related to CO<sub>2</sub> storage in geologic formations. *Computational Geosciences* 13 (4), 409–434.
- E. Commission, European Commission's Communication on Extended Impact Assessment, Brussels, Office for Official Publications of the European Communities, 2002.
- Crestaux, T., Le MaiTre, O., Martinez, J., 2009. Polynomial chaos expansion for sensitivity analysis. *Reliability Engineering & System Safety* 94 (7), 1161–1172.
- Dutton, S., Flanders, W., Barton, M., 2003. Reservoir characterization of a Permian deep-water sandstone, East Ford field, Delaware basin, Texas. *AAPG Bulletin* 87 (4), 609–628.
- Eaton, T., 2006. On the importance of geological heterogeneity for flow simulation. *Sedimentary Geology* 184 (3–4), 187–201.
- Eigestad, G., Dahlke, H., Hellervang, B., Riis, F., Johansen, W., Øian, E., 2009. Geological modeling and simulation of CO<sub>2</sub> injection in the Johansen formation. *Computational Geosciences* 13 (4), 435–450.
- Förster, A., Norden, B., Zinck-Jørgensen, K., Frykman, P., Kulenkampff, J., Spangenberg, E., Erzinger, J., Zimmer, M., Kopp, J., Born, G., et al., 2006. Baseline characterization of the CO<sub>2</sub>SINK geological storage site at Ketzin, Germany. *Environmental Geosciences* 13 (3), 145–161.
- Fajraoui, N., Ramaswamana, F., Younes, A., Mara, T.A., Ackerer, P., Guadagnini, A., 2011. Use of global sensitivity analysis and polynomial chaos expansion for interpretation of non-reactive transport experiments in laboratory-scale porous media. *Water Resources Research*, <http://dx.doi.org/10.1029/2010WR009639>.
- Foo, J., Karniadakis, G., 2010. Multi-element probabilistic collocation method in high dimensions. *Journal of Computational Physics* 229 (5), 1536–1557.
- Gerstner, T., Griebel, M., 2003. Dimension-adaptive tensor-product quadrature. *Computing* 71 (1), 65–87.
- Ghanem, R., Doostan, A., 2006. On the construction and analysis of stochastic models: characterization and propagation of the errors associated with limited data. *Journal of Computational Physics* 217 (1), 63–81.
- Ghanem, R., Spanos, P.D., 1990. Polynomial chaos in stochastic finite elements. *Journal of Applied Mechanics* 57, 197–202.
- Ghanem, R.G., Spanos, P.D., 1991. *Stochastic Finite Elements: A Spectral Approach*. Springer-Verlag, New York.
- Ghanem, R., Spanos, P., 1993. A stochastic Galerkin expansion for nonlinear random vibration analysis. *Probabilistic Engineering Mechanics* 8, 255–264.
- Hansson, A., Bryngelsson, M., 2009. Expert opinions on carbon dioxide capture and storage—a framing of uncertainties and possibilities. *Energy Policy* 37 (6), 2273–2282.
- Howell, J., Skorstad, A., MacDonald, A., Fordham, A., Flint, S., Fjellvoll, B., Manzocchi, T., 2008. Sedimentological parameterization of shallow-marine reservoirs. *Petroleum Geoscience* 14 (1), 17–34.
- Isukapalli, S.S., Roy, A., Georgopoulos, G.P., 1998. Stochastic response surface methods (srsm) for uncertainty propagation: application to environmental and biological systems. *Risk Analysis* 18 (3), 351–363.
- Jang, S.Y., Sitar, N., Kiureghian, D.A., 1994. Reliability analysis of contaminant transport in saturated porous media. *Water Resources Research* 30 (8), 2435–2448.
- Keese, A., Matthies, H.G., 2003. Sparse quadrature as an alternative to MC for stochastic finite element techniques. *Proceedings in Applied Mathematics and Mechanics* 3, 493–494.
- Kovsek, A., Wang, Y., 2005. Geologic storage of carbon dioxide and enhanced oil recovery. I. uncertainty quantification employing a streamline based proxy for reservoir flow simulation. *Energy Conversion and Management* 46 (11), 1920–1940.
- Le MaiTre, O., Knio, O., 2010. *Spectral Methods for Uncertainty Quantification: With Applications to Computational Fluid Dynamics*. Springer, New York.
- Lenzen, M., 2011. Global warming effect of leakage from CO<sub>2</sub> storage. *Critical Reviews in Environmental Science and Technology* 41 (24), 2169–2185.
- Li, H., Zhang, D., 2007. Probabilistic collocation method for flow in porous media: comparisons with other stochastic methods. *Water Resources Research* 43, 44–48.
- Manzocchi, T., Walsh, J., Nell, P., Yielding, G., 1999. Fault transmissibility multipliers for flow simulation models. *Petroleum Geoscience* 5 (1), 53–63.
- Manzocchi, T., Matthews, J., Strand, J., Carter, J., Skorstad, A., Howell, J., Stephen, K., Walsh, J., 2008. A study of the structural controls on oil recovery from shallow-marine reservoirs. *Petroleum Geoscience* 14 (1), 55–70.
- Manzocchi, T., Carter, J., Skorstad, A., Fjellvoll, B., Stephen, K., Howell, J., Matthews, J., Walsh, J., Nepveu, M., Bos, C., et al., 2008. Sensitivity of the impact of geological uncertainty on production from faulted and unfaulted shallow-marine oil reservoirs: objectives and methods. *Petroleum Geoscience* 14 (1), 3–11.
- Matthews, J., Carter, J., Stephen, K., Zimmerman, R., Skorstad, A., Manzocchi, T., Howell, J., 2008. Assessing the effect of geological uncertainty on recovery estimates in shallow-marine reservoirs: the application of reservoir engineering to the SAIGUP project. *Petroleum Geoscience* 14 (1), 35–44.
- Matthies, G., Keese, H.A., 2005. Galerkin methods for linear and nonlinear elliptic stochastic partial differential equations. *Computer Methods in Applied Mechanics and Engineering* 194, 1295–1331.
- Michael, K., Golab, A., Shulakova, V., Ennis-King, J., Allinson, G., Sharma, S., Aiken, T., 2010. Geological storage of CO<sub>2</sub> in saline aquifers - a review of the experience from existing storage operations. *International Journal of Greenhouse Gas Control* 4 (4), 659–667.
- Nobile, F., Tempone, R., Webster, C., 2008. A sparse grid stochastic collocation method for partial differential equations with random input data. *SIAM Journal on Numerical Analysis* 46 (5), 2309–2345.

- Nordbotten, J., Celia, M., Bachu, S., Dahle, H., 2005. Semianalytical solution for CO<sub>2</sub> leakage through an abandoned well. *Environmental Science & Technology* 39 (2), 602–611.
- Nowak, W., 2009. Best unbiased ensemble linearization and the quasi-linear Kalman ensemble generator. *Water Resources Research* 45, W04431, <http://dx.doi.org/10.1029/2008WR007328>.
- Oladyshevkin, S., Nowak, W., 2012. Data-driven uncertainty quantification using the arbitrary polynomial chaos expansion. *Reliability Engineering & System Safety* 106, 179–190.
- Oladyshevkin, S., Class, H., Helmig, R., Nowak, W., 2011. A concept for data-driven uncertainty quantification and its application to carbon dioxide storage in geological formations. *Advances in Water Resources* 34, 1508–1518, doi:10.1016/j.advwatres.2011.08.005.
- Oladyshevkin, S., Class, H., Helmig, R., Nowak, W., 2011. An integrative approach to robust design and probabilistic risk assessment for CO<sub>2</sub> storage in geological formations. *Computational Geosciences* 15 (3), 565–577, <http://dx.doi.org/10.1007/s10596-011-9224-8>.
- Oladyshevkin, S., de Barros, F.P.J., Nowak, W., 2012. Global sensitivity analysis: a flexible and efficient framework with an example from stochastic hydrogeology. *Advances in Water Resources* 37, 10–22.
- Reuter, U., Liebscher, M., 2008. Global sensitivity analysis in view of nonlinear structural behavior. In: Proceedings of the 7th LS-Dyna Forum, Bamberg.
- Riddiford, F., Wright, I., Bishop, C., Espie, T., Tourquai, A., 2004. Monitoring geological storage in the Salah gas CO<sub>2</sub> storage project. In: Proceedings of the 7th International Greenhouse Gas Technologies Conference, Vancouver, BC.
- Rohmer, J., Seyed, D., 2010. Coupled large scale hydromechanical modelling for caprock failure risk assessment of CO<sub>2</sub> storage in deep saline aquifers. *Oil & Gas Science and Technology-Revue de l'Institut Français du Pétrole* 65 (3), 503–517.
- Saltelli, A., 2008. *Global Sensitivity Analysis: The Primer*. Wiley, UK, Chichester.
- Saltelli, A., 2010. Global sensitivity analysis: an introduction. In: Proc. 4th International Conference on Sensitivity Analysis of Model Output, pp. 27–43.
- Sobol, I., 2001. Global sensitivity indices for nonlinear mathematical models and their Monte Carlo estimates. *Mathematics and Computers in Simulation* 55 (1–3), 271–280.
- Soize, C., Ghanem, R., 2004. Physical systems with random uncertainties: chaos representations with arbitrary probability measure. *SIAM Journal on Scientific Computing* 26 (2), 395–410.
- Sudret, B., 2008. Global sensitivity analysis using polynomial chaos expansions. *Reliability Engineering & System Safety* 93 (7), 964–979.
- Thomas, D., 2005. *Carbon Dioxide Capture for Storage in Deep Geologic Formations – Results from the CO<sub>2</sub> Capture Project*, vol. 1. Elsevier Science Ltd.
- Viebahn, P., Nitsch, J., Fischedick, M., Esken, A., Schüwer, D., Supersberger, N., Zuberbühler, U., Edenhofer, O., 2007. Comparison of carbon capture and storage with renewable energy technologies regarding structural, economic, and ecological aspects in Germany. *International Journal of Greenhouse Gas Control* 1 (1), 121–133.
- Villadsen, J., Michelsen, M.L., 1978. *Solution of Differential Equation Models by Polynomial Approximation*. Prentice-Hall, US, Mountain.
- Walton, F., Tait, J., LeNeveu, D., Sheppard, M., 2004. Geological storage of CO<sub>2</sub>: a statistical approach to assessing performance and risk. In: Proceedings of the 7th International Conference on Greenhouse Gas Control Technologies (GHGT-7).
- Wan, X., Karniadakis, G., 2007. Multi-element generalized polynomial chaos for arbitrary probability measures. *SIAM Journal on Scientific Computing* 28 (3), 901–928.
- Wiener, N., 1938. The homogeneous chaos. *American Journal of Mathematics* 60, 897–936.
- Wilson, E., Johnson, T., Keith, D., 2003. Regulating the ultimate sink: Managing the risks of geologic CO<sub>2</sub> storage. *Environmental Science and Technology* 37 (16), 3476–3483.
- Witteveen, J., Bijl, H., 2006. Modeling arbitrary uncertainties using Gram-Schmidt polynomial chaos. In: Proceedings of the 44th AIAA Aerospace Sciences Meeting and Exhibit, number AIAA-2006-0896, vol. 117, Reno, NV.
- Witteveen, J., Sarkar, S., Bijl, H., 2007. Modeling physical uncertainties in dynamic stall induced fluid-structure interaction of turbine blades using arbitrary polynomial chaos. *Computers & Structures* 85 (11), 866–878.
- Xiu, D., Hesthaven, J., 2005. High-order collocation methods for differential equations with random inputs. *SIAM Journal on Scientific Computing* 27 (3), 1118–1139.
- Xiu, D., Karniadakis, G., 2002. The Wiener–Askey polynomial chaos for stochastic differential equations. *SIAM Journal on Scientific Computing* 24 (2), 619–644.
- Xiu, D., Karniadakis, G.E., 2003. Modeling uncertainty in flow simulations via generalized polynomial chaos. *Journal of Computational Physics* 187, 137–167.
- Zhang, D., Lu, Z., 2004. An efficient, high-order perturbation approach for flow in random media via Karhunen–Loeve and polynomial expansions. *Journal of Computational Physics* 194, 773–794.
- P. Zweigel, L. Heill, Studies on the likelihood for caprock fracturing in the sleipner CO<sub>2</sub> injection case, Tech. rep., Sintef Petroleum Research Report, 2003.

## **Appendix A**

**Additional supporting material**

The papers in the appendix were prepared during the PhD studies, but do not form part of the main thesis.

# **Paper i**

## **A.1 Impact of geological heterogeneity on early-stage CO<sub>2</sub> plume migration**

Ashraf, M., Lie, K.A., Nilsen, H.M., Nordbotten, J. M., and Skorstad, A.

presented and published in the proceedings of the Computational Methods in Water Resources (CMWR) conference in Barcelona, 2010.



## IMPACT OF GEOLOGICAL HETEROGENEITY ON EARLY-STAGE CO<sub>2</sub> PLUME MIGRATION

Meisam Ashraf<sup>\*,§,1</sup>, Knut-Andreas Lie<sup>\*,§,2</sup>, Halvor M. Nilsen<sup>§,3</sup>, Jan M. Nordbotten<sup>\*,4</sup>, Arne Skorstad<sup>†,5</sup>

\*Department of Mathematics, University of Bergen, NO-5008 Bergen, Norway

§SINTEF ICT, Department of Applied Mathematics, NO-0314 Oslo, Norway

†Norwegian Computing Center, NO-0314 Oslo, Norway

<sup>1</sup>Meisam.Ashraf@uni.no, <sup>2</sup>Knut-Andreas.Lie@sintef.no, <sup>3</sup>HalvorMoll.Nilsen@sintef.no  
<sup>4</sup>Jan.Nordbotten@math.uib.no, <sup>5</sup>Arne.Skorstad@nr.no

**Key words:** CO<sub>2</sub> storage, heterogeneity, sensitivity, shallow marine

**Summary.** In an effort to determine the influence of geological heterogeneity on CO<sub>2</sub> storage efficiency, we study injection and early-stage migration of CO<sub>2</sub> in 54 different realizations of a shallow-marine reservoir.

### 1 INTRODUCTION

Academic studies of CO<sub>2</sub> injection frequently employ simplified or conceptualized reservoir descriptions in which the medium is considered nearly homogeneous. However, geological knowledge and experience from petroleum production show that the petrophysical characteristics of potential CO<sub>2</sub> sequestration sites can be expected to be heterogeneous on the relevant physical scales, regardless of whether the target formation is an abandoned petroleum reservoir or a pristine aquifer. Geological uncertainty introduces tortuous subsurface flow paths, which in turn influence reservoir behavior during injection. It is paramount that the effect of the geological heterogeneity is quantified by the research community. This will facilitate both improved understanding of subsurface flow at operational CO<sub>2</sub> injection sites, and allow comparison with simulated flow in ideal homogeneous models and upscaled versions of these.

Within oil recovery, the impact of geological uncertainty on production forecast has been thoroughly investigated in the SAIGUP project [2, 3, 4] focusing on shallow-marine reservoirs. To study different factors, synthetic realistic models were made and several thousand cases were run for different production scenarios. The results showed that realistic heterogeneity in the structural and sedimentological description had a strong influence on the production responses.

Meisam Ashraf, Knut-Andreas Lie, Halvor M. Nilsen, Jan M. Nordbotten and Arne Skorstad

---

The main objectives of CO<sub>2</sub> storage studies are to maximize the injection volume/rate and to minimize the risk of leakage [1]. The problem of CO<sub>2</sub> storage differs from oil recovery prediction not only in the objectives of study, but also in the time scales considered for the process (thousands of years compared to tens of years for CO<sub>2</sub> migration). In addition, the characteristic length scale of the flow is much larger. Working with long temporal and spatial scales and huge amounts of uncertainties poses the question of how detailed the geological description should be. The motivation of this work is mainly to answer two questions related to CO<sub>2</sub> storage:

- How sensitive is the injection and early-stage migration to uncertainty and variability in the geological description?
- What simplifying assumptions are allowed in averaging the geological attributes over scales?

To this end, we use a subset of the synthetic models from the SAIGUP study to perform a preliminary sensitivity analysis for CO<sub>2</sub> sequestration in aquifers. Heterogeneity classes are defined based on different sequence-stratigraphy parameters and levels of shale barriers. We assume two-phase flow with slight compressibility for supercritical CO<sub>2</sub>. The injection scenarios are defined based on the objectives outlined above, and important responses are discussed to evaluate the efficiency and risk of the process.

## 2 Geological descriptions

In this work we question the widespread use of simplified geological descriptions that ignore the detailed heterogeneity in modeling. Our hypothesis is that heterogeneity features like channels, barriers, sequence stratigraphy of facies, and fault intensity/geometry all have a particular effect on flow behavior, both locally and globally, and may significantly alter the injection and migration of CO<sub>2</sub> plumes.

Sound geological classifications and descriptions of key geological features are important to give a realistic description of the sensitivity of CO<sub>2</sub> storage performance. To this end, we have selected four parameter spaces of geological variations from the SAIGUP study [2, 3, 4]. The parameters span realistic intervals for progradational shallow-marine depositional systems with limited tidal influence. In the following, we give a brief description of each.

**Lobosity:** Lobosity is defined by the plan-view shape of the shore-line. As a varying parameter, lobosity indicates the level at which the shallow-marine system is dominated by each of the main depositional processes. Two depositional processes are considered in the SAIGUP study: fluvial and wave processes. The higher amount of sediment supply from rivers relative to the available accommodation space in the shallow sea, the more fluvial dominant the process will be. As the river enters the mouth of the sea, it can divide into different lobes and branches. Wave processes from the sea-side smear this effect and flatten the shoreline shape. Less wave effect produces more pronounced lobe shapes around the river mouths. Very high permeability and porosity can be found in

Meisam Ashraf, Knut-Andreas Lie, Halvor M. Nilsen, Jan M. Nordbotten and Arne Skorstad

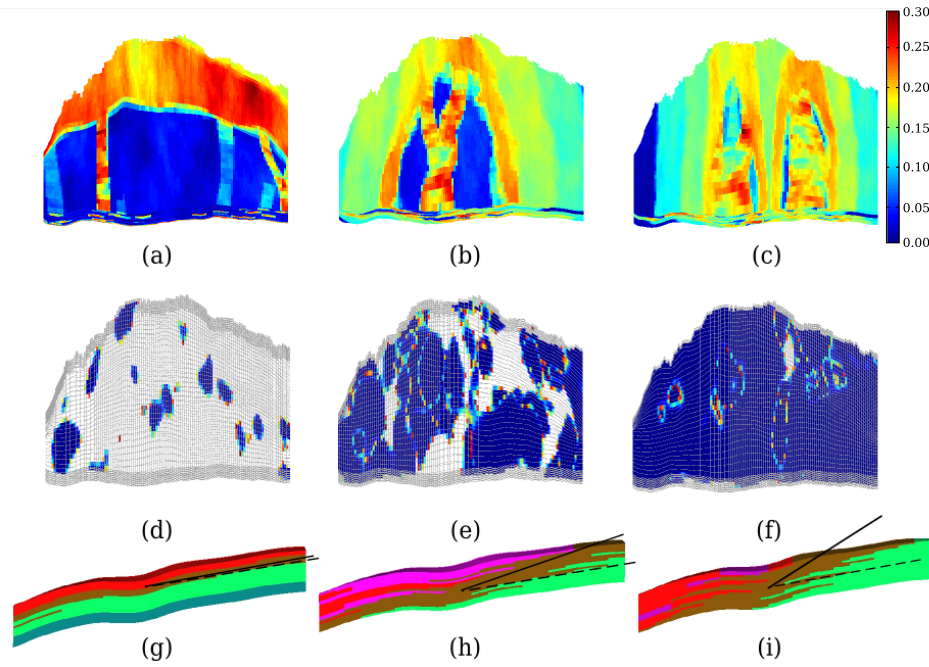


Figure 1: Different geological features considered in this study. Top row shows 'lobosity' in porosity distribution: (a) flat shore-line, (b) one lobe, (c) two lobes. The middle row shows 'barrier' by the distribution of zero transmissibility multipliers: (d) low, (e) medium, (f) high. The lower row shows 'aggradation' in rock-type distribution: (g) low angle of interface between the transitional rock-types leads to parallel layers; this angle is increasing in cases (h) and (i), which correspond to higher levels of aggradation. An up-dip progradation direction is shown in (b), and if the lobe flips over the long axis, we will have down-dip progradation.

the channeling branches, while dense rock with low permeability fills the space between them. Reservoir quality decreases with distance from the shoreface. We expect that the level of lobosity can have a considerable effect on the CO<sub>2</sub> injection and plume size in the aquifer. In this study, models of three levels of lobosity are used: flat shoreline, one lobe and two lobes, see Fig. 1.

**Barriers:** Periodic floods result in a sheet of sandstone that dips, thins, and fines in a seaward direction. In the lower front, thin sheets of sandstone are interbedded with the mudstones deposited from suspension. These mud-draped surfaces are potential significant barriers to both horizontal and vertical flow. In the SAIGUP domain used here, these barriers were modeled by transmissibility multipliers in three levels of zero value percentage: low (10%), medium (50%), and high (90%). We use the same variations in this study, see Fig. 1.

**Aggradation:** In shallow-marine systems, two main factors control the shape of the transition zone between the river and the basin: amount of deposition supplied by the river and the accommodation space that the sea provides for these depositional masses. One can imagine a constant situation in which the river is entering the sea and the flow

---

Meisam Ashraf, Knut-Andreas Lie, Halvor M. Nilsen, Jan M. Nordbotten and Arne Skorstad

---

slows down until stagnation. The deposition happens in a spectrum from larger grains depositing earlier in the land side to fine deposits in the deep basin. If the river flux or sea level fluctuates, the equilibrium changes into a new bedding shape based on the balance of these factors.

In the SAIGUP study, the progradational cases are considered in which, for example, the river flux increases and shifts the whole depositional system into the sea. The angle at which the transitional deposits are stacked on each-other because of this shifting, is called aggradation angle. Three levels of aggradation are modeled here: low, medium and high (Fig. 1). As we will observe later, aggradation can have a dramatic influence on the injection and migration process.

**Progradation:** The final factor varied is the progradation or the depositional-dip direction. Two types are considered here: up and down the dominant structural dip. Since the model is tilted a little, this corresponds to the lobe direction from flank to the crest or vice-versa (Fig. 1). This has a potential influence on the CO<sub>2</sub> flow from the injection point up to the crest.

### 3 Simulation workflow

A fully automated workflow was designed for this study, starting from variational parameters in the SAIGUP models and ending into comprehensive result outputs based on the objective of the work. As a first step, 54 representative cases are studied using a commercial simulator (Eclipse). However, the parallel aim of future work is to develop fast simulation methods that are suitable for performing thousands of runs, using e.g., a vertically-averaged formulation [5].

### 4 Scenario design

After studying several scenarios for a typical CO<sub>2</sub> injection, we ended up using an injector down in the flank and hydrostatic boundary conditions on the sides, except the faulted side on the crest (Fig. 2). No-flow boundary conditions are imposed on the top and bottom surfaces of the model. The well is completed only in the last three layers.

Simple linear saturation functions with zero capillarity are used. This can be justified because the permeability contrast in channels has the dominating effect on the flow. Also, simple PVT data for a slightly compressible supercritical CO<sub>2</sub> is used. To model the hydrostatic boundaries in Eclipse, high multipliers are used to magnify the pore volume of the outer cells in the model. About 40MM m<sup>3</sup> of supercritical CO<sub>2</sub> is injected for thirty years, which amounts to 20% of the models' pore volumes. After the injection period, seventy years of early plume migration is simulated.

### 5 Results

As our objective function, we seek to maximize the CO<sub>2</sub> storage volume and minimize the risk of leakage. These quantities are measured indirectly by various simulation outputs

Meisam Ashraf, Knut-Andreas Lie, Halvor M. Nilsen, Jan M. Nordbotten and Arne Skorstad

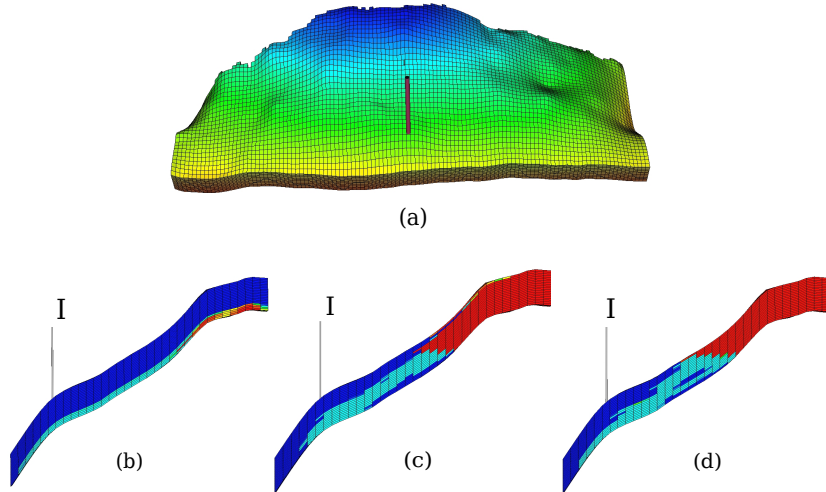


Figure 2: (a) Model geometry and well position. Model dimensions are 3km×9km×80m with 20 layers. The bottom row shows the side view of CO<sub>2</sub> distribution (in red) at the end of simulation in different aggradation cases, from low (b) to high (d). The vertical direction is exaggerated.

that are discussed below.

In all outputs, we recognize the effect of aggradation. Cases with low aggradation have continuous facies layering parallel to the horizontal direction of the grid. Because the three lowest layers, in which the well is completed, are sealing in the cross-layering direction, the flow is forced to stay in the same layers rather than accumulating in the crest (Fig. 2).

**Reservoir pressure:** The pressure response in general shows a sharp jump at the start of injection and a declining trend during the injection and plume migration. Pressure behavior of different cases at the end of the injection period is shown in Fig. 3. Low aggradation cases show higher pressure.

**Boundary fluxes:** The flux out of the open boundaries is a measure of the sweep efficiency of the CO<sub>2</sub> plume. As channeling can lead to early CO<sub>2</sub> breakthrough at boundaries, we prefer cases with less fluxes out of the boundaries. The down boundary that is closer to the injector is a potential loss for the injected volume (Fig. 4). Again, the flow is led readily to the boundaries in cases with low aggradations .

**Total mobile/residual CO<sub>2</sub>:** If the CO<sub>2</sub> saturation is below the critical value, it will be immobile in the bulk flow, although not in the molecular sense. Less mobile CO<sub>2</sub> means less risk of leakage and more residual volumes (with saturations less than the critical) resulting from a more efficient volume sweep as preferable (Fig. 4). We use critical saturation of 0.2 for both water and CO<sub>2</sub>.

**Connected CO<sub>2</sub> volumes:** To estimate the risk of leakage from the caprock, we

Meisam Ashraf, Knut-Andreas Lie, Halvor M. Nilsen, Jan M. Nordbotten and Arne Skorstad

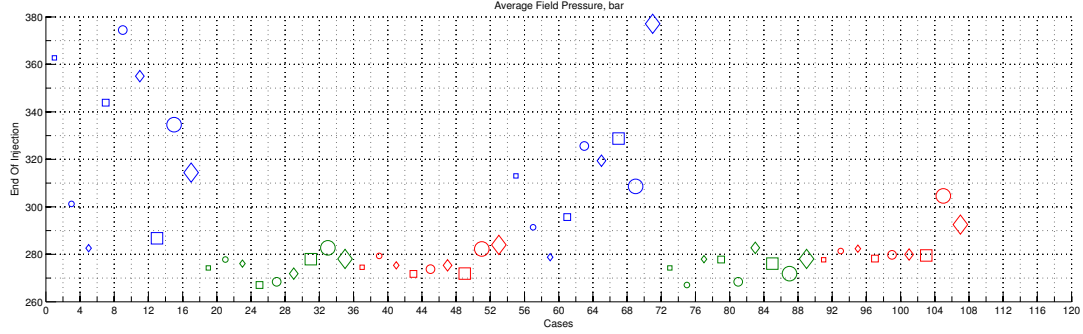


Figure 3: Average reservoir pressure plot for all cases. Colors represent 'aggradation' level: blue for low, green for medium, and red for high levels. Size represents 'barrier': small for low, medium for medium, and large for high level of barrier. Marker shape represents 'lobosity': square for flat shore-line, circle for one lobe, and diamond for two lobes. The first half of the case numbers refer to 'progradation' up-dip towards the crest, and the second half represent 'progradation' down-dip.

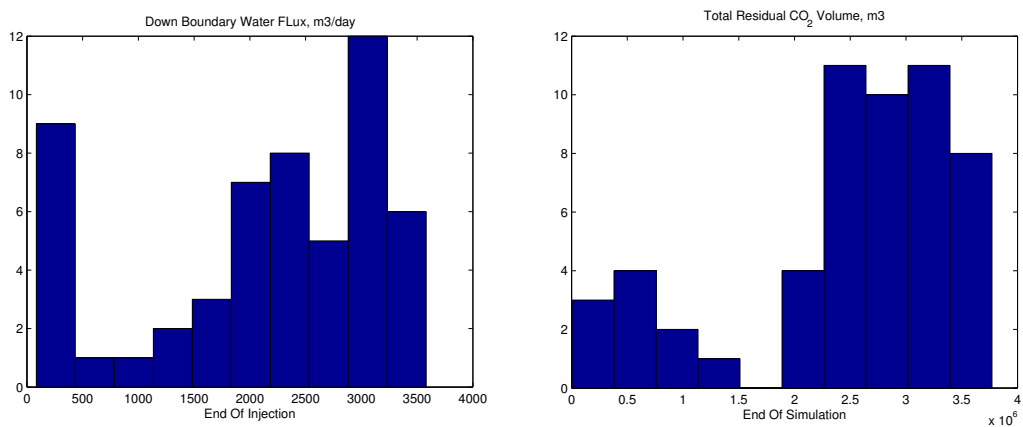


Figure 4: (a) Flux histogram for down boundary: cases with low aggradation show high values. (b) Total residual CO<sub>2</sub> volume; cases with low aggradation show less values in a separate family.

Meisam Ashraf, Knut-Andreas Lie, Halvor M. Nilsen, Jan M. Nordbotten and Arne Skorstad

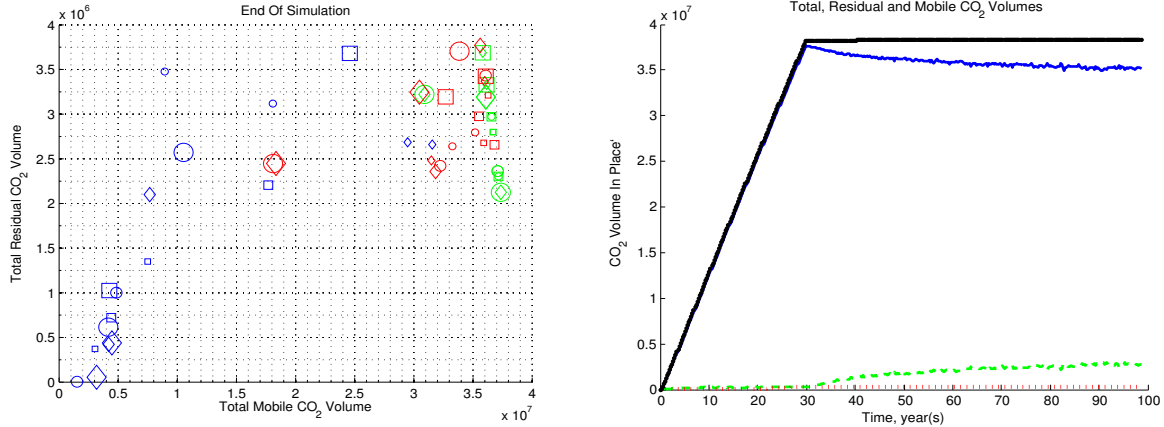


Figure 5: CO<sub>2</sub> volumes. Left: residual versus mobile volume at the end of simulation. Most of the green colored cases follow a linear trend, which is expected because the injected CO<sub>2</sub> must be conserved if no CO<sub>2</sub> leaves the system. For the rest of the cases, some CO<sub>2</sub> goes out of boundaries. Right: Total CO<sub>2</sub> volumes with time plotted for one case. Green curve is the residual volumes, dotted red denotes volumes that have left the domain, solid blue is mobile volumes, and the solid black shows the summation, which is the total volume and stays constant after injection because no more CO<sub>2</sub> is added to the system.

assume that all mobile CO<sub>2</sub> connected to a leakage point will escape out of the reservoir. Hence, it is preferable if the total mobile CO<sub>2</sub> volume is split into smaller plumes rather than forming a big mobile plume. Though the area exposed to potential leakage points will increase by splitting the plume, yet the volume reduction is overtaking the area effect.

On the other hand, the split CO<sub>2</sub> plumes can sweep more cross-areas than a big single plume. The no-flow faulted side can be considered to be connected to an imaginary large volume available for long-term plume migration. Thus, it makes sense to talk about plume sweeping cross area. Larger areas leave more residual CO<sub>2</sub> in the tail of the plume. Hence, we looked at the largest plume size, the number of plumes, and other statistical parameters. The number of plumes at the end of simulation for all cases are given in Fig. 6. Two-lobed cases include more branching channels which result in more plume numbers. Also barrier effect increases the lateral distribution of the plume.

## 6 Conclusions

Herein, we have reported on a preliminary study of the influence of various geological parameters on the injection and early-stage migration of CO<sub>2</sub> in progradational shallow-marine systems. Large variations in the flow responses show the importance of considering uncertainty in the geological parameters. In particular, our results highlight how variation in aggradation and barriers significantly change the flow direction within the medium. Therefor we believe that effort should be put into detailed geological modeling of potential injection sites. This way, one can better balance the influence of simplifications made in the models of geology and flow physics.

Meisam Ashraf, Knut-Andreas Lie, Halvor M. Nilsen, Jan M. Nordbotten and Arne Skorstad

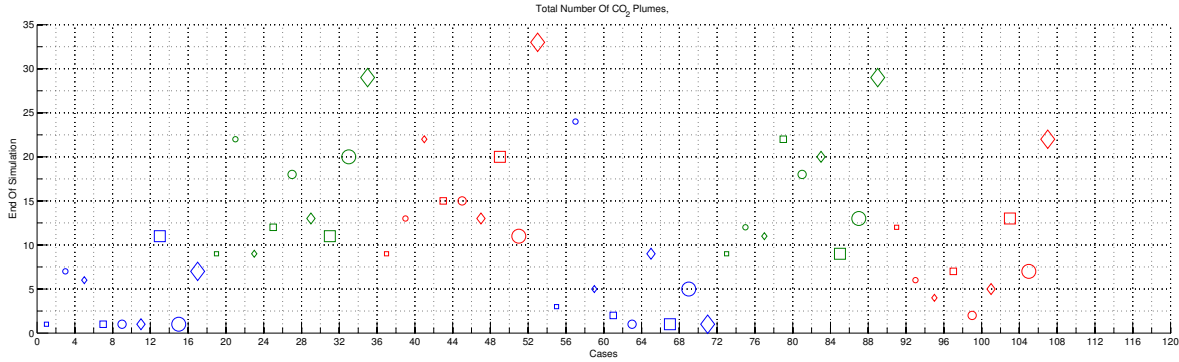


Figure 6: CO<sub>2</sub> plume number at end of simulation, see explanation in Fig. 3.

Finally, we stress that these are very preliminary conclusions drawn from a limited number of simulations performed on a suite of synthetic models that were made to study petroleum production. A more thorough investigation should generate new synthetic geological realizations that are more representative of typical injection sites.

## REFERENCES

- [1] J. M. Nordbotten: *Sequestration of Carbon in Saline Aquifers: Mathematical and Numerical Analysis*, Doctor Scientiarum Thesis, Department of Mathematics, University of Bergen, (2004).
- [2] J. A. Howel, A. Skorstad, A. MacDonald, A. Fordham, S. Flint, B. Fjellvoll, and T. Manzocchi: *Sedimentological parameterization of shallow-marine reservoirs*, Petroleum Geoscience, Vol. 14, No. 1, pp. 17-34, (2008).
- [3] T. Manzocchi, J. N. Carter, A. Skorstad, B. Fjellvoll, K. D. Stephen, J. A. Howell, J. D. Matthews, J. J. Walsh, M. Nepveu, C. Bos, J. Cole, P. Egberts, S. Flint, C. Hern, L. Holden, H. Hovland, H. Jackson, O. Kolbjørnsen, A. MacDonald, P. A. R. Nell, K. Onyeagoro, J. Strand, A. R. Syversveen, A. Tchistiakov, C. Yang, G. Yielding, and R. W. Zimmerman: *Sensitivity of the impact of geological uncertainty on production from faulted and unfaulted shallow-marine oil reservoirs: objectives and methods*, Petroleum Geoscience, Vol. 14, No. 1, pp. 3-15, (2008).
- [4] J. D. Matthews, J. N. Carter, K. D. Stephen, R. W. Zimmerman, A. Skorstad, T. Manzocchi, and J. A. Howell: *Assessing the effect of geological uncertainty on recovery estimates in shallow-marine reservoirs: the application of reservoir engineering to the SAIGUP project*, Petroleum Geoscience, Vol. 14, No. 1, pp. 33-44, (2008).
- [5] S. E. Gasda, J. M. Nordbotten, and M. A. Celia: *Vertical equilibrium with sub-scale analytical methods for geological CO<sub>2</sub> sequestration*, Computational Geosciences, Volume 13, Number 4, pp. 469-481, (2009).

# **Paper ii**

## **A.2 Impact of geological heterogeneity on early-stage CO<sub>2</sub> plume migration: sensitivity study**

Ashraf, M., Lie, K.A., Nilsen, H.M., and Skorstad, A.

Presented and published in the proceedings of the ECMOR XII in Oxford, 2010.



## IMPACT OF GEOLOGICAL HETEROGENEITY ON EARLY-STAGE CO<sub>2</sub> PLUME MIGRATION: SENSITIVITY STUDY

M. Ashraf<sup>a</sup>, K.A. Lie<sup>a</sup>, H.M. Nilsen<sup>a</sup> & A. Skorstad<sup>bc</sup>

<sup>a</sup> SINTEF ICT, Department of Applied Mathematics, NO-0314 Oslo, Norway

<sup>b</sup> Norwegian Computing Center, NO-0314 Oslo, Norway.

<sup>c</sup> Present address Roxar Software Solutions, Lysaker Torg 45, NO-1366 Lysaker, Norway

July 30, 2010

## Introduction

Academic studies of CO<sub>2</sub> injection frequently employ simplified or conceptualized reservoir descriptions in which the medium is considered nearly homogeneous. However, geological knowledge and experience from petroleum production show that the petrophysical characteristics of potential CO<sub>2</sub> sequestration sites can be expected to be heterogeneous on the relevant physical scales, regardless of whether the target formation is an abandoned petroleum reservoir or a pristine aquifer. Geological uncertainty introduces tortuous subsurface flow paths, which in turn influence reservoir behaviour during injection. It is paramount that the effect of the geological heterogeneity is quantified by the research community. This will facilitate both improved understanding of subsurface flow at operational CO<sub>2</sub> injection sites, and allow comparison with simulated flow in ideal homogeneous models and upscaled versions of these.

Within oil recovery, the impact of geological uncertainty on production forecast has been thoroughly investigated in the SAIGUP project [3, 4, 5] focusing on shallow-marine reservoirs. To study different factors, synthetic realistic models were made and several thousand cases were run for different production scenarios. The results showed that realistic heterogeneity in the structural and sedimentological description had a strong influence on the production responses.

The main objectives of CO<sub>2</sub> storage studies are to maximize the injection volume/rate and to minimize the risk of leakage [1, 2]. The problem of CO<sub>2</sub> storage differs from oil recovery prediction not only in the objectives of study, but also in the time scales considered for the process (thousands of years compared to tens of years for CO<sub>2</sub> migration). In addition, the characteristic length scale of the flow is much larger. Working with long temporal and spatial scales and huge amounts of uncertainties poses the question of how detailed the geological description should be. The motivation of this work is mainly to address two questions related to CO<sub>2</sub> storage:

- How sensitive is the injection and early-stage migration to uncertainty and variability in the geological description?
- What simplifying assumptions are allowed in averaging the geological attributes over scales?

To this end, we use a subset of the synthetic models from the SAIGUP study to perform a preliminary sensitivity analysis for CO<sub>2</sub> sequestration in aquifers. Heterogeneity classes are defined based on different sequence-stratigraphy parameters and levels of shale barriers. We assume two-phase flow with slight compressibility for supercritical CO<sub>2</sub>. The injection scenarios are defined based on the objectives outlined above, and important responses are discussed to evaluate the efficiency and risk of the process.

## Geological descriptions

In this work we question the widespread use of simplified geological descriptions that ignore the detailed heterogeneity in modelling. Our hypothesis is that heterogeneity features like channels, barriers, sequence stratigraphy of facies, and fault intensity/geometry all have a particular effect on flow behaviour, both locally and globally, and may significantly alter the injection and migration of CO<sub>2</sub> plumes.

Sound geological classifications and descriptions of key geological features are important to give a realistic description of the sensitivity of CO<sub>2</sub> storage performance. To this end, we have selected four parameter spaces of geological variations from the SAIGUP study [3, 4, 5]. The parameters span realistic intervals for progradational shallow-marine depositional systems with limited tidal influence. In the following, we give a brief description of each.

**Lobosity:** Lobosity is defined by the plan-view shape of the shore-line. As a varying parameter, lobosity indicates the level at which the shallow-marine system is dominated by each of the main depositional

processes. Two depositional processes are considered in the SAIGUP study: fluvial and wave processes. The higher amount of sediment supply from rivers relative to the available accommodation space in the shallow sea, the more fluvial dominant the process will be. As the river enters the mouth of the sea, it can divide into different lobes and branches. Wave processes from the sea-side smear this effect and flatten the shoreline shape. Less wave effect produces more pronounced lobe shapes around the river mouths. Very high permeability and porosity can be found in the channelling branches, while dense rock with low permeability fills the space between them. Reservoir quality decreases with distance from the shore-face. We expect that the level of lobosity can have a considerable effect on the CO<sub>2</sub> injection and plume size in the aquifer. In this study, models of three levels of lobosity are used: flat shoreline, one lobe and two lobes, see Fig. 1.

**Barriers:** Periodic floods result in a sheet of sandstone that dips, thins, and fines in a seaward direction. In the lower front, thin sheets of sandstone are interbedded with the mudstones deposited from suspension. These mud-draped surfaces are potential significant barriers to both horizontal and vertical flow. In the SAIGUP domain used here, these barriers were modelled by transmissibility multipliers in three levels of coverage of barrier sheet: low (10%), medium (50%), and high (90%). We use the same variations in this study, see Fig. 1.

**Aggradation:** In shallow-marine systems, two main factors control the shape of the transition zone between the river and the basin: amount of deposition supplied by the river and the accommodation space that the sea provides for these depositional masses. One can imagine a constant situation in which the river is entering the sea and the flow slows down until stagnation. The deposition happens in a spectrum from larger grains depositing earlier in the land side to fine deposits in the deep basin. If the river flux or sea level fluctuates, the equilibrium changes into a new bedding shape based on the balance of these factors.

In the SAIGUP study those cases are considered in which, for example, the river flux increases and shifts the whole depositional system into the sea. The angle at which the transitional deposits are stacked on each-other because of this shifting, is called aggradation angle. Three levels of aggradation are modelled here: low, medium and high (Fig. 1). As we will observe later, aggradation can have a dramatic influence on the injection and migration process.

**Progradation:** The next factor varied is the progradation or the depositional-dip direction. Two types are considered here: up and down the dominant structural dip. Since the model is tilted a little, this corresponds to the lobe direction from flank to the crest or vice-versa (Fig. 1). This has a potential influence on the CO<sub>2</sub> flow from the injection point up to the crest.

**Fault:** There are three variational dimensions considered for faults in the SAIGUP study: fault type, intensity and transmissibility. However we did not include all of these variations in our work and confined this step to two transmissibilities of almost open and closed faults. Fig. 2 shows the effect of fault transmissibility on the flow pattern. Here we took the compartment type of faults of medium intensity ([3, 5]).

### **Simulation workflow**

A fully automated workflow was designed for this study, starting from variational parameters in the SAIGUP models and ending into comprehensive result outputs based on the objective of the work. As a first step, 54 representative cases are studied using a commercial simulator. However, the parallel aim of future work is to develop fast simulation methods that are suitable for performing thousands of runs, using e.g., a vertically-averaged formulation [6].

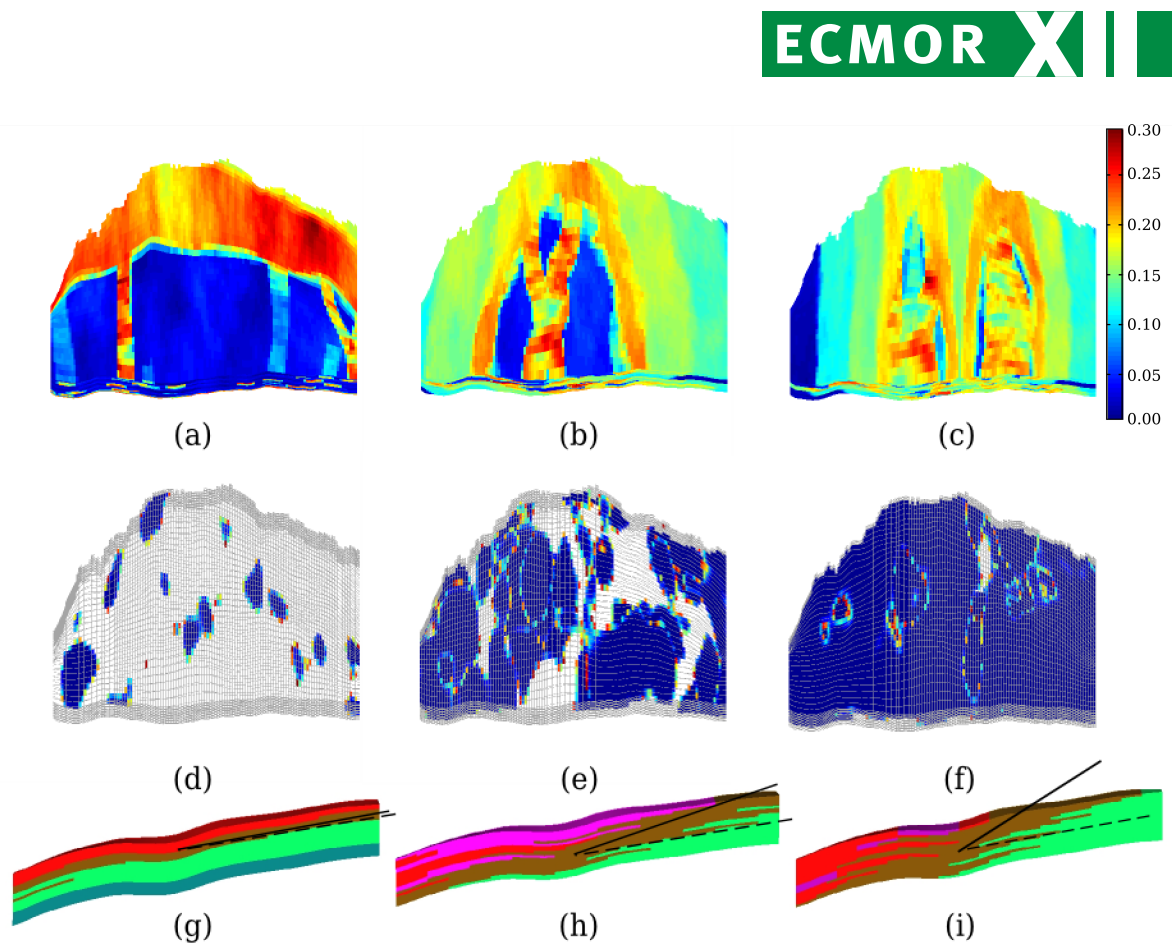


**Figure 1** Different geological features considered in this study. Top row shows 'lobosity' in porosity distribution: (a) flat shore-line, (b) one lobe, (c) two lobes. The middle row shows 'barrier' by the distribution of zero transmissibility multipliers: (d) low, (e) medium, (f) high. The lower row shows 'aggradation' in rock-type distribution: (g) low angle of interface between the transitional rock-types leads to parallel layers; this angle is increasing in cases (h) and (i), which correspond to higher levels of aggradation. An up-dip progradation direction is shown in (b), and if the lobe flips over the long axis, we will have down-dip progradation.

### Scenario design

We are using an injector down in the flank and hydrostatic boundary conditions on the sides, except the faulted side on the crest (Fig. 3). No-flow boundary conditions are imposed on the top and bottom surfaces of the model. The well is completed only in the last three layers.

Simple linear saturation functions with zero capillarity are used. This can be justified because the permeability contrast in channels has the dominating effect on the flow. Also, simple PVT data for a slightly compressible supercritical CO<sub>2</sub> is used. To model the hydrostatic boundaries in used simulator, high multipliers are used to magnify the pore volume of the outer cells in the model. About 40MM m<sup>3</sup> of supercritical CO<sub>2</sub> is injected for thirty years, which amounts to 20% of the models' pore volumes. After the injection period, seventy years of early plume migration is simulated.

### Results

As our objective function, we seek to maximize the CO<sub>2</sub> storage volume and minimize the risk of leakage. The results are discussed in three parts: first we look at model responses, then correlation between these responses. Afterwards we consider the sensitivity of each response to the studied geological feature.

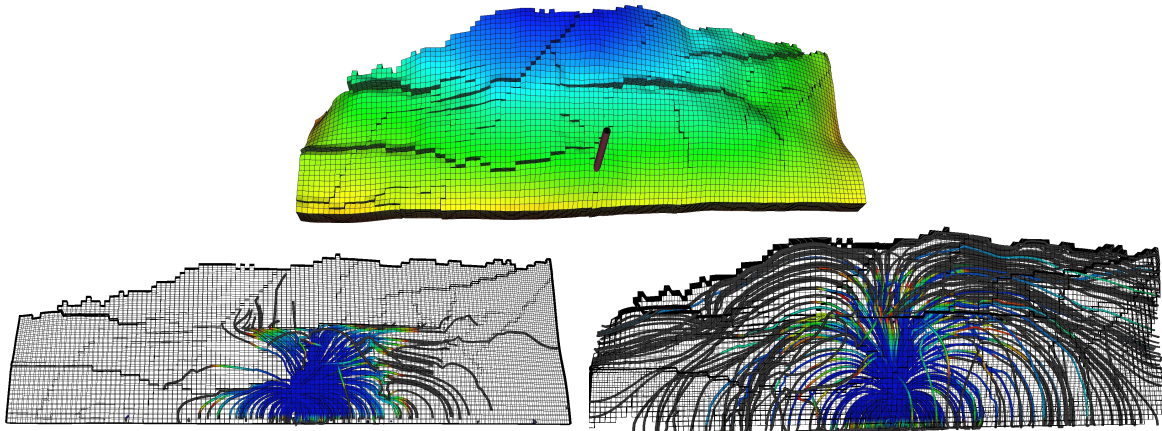


**Figure 2** The studied fault features: the picture on the top shows the orientations and intensity of the faults, down left picture shows the flow path in almost closed faults case and the one on the right is showing the flow in the almost open faulted medium. The streamlines are shown for the same time step in both pictures. Notice that the flow is confined in the closed faults model.

In all outputs, we recognize the effect of aggradation. Cases with low aggradation have continuous facies layering parallel to the horizontal direction of the grid. Because the three lowest layers, in which the well is completed, are sealing in the cross-layering direction, the flow is forced to stay in the same layers rather than accumulating in the crest (Fig. 3).

### Important responses

**Reservoir pressure:** The pressure response in general shows a sharp jump at the start of injection and a declining trend during the injection and plume migration. Pressure behaviour of different cases at the end of the injection period is shown in Fig. 4. Low aggradation cases show higher pressure.

**Boundary fluxes:** The flux out of the open boundaries is a measure of the sweep efficiency of the CO<sub>2</sub> plume. As channelling can lead to early CO<sub>2</sub> breakthrough at boundaries, we prefer cases with less fluxes out of the boundaries. The down boundary that is closer to the injector is a potential loss for the injected volume (Fig. 5(a)). Again, the flow is led to the boundaries in cases with low aggradations.

**Total mobile/residual CO<sub>2</sub>:** If the CO<sub>2</sub> saturation is below the critical value, it will be immobile in the bulk flow, although not in the molecular sense. Less mobile CO<sub>2</sub> means less risk of leakage and more residual volumes (with saturations less than the critical) resulting from a more efficient volume sweep as preferable (Fig. 5(b)). We use critical saturation of 0.2 for both water and CO<sub>2</sub>.

**Connected CO<sub>2</sub> volumes:** To estimate the risk of leakage from the cap-rock, we assume that all mobile CO<sub>2</sub> connected to a leakage point will escape out of the reservoir. Hence, it is preferable if the total mobile CO<sub>2</sub> volume is split into smaller plumes rather than forming a big mobile plume. Though the area exposed to potential leakage points will increase by splitting the plume, yet the volume reduction is overtaking the area effect.

On the other hand, the split CO<sub>2</sub> plumes can sweep more cross-areas than a big single plume. The no-flow faulted side can be considered to be connected to an imaginary large volume available for long-term plume migration. Thus, it makes sense to talk about plume sweeping cross area. Larger areas leave more residual CO<sub>2</sub> in the tail of the plume. Hence, we looked at the largest plume size, the number of plumes, and other statistical parameters. The number of plumes at the end of simulation for all cases are given

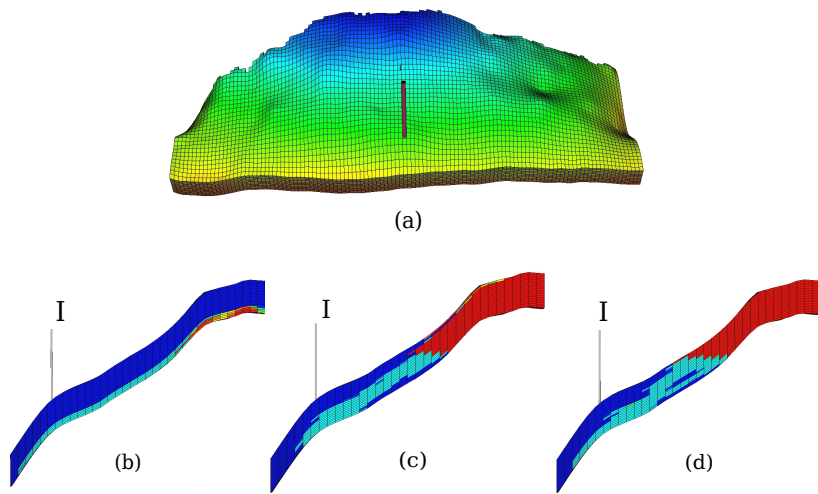


**Figure 3** (a) Model geometry and well position. Model dimensions are 3km×9km×80m with 20 layers. The bottom row shows the side view of CO<sub>2</sub> distribution (in red) at the end of simulation in different aggradation cases, from low (b) to high (d). The vertical direction is exaggerated.

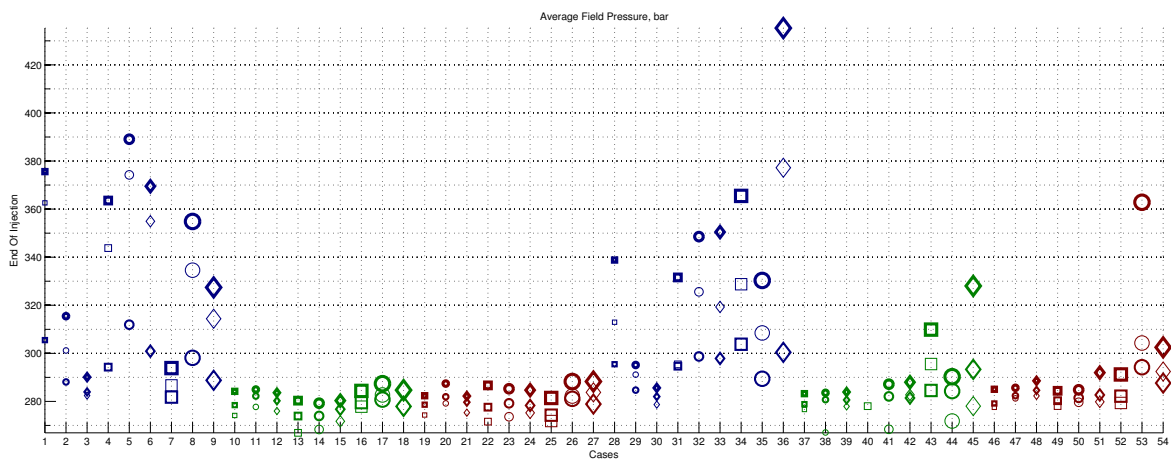


**Figure 4** Average reservoir pressure plot for all cases. Colours represent 'aggradation' level: blue for low, green for medium, and red for high levels. Size represents 'barrier': small for low, medium for medium, and large for high level of barrier. Marker shape represents 'lobosity': square for flat shore-line, circle for one lobe, and diamond for two lobes. The first half of the case numbers refer to 'progradation' up-dip towards the crest, and the second half represent 'progradation' down-dip. Thickness shows the fault criteria: thin for unfaulted, medium for open faulted and thick for closed faulted cases.

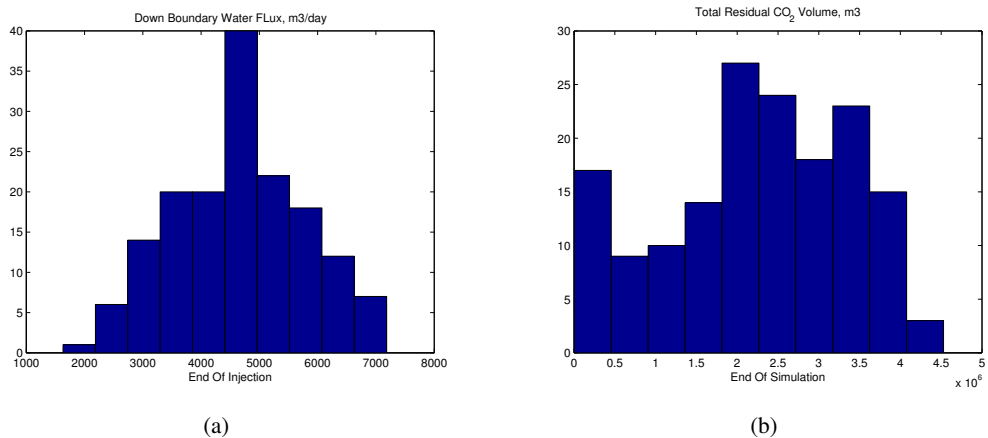


**Figure 5** (a) Flux histogram for down boundary (b) Total residual CO<sub>2</sub> volume; cases with low aggradation show less values in a separate family.

in Fig. 7. Two-lobed cases include more branching channels which result in more plume numbers. Also barrier effect increases the lateral distribution of the plume.

### Correlation between responses

Here we relate the responses by plotting them against each other. This helps in understanding the degree of correlations between the responses. By looking at these plots we can relate the trends to geological features. This in turn helps in evaluating the effect of uncertainty of each feature on the uncertainty of the simulation outputs.

Fig. 8 shows down boundary CO<sub>2</sub> flux versus average field pressure at the end of injection. Two linear trends can be recognized in the plot: first one starting from 280 bar going until 290 bar in a near vertical slope. The other one starts from 290 bar on the pressure axis and goes about 400 bar in a lower slope. The first trend shows that average pressure is not changing a lot with the increase of CO<sub>2</sub> out-flux. But the second trend shows a dramatic change in pressure corresponding to the change in the down flux rate.

The second trend is made mainly by the cases of blue colour. This is again showing the effect of low aggradation in the flow and pressure behaviour. In low aggradation cases, as the CO<sub>2</sub> flux out of the down boundary increases, the average pressure also increases in the aquifer. Effect of other geological features combined with the low aggradation dictates the amount of CO<sub>2</sub> which goes up to the crest or stays in the bottom-most layers going out from the down boundary. Since the lower layers have poor quality rock, more flow through these layers towards down boundary result in higher pressure in the aquifer.

In Fig. 9, the total number of CO<sub>2</sub> plumes are plotted against total residual CO<sub>2</sub> volumes at end of simulation. The general trend shows positive correlation between these two responses. This is consistent with our discussion in the previous section about the plume size and sweep efficiency. Split plume introduces more residual CO<sub>2</sub>. On the other hand, there is a separation in the plotted cases based on the fault criteria. Thin signs are clustered in the lower part of the graph. The medium thickness markers are clustered on the higher part of the graph and the very thick signs are sitting in between. This implies that the unfaulted cases show higher residuals with lower number of plumes, and the open faulted cases introduce more number of plumes. This can be justified by looking at a flow pattern in unfaulted and open faulted case which are shown in Fig. 10. In the open faulted cases, the flow is more laterally distributed. The closed faulted cases restrict the plume migration in the fault compartments and this

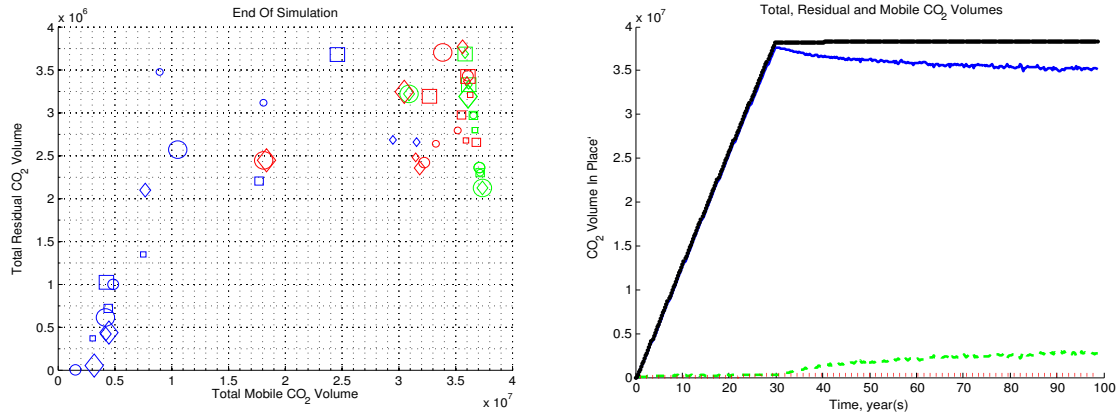


**Figure 6** CO<sub>2</sub> volumes. Left: residual versus mobile volume at the end of simulation. Most of the green coloured cases follow a linear trend, which is expected because the injected CO<sub>2</sub> must be conserved if no CO<sub>2</sub> leaves the system. For the rest of the cases, some CO<sub>2</sub> goes out of boundaries. Right: Total CO<sub>2</sub> volumes with time plotted for one case. Green curve is the residual volumes, dotted red denotes volumes that have left the domain, solid blue is mobile volumes, and the solid black shows the summation, which is the total volume and stays constant after injection because no more CO<sub>2</sub> is added to the system. The faulted cases are not included in this figure.

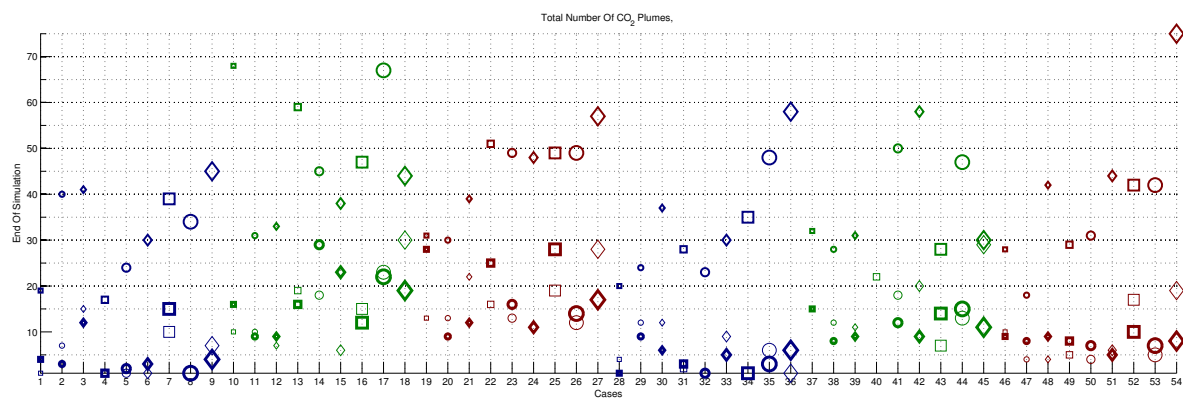


**Figure 7** CO<sub>2</sub> plume number at end of simulation, see explanation in Fig. 4.

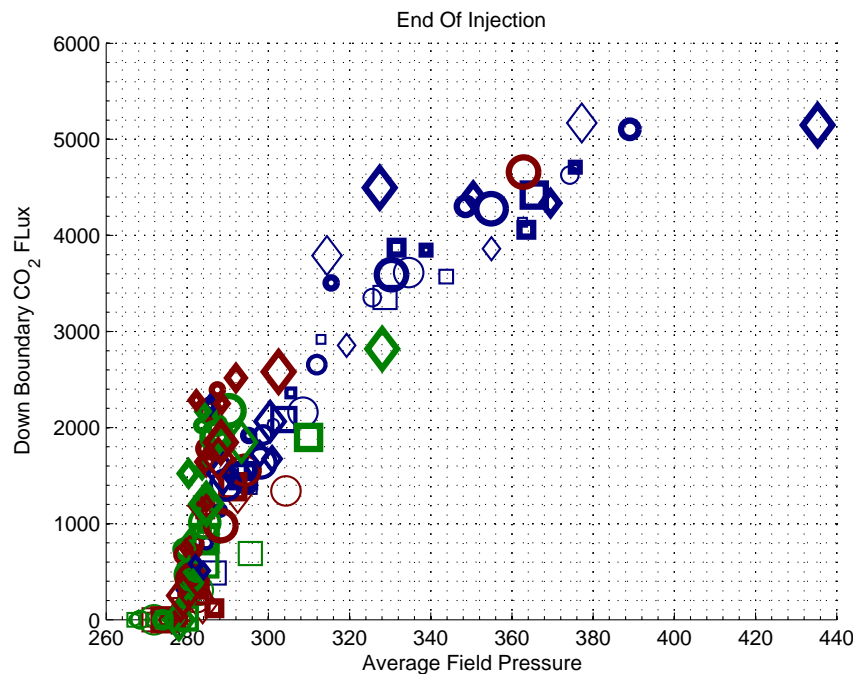


**Figure 8** Down boundary CO<sub>2</sub> flux versus average pressure, at end of injection.

introduces lower number of plumes with lower volumes of residuals which make these cases to fall in between (Fig. 2).

Finally we look at total CO<sub>2</sub> residuals versus down boundary CO<sub>2</sub> fluxes at end of injection. We can recognize a negative correlation in an almost linear trend in Fig. 11. Higher out-flux through the down boundary leaves less CO<sub>2</sub> in the domain to migrate and this lowers the residual volumes in the domain.

### Sensitivity of responses

In this section, we try to quantify the sensitivity of flow responses to each of the geological features. To achieve this, we define a gradient for each of the features. To make it clear, we use the example of barriers which are easier to explain.

We have three levels of barrier: low, medium and high. Suppose that we are interested in calculating the gradient of average field pressure with respect to barriers. We do this in two steps: first we average the average field pressure for cases of the same level of barriers. This results in three averaged pressure values corresponding to each level of barriers. In the next step, we fit a line through these three points and calculate the tangent of this line. This represents the average pressure increase due to one level increase in barriers.

For other features like fault and lobosity, we follow the same procedure. Though the feature variation is not apparent like barrier, that points to change in the type of the feature. For example, first level of fault criteria relates to unfaulted cases, the second relates to the open faulted and the third one is for the closed faulted cases. Or regarding progradation, we have two levels: up-dip and down-dip direction. The positive and negative gradient is defined based on the way we vary the defined levels.

Fig. 12 shows the average pressure sensitivity to different features at end of injection and end of sim-

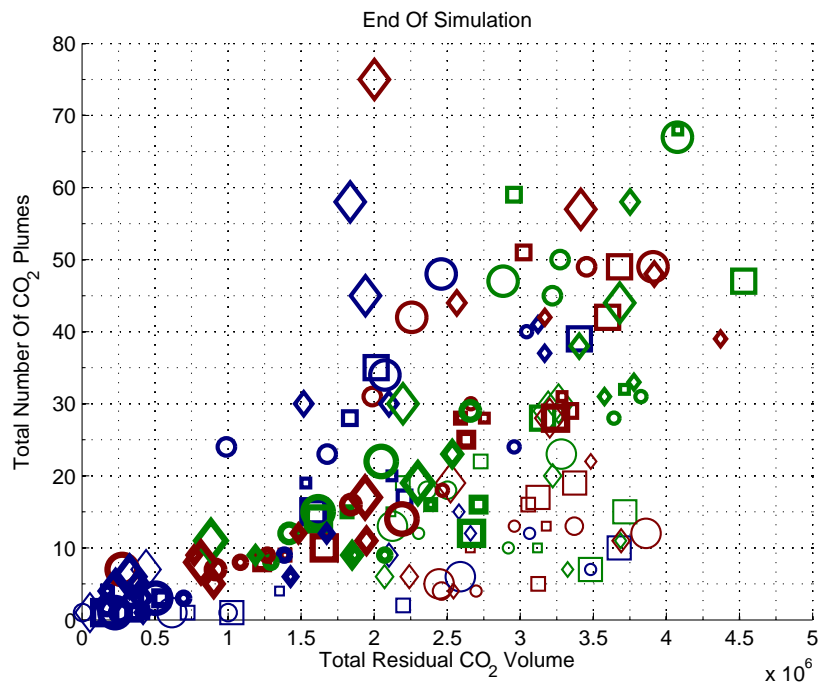


**Figure 9** Plume number versus residuals at end of simulation.

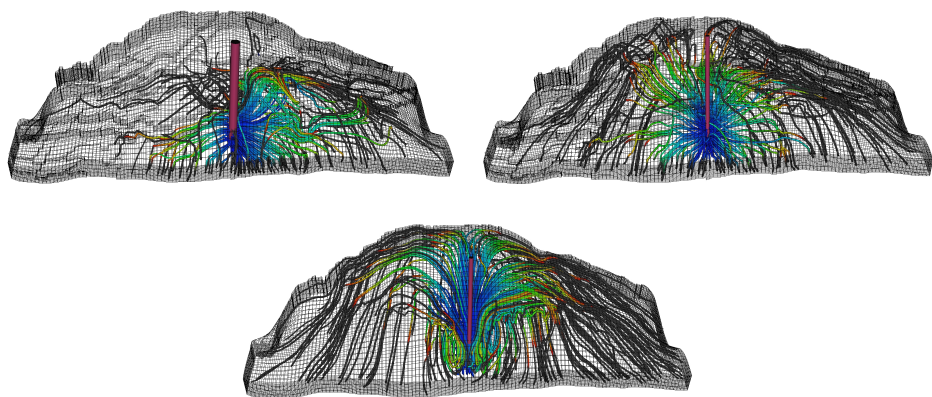


**Figure 10** Effect of fault structure on the flow pattern: top left picture shows the closed faulted case, top right picture shows the open faulted case and the bottom picture shows the unfaulted case. Open faults enhance the lateral flow, while the flow in the unfaulted case is mainly upward heading the crest.

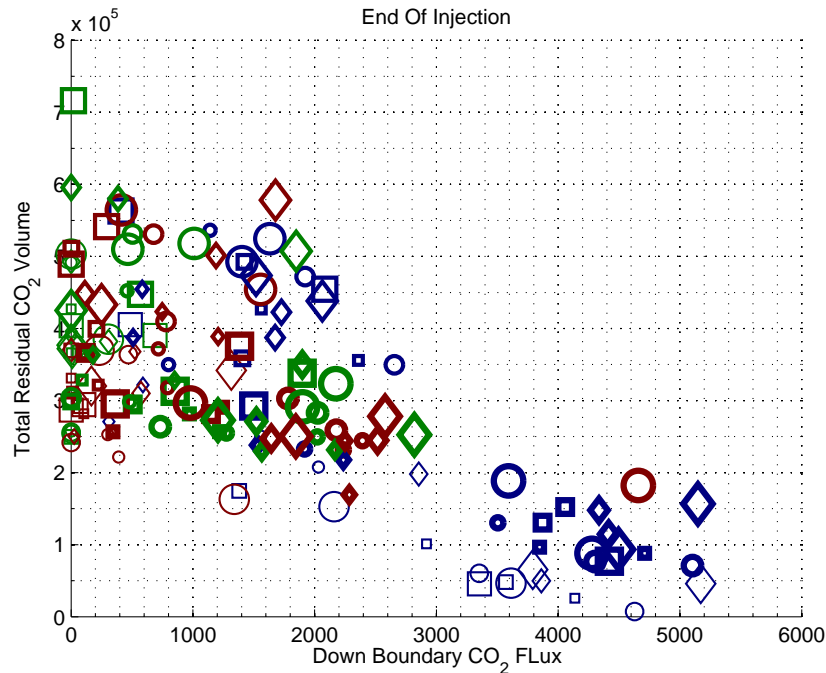


**Figure 11** CO<sub>2</sub> residual volume versus down boundary CO<sub>2</sub> flux.

ulation. These results show that in the injection period the dominating effect is related to aggradation, while at end of simulation the most influential feature is the fault criteria. During injection, the flow is dictated by the viscous force imposed by the injector. This force is more sensitive to the feature. In the low aggradation cases, flow is forced to stay in the lower layers with lower permeability values. This increase the pressure in the aquifer. In the higher aggradation level, CO<sub>2</sub> can flow upward through channels with higher permeabilities. This lowers the average pressure in the domain. This is why the gradient is negative for aggradation at end of injection, since lower aggradation level introduces higher pressure.

After stopping the injection, the dominating force is the gravity. The main flow direction is vertical and the pressure is now more sensitive to fault criteria. This is what we see in Fig. 12(b).

The effect of progradation switches from positive to negative after stopping the injection. During injection period, injecting in up-dip direction is easier than injecting in down-dip direction, while for the plume migration after injection the down-dip opens more conductive medium in front of the plumes moving towards the crest.

In Fig. 13 plume number sensitivity is shown. During injection (Fig. 13(a)), barriers are the most influential features. They enhance the lateral flow and the plume splits rather than accumulating in the crest. At end of simulation (Fig. 13(b)), progradation plays an important role relatively. Note that at this time, the open faults are introducing large number of plumes, while the unfaulted and closed faulted cases introduce small number of plumes which in average cancels out to a low gradient.

Finally Fig. 14 shows gradients for total CO<sub>2</sub> residuals. During injection (Fig. 14(a)) aggradation is the most influential feature. Fault criteria is playing the most important role in the plume migration period after injection (Fig. 14(b)).

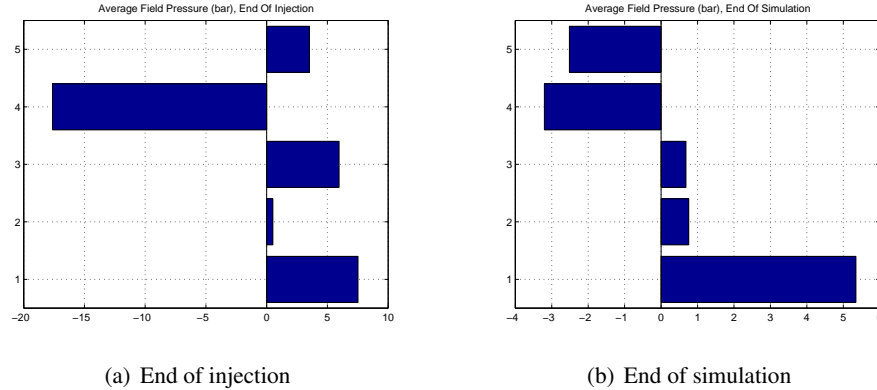


**Figure 12** Average pressure sensitivity to different geological features. In these pictures, the vertical axis shows the different geological features from bottom to top: 1-fault, 2-lobosity, 3-barrier, 4-aggradation and 5-progradation. Notice the different range in the horizontal axis at end of injection and end of simulation.

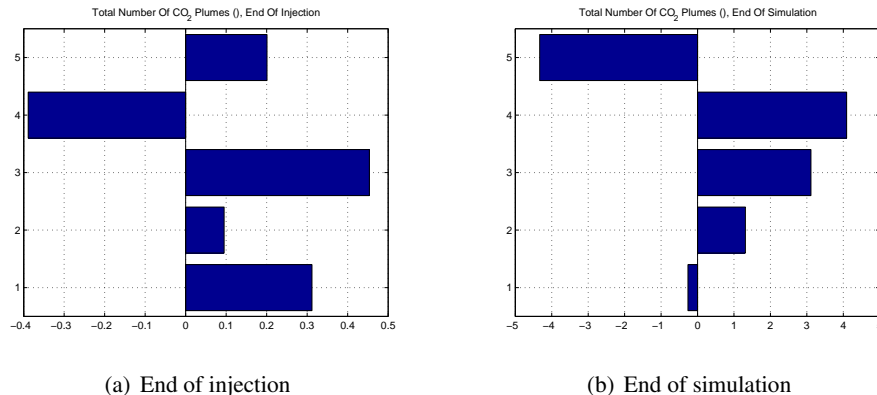


**Figure 13** CO<sub>2</sub> plume number sensitivity to different geological features. See Fig. 12 for the vertical axis explanation.

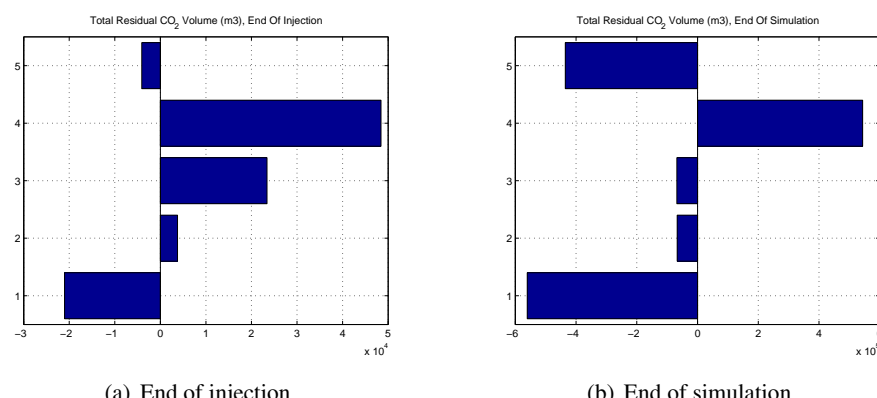


**Figure 14** Total residual CO<sub>2</sub> sensitivity to different geological features.

## **Conclusions**

Herein, we have reported on a preliminary study of the influence of various geological parameters on the injection and early-stage migration of CO<sub>2</sub> in progradational shallow-marine systems. The important responses related to storage capacity and risk of leakage are calculated for all the cases and discussed accordingly. The correlations between responses are investigated and a sensitivity measure is introduced and discussed for different responses.

Large variations in the flow responses show the importance of considering uncertainty in the geological parameters. Moreover, we have demonstrated that different geological parameters can have a different impact on the CO<sub>2</sub> migration during injection and during the later migration. In particular, our results highlight how variation in aggradation, fault criteria and barriers significantly change the flow direction within the medium. Therefore we believe that effort should be put into detailed geological modelling of potential injection sites. This way, one can better balance the influence of simplifications made in the models of geology and flow physics.

## **References**

- [1] J. M. Nordbotten: *Sequestration of Carbon in Saline Aquifers: Mathematical and Numerical Analysis*, Doctor Scientiarum Thesis, Department of Mathematics, University of Bergen, (2004).
- [2] S. Bachu: *CO<sub>2</sub> storage in geological media: Role, means, status and barriers to deployment*, Progress in Energy and Combustion Science, ELSEVIER, (2008).
- [3] J. A. Howell, A. Skorstad, A. MacDonald, A. Fordham, S. Flint, B. Fjellvoll, and T. Manzocchi: *Sedimentological parameterization of shallow-marine reservoirs*, Petroleum Geoscience, **14** (1), pp. 17-34, (2008).
- [4] T. Manzocchi, J. N. Carter, A. Skorstad, B. Fjellvoll, K. D. Stephen, J. A. Howell, J. D. Matthews, J. J. Walsh, M. Nepveu, C. Bos, J. Cole, P. Egberts, S. Flint, C. Hern, L. Holden, H. Hovland, H. Jackson, O. Kolbjørnsen, A. MacDonald, P. A. R. Nell, K. Onyeagoro, J. Strand, A. R. Syversveen, A. Tchistiakov, C. Yang, G. Yielding, and R. W. Zimmerman: *Sensitivity of the impact of geological uncertainty on production from faulted and unfaulted shallow-marine oil reservoirs: objectives and methods*, Petroleum Geoscience, **14** (1), pp. 3-15, (2008).
- [5] J. D. Matthews, J. N. Carter, K. D. Stephen, R. W. Zimmerman, A. Skorstad, T. Manzocchi, and J. A. Howell: *Assessing the effect of geological uncertainty on recovery estimates in shallow-marine reservoirs: the application of reservoir engineering to the SAIGUP project*, Petroleum Geoscience, **14** (1), pp. 33-44, (2008).
- [6] S. E. Gasda, J. M. Nordbotten, and M. A. Celia: *Vertical equilibrium with sub-scale analytical methods for geological CO<sub>2</sub> sequestration*, Computational Geosciences, **13** (4), pp. 469-481, (2009).



## **Paper iii**

### **A.3 Field-case simulation of CO<sub>2</sub> plume migration using vertical-equilibrium models.**

Nilsen , H.M., Herrera , P.A., Ashraf, M., Ligaarden , I.S., Iding , M., Hermanrud , C., Lie , K.A., Nordbotten , J.M., Dahle , H.K., and Keilegavlen , E.

Presented in GHGT10, Amsterdam, 2011. Published in 2011, Energy Procedia 4 (2011): 3801-3808.





Available online at [www.sciencedirect.com](http://www.sciencedirect.com)



Energy Procedia 4 (2011) 3801–3808

Energy  
Procedia

[www.elsevier.com/locate/procedia](http://www.elsevier.com/locate/procedia)

## Field-case simulation of CO<sub>2</sub>-plume migration using vertical-equilibrium models

Halvor Møll Nilsen<sup>a,\*</sup>, Paulo A. Herrera<sup>b</sup>, Meisam Ashrafi<sup>a,c</sup>, Ingeborg Ligaarden<sup>a</sup>, Martin Iding<sup>d</sup>, Christian Hermanrud<sup>d,e</sup>, Knut-Andreas Lie<sup>a,e</sup>, Jan M. Nordbotten<sup>e,f</sup>, Helge K. Dahle<sup>e</sup>, Eirik Keilegavlen<sup>e</sup>

<sup>a</sup>SINTEF ICT, Dept. Applied Math., Oslo, Norway

<sup>b</sup>Centre for Integrated Petroleum Research, Uni Research, Bergen, Norway

<sup>c</sup>Department of Mathematics, University of Bergen, Norway

<sup>d</sup>Statoil ASA, Trondheim, Norway

<sup>e</sup>Department of Mathematics, University of Bergen, Norway

<sup>f</sup>Department of Civil and Environmental Engineering, Princeton University, USA

### Abstract

When injected in deep saline aquifers, CO<sub>2</sub> moves radially away from the injection well and progressively higher in the formation because of buoyancy forces. Analyses have shown that after the injection period, CO<sub>2</sub> will potentially migrate over several kilometers in the horizontal direction but only tens of meters in the vertical direction, limited by the aquifer caprock [1, 2]. Because of the large horizontal plume dimensions, three-dimensional numerical simulations of the plume migration over long periods of time are computationally intensive. Thus, to get results within a reasonable time frame, one is typically forced to use coarse meshes and long time steps which result in inaccurate results because of numerical errors in resolving the plume tip.

Given the large aspect ratio between the vertical and horizontal plume dimensions, it is reasonable to approximate the CO<sub>2</sub> migration using vertically averaged models. Such models can, in many cases, be more accurate than coarse three-dimensional computations. In particular, models based on vertical equilibrium (VE) [3] are attractive to simulate the long-term fate of CO<sub>2</sub> sequestered into deep saline aquifers. The reduced spatial dimensionality resulting from the vertical integration ensures that the computational performance of VE models exceeds the performance of standard three-dimensional models. Thus, VE models are suitable to study the long-time and large-scale behavior of plumes in real large-scale CO<sub>2</sub>-injection projects [4, 1, 2, 5]. We investigate the use of VE models to simulate CO<sub>2</sub> migration in a real large-scale field case based on data from the Sleipner site in the North Sea. We discuss the potential and limitations of VE models and show how VE models can be used to give reliable estimates of long-term CO<sub>2</sub> migration. In particular, we focus on a VE formulation that incorporates the aquifer geometry and heterogeneity, and that considers the effects of hydrodynamic and residual trapping. We compare the results of VE simulations with standard reservoir simulation tools on test cases and discuss their advantages and limitations and show how, provided that certain conditions are met, they can be used to give reliable estimates of long-term CO<sub>2</sub> migration. © 2011 Published by Elsevier Ltd.

### 1. Introduction

Carbon capture and storage (CCS) is a promising technology for reducing CO<sub>2</sub> emissions to the atmosphere. To become an effective part of the solution to the climate problem, CCS technology will have to be applied at a very large scale to store a significant part of the increasing CO<sub>2</sub> emissions [6]. CO<sub>2</sub> injection into deep saline aquifers would provide large volumes to store CO<sub>2</sub>. Investigations of the risk of CO<sub>2</sub> leakage from the aquifers will require simulations that consider large temporal and spatial scales and because of the inherent uncertainty of geological characterizations, simulation of multiple realizations of a given storage scenario will be required for risk analysis. This is the main motivation for the development of fast simulation tools.

The CO<sub>2</sub>–brine system is simpler than the fluid system used in the oil industry, where black-oil or component-based formulations are standard. In particular, it is expected that at typical injection conditions, strong gravity segregation will occur over relatively short time-scales because of the large density differences between the resident brine and the injected supercritical CO<sub>2</sub>. This feature of the flow system can be used to develop fast simulation tools particularly tuned for simulating the long-term migration of the injected CO<sub>2</sub>.

Models based on a vertical equilibrium (VE) assumption have been used for long time to describe flow in porous media. Dupuit's approximation, which is commonly used in groundwater hydrology, is an example of this kind of models. In the oil industry, VE models were extended during the 50's and 60's to simulate two-phase and

\*Corresponding author

Email addresses: [Halvor.M.Nilsen@sintef.no](mailto:Halvor.M.Nilsen@sintef.no) (Halvor Møll Nilsen), [paulo.herrera@uni.no](mailto:paulo.herrera@uni.no) (Paulo A. Herrera), [jan.nordbotten@math.uib.no](mailto:jan.nordbotten@math.uib.no) (Jan M. Nordbotten), [helge.dahle@math.uib.no](mailto:helge.dahle@math.uib.no) (Helge K. Dahle)

three-phase vertically segregated flows [7, 8, 9]. The interest in VE models diminished as computational resources increased. However, interface models for scenarios with strong gravity segregation (like steam injection) were also an active research area in the 80's and 90's [10, 11].

In recent years, there has been a renewed interest in VE methods as a means to simulate large-scale CO<sub>2</sub> migration, for which a sharp-interface assumption with vertical equilibrium may be reasonable. Many authors have developed analytical solutions to study different aspects of CO<sub>2</sub> injection, assuming rapid vertical segregation and vertical equilibrium [12, 4, 1, 13, 14, 15, 16]. In particular Gasda et al. [17], extended a VE formulation with sub-scale analytic functions and demonstrated the potential of using a VE formulation to speed up simulations of CO<sub>2</sub> migration. Numerical calculations using a VE formulation compared well with full 3D simulations in a recent benchmark study [18].

Herein, we investigate the use of VE models for a realistic large-field case based on data from the Sleipner site. Our calculations consider the effects of hydrodynamic and residual trapping. We discuss the potential and limitations of VE models and show how VE models can be combined with standard methods to give reliable results both for the plume development (injection stage) and plume migration (post injection). Particularly, we focus on a model that incorporates the aquifer geometry and heterogeneity in a flexible way that enables us to utilize 3D simulations whenever needed, for example, for the injection period in heterogeneous reservoirs. To investigate large-scale CO<sub>2</sub>-injection projects with realistic rock properties over long time periods, it is crucial to reduce the computational cost. VE models enables this by using analytical solutions to capture the vertical features in the flow system, thereby reducing the dimensionality of the problem. Achieving the same in a three dimensional simulation requires prohibitively high vertical resolution.

The main objective of this paper is to compare simulations of CO<sub>2</sub> migration in the Utsira formation in the North Sea using a standard three-dimensional reservoir simulator and two-dimensional VE formulations. To our knowledge, this is one of the first comparisons between full-3D and VE calculations for a real CO<sub>2</sub> injection site. Our aims are to demonstrate the benefits of using a VE model to simulate CO<sub>2</sub> migration in a realistic setting and to discuss how VE models can be used to develop fast techniques to simulate CO<sub>2</sub> injection at the basin scale.

## 2. Mathematical formulation

In this section we present a brief summary of the derivation of a vertical equilibrium formulation. A more thorough derivation can be found in [19]. First, we assume that CO<sub>2</sub> migration in saline aquifers can be modeled as a two-phase problem with brine and CO<sub>2</sub> as the wetting (*w*) and non-wetting (*n*) fluids, respectively. Furthermore, we consider the evolution of a CO<sub>2</sub> plume in an aquifer whose mean direction makes a constant dip angle  $\theta$  with the horizontal plane as shown in Figure 1. We start the derivation by writing a mass conservation

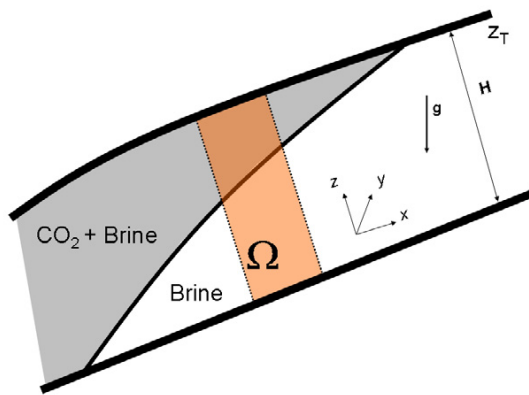


Figure 1: Schematic of the CO<sub>2</sub> plume and aquifer considered to derive a vertical equilibrium formulation for CO<sub>2</sub> migration.

equation for each fluid phase inside control volume  $\Omega = \Delta x \Delta y H$  to obtain

$$\frac{\partial}{\partial t} \int_{\Omega} \phi s_{\alpha} + \int_{\partial\Omega} \mathbf{f}_{\alpha} = \int_{\Omega} q_{\alpha}, \quad (1)$$

where  $s_{\alpha}$  is the core-scale saturation of phase  $\alpha$ ,  $\phi$  is the rock porosity,  $\mathbf{f}_{\alpha}$  are the fluid fluxes that pass through the control volume boundaries and  $q_{\alpha}$  represents source and/or sink terms. Taking the limit  $\Delta x, \Delta y \rightarrow 0$  and

assuming no flow perpendicular to the top and bottom of the aquifer, we obtain

$$\frac{\partial}{\partial t} \int_0^H \phi s_\alpha dz + \nabla_{\parallel} \cdot \int_0^H \mathbf{u}_\alpha^H dz = \int_0^H q_\alpha dz, \quad (2)$$

where  $\mathbf{u}_\alpha^H = (u_\alpha^x, u_\alpha^y)$  and  $\nabla_{\parallel} = (\partial/\partial x, \partial/\partial y)$  are two-dimensional vectors in the aquifer plane. The second term on the left hand side includes the vertical integral of the horizontal velocity of the fluid. Applying the generalized Darcy's law we have that  $\mathbf{u}_\alpha^H = -k\lambda_\alpha (\nabla_{\parallel} p_\alpha - \rho_\alpha \mathbf{g}^H)$ , so that,

$$\int_0^H \mathbf{u}_\alpha^H dz = - \int_0^H k\lambda_\alpha (\nabla_{\parallel} p_\alpha - \rho_\alpha \mathbf{g}^H) dz. \quad (3)$$

Here  $k$  is the permeability of the medium,  $\lambda_\alpha$  and  $\rho_\alpha$  are the mobility and density of phase  $\alpha$ , respectively; and  $\mathbf{g}^H$  is the projection of gravity onto the aquifer plane. To evaluate (3), we assume that [3]: i) the velocity component perpendicular to the aquifer plane is very small, and ii) the fluid density in each phase is constant. Hence the fluids are in hydrostatic equilibrium in the vertical direction. Then, pressure in each fluid phase can be written in terms of the fluid pressure at the top of the aquifer and the elevation of the top of the aquifer ( $z_T$ ), i.e. we take the caprock surface as a datum level to measure fluid pressures. Then, the pressure gradient in the aquifer plane can be evaluated as,

$$\nabla_{\parallel} p_\alpha = \nabla_{\parallel} P_\alpha - g_z \rho_\alpha \nabla_{\parallel} z_T. \quad (4)$$

Next, we define the set of vertically integrated variables and parameters listed in Table 2. Substituting (4)

Table 1: Vertically-averaged variables and parameters.

Parameter	Expression	Parameter	Expression
Gravity	$\mathbf{G} = g_z \nabla_{\parallel} z_T + \mathbf{g}^H$	Velocities	$\mathbf{U}_\alpha = \frac{1}{H} \int_0^H \mathbf{u}_\alpha^H dz$
Porosity	$\Phi = \frac{1}{H} \int_0^H \phi dz$	Saturations	$S_\alpha = \frac{1}{\Phi H} \int_0^H \phi s_\alpha dz$
Permeability	$K = \frac{1}{H} \int_0^H k dz$	Pressures	$P_\alpha = p_\alpha(z_T)$
Mobilities	$\Lambda_\alpha = \frac{1}{KH} \int_0^H k \lambda_\alpha dz$	Sources/Sinks	$Q_\alpha = \frac{1}{H} \int_0^H q_\alpha dz$

into (3) and the vertically integrated parameters into (2), we obtain a mass conservation equation for the vertically integrated fluid saturations  $S_\alpha$ . Table 2 shows a comparison between the original 3D equations and their vertically integrated equivalents.

Table 2: Equations that define the full 3D and 2D vertical equilibrium (VE) models.

3D	2D
$\frac{\partial(\phi s_\alpha)}{\partial t} + \nabla \cdot \mathbf{u}_\alpha = q_\alpha$	$\Phi \frac{\partial S_\alpha}{\partial t} + \nabla_{\parallel} \cdot \mathbf{U}_\alpha = Q_\alpha$
$\mathbf{u}_\alpha = -k\lambda_\alpha (\nabla_{\parallel} p_\alpha - \rho_\alpha \mathbf{g}^H)$	$\mathbf{U}_\alpha = -K\Lambda_\alpha (\nabla_{\parallel} P_\alpha - \rho_\alpha \mathbf{G})$
$s_w + s_n = 1$	$S_w + S_n = 1$
$\lambda_\alpha = \lambda_\alpha(s_w)$	$\Lambda_\alpha = \Lambda_\alpha(S_w)$
$p_c = p_n - p_w = p_c(s_w)$	$P_c = P_n - P_w = P_c(S_w)$

The last step in the derivation of the vertically integrated model is to evaluate the vertically integrated mobilities ( $\Lambda_\alpha$ ) and capillary pressure ( $P_c$ ) as function of the vertically integrated saturations ( $S_\alpha$ ). Assuming hydrostatic pressure distribution, so that  $p_n(z) = P_n - \rho_n g_z(z_T - z)$  and  $p_w(z) = P_w - \rho_w g_z(z_T - z)$ , we have that by definition capillary pressure as function of elevation can be computed as [3],

$$p_c(z) = p_n(z) - p_w(z) = P_n - P_w - \Delta \rho g_z(z_T - z) \quad (5)$$

where the capillary pressure at the top of the aquifer is a function of the wetting saturation at  $z_T$ ,  $P_c = P_n - P_w = p_c(s_w(z_T))$ . Then, given the wetting saturation at the top of the aquifer,  $s_w^T = s_w(z_T)$ , we can get a reconstruction of the fine scale saturation as function of  $z$  evaluation the inverse function of  $p_c(z)$ , to obtain,

$$\hat{s}_\alpha(z) = p_c^{-1}(p_c(z; s_w^T)) \quad (6)$$

Notice that  $\hat{s}_w(z)$  is not the true fine scale saturation but the one by assuming hydrostatic fluid pressure distribution in the vertical direction. Now, the vertically integrated constitutive relations can be directly computed by evaluating,  $S_\alpha = S_\alpha(\hat{s}_\alpha(s))$ ,  $\Lambda_\alpha = \frac{1}{KH} \int_0^H k \lambda_\alpha(\hat{s}_w) dz$  and  $P_c = p_c(s_w^T)$ .

### 3. Numerical simulations

In this section we compare a 3D and a VE model to simulate CO<sub>2</sub> migration in the Utsira Sand aquifer, which is a major saline aquifer in the North Sea, into which CO<sub>2</sub> separated from gas extracted from the overlying Sleipner field has been injected at a rate of approximately 1 Mt/year since 1996 [20, 21]. The Utsira Sand extends for more than 400 km in north-south direction and between 50 and 100 km in the east-west axis, covering an area of approximately  $2.6 \cdot 10^4$  km<sup>2</sup> [21]. The geometry of the aquifer is irregular and complex. While the top surface is undulatory and varies smoothly in the depth range of 550–1500 m, the bottom is more complex with multiple domes of up to 100 m high and 1–2 km wide. The aquifer thickness ranges from 300 m near the CO<sub>2</sub> injection site to 200 m farther north (200 km from the injection site). The reservoir caprock is several hundred meters thick and comprises several units of low permeability materials (shales, glacio-marine clay, and glacial till) [21]. Geophysical logs indicate that the main reservoir has a proportion of clean sand between 0.7 and 1.0 with a small shale fraction composed by multiple thin ( $\sim 1$  m) layers that constitute vertical flow barriers. The interpretation of seismic surveys, performed periodically since the CO<sub>2</sub> injection started, indicate that such shale layers have a major impact on the CO<sub>2</sub> migration because a significant part of the rising CO<sub>2</sub> has been trapped underneath these low permeability layers forming multiple quasi-independent plumes [20, 22]. Analyses of core samples of the Utsira formation sand have estimated porosity values between 35 % and 40 % and permeability in the range 1000–3000 mD [21].

#### *Model setup*

Numerical simulations were performed using a preliminary numerical model setup by the Statoil R&D group [23] to study how CO<sub>2</sub> migrates once it reaches the upper-most sand layer. Thus, the model includes the section of the aquifer immediately underneath the caprock and above the upper most shale layer as shown in Figure 2. The domain covers an area of approximately 60 km<sup>2</sup> and has an average thickness of 25 m. The numerical grid includes 120,000 hexahedral cells with constant 50 m spacing in the horizontal directions and average 5 m spacing in the vertical direction. Estimated permeability values for the top sand layer and caprock are shown in Figure 2. In the model the horizontal components of the permeability tensor are assumed isotropic and vary between 1789 and 2018 mD, while the vertical component is assigned as equal to 1/10th of the horizontal value. Because of the relative low permeability of the caprock and the underlying shale relative to the main sand aquifer, they are modeled as impermeable boundaries. The porosity of the aquifer sand was set according to a linear correlation with the permeability and has a mean value equal to 0.36. The amount of CO<sub>2</sub> that reaches the top of the aquifer was simulated as a point source with specified injection rates that increase from 0 to  $5 \cdot 10^6$  m<sup>3</sup>/year during the first 32 years and then set to zero until the end of the simulation (132 years). The total amount of CO<sub>2</sub> injected is  $5.3 \cdot 10^6$  m<sup>3</sup> at reservoir conditions.

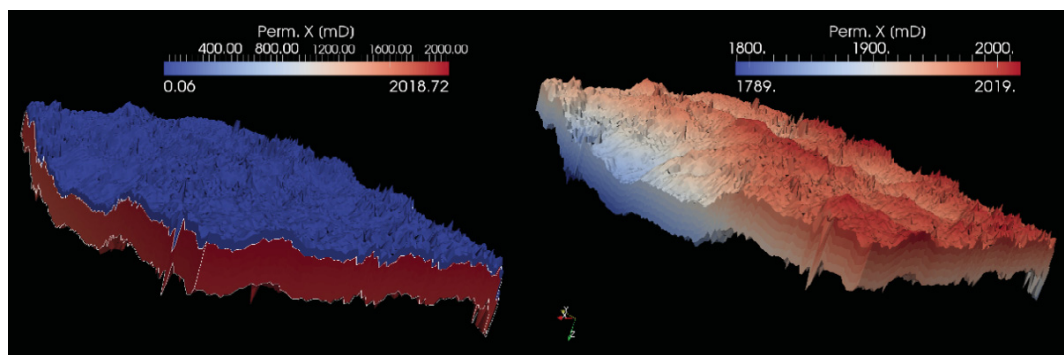


Figure 2: Estimated horizontal permeability for the upper 25 m of the Utsira Sand aquifer and lower 10 m of the caprock. There are large contrasts in permeability between the main aquifer and the caprock (left), but only moderated differences within the aquifer itself (right).

#### *Simulation results*

We present results of 3D and VE simulations carried out with the commercial ECLIPSE Reservoir simulator [24] and the VE module of the open-source Matlab Reservoir Simulation Toolbox (MRST) developed at SINTEF ICT and available at <http://www.sintef.no/Projectweb/MRST/>. In the following discussion we will refer to the different numerical solutions as ECLIPSE-3D, ECLIPSE-VE and MRST-VE. To test the sensitivity of the 3D solution with respect to the vertical discretization, we run the ECLIPSE-3D simulations using the original grid (coarse) and a refined grid (fine) that has five times more horizontal layers than the original one. Capillary forces were not included in the simulations presented below, however, as explained above, they can be easily included in the VE formulation without introducing additional computational complexity [9, 25]. The 3D simulations

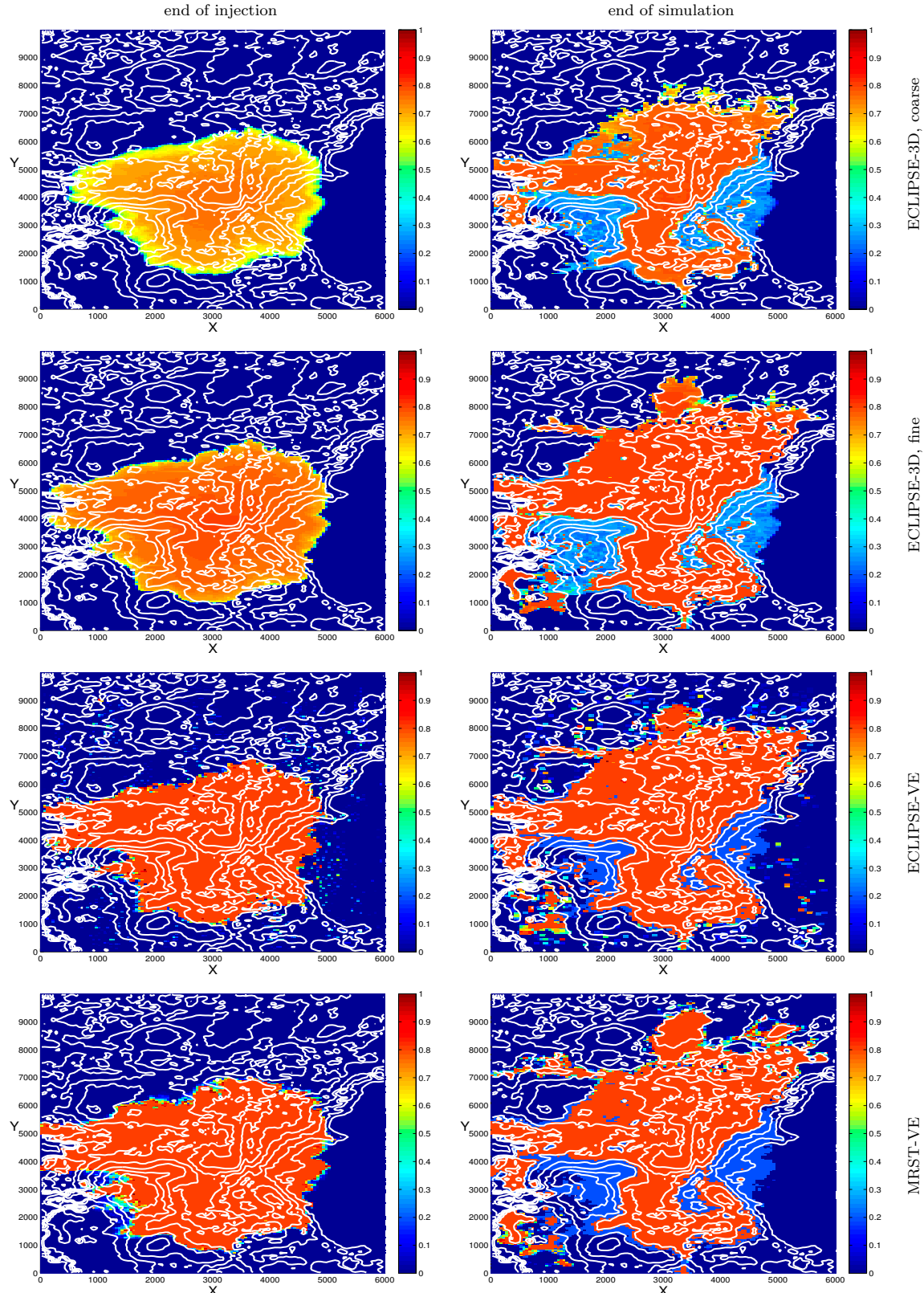


Figure 3: CO<sub>2</sub> saturation in the top cells at the end of injection (left column) and at the end of simulation (right column). Saturations computed with ECLIPSE-3D with coarse grid (first row), ECLIPSE-3D with fine grid (second row), ECLIPSE-VE (third row), and MRST-VE (fourth row). The white lines are contour lines of the height of the top of the aquifer with height distance 5 m.

3806

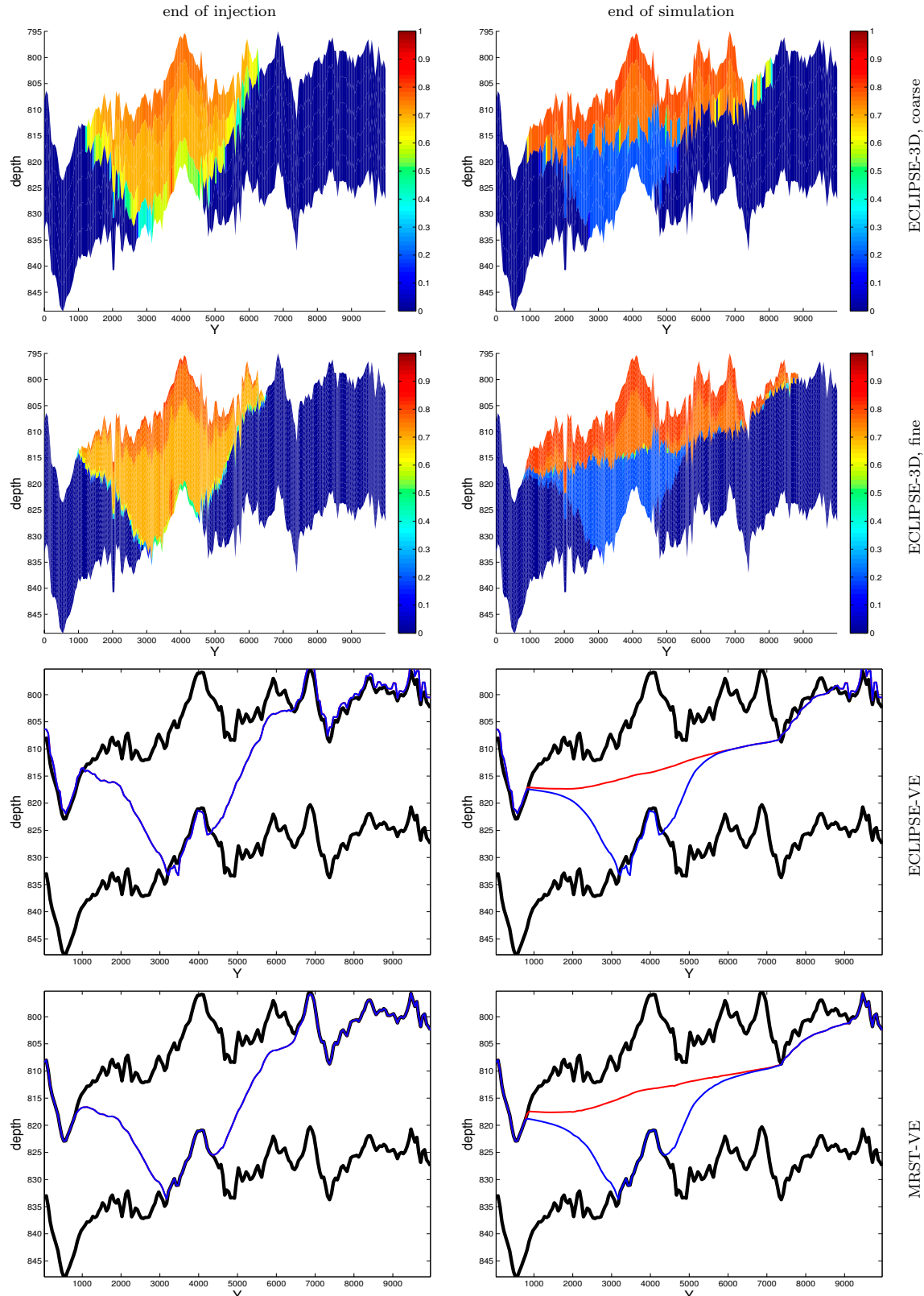
*H. Møll Nilsen et al. / Energy Procedia 4 (2011) 3801–3808*

Figure 4: CO<sub>2</sub> saturation along vertical cross-section parallel to the x-axis that passes through injection point. Saturation profiles at the end of the injection period (left column) and at the end of simulation (right column). Saturations were computed with ECLIPSE-3D with coarse grid (first row), ECLIPSE-3D with fine grid (second row), ECLIPSE-VE (third row) and MRST-VE (fourth row) simulators. Blue and red lines in the last two rows show contours of trapped and mobile CO<sub>2</sub>, respectively; black lines show the position of the bottom and top of the aquifer at the center of the cell.

were performed using both a fully implicit and an implicit-pressure, explicit-saturation (IMPES) formulation. For the coarse grid, the implicit simulation took 14 hours while the IMPES simulation took 36 minutes. The fine-grid 3D simulation took 14 hours using the IMPES option. For ECLIPSE-VE, the fully implicit option was fastest and used 19 minutes, while the IMPES time-stepping scheme used 2 hours. MRST-VE is based on a sequential splitting approach and took 12 minutes.

Figure 3 shows CO<sub>2</sub> saturation in the top cells of the model at the end of injection (32 years) and end of the simulation (132 years). Overall there is a very good agreement between the solution computed with the ECLIPSE-3D simulator in a fine grid and the two VE solutions. The difference between the two ECLIPSE-3D simulations are due to numerical errors that diminish as the grid is refined in the vertical direction. In particular, the CO<sub>2</sub> plume simulated with the coarse grid moves slower than the one simulated with the fine grid. This observation is confirmed by Figure 4, which shows simulated CO<sub>2</sub> saturations in a vertical cross-section that passes through the injection point and is parallel to the x-axis. The difference in plume speed between the coarse and fine grids is caused by CO<sub>2</sub> moving more rapidly for higher saturation values. The large cell size of the coarse grid results in a large difference between the average of the nonlinear relative permeability functions and the relative permeability functions evaluated in the average saturation. The smaller size of the cells in the refined grid reduce this effect and the CO<sub>2</sub> plume expands faster. As the CO<sub>2</sub> plume moves away from the injection area following the top of the numerical domain, it becomes thinner and the numerical errors due to poor vertical discretization become more important. This source of error is absent in the VE models because the vertical geometry of the plume is implicitly accounted for.

Figure 4 also confirms that vertical segregation of CO<sub>2</sub> and brine occurs in relatively short time and that the system reaches vertical equilibrium even before the end of the injection period. Similar patterns were observed in several other cross-sections that are not shown here. If capillary forces were included, they would not change the time required to reach vertical equilibrium, but would introduce a capillary fringe. If the capillary fringe is smaller than the vertical resolution, the vertically-averaged model will still give a better description of the system than the 3D model. Introducing capillary forces in the vertically-averaged model for our homogeneous system, however introduces very little extra computational complexity. If capillary forces were included in the simulations discussed here, the thickness of the capillary fringe would be smaller than the vertical cell spacing, hence the VE models would also give a better representation of the system than the full 3D models.

#### 4. Conclusions

We have presented results of full 3D and 2D vertical-equilibrium simulations of the migration of CO<sub>2</sub> in a realistic model of a site where CO<sub>2</sub> has been stored for more than a decade. The analysis of these results demonstrates that for the specific case of CO<sub>2</sub> migration in the Utsira Sand aquifer, VE models provide solutions that are more accurate. The VE model is much faster than corresponding 3D simulations that resolve the same dynamics. VE models are also more accurate than 3D models when full local segregation is achieved, because the vertical extension of the CO<sub>2</sub> plume is implicitly included in the model so that the VE results are independent of the vertical resolution. This is particularly important for simulations of long-term migration of CO<sub>2</sub>, where the plume thins out as it moves farther from the injection site. The VE models have reduced dimensionality compared with full 3D models and also avoid thin cells, thereby gaining a computational advantage. In addition, VE models perform better because of the weaker coupling between the pressure and transport equations [26] which make them more suitable for sequential splitting approaches. Such splitting approaches can be troublesome in three-dimensional simulations of CO<sub>2</sub> migration because of the strong coupling between the pressure and saturation equations caused by gravity.

Based on the results discussed above, we recommend that more effort should go into developing more accurate and faster VE models for simulating CO<sub>2</sub> migration. Moreover, we anticipate that the renewed interest in vertical equilibrium models will result in the development of new simulators that would be able to represent more complex physical mechanisms that affect CO<sub>2</sub> migration such as capillary pressure and CO<sub>2</sub> dissolution into brine.

#### References

- [1] M. A. Hesse, F. M. Orr, H. A. Tchelepi, Gravity currents with residual trapping, *J. Fluid Mech.* 611 (2008) 35–60.
- [2] R. Juanes, C. W. MacMinn, M. L. Szulczewski, The footprint of the CO<sub>2</sub> plume during carbon dioxide storage in saline aquifers: storage efficiency for capillary trapping at the basin scale, *Tran. Porous Media* 82 (1) (2010) 19–30.
- [3] L. W. Lake, Enhanced oil recovery, Prentice-Hall, 1989.

3808

*H. Møll Nilsen et al./Energy Procedia 4 (2011) 3801–3808*

- [4] M. A. Hesse, H. A. Tchelepi, B. J. Cantwell, F. M. Orr, Gravity currents in horizontal porous layers: transition from early to late self-similarity, *J. Fluid. Mech.* 577 (2007) 363–383.
- [5] J. M. Nordbotten, M. A. Celia, D. Kavetski, S. Bachu, A semi-analytical model estimating leakage associated with CO<sub>2</sub> storage in large-scale multi-layered geological systems with multiple leaky wells, *Environmental Science and Technology* 43 (3) (2009) 743–749.
- [6] B. Metz, O. Davidson, H. de Coninck, M. Loos, L. Meyer, *Special Report on Carbon Capture and Storage*, Cambridge University Press, UK, 2005.
- [7] J. C. Martin, Some mathematical aspects of two phase flow with application to flooding and gravity segregation, *Prod. Monthly* 22 (6) (1958) 22–35.
- [8] K. H. Coats, R. L. Nielsen, M. H. Terune, A. G. Weber, Simulation of three-dimensional, two-phase flow in oil and gas reservoirs, *Soc. Pet. Eng. J. Dec* (1967) 377–388.
- [9] J. C. Martin, Partial integration of equation of multiphase flow, *Soc. Pet. Eng. J. Dec* (1968) 370–380.
- [10] R. Godderij, J. Bruining, J. Molenaar, A fast 3d interface simulator for steamdrives, *SPE Journal* 4 (4) (1999) 400–408.
- [11] C. H. Neuman, A gravity override model of steamdrive, *J. Petrol. Tech.* 37 (1) (1985) 163–189.
- [12] M. A. Celia, S. Bachu, J. M. Nordbotten, D. Kavetski, S. Gasda, A risk assessment tool to quantify CO<sub>2</sub> leakage potential through wells in mature sedimentary basins, in: *Proceedings of the 8th Conference on Greenhouse Gas Technologies*, 2006.
- [13] C. W. MacMinn, R. Juanes, Post-injection spreading and trapping of CO<sub>2</sub> in saline aquifers: Impact of the plume shape at the end of injection, *Comput. Geosci.* 13 (2009) 483–491.
- [14] H. E. Huppert, A. E. Woods, Gravity-driven flows in porous layers, *J. Fluid Mech.* 292 (1995) 55–69.
- [15] S. Lyle, H. E. Huppert, M. Hallworth, M. Bickle, A. Chadwick, Axisymmetric gravity currents in a porous media, *J. Fluid. Mech.* 543 (2005) 293–302. [doi:10.1017/S0022112005006713](https://doi.org/10.1017/S0022112005006713).
- [16] D. Vella, H. E. Huppert, Gravity currents in a porous medium at an inclined plane, *J. Fluid Mech.* 292 (1995) 59–65.
- [17] S. E. Gasda, J. M. Nordbotten, M. A. Celia, Vertical equilibrium with sub-scale analytical methods for geological CO<sub>2</sub> sequestration, *S. of Comput. Geosci.* 13 (4) (2009) 469–481.
- [18] H. Class, A. Ebigbo, R. Helmig, H. K. Dahle, J. M. Nordbotten, M. A. Celia, P. Audigane, M. Darcis, J. Ennis-King, Y. Fan, B. Flemisch, S. E. Gasda, M. Jin, S. Krug, D. Labregere, A. N. Beni, R. J. Pawar, A. Sbai, S. G. Thomas, L. Trenty, L. Wei, A benchmark study on problems related to CO<sub>2</sub> storage in geologic formations, *Comput. Geosci.* 13 (4) (2009) 409–434. [doi:10.1007/s10596-009-9146-x](https://doi.org/10.1007/s10596-009-9146-x).
- [19] J. M. Nordbotten, M. A. Celia, *Geological Storage of CO<sub>2</sub>: Modeling Approaches for Large-Scale Simulation*, for publication with John Wiley, 2010.
- [20] M. Bickle, A. Chadwick, H. E. Huppert, M. Hallworth, S. Lyle, Modelling carbon dioxide accumulation at Sleipner: Implications for underground carbon storage, *Earth Planet. Sci. Lett.* 255 (1-2) (2007) 164–176.
- [21] R. A. Chadwick, P. Zweigert, U. Gregersen, G. A. Kirby, S. Holloway, P. N. Johannessen, Geological reservoir characterization of a CO<sub>2</sub> storage site: The Utsira Sand, Sleipner, Northern North Sea, *Energy* 29 (9-10) (2004) 1371–1381.
- [22] R. Arts, O. Eiken, A. Chadwick, P. Zweigert, L. van der Meer, B. Zinszner, Monitoring of CO<sub>2</sub> injected at Sleipner using time-lapse seismic data, *Energy* 29 (9-10) (2004) 1383–1392.
- [23] V. Singh, A. Cavanagh, H. Hansen, B. Nazarian, M. Iding, P. Ringrose, Reservoir modeling of CO<sub>2</sub> plume behavior calibrated against monitoring data from Sleipner, Norway (2010).
- [24] Schlumberger Information Systems, Eclipse technical description, Report Houston, TX (2007).
- [25] J. Nordbotten, H. Dahle, Impact of the capillary fringe in vertically integrated models for CO<sub>2</sub> storage, Under review.
- [26] I. Ligaarden, H. M. Nilsen, Numerical aspects of using vertical equilibrium models for simulating CO<sub>2</sub> sequestration, in: *Proceedings of ECMOR XII–12th European Conference on the Mathematics of Oil Recovery*, EAGE, Oxford, UK, 2010.

# Bibliography

- [1] ABRAMOWITZ, M., AND STEGUN, I., A. *Handbook of Mathematical Functions with Formulas, Graphs, and Mathematical Tables*. New York: Dover, 1965. [1.9.2](#)
- [2] ALKAN, H., CINAR, Y., AND ÜLKER, E. Impact of capillary pressure, salinity and in situ conditions on co<sub>2</sub> injection into saline aquifers. *Transport in porous media* 84, 3 (2010), 799–819. [1.7.1](#)
- [3] ALLEN, F., AND PUCKETT, D. Theoretical and experimental studies of rate-dependent two-phase immiscible flow. *SPE Production Engineering* 1, 1 (1986), 62–74. [1.7.1](#)
- [4] ARWADE, S., MORADI, M., AND LOUHGHALAM, A. Variance decomposition and global sensitivity for structural systems. *Engineering Structures* 32, 1 (2010), 1–10. [1.9.3](#)
- [5] BACHU, S. Sequestration of CO<sub>2</sub> in geological media: criteria and approach for site selection in response to climate change. *Energy Conversion and Management* 41, 9 (2000), 953–970. [1.1](#), [1.5.1](#)
- [6] BASHORE, W., ARAKTINGI, U., LEVY, M., AND SCHWELLER, W. The importance of the geological model for reservoir characterization using geostatistical techniques and the impact on subsequent fluid flow. In *SPE Annual Technical Conference and Exhibition* (1993). [1.1](#)
- [7] BEAR, J. *Dynamics of fluids in porous media*. Dover publications, 1988. [1.6.1](#)
- [8] BENSON LAB, S. U. Relative pereability explorer(rpe).  
<http://pangea.stanford.edu/research/bensonlab/relperm/index.html>. [1.6.2](#)
- [9] BENTSEN, R. Effect of neglecting viscous coupling and dynamic capillary pressure on the one-dimensional flow of two immiscible phases through a porous medium. *SPE paper*, 026016 (1993). [1.7.1](#), [1.7.1](#)
- [10] BINNING, P., AND CELIA, M. Practical implementation of the fractional flow approach to multi-phase flow simulation. *Advances in water resources* 22, 5 (1999), 461–478. [1.6.2](#)
- [11] BRADSHAW, J., AND COOK, P. Geological sequestration of carbon dioxide. *Environmental Geosciences* 8, 3 (2001), 149. [1.1](#)
- [12] CAERS, J., AND ZHANG, T. Multiple-point geostatistics: a quantitative vehicle for integrating geologic analogs into multiple reservoir models. *AAPG* (2002). [1.5](#)
- [13] CELIA, M., AND NORDBOTTEN, J. *Geological Storage of CO<sub>2</sub>: Modeling Approaches for Large-Scale Simulation*. Wiley, 2011. [1.6.1](#), [1.2](#), [1.3](#)
- [14] CHANGE, I. P. O. C. IPCC Second Assessment. *A Synthesis Report*. Geneva: WMO (1995). [1.2](#)

- [15] CHEN, Z., BODVARSSON, G., AND WITHERSPOON, P. An integral equation formulation for two-phase flow and other nonlinear flow problems through porous media. In *SPE Annual Technical Conference and Exhibition* (1990). [1.7.1](#)
- [16] CRESTAUX, T., ET AL. Polynomial chaos expansion for sensitivity analysis. *Reliability Engineering & System Safety* 94, 7 (2009), 1161–1172. [1.9.3](#)
- [17] DONG, M., AND DULLIEN, F. Effect of capillary forces on immiscible displacement in porous media. In *SPE Annual Technical Conference and Exhibition* (1999). [1.7.1](#), [1.7.1](#)
- [18] DUAN, Z., AND ZHANG, Z. Equation of state of the H<sub>2</sub>O, CO<sub>2</sub>, and H<sub>2</sub>O-CO<sub>2</sub> systems up to 10 GPa and 2573.15 K: Molecular dynamics simulations with ab initio potential surface. *Geochimica et cosmochimica acta* 70, 9 (2006), 2311–2324. [1.6.2](#)
- [19] EATON, T. On the importance of geological heterogeneity for flow simulation. *Sedimentary Geology* 184, 3-4 (2006), 187–201. [1.1](#), [1.5](#)
- [20] ELENIUS, M., AND JOHANNSEN, K. On the time scales of nonlinear instability in miscible displacement porous media flow. *Computational Geosciences* (2012), 1–11. [1.7.2](#)
- [21] ELENIUS, M., TCHELEPI, H., AND JOHANNSEN, K. CO<sub>2</sub> trapping in sloping aquifers: High resolution numerical simulations. In *XVIII International Conference on Water Resources, CIMNE, Barcelona* (2010). [1.7.2](#)
- [22] ELENIUS, M. T., NORDBOTTEN, J. M., AND KALISCH, H. Effects of a capillary transition zone on the stability of a diffusive boundary layer. *IMA Journal of Applied Mathematics* 77, 6 (2012), 771–787. [1.7.2](#)
- [23] FAJRAOUI, N., RAMASOMANANA, F., YOUNES, A., MARA, T. A. AND ACKERER, P., AND GUADAGNINI, A. Use of Global Sensitivity Analysis and Polynomial Chaos Expansion for Interpretation of Non-reactive Transport Experiments in Laboratory-Scale Porous Media. *Water Resour. Res.* (2011), doi: [10.1029/2010WR009639](https://doi.org/10.1029/2010WR009639). [1.9.2](#)
- [24] FARAJZADEH, R., AND BRUINING, J. An Analytical Method for Predicting the Performance of Gravitationally-Unstable Flow in Heterogeneous Media. In *SPE EUROPEC/EAGE Annual Conference and Exhibition* (2011). [1.7.1](#)
- [25] FAYERS, F., AND SHELDON, J. The effect of capillary pressure and gravity on two-phase fluid flow in a porous medium. *TRANS AIME* 216 (1959), 147. [1.7.1](#), [1.7.1](#)
- [26] FLETT, M., GURTON, R., AND WEIR, G. Heterogeneous saline formations for carbon dioxide disposal: Impact of varying heterogeneity on containment and trapping. *Journal of Petroleum Science and Engineering* 57, 1-2 (2007), 106–118. [1.5.1](#)
- [27] FOO, J., AND KARNIADAKIS, G. Multi-element probabilistic collocation method in high dimensions. *Journal of Computational Physics* 229, 5 (2010), 1536–1557. [1.9.2](#)
- [28] FÖRSTER, A., NORDEN, B., ZINCK-JØRGENSEN, K., FRYKMAN, P., KULENKAMPFF, J., SPANGENBERG, E., ERZINGER, J., ZIMMER, M., KOPP, J., BORM, G., ET AL. Baseline characterization of the CO<sub>2</sub>SINK geological storage site at ketzin, germany. *Environmental Geosciences* 13, 3 (2006), 145–161. [1.5.1](#)
- [29] FOUKAL, P., FRÖHLICH, C., SPRUIT, H., AND WIGLEY, T. Variations in solar luminosity and their effect on the earth's climate. *Nature* 443, 7108 (2006), 161–166. [1.2](#)

- [30] GHANEM, R., AND SPANOS, P. A stochastic galerkin expansion for nonlinear random vibration analysis. *Probabilistic Engineering Mechanics* 8 (1993), 255–264. [1.9.2](#)
- [31] GREENWOOD, H. The compressibility of gaseous mixtures of carbon dioxide and water between 0 and 500 bars pressure and 450 and 800 centigrade. *American Journal of Science* 267 (1969), 191–208. [1.6.2](#)
- [32] GUNTER, W., WIWEHAR, B., AND PERKINS, E. Aquifer disposal of CO<sub>2</sub>-rich greenhouse gases: extension of the time scale of experiment for CO<sub>2</sub>-sequestering reactions by geochemical modelling. *Mineralogy and Petrology* 59, 1 (1997), 121–140. [1.3, 1.7.2](#)
- [33] HADLEY, G., AND HANDY, L. A theoretical and experimental study of the steady state capillary end effect. In *Fall Meeting of the Petroleum Branch of AIME* (1956). [1.7.1](#)
- [34] HASSANZADEH, H., POOLADI-DARVISH, M., AND KEITH, D. Modelling of convective mixing in CO<sub>2</sub> storage. *Journal of Canadian Petroleum Technology* 44, 10 (2005). [1.7.2](#)
- [35] HITCHON, B., GUNTER, W., GENTZIS, T., AND BAILEY, R. Sedimentary basins and greenhouse gases: a serendipitous association. *Energy Conversion and Management* 40, 8 (1999), 825–843. [1.1](#)
- [36] HOUGHTON, J., ET AL. *Climate change 2001: the scientific basis*, vol. 881. Cambridge University Press Cambridge, 2001. [1.1](#)
- [37] HOVORKA, S. D., DOUGHTY, C., BENSON, S. M., PRUESS, K., AND KNOX, P. R. The impact of geological heterogeneity on CO<sub>2</sub> storage in brine formations: a case study from the Texas Gulf Coast. *Geological Society, London, Special Publications* 233, 1 (2004), 147–163. [1.5.1](#)
- [38] HOWELL, J., SKORSTAD, A., MACDONALD, A., FORDHAM, A., FLINT, S., FJELLVOLL, B., AND MANZOCCHI, T. Sedimentological parameterization of shallow-marine reservoirs. *Petroleum Geoscience* 14, 1 (2008), 17–34. [1.3, 1.5.2](#)
- [39] IEA. Key World Energy Statistics 2009. doi: [10.1787/9789264039537-en](https://doi.org/10.1787/9789264039537-en). [1.2](#)
- [40] IPPISCH, O., VOGEL, H.-J., AND BASTIAN, P. Validity limits for the van genuchten–mualem model and implications for parameter estimation and numerical simulation. *Advances in water resources* 29, 12 (2006), 1780–1789. ([document](#)), [1.21](#)
- [41] ISUKAPALLI, S., S., ROY, A., AND GEORGOPoulos, P., G. Stochastic response surface methods (srsms) for uncertainty propagation: Application to environmental and biological systems. *Risk Analysis* 18, 3 (1998), 351–363. [1.9.2](#)
- [42] JANG, Y., S., SITAR, N., AND KIUREGHIAN, A., D. Reliability analysis of contaminant transport in saturated porous media. *Water Resources Research* 30, 8 (1994), 2435–2448. [1.9.3](#)
- [43] KEESE, A., AND MATTHIES, H. G. Sparse quadrature as an alternative to Monte-Carlo for stochastic finite element techniques. *Proceedings in Applied Mathematics and Mechanics* 3 (2003), 493–494. [1.9.2](#)
- [44] LI, H., AND ZHANG, D. Probabilistic collocation method for flow in porous media: Comparisons with other stochastic methods. *Water Resources Research* 43 (2007), 44–48. [1.9.2](#)
- [45] LINDEBERG, E. Escape of CO<sub>2</sub> from aquifers. *Energy Conversion and Management* 38 (1997), S235–S240. [1.5.1](#)

- [46] LUCKNER, L., VAN GENUCHTEN, M. T., AND NIELSEN, D. A consistent set of parametric models for the two-phase flow of immiscible fluids in the subsurface. *Water Resources Research* 25, 10 (1989), 2187–2193. ([document](#)), [1.21](#)
- [47] MANZOCCHI, T., CARTER, J., SKORSTAD, A., FJELLVOLL, B., STEPHEN, K., HOWELL, J., MATTHEWS, J., WALSH, J., NEPVEU, M., BOS, C., ET AL. Sensitivity of the impact of geological uncertainty on production from faulted and unfaulted shallow-marine oil reservoirs: objectives and methods. *Petroleum Geoscience* 14, 1 (2008), 3–11. ([document](#)), [1.5.2](#), [1.5](#)
- [48] MATTHEWS, J., CARTER, J., STEPHEN, K., ZIMMERMAN, R., SKORSTAD, A., MANZOCCHI, T., AND HOWELL, J. Assessing the effect of geological uncertainty on recovery estimates in shallow-marine reservoirs: the application of reservoir engineering to the SAIGUP project. *Petroleum Geoscience* 14, 1 (2008), 35–44. [1.5.2](#), [1.5.2](#)
- [49] MATTHIES, H., G., AND KEESE, A. Galerkin methods for linear and nonlinear elliptic stochastic partial differential equations. *Computer Methods in Applied Mechanics and Engineering* 194 (2005), 1295–1331. [1.9.2](#)
- [50] MELICK, J., GARDNER, M., AND ULAND, M. Incorporating geologic heterogeneity in 3d basin-scale models for CO<sub>2</sub> sequestration: Examples from the powder river basin, ne wyoming and se montana. In *SPE International Conference on CO<sub>2</sub> Capture, Storage, and Utilization* (2009). [1.1](#)
- [51] MILLIKEN, W., LEVY, M., STREBELLE, S., AND ZHANG, Y. The effect of geologic parameters and uncertainties on subsurface flow: deepwater depositional systems. In *SPE Western Regional and Pacific Section AAPG Joint Meeting* (2008). [1.1](#)
- [52] MORRIS, M., D. Morris factorial sampling plans for preliminary computational experiments. *Technometrics*, 33 (1991), 161–174. [1.9.3](#)
- [53] NILSEN, H.M., SYVERSVEEN, A.R., LIE, K.A., TVERANGER, J., AND NORDBOTTEN, J.M. Impact of top-surface morphology on CO<sub>2</sub> storage capacity. *International Journal of Greenhouse Gas Control* 11 (2012), 221–235. [2.2](#)
- [54] NORDBOTTEN, J.M., CELIA, M.A., AND BACHU, S. Injection and storage of CO<sub>2</sub> in deep saline aquifers: Analytical solution for CO<sub>2</sub> plume evolution during injection. *Transport in Porous Media* 58, 3 (2005), 339–360. [1.7.1](#)
- [55] OLADYSHKIN, S., CLASS, H., HELMIG, R., AND NOWAK, W. A concept for data-driven uncertainty quantification and its application to carbon dioxide storage in geological formations. *Advances in Water Resources* 34 (2011), 1508–1518, doi: [10.1016/j.advwatres.2011.08.005](https://doi.org/10.1016/j.advwatres.2011.08.005). [1.9.2](#), [1.9.2](#), [1.9.2](#), [1.9.3](#)
- [56] OLADYSHKIN, S., CLASS, H., HELMIG, R., AND NOWAK, W. An integrative approach to robust design and probabilistic risk assessment for CO<sub>2</sub> storage in geological formations. *Computational Geosciences* 15, 3 (2011), 565–577, doi: [10.1007/s10596-011-9224-8](https://doi.org/10.1007/s10596-011-9224-8). [1.9.2](#), [1.9.2](#)
- [57] OLADYSHKIN, S., DE BARROS, F. P. J., AND NOWAK, W. Global sensitivity analysis: a flexible and efficient framework with an example from stochastic hydrogeology. *Advances in Water Resources In Press* (2011), doi: [10.1016/j.advwatres.2011.11.001](https://doi.org/10.1016/j.advwatres.2011.11.001). [1.9.3](#)
- [58] RAPOPORT, L., AND LEAS, W. Properties of linear waterfloods. *TRANS AIME* 198, 1953 (1953), 139–148. [1.7.1](#)

- [59] REUTER, U., AND LIEBSCHER, M. Global sensitivity analysis in view of nonlinear structural behavior. In *Proceedings of the 7th LS-Dyna Forum, Bamberg* (2008). [1.9.2](#), [1.9.3](#)
- [60] RIDDIFORD, F., WRIGHT, I., BISHOP, C., ESPIE, T., AND TOURQUI, A. Monitoring geological storage the In Salah gas CO<sub>2</sub> storage project. In *Proceedings of 7th international conference on greenhouse gas control technologies (GHGT-7), Vancouver, Canada* (2004). [1.5.1](#)
- [61] ROSADO-VAZQUEZ, F., RANGEL-GERMAN, E., AND RODRIGUEZ-DE LA GARZA, F. Analysis of capillary, gravity and viscous forces effects in oil/water displacement. In *International Oil Conference and Exhibition in Mexico* (2007). [1.7.1](#), [1.7.1](#)
- [62] SAHIMI, M. *Flow and transport in porous media and fractured rock: From classical methods to modern approaches*. Wiley-VCH, 2011. [1.6.1](#)
- [63] SALTELLI, A. *Global sensitivity analysis: the primer*. Wiley, 2007. [1.9.3](#), [1.9.3](#)
- [64] SCHLUMBERGER. Eclipse technical description manual, 2009. [1.8](#), [1.8.4](#)
- [65] SINTEF ICT. A SAIGUP realization example. <http://www.sintef.no/Projectweb/MRST/Downloadable-Resources/Download-SAIGUP-Data-Set/>. [1.5.2](#)
- [66] SINTEF ICT. MRST model of a SAIGUP realization. <http://www.sintef.no/Projectweb/MRST/Tutorials/Realistic-Reservoir-Model-II/>. [1.5.2](#)
- [67] SYVERSVEEN, A.R., NILSEN, H.M., LIE, K.A., TVERANGER, J., AND ABRAHAMSEN, P. A Study on How Top-Surface Morphology Influences the Storage Capacity of CO<sub>2</sub> in Saline Aquifers. *Geostatistics* (2012), 481–492. [1.8.2](#), [1.10.2](#), [2.2](#)
- [68] VAN DER MEER, L. The CO<sub>2</sub> storage efficiency of aquifers. *Energy Conversion and Management* 36, 6 (1995), 513–518. [1.5.1](#)
- [69] VILLADSEN, J., AND MICHELSSEN, M. L. *Solution of differential equation models by polynomial approximation*. Prentice-Hall, 1978. [1.9.2](#)
- [70] XIU, D., AND KARNIADAKIS, G. E. Modeling uncertainty in flow simulations via generalized polynomial chaos. *Journal of Computational Physics* 187 (2003), 137–167. [1.9.2](#)
- [71] YANG, W. An analytical solution to two-phase flow in porous media and its application to water coning. *SPE Reservoir Eng. J.*, 1 38 (1992). [1.7.1](#)
- [72] YORTSOS, Y., AND FOKAS, A. An analytical solution for linear waterflood including the effects of capillary pressure. *Old SPE Journal* 23, 1 (1983), 115–124. [1.7.1](#), [1.7.1](#)
- [73] ZHANG, D., AND LU, Z. An efficient, high-order perturbation approach for flow in random media via karhunen-loeve and polynomial expansions. *Journal of Computational Physics* 194 (2004), 773–794. [1.9.2](#)